THESIS AND ABSTRACT

Adipocyte autophagy in the control of obese white adipose tissue dysfunction

By Klara Piletič

Balliol College, University of Oxford

Kennedy Institute of Rheumatology, NDORMS

Thesis submitted in fulfilment of the requirements for the degree of Doctor of Philosophy, University of Oxford

Michaelmas Term 2024

Abstract

Adipocyte autophagy in the control of obese white adipose tissue dysfunction

By Klara Piletič

Thesis submitted in fulfilment of the requirements for the degree of Doctor of Philosophy, University of Oxford, Michaelmas Term 2024

Diet-induced obesity (DIO) leads to a pathological expansion of white adipose tissue (WAT), hallmarked by low-grade chronic inflammation and fibrosis. Autophagy, an evolutionary highly conserved cellular recycling pathway, positively associates with increased adiposity. However, while its role in supporting adipocyte differentiation and lipid homeostasis is well established, little is known about its role in obese adipocytes and adipose tissue dysfunction.

Here, we demonstrate that autophagy serves as a key regulator of WAT remodelling and distribution in DIO. We uncover that loss of autophagy in mature adipocytes significantly and specifically exacerbates pericellular fibrosis of gonadal WAT (gWAT), allowing for greater deposition of fat in the subcutaneous depot and supporting metabolically healthier obesity (MHO). Importantly, changes in WAT architecture are associated with increased macrophage infiltration which carry tissue-reparative and pro-fibrotic features and likely drive gWAT fibrosis. Mechanistically, we uncover that autophagy is indispensable for obesity-induced adipocyte metabolic rewiring and limits purine nucleoside catabolism. Purine catabolites, including xanthine and hypoxanthine, are secreted from adipocytes to mediate adipocyte-macrophage

crosstalk, thereby directing macrophage identity towards a tissue-reparative phenotype and contributing to excessive gWAT fibrosis.

The findings of this thesis reveal a novel role for adipocyte autophagy in the maintenance of the functional integrity and dynamic remodelling of gWAT through the limitation of obesity-associated fibrosis. Furthermore, the data presented here uncovers the role of autophagy in the regulation of adipocyte purine nucleoside metabolism and corresponding extracellular signals, which may hold therapeutic potential in fibrotic diseases.

Author's Publications, Awards, and Grants

Piletic K, Kayvanjoo AH, Richter FC, Borsa M, Lechuga-Vieco AV, Popp O, Grenet S, Long Ko JK, Zec K, Kyriazi M, Koneva L, Sansom S, Mertins P, Powrie F, Alsaleh G, Simon AK (2025) Autophagy acts as a brake on obesity-related fibrosis by controlling purine nucleoside signalling. *Manuscript in preparation.*

Piletic K, Alsaleh G, Simon AK (2023) Autophagy orchestrates the crosstalk between cells and organs. *EMBO reports*, **24**, 9.

Richter FC, Friedrich M, Kampschulte N, **Piletic K**, Alsaleh G, Zummach R, Hecker J, Pohin M, Ilott N, Guschina I, Wideman SK, Johnson E, Borsa M, Hahn P Morriseau C, Hammock BD, Schipper HS, Edwards CM, Zechner R, Siegmund B, Weidinger C, Schebb NH, Powrie F, Simon AK (2023) Adipocyte autophagy limits gut inflammation by controlling oxylipin and IL-10. *The EMBO Journal*, **42**, e112202.

MRC DTP Symposium Award for Best Student Talk (University of Oxford, 2023)

Sable Systems Award for Best Early Career Researcher Presentation (46th Meeting of the Adipose Tissue Discussion Group, University of Edinburgh, 2023)

Oxford-MRC DTP Supplementary Funding for Advanced Training in Proteomics (Medical Research Council, 2021)

Sino-British Fellowship Trust Visitorship (University of Hong Kong, 2023)

Oxford-MRC DTP Supplementary Funding for Transitions from DPhil to First Position (Medical Research Council, 2024)

Acknowledgements

Life is not measured by the breaths you take, but by the moments that take your breath away.
– Maya Angelou

When I embarked on my DPhil journey, I never imagined how deeply transformative it would be, both professionally and personally. The journey was filled with breath-taking moments of awe, discovery, but also many challenges. None of this would have been possible without the people who made Oxford feel like home, who stood by me, and whose kindness and brilliance helped shape me into who I am today. I am profoundly grateful to have had the privilege of working with some of the most extraordinary people, creating bonds that I know will last a lifetime. Through them, I discovered passions beyond science, nurturing my curiosity and belief that with imagination, anything is possible.

I will be forever grateful not only for the opportunity to pursue my DPhil at one of the best universities in the world but for the incredible people who shared this chapter of my life. Despite the inevitable ups and downs, Simon Lab has been a place of unwavering support, warm hugs, and good vibes. Mariana, Ana Vic, Lin, Felix, Dingxi, and Houfu, your generosity in answering my endless questions and the joy you brought to the everyday lab grind made even the hardest days better. I truly hope our paths cross again in the future.

To my supervisors, who have been more than mentors. Your guidance, wisdom, and encouragement have meant more than words can express. Katja, thank you for believing in me not only during the highs but especially through the lows and for your unwavering trust in my abilities. You have shown me that a fulfilling personal life can go hand-in-hand with professional success. Ghada, your delicious meals, support, and the way you showed me that empathy is just as powerful as intellect will stay with me forever. Fiona, thank you for always welcoming me with open arms and for sharing your scientific insights so generously.

I would also like to extend a huge thank you to those who made the practical aspects of my work possible. Patricia and the entire BSU team – your help with the mice was indispensable. To Amir, Ida, Jacky, Oliver, Johanna, Kristina, Jon, and Moustafa – your expertise, your patience with my endless questions, and your enthusiasm for the project enriched every step of the way. My gratitude also goes out to the students I had the privilege of supervising. Your dedication and curiosity brought fresh energy to my work and made each day more rewarding. I am deeply grateful to Kennedy Trust, Clarendon Fund, Medical Research Council, and the Ramage family for their financial support, which made this journey possible.

To all my friends who turned Oxford into a second home – Ana, Jane, Tom, the Spice Girls Anna and Matilde, Kumeren, Yavuz, Merve, Jernej, Evelina, and Markus – thank you for being there, no matter what. Vsem mojim prijateljem doma, Simoni, Daši, Anji, Ireni, Banditom in vsem ostalim, hvala ker ste si vedno vzeli čas zame in ostali v stiku kljub fizični razdalji med nami.

Največja zahvala gre mojemu partnerju in družini. Aleš, vedno si mi stal ob strani, me podpiral v vseh mojih ambicijah in mi pokazal, da se lepota življenja skriva v trenutkih, ki ti vzamejo dih in je veliko več kot le kariera. Hvala ti za vso ljubezen in pogum v težkih trenutkih. Mami in oči, hvala za vse, kar sta mi omogočila v življenju. Vajin neskončni optimizem, tolažba v najtežjih trenutkih in neomajna podpora so mi pomagali uresničiti svoje sanje. Tajda in Maj, hvala za vso podporo, zaupanje in potrpežljivost, kljub temu da sem bila tako dolgo long-distance starejša sestra in svakinja. Babi Saška, hvala za držanje pesti za srečo, brez katerih najini uspehi ne bi bili mogoči. Babi Marija, strica Borut in Boštjan, Alenka, Petra, Taj, Tim in Lora, hvala za vse vzpodbudne besede in ker ste verjeli vame. Veselim se novega poglavja v Sloveniji z vami vsemi. Ta doktorska naloga je dokaz, da je s skupnimi močmi, ljubeznijo in podporo bližnjih mogoče doseči vse.

Contents

Abbreviations

A	Adenosine
AA	Amino acid
Acetyl-CoA	Acetyl coenzyme A
ADIPOQ	Adiponectin
ADP	Adenosine diphosphate
AMP	Adenosine monophosphate
AMPK	Adenosine monophosphate-activated protein kinase
ASPC	Adipose stem and progenitor cell
ATG	Autophagy-related
ATGL	Adipose triglyceride lipase
ATM	Adipose tissue macrophage
ATP	Adenosine triphosphate
BafA1	Bafilomycin A1
BAT	Brown adipose tissue
BCAA	Branched-chain amino acid
BECN1	Beclin-1
BMI	Body mass index
C	Cytidine
C/EBP	CCAAT/enhancer binding protein

CCL	C-C motif chemokine ligand
CEM	Collagen-expressing macrophages
ChIP-seq	Chromatin immunoprecipitation sequencing
CLS	Crown-like structure
CMA	Chaperone-mediated autophagy
Col	Collagen
CR	Caloric restriction
CSF1R	Colony stimulating factor 1 receptor
DIO	Diet-induced obesity
DNL	De novo lipogenesis
ECM	Extracellular matrix
ER	Endoplasmic reticulum
EV	Extracellular vesicle
FA	Fatty acid
FABP4	Fatty acid binding protein 4
FAO	Fatty acid oxidation
FBS	Fetal bovine serum
FDR	False discovery rate
FFA	Free Fatty Acids
FMO	Fluorescence minus one
G	Guanosine

G6PD	Glucose-6-phosphate dehydrogenase
GlcNaC	N-acetylglucosamine
GLP1	Glucagon-like peptide-1
(G)M-CSF	(Granulocyte-)macrophage colony-stimulating factor
GO	Gene ontology
GSH	Glutathione (reduced)
GSSG	Glutathione (oxidised)
GTT	Glucose tolerance test
gWAT	Gonadal white adipose tissue
H&E	Haematoxylin and eosin
HDL	High-density lipoprotein
HFD	High fat diet
HK	Hexokinase
HSL	Hormone-sensitive lipase
IFN	Interferon
IL	Interleukin
ILC	Innate lymphoid cell
iNKT	Invariant NK-T cell
ITT	Insulin tolerance test
iWAT	Inguinal white adipose tissue
KO	Knock-Out

LAM	Lipid-associated macrophages
LDL	Low-density lipoprotein
MASH	Metabolic dysfunction-associated steatohepatitis
MHC	Major histocompatibility complex
MHO	Metabolically healthy obesity
Mme	Metabolically-activated macrophage
MMP	Matrix metalloproteinases
MTOR	Mammalian target of rapamycin
MTORC	Mammalian target of rapamycin complex
MUO	Metabolically unhealthy obesity
NCD	Normal chow diet
NH4Cl	Ammonium chloride
NK	Natural killer cell
NPVM	Non-perivascular-like macrophages
OPN	Osteopontin
OXPHOS	Oxidative phosphorylation
PCA	Principal component analysis
PCR	Polymerase chain reaction
PE	Phosphatidylethanolamine
PFA	Paraformaldehyde
PLIN	Perilipin

PPAR	Peroxisome proliferator-activated receptor
PPP	Pentose phosphate pathway
PSR	Picrosirius red
PVM	Perivascular-like macrophages
qRT-PCR	Real-time quantitative polymerase chain reaction
RM	Regulatory macrophages
RNA-seq	Ribonucleic acid sequencing
ROS	Reactive oxygen species
SAM	Sympathetic neuron-associated macrophages
SQSTM1	Sequestosome 1
SVF	Stromal vascular fraction
TAG	Triacylglyceride
TAL	Transaldolase
TCA	Tricarboxylic acid
Tex	Exhausted T cell
TGF	Transforming growth factor
Th	T helper
TIMP	Tissue inhibitors of matrix metalloproteinases
TKT	Transketolase
TLR	Toll-like receptor
TNF	Tumour necrosis factor

Treg	T regulatory
U	Uridine
UCP-1	Uncoupling protein-1
ULK1	Unc51-like autophagy activating kinase 1
VAM	Vasculature-associated macrophages
visWAT	visWAT Visceral white adipose tissue
WAT	White adipose tissue
WT	Wild-type

List of Figures

List of Tables

1 General Introduction

1.1 Obesity

1.1.1 Epidemiology

Obesity, a 21st-century epidemic, is proving to be a heavy burden on the global socio-economy. Notably, this public health problem is not restricted to the industrialized and economically advanced countries of the world. As of 2022, one in eight people was living with obesity worldwide, a staggering statistic that has more than doubled since 1990 (WHO, 2024). The escalating obesity prevalence highly varies by region and ethnicity, with the highest occurrence among African Americans in the United States. In England alone, 25.9 % of adults aged 18 years and over are living with obesity, with a further 37.9 % of people being overweight (NHS, 2022). Obesity is commonly defined by a body mass index (BMI) greater or equal to 30 that grossly estimates adiposity based on people's weight and height (BMI = weight (kg)/height² (m²)) (González-Muniesa et al., 2017).

1.1.2 Mechanisms and Pathophysiology

While the aetiology of obesity is complex, excessive fat deposition is generally considered the primary hallmark of obesity. Expanded adipose tissue significantly contributes to increased body mass in obesity. Increased adiposity is a result of different environmental or genetic influences, impacting eating behaviour, physical activity, and regional fat distribution in the body through various neural and endocrine cues (González-Muniesa et al., 2017). Higher caloric intake compared to energy expenditure results in a net positive energy balance, contributing to cumulative weight gain. The detrimental impact of weight gain is also dictated by the regional accumulation of fat. In contrast to a subcutaneous deposition of fat in the leg and hip region, concentration of fat in the abdominal or visceral area is considered more detrimental in obesity pathophysiology (Després, 2021). Visceral obesity positively correlates

with the development of metabolic pathologies. Failure of effective lipid storage in these depots results in ectopic fat deposition, where fat deposits in and around normally lean tissues, including the liver, muscle, and the heart, impacting their function and majorly contributing to insulin resistance (James et al., 2021).

1.1.3 Prevention and Management

Obesity prevention and management include maintenance of weight loss and strategies to lose weight. These are primarily focused on dietary interventions and exercise, with pharmacotherapy and bariatric surgery serving as second-line treatment options (González-Muniesa et al., 2017). Recent advances in developing a new class of anti-obesity drugs, glucagon-like peptide-1 (GLP-1) agonists, show great promise. Primarily aimed at promoting insulin release and reducing food intake, these drugs demonstrate a promising reduction in body weight together with the improvement of several metabolic markers (Andersen et al., 2018). On the other hand, bariatric surgery is mostly adopted in patients with severe obesity, significantly reducing body weight and improving glucose control (Osorio-Conles et al., 2021).

Despite these available treatment strategies, we still lack a better understanding of the mechanistic underpinnings of obesity that would enable the development of therapies aimed at prolonged improvement of metabolic health (Després, 2021). This is particularly critical considering numerous obesity-associated comorbidities that develop as a consequence of excessive weight gain. The most common obesity-related comorbidity is the development of metabolic syndrome, which is diagnosed when three of the five criteria are fulfilled, including visceral obesity, hypertriglyceridemia, low high-density lipoprotein (HDL) cholesterol, elevated blood pressure and increased glucose levels (González-Muniesa et al., 2017). Obesity also represents an important risk factor for developing many other pathological conditions, including type 2 diabetes mellitus, metabolic dysfunction-associated steatohepatitis (MASH), cardiovascular diseases, and cancer, as well as is an important predisposing factor for adverse

outcomes in non-related diseases, including respiratory diseases such as COVID-19 (Stefan et al., 2020, Lin and Li, 2021). Despite numerous efforts, the obesity disease burden is expected to increase further (WHO, 2024). Therefore, a better understanding of molecular mechanisms, disease progression, as well as adverse health consequences is imperative to address this emerging global problem.

1.2 Adipose tissue function and dysfunction

1.2.1 White and brown adipose tissue

Adipose tissue is divided into three subtypes: white, brown, and beige. White adipose tissue (WAT) is primarily found in both mice and humans' subcutaneous and visceral locations. Subcutaneous WAT is located under the skin in the abdominal and gluteofemoral regions in humans or the inguinal and axillary regions in mice. In contrast, visceral WAT is found in the peritoneal cavity as the omental and mesenteric depot, with analogous gonadal, perirenal and mesenteric depots in mice (Emont et al., 2022). The main function of WAT is energy storage in the form of large lipid droplets, and energy release. These two processes are controlled by lipid uptake or synthesis (lipogenesis) and lipid release (lipolysis), and their balance ultimately drives tissue expansion and contraction in response to systemic energy demand (Maniyadath et al., 2023). WAT also serves as an important modulator of multiple physiological functions through its endocrine function, plays a mechanical role in the body by cushioning the organs and serves as thermal insulation (Sakers et al., 2022).

On the other hand, brown adipose tissue’s (BAT) primary role is heat production for body temperature regulation and adaptation to environmental cold. It is found in multiple smaller depots at paravertebral, cervical, perirenal, and perivascular locations in humans and mice (Villarroya et al., 2017). In contrast to WAT which is comprised of unilocular (single) lipid droplet adipocytes, brown adipocytes display a multilocular lipid droplet phenotype. In addition, they

are characterized by high mitochondrial density and expression of uncoupling protein 1 (UCP1), which supports thermogenesis by separating nutrient catabolism from ATP synthesis. Through this, BAT can also serve as an important metabolic sink for excess nutrients (Villarroya et al., 2018). Similar to BAT, beige adipose tissue also serves as thermogenic fat, however, develops in response to cold exposure in WAT depots (Sakers et al., 2022).

1.2.2 Metabolic plasticity of white adipose tissue

Unlike other tissues, adipose tissue possesses a unique capability to undergo profound metabolic, structural, and phenotypic remodelling in response to physiological and environmental cues (Sakers et al., 2022). Preserving its remarkable plasticity during pathophysiological challenges is therefore imperative. The metabolic plasticity of WAT enables the organism to meet its energetic demands and is characterized by the ability to switch between two opposing processes: nutrient storage and release. Surplus nutrients such as glucose, amino acids (AAs), and fatty acids are taken up from the bloodstream and stored in lipid droplets as triglycerides (TAGs) through the process of *de novo* lipogenesis (DNL) (Chouchani and Kajimura, 2019). In contrast, when nutrients are scarce, TAGs are broken down and released in the form of free fatty acids (FFA) and glycerol through the process of lipolysis (Duncan et al., 2007). The balance between DNL and lipolysis is regulated by endocrine and neuronal factors. Insulin, an important anabolic hormone, is secreted from pancreatic β-cells in response to high circulating levels of glucose and fatty acids, stimulating their uptake and DNL while inhibiting lipolysis (James et al., 2021). On the other hand, catecholamines and glucagon stimulate hydrolysis of TAGs. Tight regulation of these processes is critical for the adipose tissue to adapt to the daily flux of nutrients and support whole-body metabolic homeostasis (Chouchani and Kajimura, 2019).

1.2.3 Structural plasticity of white adipose tissue

Adipose tissue expansion is supported by a combination of adipocyte hypertrophy (increase in cell size) and adipocyte hyperplasia (increase in cell number). Hypertrophy denotes the enlargement of existing adipocytes. It helps to buffer excess nutrient availability through the increase of lipid storage and is therefore commonly associated with impairing metabolic health (Sakers et al., 2022).

On the other hand, hyperplastic growth is generally more metabolically favourable. Since mature adipocyte lose their ability to proliferate, adipocyte hyperplasia relates to *de novo* adipocyte differentiation, also termed adipogenesis. Adipocyte number increases throughout childhood and adolescence and is maintained in adulthood (Maniyadath et al., 2023). Adipogenesis is a two-step process, whereby a multipotent mesenchymal precursor (fibroblast-like progenitor) becomes restricted to the adipogenic lineage, followed by differentiation. During this process, committed preadipocytes clonally expand, enter growth arrest, accumulate lipids, and become fully functional mature adipocytes. Adipocyte differentiation requires extensive cytoplasmic remodelling to remove organelles and make space for a large lipid droplet. The adipogenic trajectory is controlled by two master adipogenic transcription factors, i.e. peroxisome proliferator-activated receptor (PPARγ) and C/EBPα, which activate the expression of adipocyte-selective genes and adipogenic growth factors, such as adiponectin and fatty acid-binding protein (FABP) 4 (Ghaben and Scherer, 2019). Preadipocytes constitute the so-called stromal vascular fraction (SVF) of WAT, which also includes highly heterogeneous populations of endothelial, immune, and other mesenchymal stromal cells (Emont et al., 2022). As such, SVF additionally plays a critical role in vascularization and immunoregulatory functions in the tissue.

Changes in WAT cellular composition in response to physiological and environmental inputs are accompanied by changes in tissue remodelling. The extracellular matrix (ECM) regulates

the structural plasticity of WAT expansion and contraction. Built as a three-dimensional network, it provides mechanistic and structural support, supports tissue elasticity as well as facilitates cell differentiation, migration, survival, and signalling (Gliniak et al., 2023). The physical integrity of the tissue is provided by a highly organized matrix of collagens and non-collagenous proteins, including fibronectin, elastin, hyaluronan, and polysaccharides. Their constant turnover is mediated by different WAT cells who are actively constructing, reshaping, and degrading the ECM through the secretion of enzymes and other components (Marcelin et al., 2022).

1.2.4 Adipose tissue as a secretory organ

WAT is the body's largest endocrine organ. Collectively termed adipokines, adipocyte-derived hormones control energy and metabolic homeostasis, insulin sensitivity, as well as inflammation in intra- and inter-tissue manner. Their production is dynamically regulated by various pathophysiological conditions, such as obesity (González-Muniesa et al., 2017). One such example is leptin, a pro-inflammatory adipokine that is upregulated in the obese state. It controls feeding behaviour by stimulating the central nervous system and promotes pro-inflammatory cytokine secretion by immune cells. Pro-inflammatory adipose tissue-derived factors also include cytokines such as tumour necrosis factor α (TNFα), interleukin-6 (IL-6), and interleukin-1β (IL-1β), which can be secreted by both adipocyte and non-adipocyte cell types and support chronic inflammation. In contrast, plasma adiponectin negatively correlates with adipose mass and is specifically produced in mature adipocytes. It acts to alleviate obesity-associated metabolic dysfunction and promote insulin sensitivity by supporting fatty acid oxidation. The ratio between adiponectin and leptin is considered a biomarker of WAT inflammation (Ouchi et al., 2011).

In addition to proteinaceous factors, WAT also secretes large amounts of extracellular vesicles (EVs) which serve as local and interorgan signalling messengers (Bond et al., 2022). Their

endocrine and paracrine functions both maintain metabolic homeostasis and drive disease through various cargo, including nucleic acids, mitochondria, and lipids (Thomou et al., 2017). As their content changes according to the metabolic state of the tissue, EVs have been proposed as diagnostic biomarkers of adipose tissue health and disease.

1.2.5 Obesity-associated adipose tissue dysfunction

Continued surplus caloric intake leads to the development of metabolic disorders, during which WAT massively expands to adapt the metabolic homeostasis of the organism to changing environmental conditions. This results in WAT maladaptation that is characterised by five hallmarks: hypoxia, chronic inflammation, fibrosis, impaired adipogenesis, and metabolic inflexibility (Sakers et al., 2022) (Fig 1). These processes are continuous and intricately linked, therefore understanding the cause versus consequence has proven difficult.

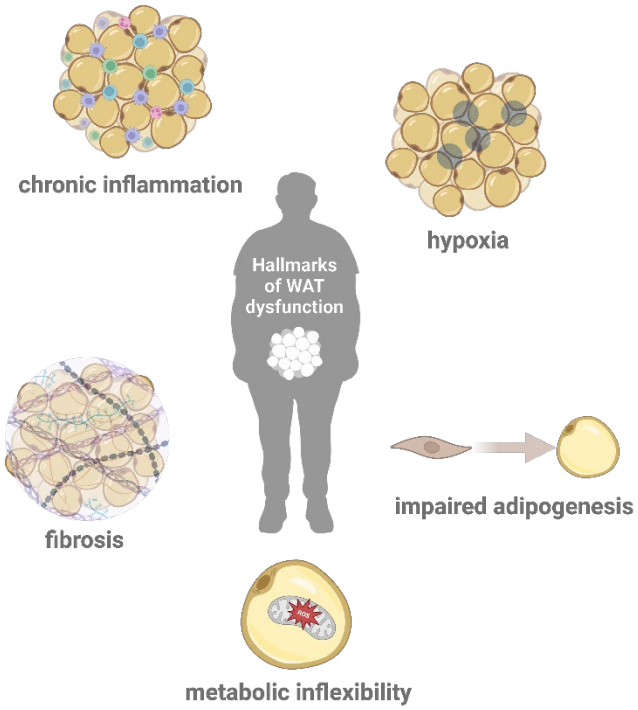

Figure 1: The hallmarks of white adipose tissue (WAT) dysfunction in obesity. Maladaptation of WAT during obesity results from five intricately linked processes, including hypoxia that inhibits adipogenesis, fibrosis, and chronic inflammation, which are both a consequence of metabolically impaired obese adipocytes. Created with BioRender.com.

During obesity, adipocytes store excess nutrients and grow through hypertrophy. As their size exceeds the diffusional limit of oxygen, this leads to local hypoxia, triggering an inflammatory response. Furthermore, massive WAT growth also results in persistent tissue hypoxia due to insufficient angiogenic potential of the tissue, inducing fibrosis (Marcelin et al., 2022). Hypoxia further inhibits adipogenesis, deeming the tissue unable to further expand through hyperplastic growth (Ghaben and Scherer, 2019). These morphological limitations to fat storage and cell size result in a chronic stress response in adipocytes (Maniyadath et al., 2023).

Adipocyte apoptotic or necrotic cell death fuels WAT inflammation through increased cytokine release and immune cell infiltration. Obese WAT is tightly associated with the recruitment of monocytes that accumulate in the tissue and form crown-like structures around damaged adipocytes to preserve tissue integrity. By switching to a pro-inflammatory phenotype, these adipose tissue macrophages (ATMs) significantly contribute to systemic low-grade inflammation (Sarvari et al., 2021).

Dysfunctional adipose tissue is also characterized by excessive ECM accumulation, leading to fibrosis. Stiffening of the WAT interferes with healthy remodelling and expansion as it negatively impacts adipogenesis and mature adipocyte function, as well as cell-to-cell interactions and signalling (Gliniak et al., 2023).

Nutrient uptake and release as well as catabolic and anabolic signals are limited in fibrotic tissue, leading to adipocyte metabolic dysfunction. Dysregulation of mitochondrial synthesis and metabolism impairs lipolysis and adipokine secretion, resulting in cell death, and further reinforcing WAT inflammation (Chouchani and Kajimura, 2019). Obesity-associated adipose tissue dysfunction is a key driver of many obesity-related complications, including type 2 diabetes, cardiovascular diseases, and MASH (Osorio-Conles et al., 2021).

1.3 Autophagy

1.3.1 Overview of autophagy

Autophagy (derived from the Greek word for “self-eating”) is an evolutionary highly conserved catabolic process. The discovery of the pathway in yeast earned Dr Yoshinori Ohsumi the Nobel Prize in Physiology or Medicine in 2016. It serves as a cellular degradation process that recycles cytoplasmic proteins, lipids, and organelles, such as the endoplasmic reticulum, nucleus, mitochondria, and ribosomes. As such, autophagy serves as an important quality control mechanism and mediator of cellular proteostasis (Dikic and Elazar, 2018).

Besides its role in degradation, autophagy is also critical for the provision of cellular energy and anabolic precursor pools (Kaur and Debnath, 2015). Therefore, it has been recognized as a master regulator of cellular metabolism (Deretic and Kroemer, 2022, Rabinowitz and White, 2010). Through modulation of these processes, autophagy is indispensable for cellular differentiation, and consequently organ development, survival, homeostasis, and ultimately function. Starvation, i.e., reduced nutrient and energy availability, is the main inducer of the autophagic process. In addition, stress conditions, growth factors, and hormones also control autophagy activation (Levine and Klionsky, 2004).

Autophagy is a tightly regulated multi-step process during which autophagosomal cargo is delivered to the lysosome for degradation. The mechanism by which the cargo is engulfed into the autophagosome differentiates between three main types of autophagy: macroautophagy, microautophagy, and chaperone-mediated autophagy (CMA). During the most prevalent form – macroautophagy – autophagosomes engulf cytoplasmic components in double membrane-bound vesicles, which are trafficked to the lysosomes for degradation (Parzych and Klionsky, 2014). In contrast, microautophagy and CMA don’t utilize autophagosomal delivery to the lysosome. Instead, cytoplasmic components are delivered to the lysosome by either direct

engulfment or delivery through a chaperon, respectively (Dikic and Elazar, 2018). Macroautophagy is initiated through mammalian target of rapamycin 1 (mTORC1) and the adenosine monophosphate-activated protein kinase (AMPK) signalling axis (Fig 2). This results in the formation and subsequent elongation of the autophagosome which is facilitated by several ATG factors (Levine and Klionsky, 2004). Once the cytoplasm gets engulfed into the membrane, the autophagosome expands and matures, during which ATG7 facilitates LC3 lipidation. Finally, upon fusion with the lysosome, autophagosomal contents are degraded and recycled as macromolecules for other cellular processes (Feng et al., 2014).

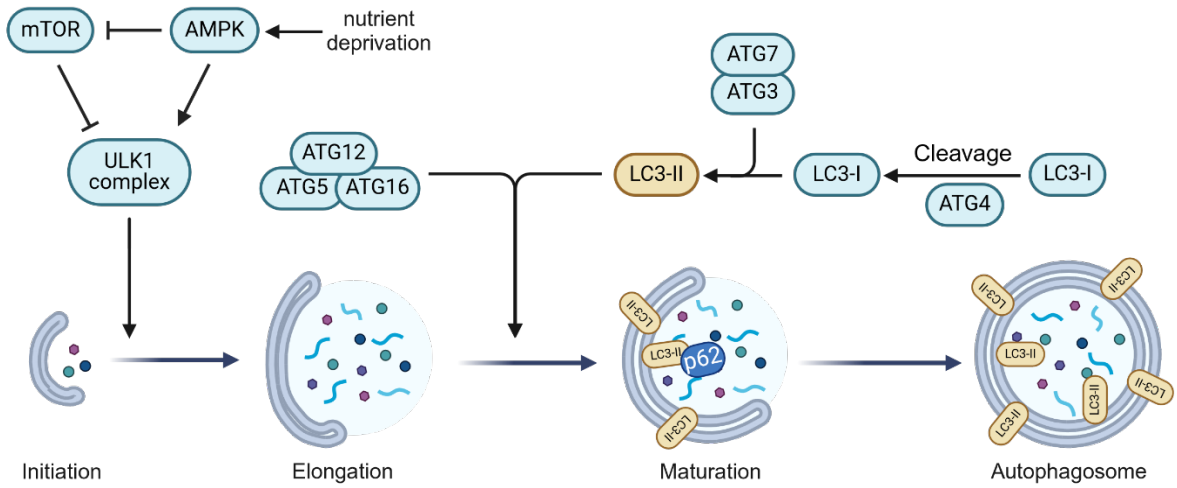

Figure 2: Overview of the three key macroautophagy steps in the formation of the autophagosome. Nutrient deprivation activates the AMPK and ULK1 complex, resulting in phagophore initiation. Through the process of elongation and maturation, cytosolic LC3-I is lipidated by the addition of PE through E1-ligase ATG7 activity. Membrane-bound LC3-II serves as a binding site for autophagy receptors (e.g. p62) which specifically target proteins and organelles for degradation. Finally, the mature autophagosome is formed and fused with the lysosome, resulting in the degradation of autophagic cargo and nutrient recovery. For more details refer to the main text. ATG: autophagy-related protein. Created with BioRender.com.

1.3.2 The role of autophagy in white adipocytes

The role of autophagy in adipocytes was first addressed in 2009, when three groups independently demonstrated that white preadipocytes highly rely on autophagy for their differentiation both *in vitro* and *in vivo* (Zhang et al., 2009, Singh et al., 2009b, Baerga et al.,

2009) (Table 1). Constitutive depletion of *Atg7* and *Atg5* resulted in leaner mice with a notable reduction in WAT mass, plasma triglycerides and cholesterol, and improved insulin sensitivity (Zhang et al., 2009, Singh et al., 2009b). Furthermore, white adipocytes obtained features of brown adipocytes, with increased mitochondrial content, reduced lipid accumulation and enhanced fatty acid oxidation. While this seminal work uncovered how autophagy impacts WAT homeostasis and function through its role in adipogenesis, the role of autophagy in mature adipocytes remained unaddressed for almost a decade.

The generation of a mouse model with an inducible depletion of autophagy offered insight into its role post adipose tissue development (Cai et al., 2018) (Table 1). Deletion of *Atg3*, *Atg16l1*, and *Atg7* uncovered that autophagy in mature adipocytes does not control body weight (Cai et al., 2018, Sakane et al., 2021). In addition, deletion of different ATG proteins had a differential effect on insulin sensitivity, further indicating its differential role in preadipocytes compared to mature adipocytes. Both studies uncovered the role of adipocyte autophagy in adipose-liver crosstalk. It has been proposed that in mature adipocytes, autophagy is indispensable for mitochondrial and redox homeostasis, which can be signalled to the liver (Cai et al., 2018). Furthermore, the work done in our lab demonstrated that during inflammatory bowel disease, autophagy limits gut inflammation by maintaining lipid homeostasis in adipocytes, including oxylipin metabolism and FFA release through lipolysis (Richter et al., 2023).

Besides macroautophagy, substrate-specific selective autophagy has also been described to play a role in adipocyte biology. Lipophagy is a specialized form of autophagy that is used to mobilize lipids and lipid droplets in several different cell types (Singh et al., 2009a). In adipocytes, lipophagy plays a role in both lipid droplet biogenesis, as well as degradation, and its depletion has been associated with a reduction in adipocyte lipid droplet content (Clemente-Postigo et al., 2020). The mechanistic underpinnings, however, remain unknown.

Table 1: The role of macroautophagy in white adipose tissue.

Genotype	Knockout	Target organ	Model	Phenotype	Reference
Atg5$^{-/-}$	Constitutive	Whole body	Primary embryonic fibroblasts, mice	Decreased adipogenesis, reduced neonatal subcutaneous adipocytes	(Baerga et al., 2009)
aP2 (Fabp4)-Cre Atg7$^{-/-}$	Constitutive	Adipose tissue	NCD or HFD, mice	Decreased WAT mass, increased insulin sensitivity, resistant to DIO, increased fatty acid metabolism	(Zhang et al., 2009)
aP2 (Fabp4)-Cre Atg7$^{-/-}$	Constitutive	Adipose tissue	NCD or HFD, mice	Decreased WAT mass, increased insulin sensitivity, resistant to DIO, increased fatty acid metabolism	(Singh et al., 2009b)
Adipoq-Cre Atg3$^{-/-}$, *Adipoq-Cre Atg16*$^{-/-}$	Conditional	Adipose tissue	NCD or HFD, mice	Insulin resistance, mitochondrial dysfunction, increased lipid peroxidation	(Cai et al., 2018)
Adipoq-Cre Atg7$^{-/-}$	Conditional	Adipose tissue	NCD or HFD, mice	iWAT hypertrophy, decreased serum FFA levels, reduced DIO-related liver steatosis	(Sakane et al., 2021)
Adipoq-Cre Atg7$^{-/-}$	Conditional	Adipose tissue	Intestinal inflammation, mice	Decreased serum FFA levels, oxylipin imbalance, increased colonic inflammation	(Richter et al., 2023)

1.3.3 The role of autophagy in obesity

Autophagy is highly sensitive to changes in metabolic parameters, including AAs, glucose, and lipids which convey organismal and cellular nutrient status. This is particularly obvious during opposing states, such as starvation or high caloric food intake, which both substantially alter

autophagy levels (Nuñez et al., 2013). These changes are further influenced by the duration of the stress, experimental models, cell types, organs, and techniques used for the assessment of autophagic activity (Zhang et al., 2018b). In addition, autophagy is not only regulated by energy imbalance but also regulates it, influencing both local and global metabolism (Kaur and Debnath, 2015). Therefore, the interplay of these influences on autophagy levels, and ultimately organismal physiology is highly complex. As dysregulation of autophagy (enhancement or suppression) is characteristic of several metabolic disorders, including obesity, diabetes mellitus, and atherosclerosis, there is an emerging interest in its regulation and role (Klionsky et al., 2021b). A need for a better understanding of the underlying molecular mechanisms is further supported by the challenges in the clinical translation of autophagy-targeting therapies due to differential organ dependency, off-target effects, and toxicity (Zhang et al., 2018b).

In contrast to most of the metabolic tissues, including the heart, liver, and pancreas, autophagy in adipose tissue during obesity is upregulated (Zhang et al., 2018b) (Table 2). This observation has been reported in several studies in humans and mice (Jansen et al., 2012, Kosacka et al., 2015, Kovsan et al., 2011, Mizunoe et al., 2017, Nuñez et al., 2013, Öst et al., 2010), with only one study to date opposing these findings (Soussi et al., 2015). Despite numerous reports as well as some more recent mechanistic studies, it remains unclear what is the mechanism and function of elevated autophagy and whether this change is causal or it just coincides with obesity. Autophagy has been reported to be stimulated through the pro-inflammatory environment of WAT in obese mice, leading to impaired triglyceride storage and lipid metabolism in adipocytes (Ju et al., 2019). In contrast, autophagy suppression, rather than enhancement has been linked to dysregulated systemic lipid homeostasis (Cai et al., 2018), albeit observations were only partially confirmed in obesity. Furthermore, these mice displayed reduced adipocyte size, peripheral insulin resistance, and increased accumulation of macrophages upon loss of adipocyte autophagy. On the other hand, a third study reporting the

role of adipocyte autophagy in obesity concluded that loss of autophagy had no effect on insulin resistance and adipocyte size, but did, however, differentially impact body fat deposition and serum FFA concentration (Sakane et al., 2021). These contradictory reports highlight a complex and yet understudied role of elevated autophagy in obese WAT.

Table 2: Changes in autophagy in WAT in obesity.

Obesity model	Organism	Autophagy change	Assessment of autophagy	Reference
Obese subcutaneous WAT with type 2 diabetes	Human	Enhanced	Increased autophagosomes (electron microscopy), increased LC3 immunofluorescence	(Öst et al., 2010)
Obese oWAT and subcutaneous WAT	Human	Enhanced	Increased ATG5, ATG12-ATG5, LC3-II, no change in p62, increased autophagy flux (p62 (Inh) /p62 (Veh)), increased *Atg5*, *Lc3a* and *Lc3b* mRNA expression	(Kovsan et al., 2011)
Obese subcutaneous WAT, *ob/ob* gWAT	Human, mouse	Enhanced	Increased LC3-II	(Jansen et al., 2012)
Obese subcutaneous WAT, HFD for 8 weeks (gWAT)	Human, mouse	Enhanced	Increased Beclin-1 and p62, increased autophagosomes (electron microscopy)	(Nuñez et al., 2013)
Obese visceral and	Human	Enhanced	Increased LC3 immunofluorescence, increased *Atg5* and *Lc3a* mRNA expression, increased	(Kosacka et al., 2015)

subcutaneous WAT			ATG12-ATG5 and LC3-II, decreased p62	
HFD for 8, 18 and 30 weeks (gWAT)	Mouse	Enhanced	Increased LC3-II and p62, increased *Lc3b* and *p62* mRNA expression	(Mizunoe et al., 2017)
Obese oWAT, HFD for 24 weeks (gWAT)	Human, mouse	Enhanced	Increased LC3-II, increased expression of autophagic genes	(Ju et al., 2019)
HFD for 8 weeks (iWAT and gWAT)	Mouse	Enhanced	Increased autophagy flux (LC3-II (Inh) /LC3-II (Veh)), decreased p62	(Sakane et al., 2021)
Obese subcutaneous WAT, *ob/ob* gWAT	Human, mouse	Suppressed	Decreased LC3-II after the inhibition of autophagy flux, increased p62, increased *p62* mRNA expression	(Soussi et al., 2015)

1.4 Autophagy-mediated crosstalk between cells and organs

Traditionally, autophagy has been mostly viewed as a cell-intrinsic pathway, i.e., modulating the cytosolic landscape of individual cells. However, many recent reports suggest that autophagy also participates in extracellular communication, either actively or passively, thereby functionally modulating recipient cells and organs (Piletic et al., 2023).

The active form of non-cell autonomous autophagy is termed secretory autophagy and closely overlaps with endo- and exocytotic pathways as well as with lysosomal exocytosis (Leidal et al., 2020) (Fig 3). It is activated during times of stress, including starvation, ER stress, unfolded protein response, and dysregulated intracellular trafficking (Jahangiri et al., 2022). While the

exact mechanism of the secretory pathway is not yet understood in detail, it has been suggested that autophagosomes/endosomes can be re-directed to the cytoplasmic membrane, thereby releasing soluble proteins, extracellular vesicles (EVs), and secretory lysosomes into the extracellular space (Nguyen and Debnath, 2022). Most of the studies to date focus on the non-degradative aspect of secretory autophagy, with secreted messengers exerting biological activity, including cytokines, hormones, and RNA-loaded EVs (Piletic et al., 2023).

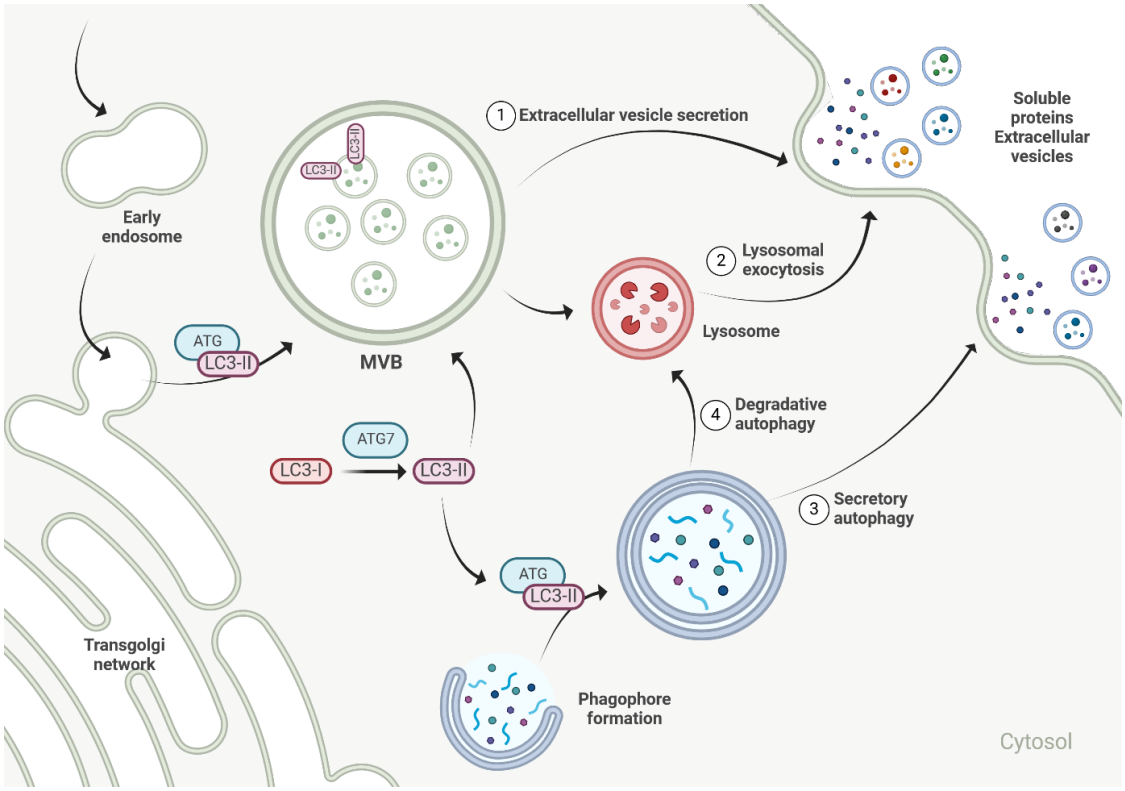

Figure 3: Secretory autophagy tightly overlaps with endo- and exocytosis. Secretory autophagy (3) overlaps with traditional endo- and exocytotic pathways (1) and lysosomal exocytosis (2). Secretory autophagy branches away from degradative autophagy (4), which can also exert non-cell autonomous effects. Key overlapping processes are highlighted here. For more details refer to the main text. Adapted from (Piletic et al., 2023). MVB = multivesicular bodies.

On the other hand, the passive form of non-cell autonomous autophagy is often a consequence of dysregulated intracellular recycling, whereby changes in autophagy activity result in altered metabolism and/or proteostasis inside the cell. In turn, the affected cells signal these changes

through the release of nutrients, thereby modulating their microenvironment (Fig 4). The secretion of AAs (including arginine and alanine), lipids (lipid peroxides and oxylipins), and other metabolites (adenosine triphosphate (ATP)) is a result of protein degradation or enzymatic conversion (Piletic et al., 2023). This nutrient-generating non-cell-autonomous function of autophagy has been mainly described in pathophysiological conditions, including cancer, obesity, and intestinal inflammation (Martins et al., 2014, Sousa et al., 2016, Katheder et al., 2017, Poillet-Perez et al., 2018, Cai et al., 2018, Richter et al., 2023). By redirecting cellular waste outside of the cell, autophagy can therefore obtain a signalling function, shaping cell fate, tissue microenvironment, and ultimately systemic metabolism.

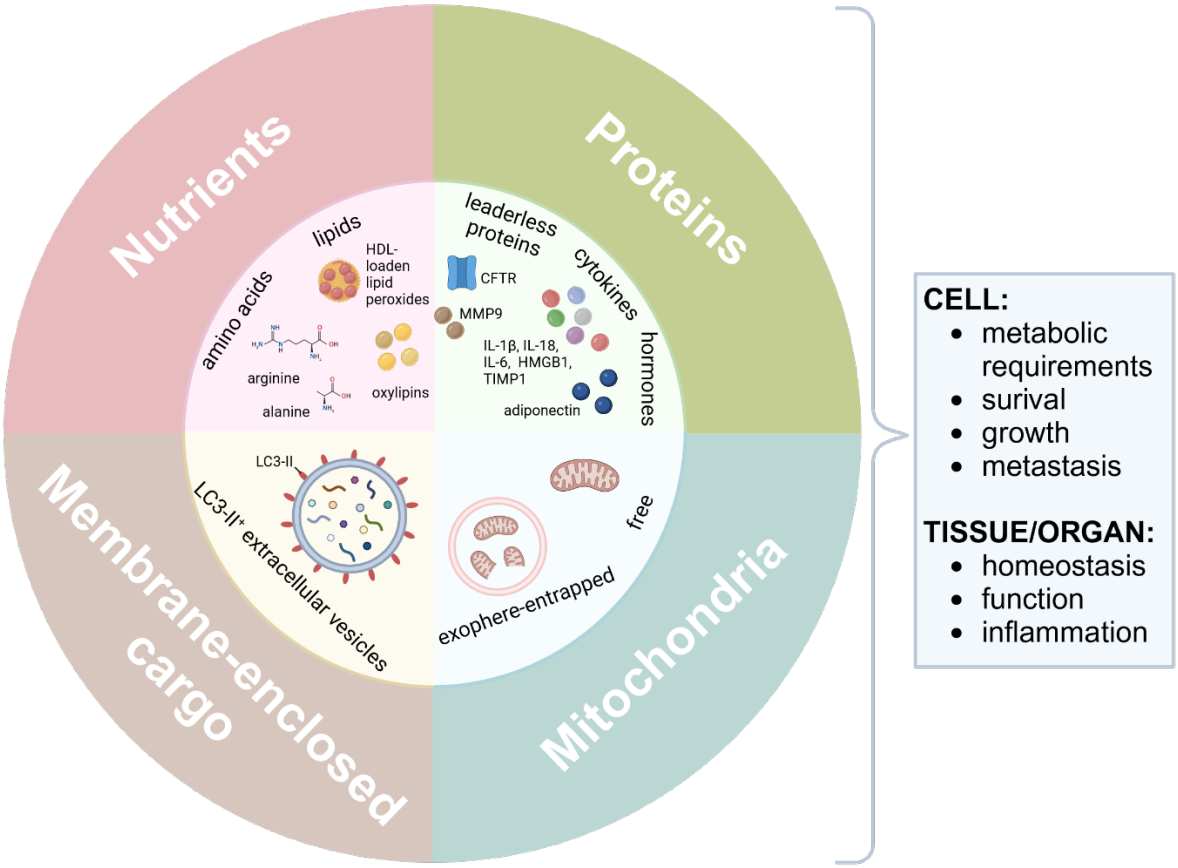

Figure 4: The role of autophagy in intercellular and interorgan crosstalk. Cells, tissues and organs communicate their homeostatic status and needs to their environment via autophagy. The diverse nature of these autophagy-derived messengers includes amino acids, lipids, proteins, mitochondria, and membrane-bound cargo. For more details refer to the main text. Adapted from (Piletic et al., 2023).

1.4.1 Autophagy in the control of cell-to-cell communication

Efficient cell-to-cell communication is key to maintaining tissue homeostasis and can be facilitated by autophagy (Fig 4). Nutrient and energy demands as well as cellular stress and damage need to be communicated between cells of different cell types to support tissue function and ultimately the organism. The role of autophagy in this crosstalk is especially apparent in the case of functionally highly specialized cells with specific metabolic adaptations and needs as well as a low turnover, such as cancer and immune cells.

In healthy conditions, secretory autophagy facilitates communication between immune and non-immune cells in the heart. By supporting the release of damaged mitochondria via vesicular particles called exophers, autophagy supports the crosstalk between parenchymal cells and cardiac-resident macrophages (Nicolás-Ávila et al., 2020). By eliminating dysfunctional mitochondria through autophagy, cardiac cells can maintain their proteostasis and ultimately heart function. A similar autophagy-dependent degradation of mitochondria has also been predicted between adipocytes and macrophages but remains to be experimentally validated (Crewe et al., 2021).

Furthermore, the importance of communication between cells is especially evident in times of distress, such as cancer. Autophagy mediates local as well as systemic metabolic and cytokine crosstalk between cancer cells and tumour microenvironment. These autophagy-dependent interactions are highly evolutionary-conserved and have been described in *Drosophila melanogaster*, mouse, and human cell lines (Katheder et al., 2017, Sousa et al., 2016, Poillet-Perez et al., 2018, Michaud et al., 2011). Cancer cells display a dysregulated metabolic demand compared to healthy cells due to their increased proliferation and growth as well as the accumulation of damaged mitochondria. Autophagy can support this metabolic adaptation by providing nutrient sources in the microenvironment, resulting in improved cell survival, proliferation, and tumour malignancy. In the case of pancreatic ductal adenocarcinoma,

stromal pancreatic stellate cells promote tumour initiation through autophagy-mediated secretion of alanine, which serves as an alternative metabolic source to support tumour growth (Sousa et al., 2016). Host autophagy can also indirectly support the growth of arginine-auxotrophic tumours such as melanoma, urothelial carcinoma, and non-small-cell lung cancer by limiting the release of arginine-depleting enzyme arginase I from the liver, therefore increasing the systemic availability of arginine in the circulation (Poillet-Perez et al., 2018). In addition to AA exchange, autophagy is also required for the release of ATP in the colorectal carcinoma tumour microenvironment, which triggers immunogenic cell death and improves chemotherapy response (Michaud et al., 2011).

1.4.2 Autophagy in the control of organ-to-organ communication

In addition to intercellular crosstalk, autophagy also controls secreted messengers between distant organs and tissues, resulting in the regulation of organ function, whole-body metabolism and energy balance (Fig 4). Since most of the cell-to-cell crosstalk studies have looked at the role of autophagy in metabolically demanding, functionally specialized, and non-proliferative cells, it is not surprising that the majority of reports on autophagy in organ-to-organ communication relate to adipose tissue.

The best studied example of autophagy-mediated organ-to-organ communication is between adipose tissue and the liver (Fig 5). In the lean state, depletion of autophagy in mature adipocytes results in the activation of gluconeogenesis and detoxification pathways in the liver, and it has been proposed that the extent of adipose tissue damage is conveyed to the liver in the form of lipid peroxides (Cai et al., 2018). When adipocyte autophagy is depleted in obesity, this leads to a reduction in FFA-mediated crosstalk alleviating liver steatosis, inflammation, and fibrosis, however, the mechanism remains elusive (Sakane et al., 2021). Furthermore, autophagy-mediated adipose tissue-to-liver communication was also identified in a model of autophagy upregulation through hyperactivation of Becn1 protein. In a lean state, adipocyte

autophagy promotes adiponectin secretion in exocyst secretory vesicles, which improves lipid metabolism and insulin sensitivity in the liver and skeletal muscle (Kuramoto et al., 2021). Different outcomes of these independent studies suggest further understanding of adipose tissue-liver crosstalk is needed to better understand the contribution of autophagy to this interaction.

In addition, our group has previously identified that autophagy also mediates adipose tissue-gut crosstalk through the control of local inflammatory responses in fat (Richter et al., 2023) (Fig 5). By controlling the secretion of oxylipins (oxidised lipid species) WAT autophagy acts to limit intestinal inflammation through stimulation of anti-inflammatory interleukin 10 (IL-10) production.

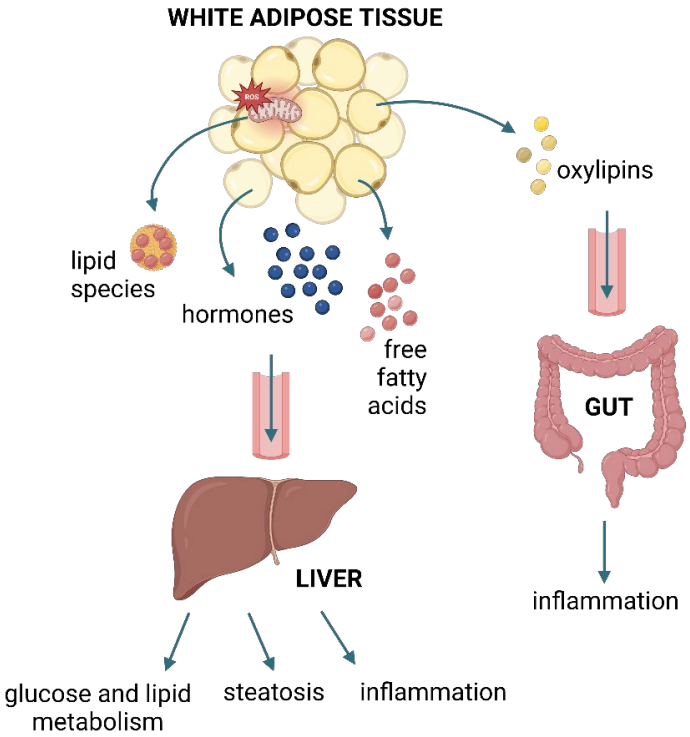

Figure 5: The role of autophagy in the crosstalk between adipose tissue and liver or gut. Adipose tissue communicates its status of damage and metabolic needs to distinct organs via autophagy. Autophagy-derived functional molecules from adipose tissue have various downstream effects on target organs, such as the liver and gut. For more details refer to the main text. Adapted from (Piletic et al., 2023).

1.5 Thesis hypothesis and objectives

Cells utilise autophagy to rewire biosynthetic pathways and cellular metabolism allowing them to better adapt to intra- as well as intercellular stressors. While it is well accepted that adipocyte autophagy positively associates with body weight gain, little is known about the functional impact of this increase on obesity outcomes. Furthermore, it remains poorly understood if and how adipocyte autophagy shapes obese WAT dysfunction. As a close link between autophagy-controlled adipogenesis and WAT maladaptation has already been established, we set out to study the role of autophagy in mature adipocytes during diet-induced obesity (DIO). We hypothesised that adipocyte autophagy impacts obese adipose tissue dysfunction in a cell-intrinsic and cell-extrinsic manner. To test this hypothesis, we established the following objectives:

1. Assess the role of adipocyte autophagy in systemic metabolism during obesity.
2. Investigate the impact of adipocyte autophagy on adipose tissue dysfunction during obesity.
3. Understand the mechanistic underpinnings of adipocyte autophagy during obesity-related adipose tissue remodelling.

These objectives are addressed throughout chapters 3-5, respectively. As this thesis describes, we have uncovered novel roles for adipocyte autophagy in i) visceral WAT distribution and ii) limiting pericellular adipose tissue fibrosis. Mechanistically, we observed that during obesity, autophagy is upregulated to support adipocyte metabolic adaptation. Failure to meet adipocyte metabolic demand leads to nucleoside-mediated crosstalk with macrophages, driving their tissue-reparative phenotype and ultimately contributing to excessive WAT fibrosis. Overall, this thesis highlights the critical role of autophagy in the maintenance of adipose tissue integrity during DIO.

2 Materials and Methods

2.1 Mouse models

Adipoq-Cre^{ERT2} mice (Sassmann et al., 2010) were purchased from Charles River, UK (JAX stock number: 025124) and crossed to floxed *Atg7* (*Atg7*$^{fl/fl}$) mice (Komatsu et al., 2005). Wild-type C57BL/6J and C57BL/6 SJL CD45.1 mice were bred in-house. All mice used in the experiments were on a C57BL/6J background. Experimental cages were sex- and age-matched and balanced for genotypes. Littermate *Cre*$^{-}$ mice were used as controls for the experimental animals. Genetic recombination was induced at 6-8 weeks of age by oral gavage of 4 mg tamoxifen (T5648, Sigma) per mouse per day for five consecutive days. Tamoxifen was given to both control and experimental groups of mice. Two days after receiving the last tamoxifen dose, mice were subjected to an altered diet regime with either a high-fat diet with 60 kcal% fat (D12492i, Research Diets) or a complementary normal chow diet with 10 kcal% fat (D12450Ji, Research Diets) for 6-26 weeks. All mice were housed under specific pathogen-free conditions and subjected to a 12-hour dark/light cycle. They were housed in groups of 3-5 with unlimited access to water and food. The housing temperature was kept between 20 and 24 °C, with a humidity level of 45–65%. All experiments were performed in accordance with approved procedures by the Local Review Committee and the Home Office under the project license (PPL30/3388 and P01275425).

2.2 Bone marrow chimera generation

Recipient *Adipoq-Cre*$^{+}$ and *Adipoq-Cre*$^{-}$ *Atg7*$^{fl/fl}$ mice on CD45.2^{+} background were lethally irradiated with 5.5 Gray doses per cycle for two irradiation cycles, 4 hours apart, before intravenously injecting 300,000 donor cells. Donor cells were prepared from the femur and tibia from C57BL/6 SJL CD45.1 mice. Following the transplantation, mice were kept on antibiotics (Baytril, Bayer) in drinking water for two weeks to avoid infections and the cell replenishment

was followed bi-weekly. Five weeks after irradiation, mice were treated with tamoxifen for genetic deletion and fed a high-fat diet for a total of 12 weeks (as described above).

2.3 Caloric restriction

Mice were treated with tamoxifen to induce genetic recombination and fed HFD as described above. Starting after 16 weeks of HFD feeding, mice were subjected to a caloric restriction regimen, whereby access to HFD was limited in a 2:1 ratio (2 days unlimited access, 1 day no access) (Lee et al., 2020). Access to food was restricted for 8 consecutive weeks.

2.4 Macrophage depletion models

Mice were treated with tamoxifen to induce genetic recombination and fed HFD as described above. Starting after 8 weeks of HFD feeding, mice were treated with inducers of macrophage depletion. For clodronate-induced macrophage depletion, *Adipoq-Cre*$^{+}$ and *Adipoq-Cre*$^{-}$ *Atg7*$^{fl/fl}$ mice were intraperitoneally injected with 200 µl of clodronate- or PBS-loaded liposomes (CP-005-005, Liposoma BV) once a week for 4 weeks. For antibody-induced macrophage depletion, *Adipoq-Cre*$^{+}$ and *Adipoq-Cre*$^{-}$ *Atg7*$^{fl/fl}$ mice were intraperitoneally injected with rat IgG2a (BE0089, Bio X Cell) or Armenian hamster polyclonal IgG (BE0091, Bio X Cell) isotype controls or anti-CSF1R (BE0213, Bio X Cell) or anti-CCL2 (BE0185, Bio X Cell) blocking antibody, twice, one week apart. Mice received 35 µg (α-CSF1R) or 5 µg (α-CCL2) antibodies per gram of body weight. In total, mice were fed HFD for 12 weeks.

2.5 Human samples

Human omental white adipose tissue (oWAT) samples were obtained from Associate Professor Emma Börgeson at the University of Aarhus, Denmark. The samples were collected from lean participants (BMI 18.5-25 kg/m^2) undergoing cholecystectomy (gallbladder removal) or obese patients (BMI 35-55 kg/m^2) undergoing gastric bypass surgery, as part of the Adipos2 Cohort

clinical study. Key exclusion criteria included gastrointestinal or inflammatory diseases, recent use of anti-inflammatory or immunosuppressive drugs, alcohol and tobacco intake. Tissue collection and ethics were approved and registered as Ethical Approval ID: Dnr 682-14 and Clinical Trials ID: NCT02322073. We obtained access to 14 patients, 11 females and 3 males, aged between 22-60 years. Autophagy and histology assays were performed as described in the sections below.

2.6 Genotyping

Clips were collected from the ears and lysed in 100 µl 50 mM NaOH for 1 hour at 100°C. To quench the lysis, 13 µL of 1M Tris-HCl solution at pH~8 was added. Tubes were shortly centrifuged to pellet the undigested tissue. Polymerase chain reaction (PCR) was performed for individual transgenes using My-Taq™ Red Mix (BIO-25044, Bioline) in 20 µL reaction volume. All primers were used at a concentration of 100 µM. To visualise the genotypes, agarose was mixed with TAE buffer (40 mM Tris-Acetate, 1 mM EDTA) and SYBR® Safe DNA Stain (Invitrogen, S33102, dilution 1:10000). PCR products were separated on a 2% agarose gel at 120V for 25 min. Bands were visualized using G-Box (Syngene).

Table 3: Primer sequences for *Atg7^{Ad}* genotyping.

Adipoq-Cre PCR	Adipoq-21173	5'- CCG CAT CTT CTT GTG CAG T -3'
	Adipoq-21175	5'- ATC ACG TCC TCC ATC ATC C -3'
	Adipoq-22925	5'- GAG TCT GCC TTT CCC ATG AC -3'
	Adipoq-22926	5'- TCC CTC ACA TCC TCA GGT TC -3'
Atg7$^{fl/fl}$ PCR	Atg7-14R	5'- GTC CAG AGT CCG GTC TCT GGT TG -3'
	Atg7-752	5'- CCA TGC TGA TGG CTA ATG TCT C -3'
	Atg7-753	5'- CTG CAG GAA TTC GAT ATC ATA ACT TCG -3'

Reaction:

10 µl 2x MyTaq RedMix
0.25 µl of each primer (at 100 µM)
2 µl DNA sample
up to 20 µl RNase/DNase-free water

PCR settings:

Step	*Adipoq-Cre*	*Atg7$^{fl/fl}$*
1	94°C, 2 min	95°C, 1 min
2	94°C, 20 sec	95°C, 15 sec
3	65°C, 15 sec	64°C, 30 sec
4	68°C, 10 sec (to step 2, 10 cycles)	70°C, 10 sec (to step 2, 32 cycles)
5	94°C, 15 sec	70°C, 2 min
6	60°C, 15 sec	4°C, hold
7	72°C, 10 sec (to step 5, 28 cycles)	
8	72°C, 2 min	
9	4°C, hold	

2.7 Blood glucose monitoring and serum chemistry

Mice were subjected to 6-12 hours fast before measuring fasted glucose levels in blood collected from the tail vein. A glucose tolerance test (GTT) was performed by injecting 1.5 g bolus glucose per kg of body mass intraperitoneally. An insulin tolerance test (ITT) was performed by injecting 1 U/kg body weight of insulin for lean mice and 2 U/kg body weight of insulin for obese mice. For both tests, blood glucose levels were measured at 15, 30, 60, 90, 120, and 180 min after injection with a glucose meter (Freestyle Lite, Abbott). For serum chemistry, serum from overnight fasted mice was collected by a cardiac puncture in Microtainer tubes. These were centrifuged for 90 s at 15,000 g and serum was sent for analysis. Triglycerides, FFAs and cholesterols were measured using a Beckman Coulter AU680 clinical chemistry analyser at Mary Lyon Centre at MRC Harwell, UK.

2.8 Adipose tissue *ex vivo* explant culture

White adipose tissues were collected from mice in a fat medium (DMEM high glucose (D5796, Sigma) supplemented with 1% fatty acid-free BSA (126609, Sigma) and 5% HEPES (15630-056, Gibco)). Tissues were washed in PBS and cut finely into approximately 10 mg pieces for explant culturing. Autophagy flux was assessed by incubating 100 mg of adipose tissue explants in 500 µl full DMEM supplemented with 100 nM Bafilomycin A1 (B1793, Sigma) and 20 mM NH_4Cl (213330, Sigma) for 4 hours at 37°C. DMSO (D8418, Sigma) was used as a

'vehicle' control. To measure cytokine secretion, 200 mg adipose tissue explants were cultured for 6 hours in 1 ml full RPMI-1640 ((R8758, Sigma), supplemented with 100U/ml Pen-Strep (P/S) and 10 % fetal bovine serum (FBS)). After incubation, the supernatant was collected, centrifuged at 400 g for 5 min to remove cell debris and snap-frozen until further analysis.

2.9 Adipose tissue processing

Adipose tissue digestion was performed as previously described (Richter et al., 2023). Adipose tissues were weighed upon collection and placed in the fat medium. They were digested in 2 ml of a digestion medium, i.e., high glucose DMEM supplemented with 1 % fatty acid-free BSA, 5 % HEPES, 0.2 mg/ml Liberase TL (5401020001, Roche), and 20 µg/mL DNaseI (11284932001, Roche). Tissues were minced in a digestion medium and incubated for 25-30 min at 37°C under agitation (180 rpm). Digested tissue was broken up using wide bore and standard-size pipette tips and strained through a 300 µm mesh (43-50300-01, pluriSelect). The digestion was quenched by adding PBS supplemented with 0.5 % BSA (A7030, Sigma) and 2 mM EDTA (15575-020, Invitrogen). Floating adipocyte and pelleted stromal vascular fraction were separated by 7 min centrifugation at 500 g and collected for further analysis.

2.10 Primary cell culture

For primary macrophage cell culture, visWAT was collected from lean or obese mice and digested as described above. The pelleted SVF was depleted of red blood cells with RBC lysis buffer (00-4333-57, Invitrogen) and enriched for $CD11b^+$ cells using CD11b MicroBeads (130-049-601, Miltenyi Biotec) according to manufacturers' instructions. Isolated $CD11b^+$ cells were counted using a haemocytometer and 400,000 cells were seeded in 24-well tissue-culture-treated plates in full RPMI-1640 containing 10 % FBS and 1 % P/S. Isolated cells were incubated overnight to allow macrophages to attach. The next day, macrophages were further enriched by washing the wells with warm PBS before proceeding with the experiment. For

conditioned medium treatment, RPMI containing 10 % FBS and 1 % P/S was supplemented with the conditioned medium in a 2:1 ratio and applied to the cells for 72 hours. For nucleoside treatment, macrophages were cultured for 72 hours in RPMI containing 10 % FBS and 1 % P/S and 50 ng/ml M-CSF and treated with 10/100 µM of either adenosine, guanosine, hypoxanthine or xanthine.

The conditioned medium was generated by collecting adipocytes after the digestion process using wide-bore tips. Adipocytes were centrifuged for 5 min at 300 g and washed three times with PBS. 250 µl of the packed adipocytes were collected and seeded in 500 µl of RPMI containing 10 % FBS and 1 % P/S and incubated for 24 hours at 37°C. Following the incubation, the medium and cells were harvested, centrifuged at 300 g for 5 min and purified medium was collected and snap-frozen for *in vitro* experiments.

2.11 Flow cytometry

Cells analysed by flow cytometry staining were isolated as described above. Single-cell suspensions were first stained in PBS for live dead and surface staining with LIVE/DEAD fixable near-IR, aqua, or blue dead cell stains (Invitrogen) and fluorochrome-conjugated primary antibodies (see below) for 25 min on ice. Fc receptor block antibody was added to the mix to prevent nonspecific binding of immune cell Fc receptors to antibodies. Following the initial staining, cells were washed and fixed with 4 % paraformaldehyde for 10 min at room temperature or eBioscience™ Foxp3/Transcription Factor Staining Set (00-5523-00, Invitrogen) for 30 min at 4°C if performing intracellular staining. Intracellular transcription factor staining was performed after fixation and permeabilization with fluorescently labelled primary antibodies. Unstained cells and bead compensation controls were prepared for individual fluorophores for compensation and spectral unmixing. For counting the cells, 20,000 PE/FITC-fluorescent BD Calibrite™ Beads (349502, BD Bioscience) were added per sample before sample acquisition. Samples were acquired on the Fortessa X-20 flow cytometer (BD

Biosciences) or the Aurora spectral flow cytometer (Cytek). Data were analysed with FlowJo v10.8.0 or OMIQ (for spectral flow data).

Flow cytometry antibodies	Clone	Dil.	Ref.	Supplier
BV510 anti-mouse CD45	30-F11	1:200	563891	BD Biosciences
PE-Cyanine7 anti-mouse CD31	390	1:200	25-0311-81	Invitrogen
PE anti-mouse CD140a (PDGFRa)	APA5	1:200	135905	Biolegend
PerCP anti-mouse CD45	30-F11	1:200	103130	Biolegend
BV785 anti-mouse/human CD11b	M1/70	1:200	101243	Biolegend
BV605 anti-mouse F4/80	BM8	1:200	123133	Biolegend
BV711 anti-mouse CD64	X54-5/7.1	1:200	139311	Biolegend
PE anti-mouse CD170 (Siglec-F)	S17007L	1:200	155505	Biolegend
APC anti-mouse NK-1.1	PK136	1:200	108709	Biolegend
PE-Cyanine7 anti-mouse Ly6G	1A8	1:200	127618	Biolegend
PE-Cyanine7 anti-mouse TCR b chain	H57-597	1:200	109221	Biolegend
BV785 anti-mouse CD19	6D5	1:200	115543	Biolegend
BV421 anti-mouse CD3ε	145-2C11	1:200	100335	Biolegend
Pacific Blue anti-mouse CD8a	53.6.-7	1:400	100725	Biolegend
BV605 anti-mouse CD4	GK1.5, RM4-5	1:400	100451	Biolegend
PE anti-mouse CD45.1	A20	1:200	110707	Biolegend
BV711 anti-mouse CD45.2	104	1:200	109847	Biolegend
APC anti-mouse CD9	MZ3	1:200	124811	Biolegend
PerCP/Cyanine5.5 anti-mouse CD63	NVG-2	1:200	143911	Biolegend
eFluor450 anti-mouse Lyve1	ALY7	1:200	48-0443-82	Invitrogen
PerCP/Cyanine5.5 anti-mouse I-A/I-E (MHCII)	M5/114.15.2	1:200	107626	Biolegend
Mouse CD16/32	/	1:200	101302	Biolegend
BUV496 anti-mouse CD11b	M1/70	1:200	749864	BD Biosciences
BUV737 anti-mouse F4/80	T45-2342	1:200	749283	BD Biosciences
FITC anti-mouse CD163	TNKUPJ	1:200	11-1631-82	Thermo Fisher
Spark NIR 685 anti-mouse Ly6G	1A8	1:200	127665	BioLegend
Bv785 anti-mouse Ly6C	HK1.4	1:200	128041	BioLegend
Spark Blue 550 anti-mouse I-A/I-E (MHCII)	M5/114.15.2	1:200	107661	BioLegend
Spark YG 570 anti-mouse CD206	C068C2	1:200	141737	BioLegend
Bv711 anti-mouse CD64	X54-5/7.1	1:200	139311	BioLegend
BUV661 anti-mouse CCR2/CD192	475301	1:200	750042	BD Biosciences

Bv480 anti-mouse CD9	KMC8	1:200	746438	BD Biosciences
PE Fire 810 anti-mouse CD11c	QA18A72	1:200	161105	BioLegend
Super Bright 436 anti-mouse Siglec F	1RNM44N	1:200	62-1702-82	Thermo Fisher
BUV395 anti-mouse CD45	30-F11	1:200	565967	BD Biosciences
BUV615 anti-mouse CD69	H1.2F3	1:200	751593	BD Biosciences
PE Cy5 anti-mouse EOMES	Dan11ma	1:100	15-4875-80	Thermo Fisher
eFluor 450 anti-mouse CD8a	53-6.7	1:200	48-0081-80	Thermo Fisher
Alexa Fluor 647 anti-mouse CD39	Duha59	1:200	143807	BioLegend
Bv570 anti-mouse CD62L	MEL-14	1:200	104433	BioLegend
Bv650 anti-mouse Ly108	13G3	1:200	740628	BD Biosciences
PE Cy7 anti-mouse PD-1	J43	1:200	25-9985-80	Thermo Fisher
PE Dazzle 594 anti-mouse CD44	IM7	1:200	103055	BioLegend
PE anti-mouse TCF1	S33-966	1:100	564217	BD Biosciences
APC Fire 810 anti-mouse CD4	GK1.5	1:400	100479	BioLegend

2.12 Enzyme-linked immunosorbent assay (ELISA)

Cytokine levels in serum, adipose tissue or cellular secretome were measured by commercially available ELISA kits following the manufacturer's protocols. The following ELISA kits were used: IL1 beta (88-7013A-88, Invitrogen), IL-10 (88-7105-86, Invitrogen), IL-6 (88-7064-88, Invitrogen), TGF beta-1 (88-8350-88, Invitrogen), TNF alpha (88-7324-88, Invitrogen), Adiponectin (KMP0041, Invitrogen), Mouse Magnetic Luminex Assay (OPN) (LXSAMSM, Luminex), and Leptin (KMC2281, Invitrogen). All cytokine levels were normalized to input tissue weight or cell number.

2.13 Western blot

Protein extraction was performed as previously published (An and Scherer, 2020). Per 100 mg of WAT, 500 µL of RIPA lysis buffer containing protease inhibitors (04693159001, Roche) and PhosphoStop (04906837001, Roche) but without TritonX-100 was added. Tissues were homogenised using TissueLyser II (Qiagen) and homogenate was centrifuged at 6000 g for 15 min. The top lipid layer was removed and the tissues were lysed for one hour on ice by adding Triton X-100 (T9284, Sigma) at a 1 % final concentration. Lipid contamination was removed through serial centrifugation at 12000 g for 15 min. Protein content was measured with a BCA Protein Assay kit (23227, Thermo Fisher). 10-15 µg of protein samples and prestained protein ladder (ab116028, Abcam) were separated on a 4-12% Bis-Tris SDS PAGE gel (NP0336, Invitrogen) for 90 min at 130 V. Proteins were transferred onto a PVDF membrane using wet-transfer technique for 2 hours at 300 mA. Membranes were blocked in 5 % skimmed milk (70166, Sigma) in TBST for one hour at room temperature, and incubated with primary antibodies overnight. The following primary antibodies were used: rabbit anti-LC3 (L8918, Sigma) (1:1500), rabbit anti-ATG7 (ab133528, Abcam) (1:1500), rabbit anti-vinculin (13901, CST) (1:2000). Proteins were visualized on a membrane using IRDye 800 secondary antibodies (926-32211, LI-COR Biosciences) at the dilution 1:10,000. Quantification was performed with ImageStudio software (LI-COR). Autophagy flux was calculated as: (LC3-II (Inh) – LC3-II (Veh))/(LC3-II (Veh)), as previously described (Zhang et al., 2019).

2.14 Histology and immunohistochemistry

For histological analysis, adipose tissues and the liver were fixed in 10 % neutral buffered formalin (HT501128, Sigma) for 24 and 48 hours, respectively. Following the fixation, tissues were transferred to 70 % ethanol and submitted to the Kennedy Institute of Rheumatology Histology service for paraffin embedding, sectioning (section thickness 5 µm), and staining. Haematoxylin and eosin (H&E) (3801560E, Leica microsystems and RBC-0100-00A, Cell

Path, respectively) and picrosirius red staining (ab24683, Abcam) were performed according to the standard histology protocols. Slides were mounted with Di-n-butylphthalate (DPX) mounting media (06522, Sigma). Whole tissue scans were acquired using a Zeiss Axioscan 7 scanning microscope. Picrosirius red staining analysis and quantification were performed by Dr Jacky Ka Ko Long at the Oxford Zeiss Centre of Excellence using QuPath, Image J, and an in-house developed script (available at https://github.com/Oxford-Zeiss-Centre-of-Excellence/pyHisto). In summary, the blind colour deconvolution method was used based on a stain vector estimation (Ruifrok and Johnston, 2001), followed by Otsu thresholding and determination of collage-to-area ratio.

For immunohistochemistry analysis, adipose tissues were fixed in 4 % paraformaldehyde (043368.9M, Thermo Fisher) for 24 hours at 4°C, embedded and sectioned as described above. After sectioning, tissues were deparaffinized in a series of xylene, 100 %, 95 %, 70 % and 50 % ethanol, 0.3 % Triton-X in PBS and PBS. Antigens were heat-retrieved in a pressure cooker at 100°C for 20 min using citrate antigen retrieval solution (H-3300, Vector Laboratories, pH 6.0), and allowed to cool naturally in Tris antigen retrieval solution (10 mM, pH 8.8-9.0). Slides were washed twice in PBS and blocked overnight in 10 % donkey serum (D9663, Sigma) and 3 % BSA. The next day, slides were incubated with DAPI (D3571, Thermo Fisher) for 15 min and mounted with glycerol. A background scan was recorded and coverslips were removed. Slides were incubated for 20 min with Fc block reagent (1:200 in 3 % BSA, 130-092-575, Miltenyi Biotec), followed by primary antibody incubation overnight at 4°C. The following primary antibodies were used: mouse anti-CD45 (1:500) (AF114, R&D Systems), rabbit anti-CD68 (1:100) (ab125212, Abcam), rat anti-F4/80 (1:100) (MCA497A488T, BioRad), rabbit anti-Perilipin 1 (D1D8) (1:100) (9349, CST), mouse anti-caveolin (1:500) (610406, BD Bioscience), and rabbit anti-p62 (1:250) (BML-PW9860, Enzo Life Sciences). The next day, slides were washed twice for 5 min PBS-T and once in PBS, and incubated with secondary antibodies diluted in 3 % BSA for one hour at room temperature. Secondary antibodies used

were donkey anti-rat IgG H&L (Alexa Fluor 647) (1:500) (ab150155, Abcam), donkey anti-rabbit IgG H&L (Alexa Fluor 555) (1:500) (ab150074, Abcam), donkey anti-rabbit IgG (Alexa Fluor 647) (1:350) (A31573, Life Technologies), and goat anti-mouse IgG (Alexa Fluor 488) (1:250) (A11029, Life Technologies). After repeating the washes, slides were mounted with glycerol, and images were acquired with a GE Cell DIVE multiplex imager.

2.15 Gene expression analysis (qRT-PCR)

To isolate RNA, adipose tissues were homogenized in TRI reagent (T9424, Sigma) using 2 ml tubes containing ceramic beads (KT03961-1-003.2, Bertin Instruments) on a Precellys 24 homogenizer (Bertin Instruments). RNA was isolated from enriched adipocyte fractions by following the TRI reagent extraction method. RNA was extracted using RNeasy Mini or Micro Kit (74104, Qiagen) following the manufacturer's protocol. RNA yield and quality were quantified using a NanoDrop and cDNA was synthesized using a High-Capacity RNA-to-cDNA™ kit (4387406, Applied Biosystems). Gene expression analysis was performed using validated TagMan™ probes and TaqMan™ Fast Advanced Master Mix (4444557, Applied Biosystems) on a ViiA7 real-time PCR system (Thermo Fisher). Values were normalized to *Ppia* reference gene using the comparative Ct method to calculate fold change ($2^{-\Delta\Delta Ct}$). Settings: 95°C 20 sec, (95°C 1 sec, 60°C 20 sec) x 40 cycles.

TaqMan™ probes: *Atg7 (Mm00512209 m1), Col1a1 (Mm00801666_g1), Col3a1 (Mm01254476_m1), Col6a3 (Mm00711678_m1), Fn1 (Mm01256744_m1), Mmp14 (Mm00485054_m1), Timp1 (Mm01341361_m1), Acta2 (Mm00725412_s1), Il1b (Mm00434228_m1), Ppia (Mm02342430_g1)*.

2.16 Transcriptomics (bulk RNA sequencing)

Macrophages and T cells were isolated by FACS and adipocytes were isolated as enriched adipocyte fraction by floating method. RNA was extracted as described above and further processed by the Oxford Genomics Centre (University of Oxford) or Novogene Sequencing Company. To generate PolyA libraries, cDNA was end-repaired, A-tailed and adapter-ligated. Libraries were size-selected, multiplexed, quality-controlled, and sequenced using a NovaSeq6000. Quality control of raw reads was performed with a pipeline readqc.py (https://github.com/cgat-developers/cgat-flow). The pseudoalignment method Salmon (Patro et al., 2017) was used to align the resulting reads to the GRCm38/Mm10 reference genome. Batch effects attributed to sex were corrected using the limma package (v3.54.1) (Ritchie et al., 2015). Differential gene expression analysis was performed with DEseq2 (v1.38.3) (Love et al., 2014). The workflow included the estimation of size factors, dispersion estimation, and fitting of a negative binomial generalized linear model. Genes were considered significantly differentially expressed based on an adjusted p-value threshold of <0.05, after correcting for multiple testing using the Benjamini-Hochberg procedure. Finally, gene set enrichment analysis was performed to explore the biological implications of the differentially expressed genes using the clusterProfiler package (v4.6.0).

2.17 Proteomics

Adipocytes were isolated as a floating fraction upon digestion of adipose tissue and a conditioned medium was generated after 24-hour incubation in serum-free medium as described above. Samples were snap frozen and sent to Dr Oliver Popp at the Max-Delbrück Center for Molecular Medicine in the Helmholtz Association, Germany, for further processing. Equal volumes of conditioned medium or a pellet of 100 µl packed adipocytes were lysed in SDC buffer containing 2% (w/v) sodium deoxycholate (SDC; Sigma), 20 mM dithiothreitol (Sigma), 80 mM chloroacetamide (Sigma), and 200 mM Tris-HCl (pH 8). After heating at 95°C

for 10 minutes, the lysates were enzymatically digested using endopeptidase LysC (Wako) and sequence grade trypsin (Promega) at a protein:enzyme ratio of 50:1. The digestion process occurred overnight at 37°C. For reversed-phase liquid chromatography coupled to mass spectrometry (LC-MS) analysis, each sample replicate was injected with 1 µg of peptide amount into an EASY-nLC 1200 system (Thermo Fisher) for separation, using a 110-minute gradient. Mass spectrometric measurements were made with the Exploris 480 (Thermo Fisher) instrument in data-independent acquisition (DIA) mode, utilising an isolation scheme with asymmetric isolation window sizes. The raw files were analysed using DIA-NN version 1.8.1 (Demichev et al., 2020) in library-free mode, with a false discovery rate (FDR) cutoff of 0.01 and relaxed protein inference criteria, while employing the match-between runs option. The spectra were compared to a Uniprot mouse database (2022-03), including isoforms. The protein intensities were normalised using MaxLFQ and filtered to ensure that each protein had at least 50% valid values across all experiments, with an additional filter to retain at least 3 valid values in at least one experimental group. The limma package (Ritchie et al., 2015) was used to calculate two-sample moderated t-statistics for significance calling. The nominal P-values were adjusted using the Benjamini-Hochberg method.

2.18 Metabolomics

Adipocytes and conditioned medium were obtained as described above, snap frozen and submitted to Dr Johanna ten Hoeve-Scott based at the UCLA Metabolomics Center, USA. Metabolite extractions from frozen cell pellets were done through a two-phase extraction with 80 % MeOH and chloroform. When just thawed, cells were resuspended in 500 µl ice-cold 80 % MeOH, vortexed and sonicated in an ice bath for 6 min. Following one hour of incubation on dry ice, tubes were centrifuged at 16,000 g for 10 min at 4°C, and supernatants were mixed with water and chloroform in 1:1:1 ratio. Each sample was vortexed for 1 min and centrifuged at top speed for 15 min at 4°C. Finally, 600 µl of the top aqueous layer was transferred to a glass vial and evaporated using an EZ-2Elite evaporator (Genevac). Samples were stored at

−80 °C before analysis. The BCA assay was performed on the airdried pellets, resuspended in 200 µl of 0.2 M NaOH and heated at 95°C for 20 min. Metabolite extractions from frozen conditioned medium precleared from cells and cell debris were performed after removing cells and cell debris by mixing 20 µl of clarified medium with 500 µl ice-cold 80 % MeOH/20 % H_2O. After vortex and 30 min incubation at -80°C, samples were centrifuged at 16,000 g for 10 min at 4°C, transferred to a glass vial and evaporated using an EZ-2Elite evaporator (Genevac). Dried extracts were stored at −80 °C before analysis. Dried metabolites were resuspended in 100 ul 50% ACN:water and 5 ul was loaded onto a Luna NH_2 3um 100A (150 × 2.0 mm) column (Phenomenex) using a Vanquish Flex UPLC (Thermo Fisher). The chromatographic separation was performed with mobile phases A (5 mM NH_4AcO pH 9.9) and B (ACN) at a flow rate of 200 µl/min. A linear gradient from 15% A to 95% A over 18 min was followed by 7 min isocratic flow at 95% A and re-equilibration to 15% A. Metabolites were detected with a Thermo Fisher Q Exactive mass spectrometer run with polarity switching in full scan mode using a range of 70-975 m/z and 70.000 resolution. Maven (v 8.1.27.11) was used to quantify the targeted polar metabolites by AreaTop, using expected retention time and accurate mass measurements (< 5 ppm) for identification. Data analysis, including principal component analysis and heat map generation, was performed using in-house R scripts. In brief, metabolite intensities (area under the curve) were normalized to protein content and analysed with one-way ANOVA (ANOVA column). Metabolites with a p-value < 0.05 were termed as significant. Heatmaps are z-score normalized assuming a normal distribution. Bar plots display relative amounts for each metabolite, calculated by averaging amounts for each condition (a condition with the lowest average value set to 1).

2.19 Metabolic assays

Metabolite levels in live cells, cell homogenates and conditioned medium were measured using commercially available kits according to the manufacturer’s protocols. Intracellular ATP was measured in living cells using ATP bioluminescence assay kit CLS II (11699695001, Roche).

The concentration of xanthine and hypoxanthine (ab155900, Abcam), adenosine (ab211094, Abcam), L-lactate (ab65331, Abcam), and H_2O_2 (A22188, Invitrogen), GSH/GSSG ratio (V6611, Promega) and the activity of xanthine oxidase (A22182, Invitrogen) were measured in cell homogenates and conditioned medium. To homogenise cells, these were resuspended in an ice-cold homogenisation medium (0.32 M sucrose, 1 mM EDTA, and 10 mM Tris–HCl, pH 7.4) and processed with 72 strokes using a tight pestle. After brief sonication at 40 % Amp, homogenates were centrifuged at 2000 g for 5 min at 4°C to remove the lipid layer. Protein concentration in homogenates was determined using a BCA assay to normalize between conditions. 24 µg of protein was used per assay condition.

2.20 Quantification and statistical analysis

Experiments were conducted as 3 independent repeats unless otherwise indicated. Mice were randomly grouped in experimental groups and all data shown except proteomics and metabolomics are pooled from both sexes. Data were analysed and visualized using GraphPad Prism 9, except for omics data where R software was used for visualisation and statistics calculation. The normal distribution of data was tested before applying parametric or nonparametric testing. For comparison between two independent groups, unpaired Student's t-tests or non-parametric Mann-Whitney tests were applied. Comparisons across more than two groups were performed using one-way or two-way ANOVA with Šídák, Tukey or Dunnett multiple testing correction. Data were considered statistically significant when p value < 0.05. For transcriptomics and proteomics analyses, hits were considered differentially expressed if a multiple testing with limma package (Ritchie et al., 2015) and adjusted with Benjamini-Hochberg method returned a p-value <0.05. For metabolomics, metabolite intensities (area under the curve) were analysed with one-way ANOVA and hits with a p-value < 0.05 were considered significant.

3 Adipocyte autophagy controls fat tissue distribution and metabolic syndrome in obesity by limiting fibrosis

3.1 Introduction

3.1.1 Murine models of obesity

Animal models have been extensively utilized in obesity research. Murine models of obesity are broadly divided into monogenic, polygenic, and dietary models. The most common monogenic models that spontaneously develop morbidly obese phenotypes are mice with a defect in the leptin signalling pathway. These include the leptin-deficient *ob/ob* mouse and the leptin receptor-deficient *db/db* mouse. As monogenic obesity is rare in humans, polygenic mouse obesity models are more relevant when studying genetic predisposition to obesity, including New Zealand Obese and Tsumura Suzuki Obese Diabetes mouse models (Kanasaki and Koya, 2011).

In contrast to genetically modified models, DIO models most closely mimic human obesity, especially considering that current obesity prevalence is in large part due to unhealthy lifestyle, i.e. poor diet and lack of exercise. DIO models are fed high-fat diets (HFD), where more than 30% of energy comes from fat, fat- and sugar-rich diets (e.g. cafeteria diet) or saturated fatty acids- and simple sugars-rich diets (e.g. western diet) (Lutz and Woods, 2012). An increase in adiposity due to dietary fat intake is strain-specific, with the C57BL/6J strain commonly used as it develops similar abnormalities to humans, including severe obesity, glucose tolerance, and moderate insulin resistance. While fat mass gain is generally rapid and massive in experimental mouse models compared to a gradual increase in humans, the secondary development of insulin resistance is very similar between the species (Kleinert et al., 2018). Besides strain-specific effects, sex is another susceptibility factor for DIO, with male mice prone to develop obesity sooner and to a greater extent than female mice. This is in contrast

with humans, where females are more prone to develop obesity. In addition, their WAT is highly responsive to reproductive hormones, which is less pronounced in female rodents (Lutz and Woods, 2012).

In addition to obesity induction differences in humans versus mouse models, there are significant differences in the location and function of adipose tissue depots. Humans don't possess analogues of gonadal WAT, which is the most widely studies WAT depot in mice. Omental WAT (oWAT) expands the most in human obesity but is relatively small in mice (Lempesis et al., 2022). Despite different challenges of dietary and genetic modifications that limit translation to human obesity, DIO models are nevertheless commonly used in obesity research showing good validity with human obesity (Kleinert et al., 2018).

3.1.2 Metabolic syndrome

Obesity is broadly stratified into metabolically healthy (MHO) versus unhealthy (MUO) obesity. The predominant type, MUO is characterized by a development of metabolic syndrome, which is defined by a combination of pathophysiological factors. Individuals with metabolic syndrome and MUO have an increased risk of developing endocrine disorders such as type 2 diabetes mellitus, fatty liver disease and cardiovascular diseases (Bluher, 2020). Therefore, understanding the molecular mechanisms behind the development of metabolic syndrome and MUO is critical to developing obesity management therapies aimed at alleviating the risk of obesity-associated comorbidities.

The core pathophysiological factors underlying metabolic syndrome are abdominal adiposity and insulin resistance, which are tightly correlated. Insulin resistance versus sensitivity are defined as a response to a glucose or insulin stimulus. Obese insulin-resistant individuals display impaired glucose metabolism or tolerance upon glucose challenge and elevated fasting glucose levels. A critical contributor to insulin resistance is expanded adipose tissue, which

drives metabolic syndrome pathophysiology through elevated FFA release. This leads to an increase in inflammation and pancreatic insulin secretion, resulting in hyperinsulinemia and a further increase in FFA secretion. Ultimately, excess FFAs are redirected to other organs, such as the liver, where their deposition leads to inflammatory lesions and the development of MASH (Cornier et al., 2008). This notion is further supported by the adipose tissue expendability theory proposed by Vidal-Puig and Virtue, who claim that the capacity for WAT expansion is limited, and once reached, leads to ectopic deposition of lipids in non-adipocyte cells. This leads to lipotoxicity and ultimately insulin resistance and type 2 diabetes mellitus (Virtue and Vidal-Puig, 2010).

3.1.3 Adipose tissue fibrosis

Obesity contributes to the development of adipose tissue fibrosis (Sakers et al., 2022). This process is characterized by excessive production and reduced degradation of ECM components. These include collagens (Col I-VI), fibronectin, thrombospondin, hyaluronic acid, and elastin, as well as enzymes that dynamically remodel ECM components, such as collagenases and matrix metalloproteinases (MMPs). Tissue inhibitors of MMPs (TIMPs) also critically regulate ECM dynamics (Sun et al., 2023). Pericellular accumulation of collagen, the degree of collagen covalent cross-linking with other ECM components, and dysregulation of remodelling enzymes negatively impact ECM turnover, limiting WAT expandability and plasticity. Deposition of fibrosis physically constrains the dynamic adipose tissue remodelling (Marcelin et al., 2022). The enhanced stiffness of adipose tissue leads to mechanical stress, which triggers cell necrosis and the release of FFAs and pro-inflammatory factors, leading to systemic lipotoxicity. This positions fibrosis as a key modulator of local and systemic metabolic outcomes (Gliniak et al., 2023). Fibrosis is fine-tuned by multiple cell types in obese adipose tissue, including adipocytes, immune cells, pre-adipocytes, (myo)fibroblasts, and endothelial cells (DeBari and Abbott, 2020).

While the molecular mechanisms of adipose tissue fibrosis are becoming better understood, no targeted therapy exists to slow or reverse its progression. This is mostly due to a complex interplay of fibrosis with other processes that result from unhealthy expansion of WAT, including hypoxia and inflammation. While it is well-accepted that these three processes are intimately linked and reinforce each other, the exact sequence and kinetics remain unclear (Reggio et al., 2013). The first hypothesis suggests that hypoxia stimulates pro-fibrotic signalling pathways, initiating fibrosis early during obesity onset. This results in adipocyte necrosis and recruitment of immune cells in WAT, ultimately inducing chronic low-grade inflammation (Halberg et al., 2009). Another model proposes that hypertrophic expansion of WAT triggers local inflammation that precedes the development of fibrosis. The pro-fibrotic program is then initiated through pro-inflammatory cytokine stimulation to resolve chronic inflammation (Wynn, 2007).

What also remains debatable are the beneficial versus deleterious effects of adipose tissue fibrosis concerning metabolic homeostasis. On one hand, maladaptive fibrosis has been described to reversely correlate with body-weight loss following bariatric surgery (Abdennour et al., 2014). On the other hand, adaptive fibrosis has been reported to limit the excessive growth of adipocytes, thereby improving metabolic outcomes (Datta et al., 2018). Therefore, a better understanding of the cellular and molecular mechanism underlying adipose tissue fibrosis is necessary and will ultimately lead to the development of targeted therapies.

3.1.4 Chapter aims

WAT autophagy increase during obesity is broadly reported (Zhang et al., 2018b), however, understanding its functional consequence remains largely elusive. We set out to investigate whether loss of autophagy in mature adipocytes impacts obesity development and progression. We hypothesised that an increase in autophagy observed in obese subjects impacts their adiposity, metabolic outcomes, and adipose tissue biology. The aim of this

chapter is (1) to validate the increase in autophagic flux during obesity, (2) to investigate the impact of adipocyte autophagy loss on obesity phenotype, (3) to examine whether fibrotic WAT is an adaptive or maladaptive response, and (4) understand whether some of our findings can translate to humans.

3.2 Results

3.2.1 Obesity induces adipocyte autophagy which impacts fat distribution and ameliorates metabolic syndrome

Autophagy in adipose tissue increases during obesity both in humans and mice (Jansen et al., 2012, Kosacka et al., 2015, Kovsan et al., 2011, Mizunoe et al., 2017, Nuñez et al., 2013, Öst et al., 2010, Soussi et al., 2016). To confirm previous observations are true in our DIO mouse model, we fed C57BL/6J wild-type (WT) mice HFD with 60% of calories coming from fat for 16 weeks. Assessment of autophagic flux by accumulation of mature autophagosome marker LC3-II upon inhibition confirmed that autophagy in both main mouse WAT depots, i.e., inguinal and gonadal WAT (iWAT and gWAT, respectively) positively correlated with increased adiposity (Fig 6A-B).

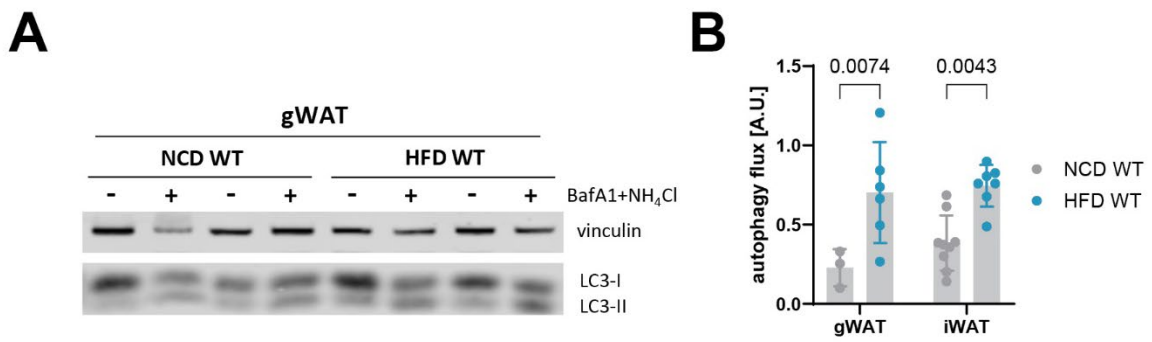

Figure 6: Adipocyte autophagy is increased in obese WAT. WT and *Atg7*^{Ad} mice were fed a normal chow diet (NCD) or high-fat diet (HFD) for 16 weeks before isolation of gonadal and inguinal white adipose tissues (gWAT and iWAT, respectively). (A) Representative western blot analysis of LC3-II accumulation to measure autophagy flux in gWAT, in the presence of 100 nM BafA1 and 20 mM NH_4Cl. (B) Quantification of autophagy flux in gWAT and iWAT.

Autophagy flux was calculated as: (LC3-II (Inh) – LC3-II (Veh))/(LC3-II (Veh)). Data are presented as mean ± SD. Each data point represents one biological replicate. Statistical analysis by two-way ANOVA with Šídák multi comparisons test. Representative of 3 independent experiments.

To understand the pathophysiological function of induced WAT autophagy during DIO, we took advantage of a previously validated *Atg7*^{Ad} mouse model with an adipocyte-specific deletion of autophagy developed in our group (Richter et al., 2023). In contrast to constitutive depletion of adipocyte autophagy (Zhang et al., 2009, Singh et al., 2009b, Baerga et al., 2009), this experimental model enables inducible depletion after adipose tissue has fully developed (between 6 and 8 weeks of age), circumventing defects in adipogenesis and consequences thereof. *Adipoq*-driven Cre ERT2 recombinase system specifically targets mature adipocytes within adipose tissues upon tamoxifen administration, allowing for spatial-temporal control of gene depletion (Sassmann et al., 2010) (Fig 7A). Autophagy is blocked through a loss of ATG7 protein expression, a critical catalyst of autophagosome formation through the mediation of LC3 lipidation (Feng et al., 2014). *Atg7*^{Ad} mice fed standard chow diet show no phenotype (data not shown).

Inducing *Atg7* deletion and feeding mice HFD for 16 weeks to develop DIO (Fig 7B-C) resulted in a block of autophagy flux in both iWAT and gWAT (Fig 7D-E). Mice displayed a comparable caloric intake between the two diets (Fig 7F). Body weight gain between WT and *Atg7*^{Ad} mice showed no difference either when mice were fed control (NCD) or HFD (Fig 7G). Following body weight gain, obese mice increased their serum leptin concentration (Fig 7H). Within the obese group, no significant difference in adiponectin/leptin ratio was observed between WT and *Atg7*^{Ad} mice, although there was a downward trend in *Atg7*^{Ad} mice (Fig 7I). The adiponectin/leptin ratio is a biomarker tightly correlating with increased body weight and comorbidity risk, whereby a lower ratio is associated with elevated WAT dysfunction (Fruhbeck et al., 2018). Despite no change to body adiposity, we observed a significant difference in fat distribution between WT and *Atg7*^{Ad} mice on HFD, with a reduced gWAT but elevated iWAT

expansion in obese *Atg7*^{Ad} mice (Fig 7J). This observation sparked our interest considering that gWAT, mimicking human visceral WAT, is the most pathophysiological WAT depot (Lutz and Woods, 2012). In addition, increased iWAT growth is believed to buffer the detrimental impact of visceral obesity (González-Muniesa et al., 2017), and people with MHO tend to have a higher ratio of gluteofemoral (analogous to iWAT) to visceral WAT (Bluher, 2020).

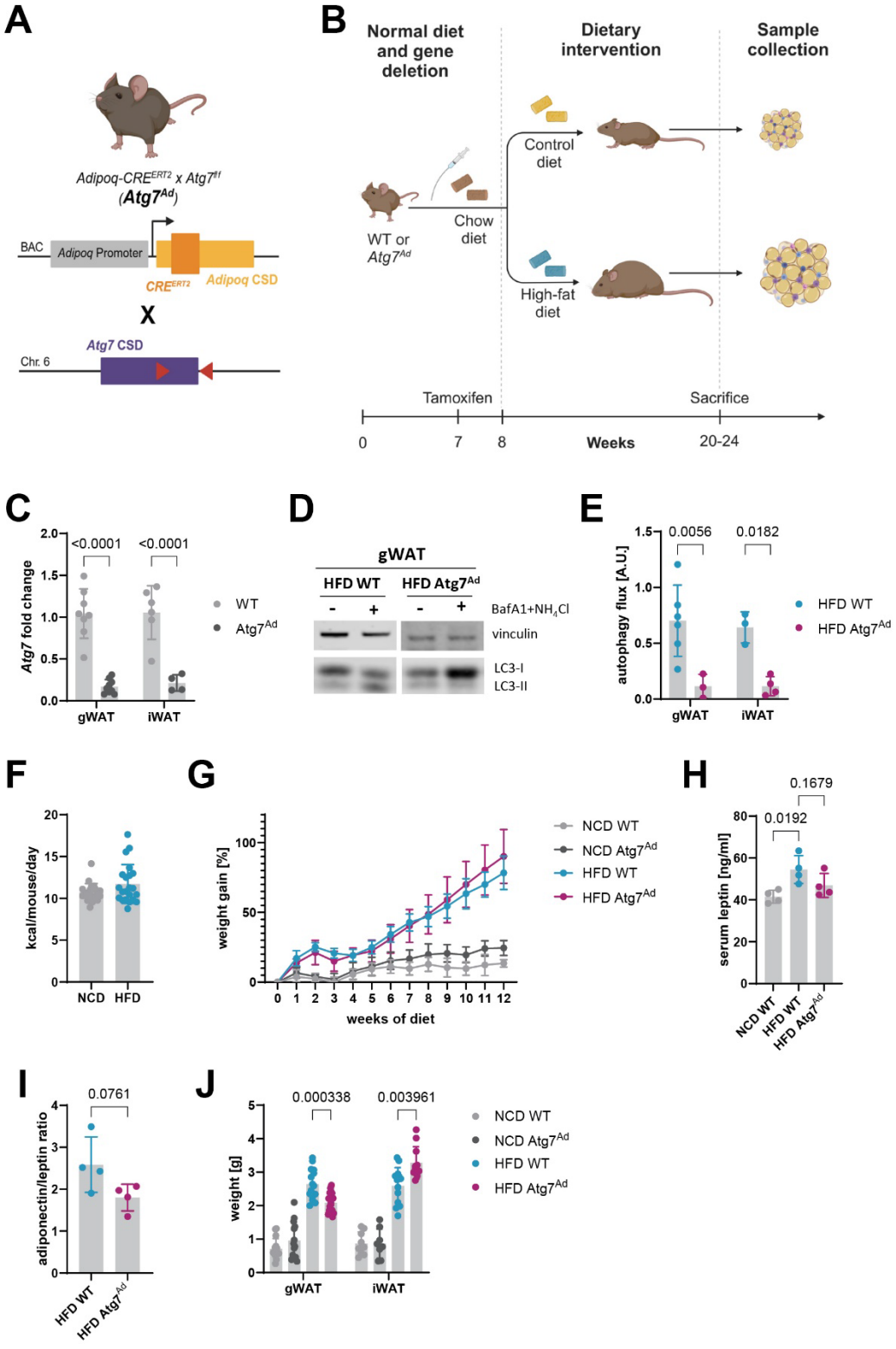

Figure 7: Adipocyte autophagy differentially regulates WAT expansion. (A) Schematic representation of *Atg7*^{Ad} genetic model. Red triangles denote flox sites. (B) Experimental set-up to study the role of adipocyte autophagy in DIO. (C) Relative mRNA expression of *Atg7* in gWAT and iWAT of WT and *Atg7*^{Ad} mice measured by qRT-PCR. n = 8-9 mice. (D) Representative western blot analysis of LC3-II accumulation to measure autophagy flux in gWAT upon treatment with 100 nM BafA1 and 20 mM NH_4Cl. (E) Quantification of autophagy

flux in obese gWAT and iWAT. Autophagy flux was calculated as: (LC3-II (Inh) – LC3-II (Veh))/(LC3-II (Veh)). (F) Daily intake of calories between NCD and HFD-fed mice. The caloric intake per mouse per day was calculated by weighing the administered food weekly, then dividing the total kcal consumed per week by the number of animals in the cage and the number of days in the week. (G) Relative weight gain over 12 weeks of alternative diet. n = 4 mice. (H) Serum concentration of leptin. (I) Adiponectin to leptin ratio measured in serum. (J) Fat pad weight after 16 weeks of NCD or HFD feeding. Data are merged from 3 independent experiments. Data are presented as mean ± SD. Each data point represents one biological replicate. Statistical analysis by two-way ANOVA with Šídák multi comparisons test (C, E), one-way ANOVA (H), unpaired t-test (I), or multiple unpaired t-test (J). Representative of 3 independent experiments unless otherwise indicated. Created with BioRender.com (A-B).

This prompted us to assess whether obese *Atg7*^{Ad} mice develop metabolic syndrome to the same extent as obese WT mice. To this end, we assessed the development of insulin resistance by performing a glucose tolerance test (GTT), where fasted mice were challenged with bolus glucose and monitored for their response (Bowe et al., 2014). We observed that obese *Atg7*^{Ad} mice showed a trend of improved glucose homeostasis compared to WT counterparts, as evidenced by a more efficient cellular uptake of blood glucose upon challenge (Fig 8A-B). This was also true for NCD-fed mice, suggesting that improved glucose tolerance in *Atg7*^{Ad} mice may not be associated with the development of obesity. Fasted glucose and insulin levels between WT and *Atg7*^{Ad} mice were comparable between the diets, with HFD-fed WT displaying a tendency for higher glucose and insulin levels compared to NCD-fed WT, as expected (Fig 8C-D). Surrogate assessment of insulin resistance can be performed by an insulin tolerance test (ITT), where blood glucose is monitored after insulin administration in contrast to glucose loading. While no difference in insulin resistance by ITT was observed, obese WT mice seemed to be more insulin resistant compared to lean counterparts, as expected (Fig 8E). Metabolic syndrome is also diagnosed by an increase in serum triglycerides and FFAs and dysregulated cholesterol levels (Després, 2021). We observed no differences in serum triglycerides or FFAs but a tendency for a general dysregulation of cholesterol metabolism, whereby total as well as both “good” (HDL) and “bad” (LDL) cholesterol were somewhat upregulated in obese mice (Fig 8F-J). No difference could be observed between obese WT and *Atg7*^{Ad} mice.

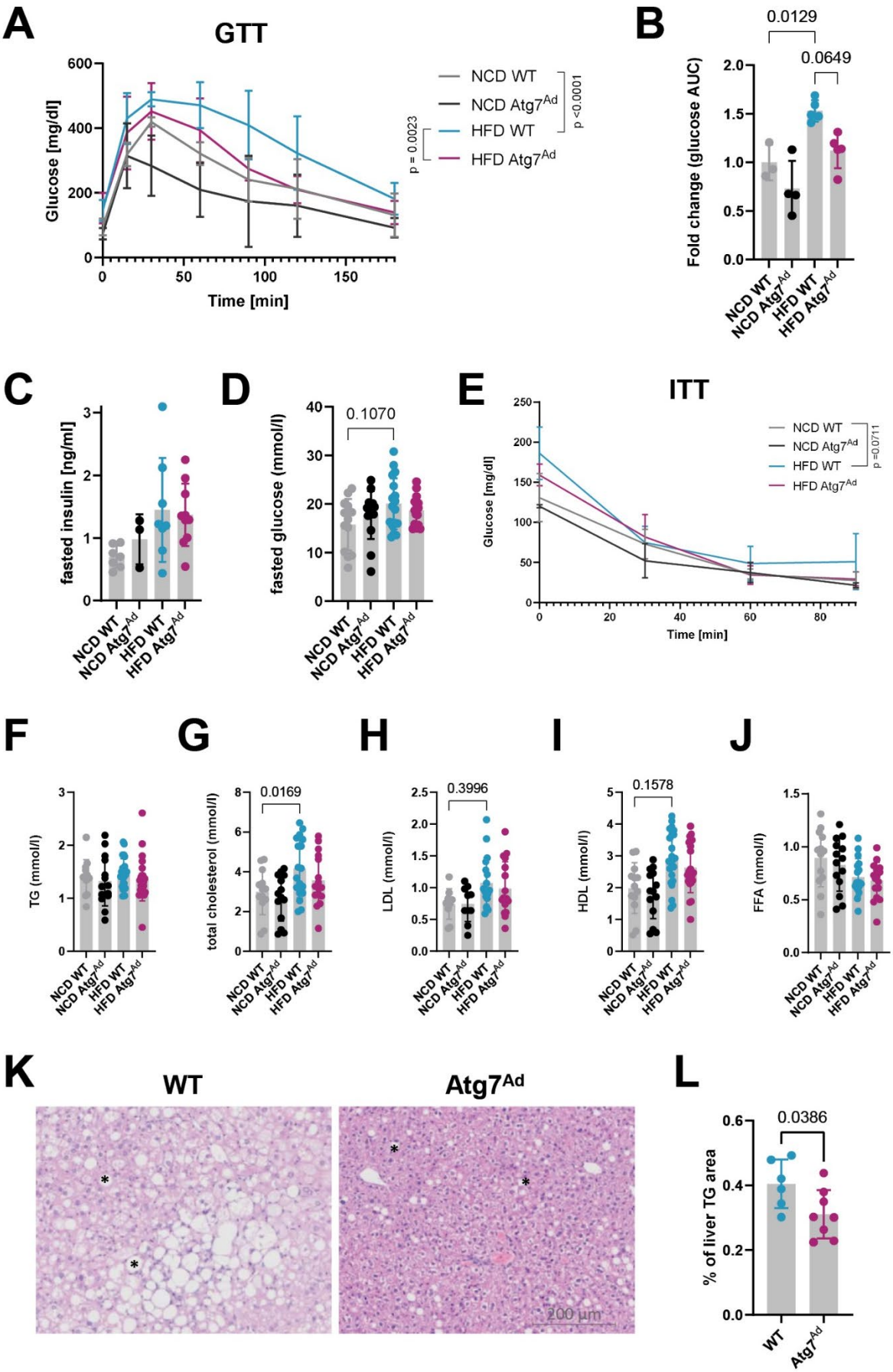
A
GTT
Glucose [mg/dl]
Time [min]
NCD WT
NCD Atg7Ad
HFD WT
HFD Atg7Ad
p = 0.0023
p <0.0001
B
0.0129
0.0649
Fold change (glucose AUC)
C
fasted insulin [ng/ml]
D
0.1070
fasted glucose (mmol/l)
E
ITT
Glucose [mg/dl]
Time [min]
p =0.0711
F
TG (mmol/l)
G
0.0169
total cholesterol (mmol/l)
H
0.3996
LDL (mmol/l)
I
0.1578
HDL (mmol/l)
J
FFA (mmol/l)
K
WT
Atg7Ad
200 µm
L
0.0386
% of liver TG area

Figure 8: Loss of adipocyte autophagy alleviates metabolic syndrome in DIO mice. WT and *Atg7*^{Ad} mice were kept on NCD or HFD for 12-16 weeks before the assessment of their metabolism. (A) Glucose tolerance test (GTT) was performed at 12 weeks of HFD feeding. n = 4 mice. (B) Quantification of GTT response by area under the curve (AUC). (C-D) Serum concentration of insulin (C) and glucose (D) following an overnight fast. Data are merged from 3 independent experiments. (E) Insulin tolerance test (ITT) performed at 12 weeks of HFD feeding. n = 3 mice. (F-J) Serum concentration of triglycerides (TG, F), total cholesterol (G), low-density lipoprotein (LDL, H), high-density lipoprotein (HDL, I), and free fatty acids (FFA, J). Data are merged from 3 independent experiments. (K) Representative haematoxylin and eosin (H&E) staining of liver from WT and *Atg7*^{Ad} mice after 16 weeks of DIO. Examples of fat deposition marked with asterisk, scale bar, 200 µm. (L) Quantification of white (lipid) area from (K). Data are presented as mean ± SD. Each data point represents one biological replicate. Statistical analysis by two-way ANOVA with Tukey multi comparisons test (A-I) or unpaired t-test (L). Representative of 3 independent experiments unless otherwise indicated.

Tightly linked to insulin sensitivity is ectopic fat deposition, primarily in the liver. Obese *Atg7*^{Ad} mice displayed a marked decrease in lipid accumulation in the liver compared to obese WT mice assessed by histological staining (Fig 8K-L). This suggests that loss of adipocyte autophagy improves WAT buffering of excess lipids, limiting FFA storage to non-adipocyte cells and organs.

Considering the subtle impact of autophagy loss on the metabolic health of obese mice, we asked whether these mice when exposed to a longer period of HFD feeding or aging develop different pathologies to WT mice. To this end, WT and Atg7^{Ad} mice were either fed HFD continuously for 26 weeks or fed HFD for 16 weeks followed by 75 weeks on a normal chow diet (reaching 100 weeks of age). In contrast to our expectations, no differences in obesity co-morbidities, including cardiovascular complications, steatosis, and tumours, could be observed between WT and Atg7^{Ad} mice when assessing serum markers of the heart (creatine kinase-MB) and liver function (alanine transaminase, aspartate transaminase, and alkaline phosphatase) as well as histological analysis of tissues (data not shown).

Taken together, our results demonstrate that obesity-induced adipocyte autophagy governs regional WAT distribution independent of body weight gain. By specifically limiting gWAT expansion, lack of adipocyte autophagy results in the improvement of metabolic syndrome,

including reduced visceral obesity and improved insulin sensitivity. The development of metabolically healthier obesity in the context of adipocyte autophagy loss is further evident by a reduction in ectopic fat deposition.

3.2.2 Visceral WAT expansion is specifically limited by pericellular fibrosis

Adipose tissue expansion is mediated by two complementary processes: hypertrophy and hyperplasia. Noticing that loss of adipocyte autophagy results in a limitation to gWAT but not iWAT expansion, we sought to investigate whether this could be due to defects in these growth processes. We assessed adipocyte number (hyperplasia) and size (hypertrophy) by quantifying the number and size of unilocular lipid droplets in both WATs, which occupy most of the adipocyte volume and thereby contribute the most to the cell size (Ghaben and Scherer, 2019). Analysis of histological images revealed that the difference in gWAT deposition between *Atg7*^{Ad} and WT could not be attributed to changes in cell number and/or size (Fig 9A-B). The same was true for iWAT (Fig 9C-D), suggesting that another process was contributing to significantly altered adipose tissue deposition.

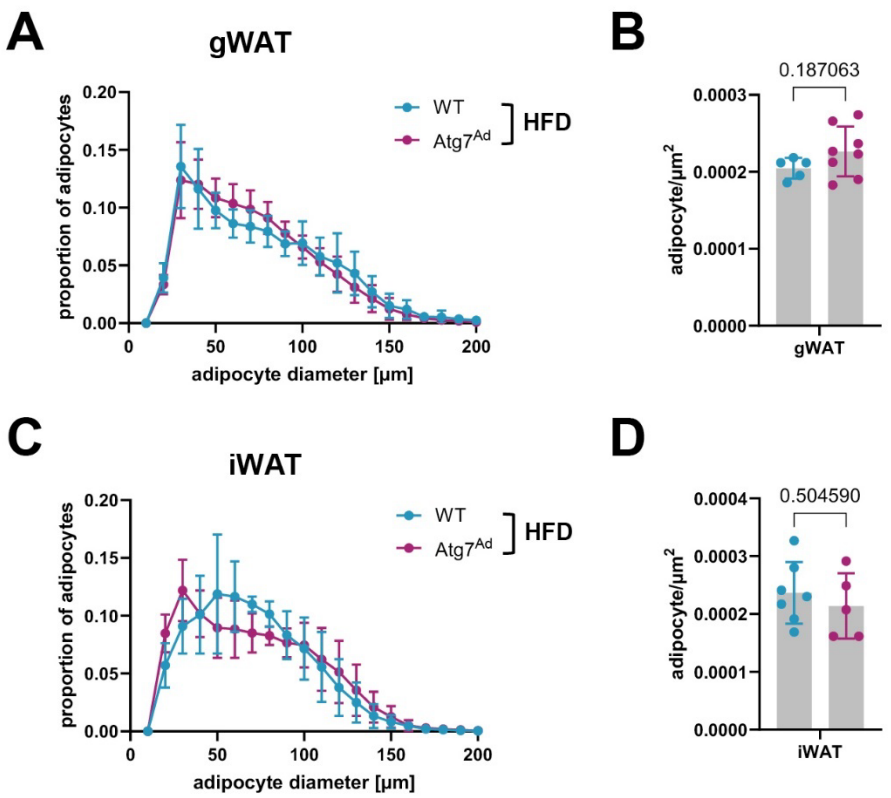

Figure 9: Autophagy does not impact adipocyte hyperplasia and hypertrophy. (A, C) Quantification of adipocyte diameter and their proportion across cell sizes in gWAT (A) and iWAT (C). n = 6 mice. (B, D) Quantification of adipocyte number per area in gWAT (B) and iWAT (D). Data are presented as mean ± SD. Each data point represents one biological replicate. Statistical analysis by unpaired t-test (B, D). Representative of 3 independent experiments.

Our postulation was further supported by a macroscopic tissue phenotype, where changes in tissue shape, colour, and stiffness were evident (Fig 10A). Tissue shape and stiffness are tightly dictated by ECM deposition and turnover (Sun et al., 2023). To evaluate ECM-related morphological changes, we stained WATs with picrosirius red (PSR), which is a standard method to visualise collagen I and III fibres (Lattouf et al., 2014). Strikingly, collagen staining was highly pronounced in the gWAT of obese *Atg7^{Ad}* mice compared to obese controls, indicating a highly exacerbated pericellular fibrosis (Fig 10B-C). As expected, fibrosis also developed in the gWAT of obese WT mice, albeit to a much more limited extent. In contrast, iWAT displayed no difference in the staining between the genotypes, suggesting that its expansion is not limited by ECM remodelling in our experimental model (Fig 10B-C). These

observations were further confirmed by an extensive gene expression panel of ECM components and enzymes, with a significantly elevated expression of key ECM modulators, including *Col3a1*, *Fn1*, *Mmp14*, and *Timp1* in *Atg7*^{Ad} gWAT but not iWAT (Fig 10D-E). In addition, we observed an elevated secretion of cytokines contributing to excessive ECM accumulation when culturing gWAT and iWAT ex vivo for six hours (Fig 10F-G). This included increased secretion of transforming growth factor β (TGFβ), a master regulator of tissue fibrosis (Meng et al., 2016) (Fig 10F), and osteopontin (OPN), a glycoprotein stimulating and building ECM in wound healing, inflammation, and fibrosis (Icer and Gezmen-Karadag, 2018) (Fig 10G). While the secretion of TGFβ was only induced from obese *Atg7*^{Ad} gWAT, both tissues displayed increased OPN secretion, albeit 20-fold lower in iWAT compared to gWAT (Fig 10F-G).

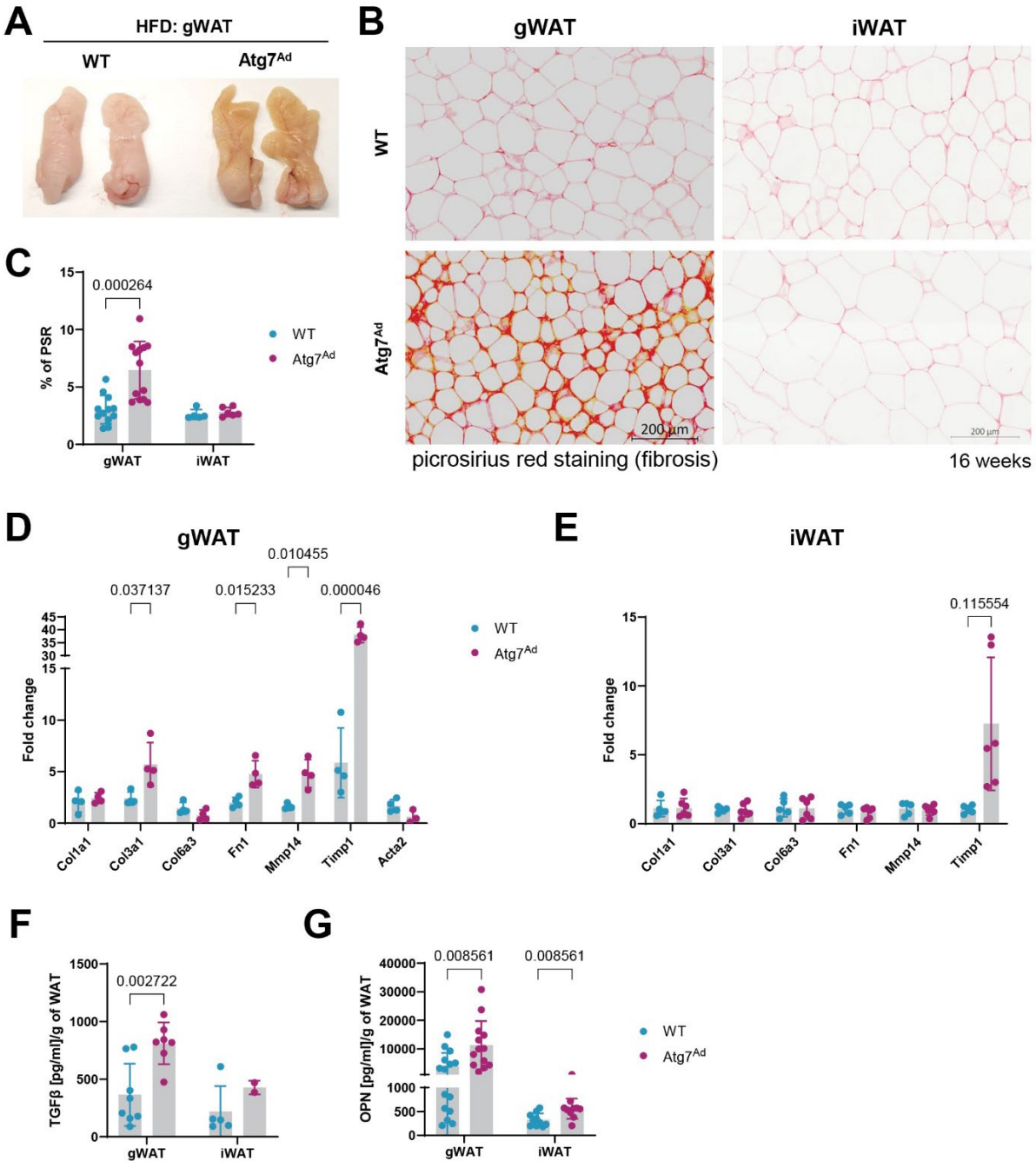

Figure 10: Adipocyte autophagy selectively limits gWAT expansion through pericellular fibrosis. (A) Photograph of WT and *Atg7*^{Ad} gWAT fat pads after 16 weeks of HFD feeding. (B) Picrosirius red (PSR) staining of collagen I and III in gWAT and iWAT after 16 weeks of HFD feeding. Scale bar, 200 µm. (C) Quantification of PSR staining area presented as a percentage of total tissue area from (B). (D-E) ECM-related genes' relative mRNA expression measured by qRT-PCR in gWAT (D) and iWAT (E). (F-G) Secretion of TGFβ (F) and osteopontin (OPN) (G) from gWAT and iWAT assessed by ELISA. For (G) data are merged from 3 independent experiments. Data are presented as mean ± SD. Each data point represents one biological replicate. Statistical analysis by multiple unpaired t-test (C-G). Representative of 3 independent experiments unless otherwise indicated.

To better understand the kinetics of the fibrotic process in the context of gWAT growth, we assessed WAT fibrosis during early body weight gain. Collagen accumulation appeared gradual, starting between 6 and 9 weeks of HFD feeding in obese *Atg7*^{Ad} mice (Fig 11A-B), indicating that fibrosis is an early event in gWAT pathophysiology in these mice. In addition, we wanted to understand the causation between DIO and adipocyte autophagy deletion. To this end, we initially fed mice HFD for 12 weeks and only later induced gene deletion by tamoxifen administration. When assessing gWAT morphology 4 weeks post-deletion, we observed similar excessive fibrosis developed as when autophagy deletion preceded DIO (data not shown), clearly demonstrating the therapeutic potential for adipocyte autophagy modulation in DIO.

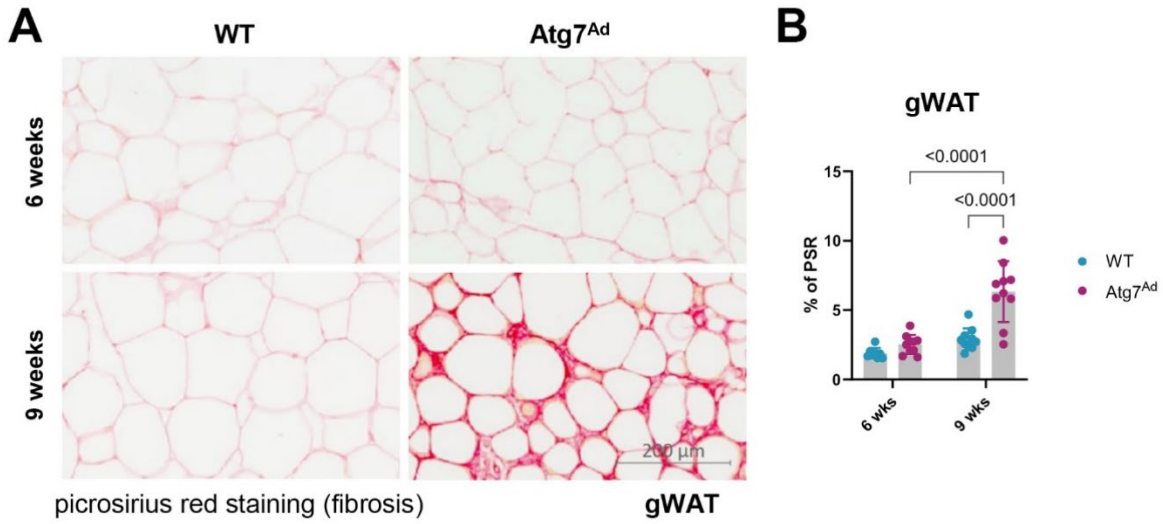

Figure 11: Fibrotic onset in *Atg7*^{Ad} is gradual and develops during early weight gain. (A) PSR staining of gWAT after 6 and 9 weeks of HFD feeding. Scale bar, 200 µm. (B) Quantification of PSR staining area presented as a percentage of total tissue area from (A). Data are presented as mean ± SD. Statistical analysis by two-way ANOVA with Fisher test. Each data point represents one biological replicate. Representative of 3 independent experiments.

In summary, our findings uncover a novel role of adipocyte autophagy in the modulation of visceral WAT architecture by supporting ECM remodelling and limiting fibrosis.

3.2.3 Adipose tissue fibrosis is maladaptive for tissue structural plasticity upon caloric restriction challenge

Fibrosis can serve as an adaptive or maladaptive tissue response. As an adaptive response, fibrosis serves to repair tissue injury and prevent excessive inflammation. In contrast, it becomes maladaptive when fibrotic lesions obstruct the normal function of tissues and organs, as the scars are inflexible, irreversible and functionally disabling (Datta et al., 2018). To understand whether exacerbated fibrosis observed in gWAT is an adaptive or maladaptive response, we challenged the mice to assess the functional response of fibrotic gWAT. As a challenge, we selected caloric restriction, which can reduce caloric intake without malnutrition by limiting access to food in a 2:1 ratio (2 days unlimited access, 1 day no access). As the reduced availability of nutrients changes systemic energy demand, the function of healthy WAT is to balance this need by releasing energy in the form of lipids via lipolysis (Chouchani and Kajimura, 2019).

By limiting access to food every two days while simultaneously keeping them on HFD once mice have developed chronic obesity, we observed no significant change in weight loss over the 8 weeks in WT and *Atg7*^{Ad} mice (Fig 12A). In addition, no change in weight gain was evident between the experimental groups kept continuously on HFD for 24 weeks and groups who were calorically restricted for the last 8 weeks (Fig 12B). When assessing WAT distribution, we found that the previous differences seen in gWAT deposition between WT and Atg7^{Ad} mice were lost after chronic administration of HFD (Fig 12C). No reduction of gWAT expansion was observed after 24 weeks of HFD feeding, and simultaneously, no difference was observed upon CR challenge. It is plausible that gWAT of WT dynamically remodels and adapts to continuous HFD administration, therefore masking the differences. In contrast, we noticed that increased accumulation of iWAT between WT and *Atg7*^{Ad} mice was also true after 24 weeks of HFD feeding (Fig 12D). In addition, this trend persisted after CR in *Atg7*^{Ad}, albeit the difference was much less pronounced and non-significant (Fig 12D). The data revealed an interesting

shift in iWAT distribution between HFD and CR HFD mice, whereby iWAT of CR *Atg7*^{Ad} mice shrunk compared to WT. This could potentially indicate that under CR, iWAT reduction serves to meet the change in organismal energy demands mice utilise in contrast to fibrotic gWAT which cannot shrink upon nutrient limitation. Nevertheless, more data would be needed to further support this hypothesis.

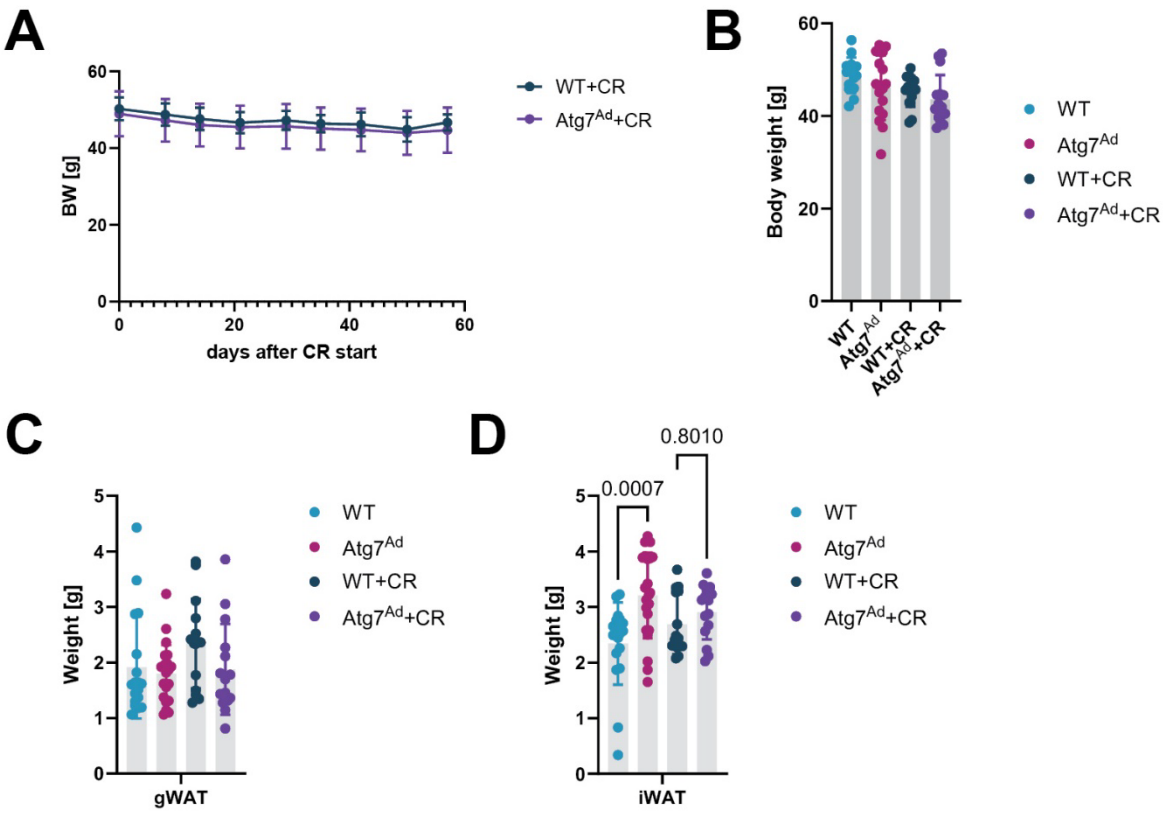

Figure 12: Impact of caloric restriction on body weight and fat distribution. Mice were continuously fed HFD for 24 weeks. Caloric restriction (CR) was initiated after 16 weeks of HFD feeding for a total duration of 8 weeks. (A) Body weight gain throughout the 8 weeks of CR. n = 10 mice. (B) Mouse body weight after 24 weeks of HFD±CR. (C-D) Weight of gWAT (C) and iWAT (D) fat pads after HFD±CR. Statistical analysis by one-way ANOVA (D). Data are presented as mean ± SD. Each data point represents one biological replicate. Data are merged from 3 independent experiments.

Caloric restriction and fasting are some of the most potent non-genetic inducers of non-selective autophagy (Bagherniya et al., 2018). To evaluate whether CR indeed led to the upregulation of WAT autophagy, we assessed autophagic flux in WAT explants isolated from

obese caloric-restricted mice. The ratio of LC3-II to LC3-I demonstrated that autophagy-sufficient obese WT mice highly increased gWAT autophagic flux, while *Atg7*^{Ad} mice with a genetic block in the autophagy pathway showed a much lower but still significant elevation of gWAT autophagy upon CR (Fig 13A).

As we have observed that adipocyte autophagy limits the development of gWAT fibrosis, we were curious if additional non-selective induction of autophagy with CR in obese WT mice can play a role in fibrosis resolution. While obese *Atg7*^{Ad} mice developed marked gWAT fibrosis, collagen accumulation and fibrosis also developed in WT WAT under obese conditions, albeit to a lower extent. In contrast to our expectations, increased autophagy in gWAT of obese WT mice did not resolve fibrosis, with comparable levels of fibrotic WAT between the groups (Fig 13B-C). This suggests that induction of non-selective autophagy per se cannot act to resolve fibrosis once it has been established. In addition, we unexpectedly found that CR advanced fibrotic deposition in gWAT of obese *Atg7*^{Ad} mice compared to HFD-fed counterparts (Fig 13B-C), indicating that additional WAT stress imposed with CR further contributed to collagen deposition.

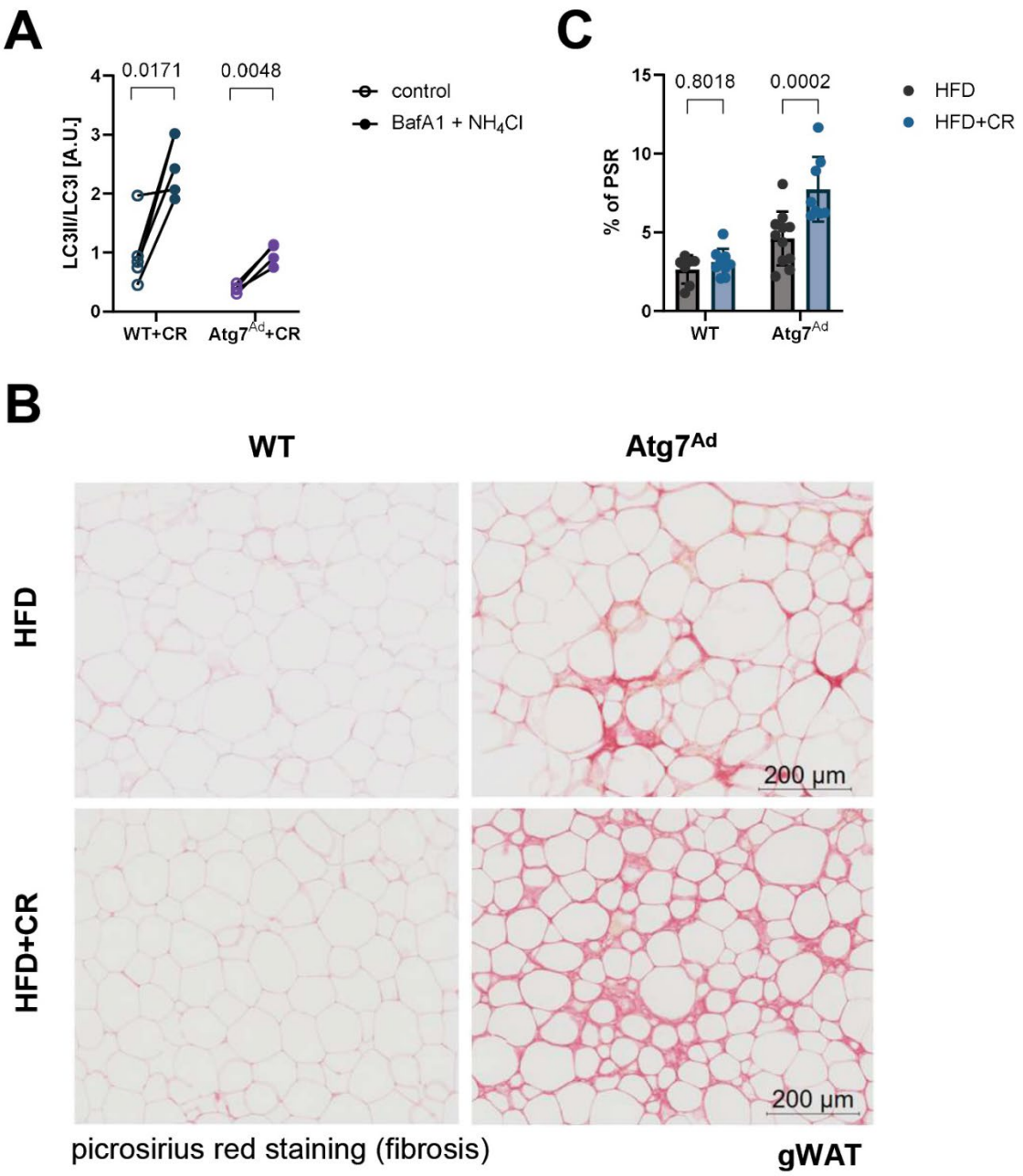

Figure 13: Induction of autophagy does not resolve fibrosis. Mice were continuously fed HFD and exposed to CR for the last 8 weeks of the feeding. (A) Quantification of autophagy flux as the ratio of LC3-II to LC3-I accumulation by western blot upon treatment with 100 nM BafA1 and 20 mM NH_4Cl. (B) PSR staining of gWAT after HFD±CR treatment. Scale bar, 200 µm. (C) Quantification of PSR staining area presented as a percentage of total tissue area from (B). Data are presented as mean ± SD. Each data point represents one biological replicate. Data are merged from 3 independent experiments. Statistical analysis by paired t-test (A) or two-way ANOVA with Šídák multi comparisons test (C).

To summarize, our results unveil that excessive collagen deposition deems gWAT inflexible upon CR challenge and is thus maladaptive in terms of its structural flexibility. It remains unclear whether it is also maladaptive for tissue metabolic plasticity. Despite induction with CR, non-selective autophagy in WT gWAT could not resolve obesity-associated fibrosis and was further pronounced in *Atg7*^{Ad} gWAT.

3.2.4 Autophagy and WAT fibrosis do not correlate with metabolic health in obese humans

A critical challenge in experimental models of obesity is their translation into human research (Lempesis et al., 2022). The main reasons for this are the scarcity of omental WAT (oWAT) available for basic research, anatomical differences between mice and humans, and a difference in clinical versus research protocols. During this DPhil project, we established a collaboration with a research group based at the University of Aarhus, Denmark, led by associate professor Emma Börgeson, who focuses on metabolic health and inflammation in obese patients and their association with cardiometabolic diseases. She offered us to study clinical samples from the Adipos2 Cohort (Ethical Approval ID Dnr 682-14, Clinical Trials ID NCT02322073), which is aimed at studying obesity-induced inflammation and includes lean and obese omental WAT (oWAT) collected from patients undergoing cholecystectomy (gallbladder removal) or gastric bypass surgery, respectively. Obese patients with a BMI of 35-55 scheduled for laparoscopic Roux-en-Y gastric bypass were recruited and underwent a 3-week calorie restriction (800 calories/day) before surgery. Lean patients were classified as having a BMI of 18.5 - 24.9 and were scheduled for cholecystectomy surgery. As we had access to a very limited number of samples (3-11 per condition), we tried to initially address a simple hypothesis before moving onto a larger sample size, depending on the outcomes. We aimed to evaluate whether adipose tissue autophagy and fibrosis correlate, also with respect to the metabolic health of individuals. To address this question, we stratified the Adipos2 cohort into two sub-cohorts based on metabolic health at the time of surgery and sample collection.

Classification strategy 1 was based on patients' responses to pre-surgical diet. Patients were classified as obese responders (reduced fasted blood sugar post-diet, n = 5), obese non-responders (no change or elevated fasted blood sugar post-diet, n = 4), and lean individuals (n = 3) (Table 4). Their fasted blood sugar in response to the presurgical diet was measured before starting the diet, on the date of the surgery, i.e., after 3 weeks of the pre-surgical diet, and 12 months post-surgery. Obese participants were classified based on the concentration of fasted blood sugar on the date of the surgery compared to pre-surgery levels. Lean participants were not classified.

Table 4: Classification strategy 1. Patients were stratified into obese responders, obese non-responders and lean groups depending on the criteria described in the main text at the time of the surgery. FBS = fasted blood sugar, NA = not available.

patient ID	sex	phenotype	age	BMI	FBS pre-surgery [mmol/L]	FBS surgery date [mmol/L]	FBS 12-month post-surgery [mmol/L]	group
1	F	obese	55	46.29	7.84	7.2	5.4	obese responder
2	M	obese	39	38.99	7.1	6.2	6.2	obese responder
3	F	obese	22	40.56	5.8	6.4	5.4	obese non-responder
4	F	obese	22	41.03	6.4	5.6	5.2	obese responder
5	F	obese	48	41.43	6.4	6.4	5.6	obese non-responder
6	F	obese	60	37.38	6.9	6.3	6.5	obese responder
15	F	obese	42	38.82	5.9	6.2	6.4	obese non-responder
16	F	obese	42	37.65	7.4	7.5	4.1	obese non-responder
22	F	obese	57	32.86	12.7	6	8	obese responder
61	M	lean	34	22.39	5.9	NA	NA	lean
101	F	lean	40	22.68	5.3	NA	NA	lean
102	F	lean	46	21.51	5.1	NA	NA	lean

Classification strategy 2 was based on the development of diabetes and patients were stratified into diabetic (n = 4), non-diabetic (n = 7), and lean controls (n = 3) (Table 5). Patients were classified as diabetic if they had increased HbA1c (≥ 39 mmol/L) or were taking anti-diabetes medication (metformin, insulin, dapagliflozin). None of the patients in the study was diagnosed with type 1 diabetes mellitus. All the lean controls were diabetes-free.

Table 5: Classification strategy 2. Patients were stratified into diabetic, non-diabetic and lean groups if they had increased HbA1c (≥ 39 mmol/L) or were taking anti-diabetes medication.

patient ID	sex	age	BMI	phenotype	HbA1c [mmol/L]	diabetic medication	group
1	F	55	46.29	obese	48	0	diabetic
2	M	39	38.99	obese	34	0	non-diabetic
3	F	22	40.56	obese	35	0	non-diabetic
4	F	22	41.03	obese	33	0	non-diabetic
5	F	48	41.43	obese	28	0	non-diabetic
6	F	60	37.38	obese	33	0	non-diabetic
14	M	47	37.66	obese	42	0	diabetic
15	F	42	38.82	obese	32	0	non-diabetic
16	F	42	37.65	obese	60	metformin, insulin	diabetic
22	F	57	32.86	obese	81	metformin, dapagliflozin	diabetic
82	F	26	40.23	obese	33	0	non-diabetic
61	M	34	22.39	lean	25	0	lean
101	F	40	22.68	lean	33	0	lean
102	F	46	21.51	lean	30	0	lean

To assess the levels of autophagy, we took advantage of paraffin-embedded tissue sections to detect protein p62 (Fig 14A), which is degraded by autophagy and thus inversely correlates with active autophagy (Watson and Soilleux, 2015). We found that autophagy is upregulated in obese compared to lean human WAT as evidenced by decreased p62 levels in obese, supporting our observations in mice (Fig 14B). As in mice, the fibrosis of oWAT was assessed

with PSR staining (Fig 14C). Image analysis workflow was designed in collaboration with Dr Jacky Ka Long Ko from Oxford-ZEISS Centre of Excellence at the Kennedy Institute of Rheumatology. Analysis of human samples revealed that regardless of the classification strategy, the levels of oWAT autophagy and fibrosis do not correlate (Fig 14D-E). We did, however, observe a slight trend of reduced autophagy (more p62 accumulation) associated with lower levels of fibrosis (not significant), which is the opposite of our findings in the DIO experimental mouse model.

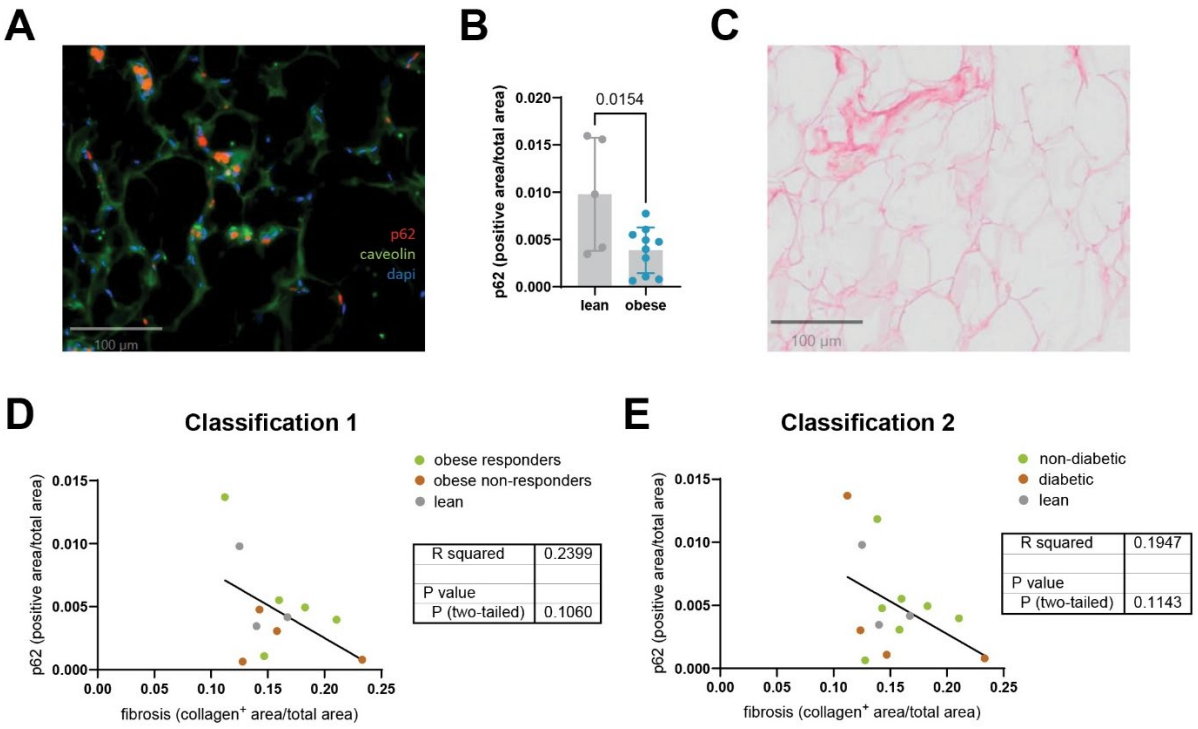

Figure 14: Autophagy does not correlate with fibrosis and metabolic health in obese human oWAT. (A) Samples were stained for active autophagy by p62 accumulation. (B) The accumulation of p62 in lean and obese oWAT samples was quantified as a positive p62 staining area normalised to the total tissue area. (C) Collagen deposition was assessed by PSR staining, quantified as an area of positive collagen staining normalised to the total tissue area. (D-E) Human oWAT samples were stratified based on metabolic status. Simple linear regression analysis was performed as a correlative analysis of fibrosis and autophagy. Colours denote the metabolic health of individuals, which were categorised according to classification 1 (D) or 2 (E). Each data point represents one biological replicate.

In conclusion, and given the small number of samples, we observed no correlation between adipose tissue autophagy and fibrosis in the context of metabolic health in obese humans. The limitations of this experimental setup will be discussed below.

3.3 Discussion

3.3.1 Adipocyte autophagy selectively modulates gWAT growth and expansion

Adipose tissue body distribution is one of the main determinants of metabolic health in obese individuals (Bluher, 2020). While the molecular mechanisms that underlay lipid distribution between different fat depots are not well understood, genetic predisposition, sex hormones, and certain drugs have been proposed to serve as the main drivers (Archer et al., 2013, Marcelin et al., 2022). On the other hand, the molecular mechanisms of WAT expansion are much better understood, and the susceptibility of different WAT depots to distinct processes, including hypertrophy, hyperplasia, immune cell composition, and oxidative stress sensitivity, could indirectly govern regional fat distribution (Ghaben and Scherer, 2019, Okuno et al., 2018, Sakers et al., 2022). Expansion of gWAT is dictated by both hypertrophy and hyperplasia, while iWAT predominantly expands via hypertrophy (Chouchani and Kajimura, 2019). Furthermore, it has been proposed that these fat depots may arise from two different progenitor cells as the kinetics of their development are different, however, this has not been experimentally proven (Datta et al., 2018). As we did not observe differences in cell size or number between gWAT and iWAT depots in obese WT and *Atg7*^{Ad} mice, it is likely that adipocyte autophagy does not influence these core growth processes but rather governs the selective expansion of gWAT through the control of ECM remodelling.

Metabolic health during obesity positively correlates with fat deposition in the subcutaneous area, also due to the ability of the subcutaneous WAT to buffer the detrimental impact of visceral WAT expansion (Sakers et al., 2022, Marcelin et al., 2022). In line with this, we noted

that increased iWAT at the expense of gWAT resulted in an improvement of metabolic health in *Atg7*^{Ad} obese mice, as measured by improved glucose homeostasis and lessened ectopic fat deposition in the liver. While we observed some disparities between GTT and ITT assessment of glucose homeostasis, this could be explained by the principle of the ITT assay, which predominantly measures response to insulin administration in the liver and skeletal muscle (Bowe et al., 2014). As we are impacting autophagy in adipocytes, favourable insulin sensitivity outcomes observed in obese *Atg7*^{Ad} mice are likely related to glucose uptake to the adipose tissue, however, this hypothesis would have to be experimentally validated.

3.3.2 Fibrosis limits gWAT expansion and functionality

We found that depletion of adipocyte autophagy resulted in WAT fibrosis that was specifically limited to gWAT. While the role of autophagy in WAT fibrosis has been suggested before, it remained experimentally unproven (Oh et al., 2023). The development of adipose tissue fibrosis is associated with pathological ECM deposition or dysfunctional turnover. Its resolution remains difficult to experimentally interrogate (Marcelin et al., 2022). The quest for anti-fibrotic or fibrosis-resolving therapies mostly stems from a traditional view, which recognises fibrosis as a detrimental factor in WAT development, plasticity, and ultimately function due to the mechanical stiffness it imposes on the tissue (Gliniak et al., 2023). Nevertheless, fibrosis also serves as a key adaptive response of tissue repair, acting to limit tissue damage and restore tissue architecture, thereby supporting its function, recovery, and survival (Henderson et al., 2020). When tissue injury is persistent or severe, however, fibrotic lesions disrupt tissue architecture, interfere with its biological function, and can ultimately result in organ failure (Medzhitov, 2021). Chronic progression of gWAT fibrosis was apparent in obese WT mice but much more pronounced in adipocyte autophagy-depleted obese mice. We hypothesise that initially, fibrosis serves as an adaptive response to prevent acute tissue damage. Eventually, however, progressive impairment of ECM remodelling leads to broader adipose tissue dysfunction, and fibrosis becomes maladaptive, with similar conclusions drawn recently in the

pancreas (Baer et al., 2023). The body-wide maladaptive outcomes of chronic WAT fibrosis are, however, difficult to discern as the WAT is not functionally compartmentalised and the effect is interestingly highly specific for a single WAT depot.

Our hypothesis could also help explain the inconsistency of our results with a broadly accepted observation of adipose tissue fibrosis contributing to the pathogenesis of insulin resistance (Lawler et al., 2016, Gliniak et al., 2023). As the fibrotic effect in the adipocyte autophagy-deficient model is highly specific to visceral WAT, this allows for metabolic buffering and forced expansion of iWAT, which is known to limit insulin resistance in MHO (James et al., 2021). Furthermore, since our mice on C57BL/6J background do not tend to fully develop type 2 diabetes but instead model early stages of the disease (Kleinert et al., 2018), it is difficult to discern the long-term effects of exacerbated gWAT fibrosis on (un)favourable chronic metabolic outcomes. Nevertheless, to get a better understanding of how gWAT fibrosis impacts WAT function, we could assess the lipolytic function of the tissue by measuring markers of active lipolysis, i.e., phosphorylated (activated) hormone-sensitive lipase (p-HSL) and adipose triglyceride lipase (ATGL).

A notable observation was that DIO WT mice that were subjected to caloric restriction further elevated their adipose tissue autophagy. While making a different conclusion, a previous study showed a drop in p62 accumulation, suggesting active autophagy, when mice were calorically restricted post-DIO compared to DIO in visceral WAT (Nuñez et al., 2013). Considering two independent but similar outcomes, these suggest that while autophagy is upregulated in obese WAT, this upregulation might not be sufficient to preserve the integrity of obese adipocytes, healthy ECM remodelling and the dynamic expansion of WAT.

3.3.3 Human data does not recapitulate the DIO experimental model

Rodent models are currently the most comprehensive models available in obesity research. Despite this recognition, many limitations make translation to humans challenging, including adipose tissue anatomy, weight gain kinetics, diet composition, and sex-specific differences (Lutz and Woods, 2012, Lempesis et al., 2022). We fed mice with HFD where 60 % of calories are fat-derived, in contrast to most human diets, where ~30% of daily calories come from fat (Lempesis et al., 2022). Nevertheless, highly caloric diets are still commonly used in DIO mouse models, predominantly as they greatly reduce the speed at which obesity phenotype can be studied. To mitigate sex-specific limitations, we have included both females and males in our study, and all the results presented in this chapter reflect both sexes.

We have found that the levels of autophagy do not correlate with the development of fibrosis, neither in the context of MHO or MUO. Besides the limitations of the translation of mouse models into clinical research, we believe that the observed disparity could be explained by differences in experimental endpoints and sample collection. Human adipose tissue samples were collected after a 3-week long strict pre-surgical diet, which comprised of only 800 calories per day. Considering that their caloric input beforehand was higher, this could suggest that oWAT autophagy was upregulated in response to caloric restriction, as we have demonstrated in mice, as well as previously described (Chung and Chung, 2019). In addition, we have demonstrated that caloric restriction-stimulated non-selective autophagy does not resolve fibrosis in WT mice, and the same could be true for human participants. This could help explain why we observed a trend in positive correlation between autophagy and fibrosis. These limitations could be overcome by better aligning the experimental model with the clinical cohort, however, due to time constraints, those adjustments were out of the scope of this DPhil project.

3.4 Conclusion

In this chapter, we have sought to understand the impact of adipocyte autophagy on WAT pathophysiology during obesity. We found that obesity-induced autophagy dictates local fat distribution by promoting gWAT expansion. Tissue growth is supported by the restriction of pathological ECM remodelling and fibrosis. In the next chapter, we will aim to understand the mechanisms by which adipocyte autophagy controls gWAT remodelling and architecture.

4 Adipocyte autophagy controls adipose tissue inflammation

4.1 Introduction

4.1.1 Immune cells shaping adipose tissue in health and disease

Adipose tissue was identified as a source of TNFα and inflammation in obesity more than 30 years ago (Hotamisligil et al., 1993). Research over the past three decades has identified a variety of innate and adaptive immune cells residing in WAT having an important tissue regulatory role in both health and disease. Immune cells in adipose tissue importantly contribute to whole-body inflammatory homeostasis. Memory T cells home to WAT after the infection, making adipose tissue an important immune reservoir for memory and recall responses (Han et al., 2017). Furthermore, adipose tissue serves as an infection site for various parasitic and viral pathogens, thereby orchestrating whole-body immune response to infection and antiviral therapies (Mathis, 2013). In addition, immune cells in adipose tissue carry out non-immune functions. They regulate adipocyte homeostasis through the control of preadipocyte proliferation and differentiation, adipocyte cell death, insulin sensitivity, and their metabolic homeostasis through control of lipid uptake and lipolysis. In beige adipose tissue and BAT, they importantly contribute to adipocyte browning and thermogenesis regulation (Trim and Lynch, 2022).

Lean WAT is characterized by an anti-inflammatory (type II) profile. Tissue homeostasis is established by many WAT resident anti-inflammatory immune cells, including anti-inflammatory macrophages, eosinophils, regulatory T cells (T_{reg}), natural killer (NK) cells, invariant natural killer T cells (iNKT), and type 2 innate lymphoid cells (ILC2s) (Ferrante, 2013). Obesity-induced changes in adipocyte secretome, hypertrophy, and lipid-induced endoplasmic reticulum (ER) stress, however, lead to a pro-inflammatory shift in the obese WAT microenvironment. This is

characterized by an increased proliferation and recruitment of inflammatory macrophages, neutrophils, $CD8^+$, $CD4^+$ T helper 1 (T_H1) and B cells, and a reduced abundance of anti-inflammatory immune cells (Trim and Lynch, 2022). This shift leads to impaired local and systemic low-grade chronic inflammation and has also been related to metabolic disorders, although the causality of this relationship requires further investigation.

4.1.2 Adipose tissue $CD8^+$ and $CD4^+$ T cells

T cells are central to adaptive immune response and are divided into $CD4^+$ and $CD8^+$ subtypes based on the expression of surface markers. Naïve $CD4^+$ T cells differentiate into multiple T helper (T_H) subsets with distinct transcription factor and cytokine profiles. While they respond to antigens presented on MHC class II (MHCII), $CD8^+$ T cells produce cytolytic substances and regulate the activation of other immune cells upon activation by MHC class I (MHCI) antigens (Mraz and Haluzik, 2014). Adipose tissue T cell composition is dynamic between lean and obese states. In lean mice and humans, $CD4^+$ T_H2 and Treg cells help maintain WAT homeostasis and an anti-inflammatory environment. With obesity, their numbers are reduced in favour of pro-inflammatory $CD4^+$ T_H1 and T_H17 as well as $CD8^+$ T cells, which rapidly increase in abundance due to clonal expansion. In addition, they often acquire an exhausted phenotype due to chronic antigen stimulation and prolonged activation. Through the recruitment and cytokine-mediated stimulation of other pro-inflammatory cells, these cells support immunometabolic WAT dysfunction (Jacks and Lumeng, 2024). WAT also serves as a reservoir for memory T cells, which home to the tissue following infection and clonal expansion, and might therefore importantly contribute to immunological memory (Trim and Lynch, 2022).

4.1.3 Adipose tissue macrophages

Macrophages are haematopoietic cells of the myeloid lineage that play a critical role in protection against infection and injuries. They play an important role in innate immune defence

as well as support organ and systemic homeostasis in a tissue-specific manner. These functions are achieved through specialization in phagocytosis to degrade and detoxify engulfed cargo, as well as through secretion and response to cytokines and chemokines to communicate in their microenvironment (Epelman et al., 2014). Macrophages colonize most organs in the body either through embryonical seeding, followed by self-renewal and longevity or through continuous derivation from circulating monocytes (Gomez Perdiguero et al., 2015). Their dynamic response to environmental signals and marked plasticity enable macrophages to fulfil highly specific functions in different tissues (Guilliams and Scott, 2017). This plasticity is considered their key ability to switch from tissue-specific homeostatic functions to a pathogen-eliminating inflammatory state. Macrophage phenotype is largely impacted by developmental origin, tissue location and time spent in the tissue, local microenvironment, and inflammation status (Bleriot et al., 2020). Their specialization is defined by tissue- and lineage-specific transcription factors, cytokines and chemokines, danger-associated molecular patterns and metabolic cues. Differentiated macrophages can be reprogrammed when transferred into a new microenvironment (Lavin et al., 2014), emphasizing that environmental factors are key to influencing their specialisation. Despite their multifaceted phenotypes, several core populations of macrophages have been identified as coexisting across tissues. Among monocyte-derived macrophages, two distinct populations were identified in subtissular niches, including antigen-presenting macrophages residing adjacent to nerves (identified as Lyve1^{lo} MHCII^{hi}, also known as non-perivascular-like macrophages (NPVM)) and wounding and tissue repair macrophages found in proximity to blood vessels (identified as Lyve1^{hi} MHCII^{lo}, also known as perivascular-like macrophages (PVM)) (Chakarov et al., 2019). Another study identified three distinct populations based on their life cycle and tissue residency properties, including TFL^{+} macrophages (TIM4^{+} and/or LYVE1^{+} and/or FOLR2^{+}) maintained through self-renewal, CCR2^{+} macrophages (TIM4^{-} LYVE1^{-} FOLR2^{-}) replaced by monocytes, and MHCII^{hi} macrophages (TIM4^{-} LYVE1^{-} FOLR2^{-} CCR2^{-}) with a modest monocyte contribution (Dick et al., 2022).

Adipose tissue macrophages (ATM) represent around 10 % of total immune cells in lean WAT. They support WAT through dynamic and multifaceted functions involving adipocyte clearance, extracellular remodelling, supporting angiogenesis and adipogenesis, promoting insulin sensitivity, controlling adipocyte metabolism and T cell activation, and scavenging lipids (Matz et al., 2023). Their number profoundly increases to more than 50 % of $CD45^+$ upon obesity as a result of both recruitment and proliferation, making them the most abundant immune cell population (Weisberg et al., 2003, Amano et al., 2014). Their accumulation in obese WAT has traditionally been associated with crown-like structure (CLS) formation around dead/dying adipocytes to uptake debris, leading to exacerbated local and systemic inflammation and insulin resistance (Cinti et al., 2005). Therefore, they are often referred to as master regulators of WAT inflammation and are the most well-studied immune cell type in WAT. Determining their phenotype in WAT inflammation would traditionally rely on the paradigm of M1/M2 macrophages, delineating their classical (pro-inflammatory) activation (M1) and alternative (anti-inflammatory) activation (M2). However, with the emergence of single-cell techniques, this oversimplified M1/M2 paradigm quickly became outdated (Nance et al., 2022). With recent advances in macrophage heterogeneity, we now have a better understanding of ATM diversity, which spans a spectrum of ATM functions and phenotypes (Fig 15). Novel subtypes of ATM have been identified with critical tissue regulatory functions beyond inflammation. It has been shown that the metabolic state of WAT not only controls ATM abundance but also their composition, as they are highly plastic in response to external stimuli (Matz et al., 2023). This led to a postulation that while initially serving as a protective physiological response, their accumulation due to chronic stimuli leads to a pathogenic response. As such, macrophages were proposed to be a critical link between adipose tissue, systemic metabolism and the immune system in obesity (Trim and Lynch, 2022).

Lipid-associated macrophages (LAMs) actively engage in lipid homeostasis in obese WAT by promoting local lipid turnover. They sequester lipids from cell death-prone hypertrophic

adipocytes through CLS formation and phagocytosis and have a highly active lipid catabolism (Xu et al., 2013a). The lipid-loading of $CD9^+$ $CD63^+$ macrophages results in a metabolic reprogramming, which leads to a pro-inflammatory or tissue-protective function in a lipid sensor TREM2-dependent manner (Jaitin et al., 2019, Hill et al., 2018). Another subset of ATMs responding to metabolic stimuli are metabolically activated macrophages (MMes). Their phenotype is driven by high levels of insulin, glucose, and FFAs in WAT (Kratz et al., 2014). Similar to LAMs, MMes prevent lipotoxicity through the sequestration of lipids and dead adipocyte clearance. They display both detrimental and beneficial functions depending on the obesity progression in a *Nox2*-dependent manner (Coats et al., 2017). On the other hand, vasculature-associated macrophages (VAMs) predominantly maintain tissue homeostasis by supporting WAT angiogenesis and extracellular remodelling. By residing in the proximity to blood vessels, they serve as a communication interface between systemic circulation and the WAT microenvironment, monitoring their microenvironment and removing adipocyte-derived catabolites through their high endocytic capacity (Silva et al., 2019). Due to their location and function as well as anti-inflammatory and tissue repair gene signature, they closely relate to PVM found across multiple tissues (Chakarov et al., 2019). Besides these three well-defined subtypes, ATMs further include proliferative LAM (P-LAM), collagen-expressing macrophages (CEM), regulatory macrophages (RM), and sympathetic neuron-associated macrophages (SAM) (Sarvari et al., 2021, Pirzgalska et al., 2017). In addition, their ontogeny and function also allow classification based on CD206, TIM4, CD163, and MHCII (Félix et al., 2021).

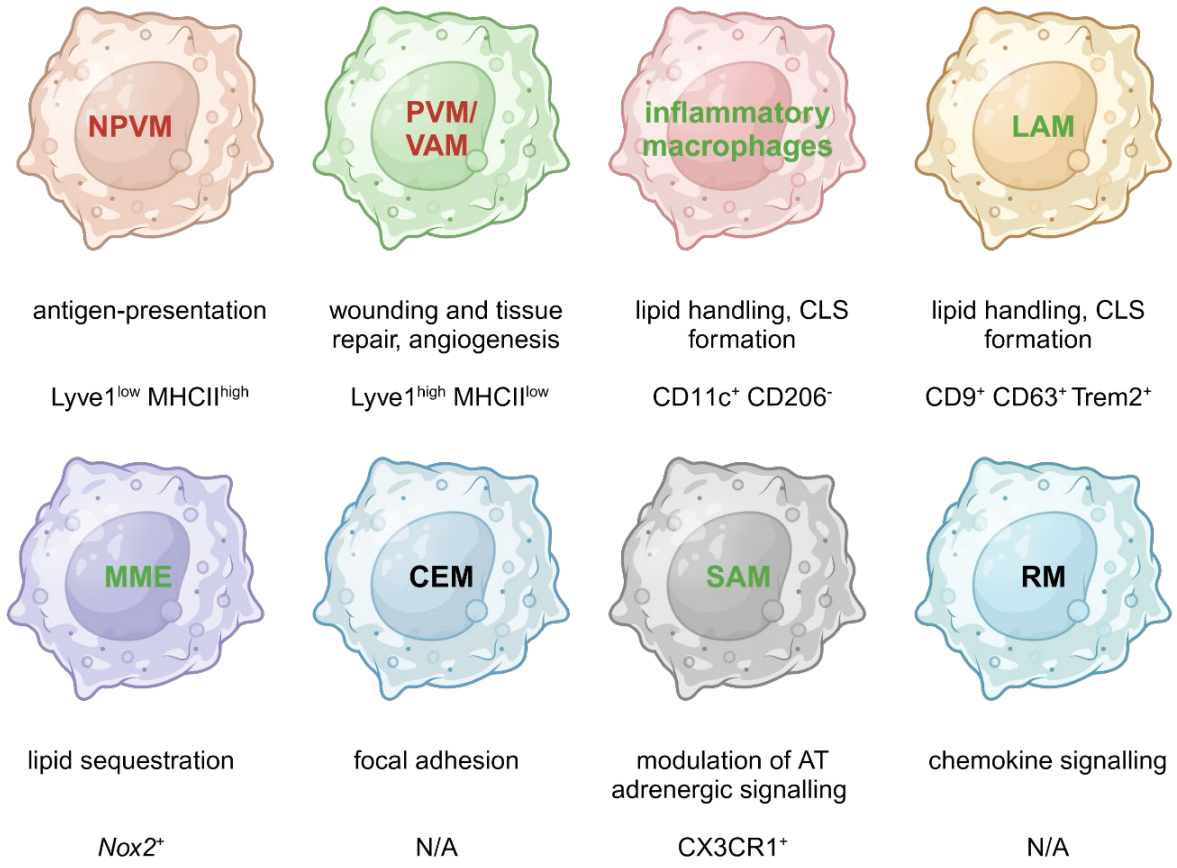

Figure 15: Adipose tissue macrophage heterogeneity. Summary of different subsets found in WAT, their typical role and characteristic markers. Subsets that accumulate with obesity are denoted in green, while the subsets that decrease with obesity are denoted in red. Black denotes subsets which have not been studied in relation to obesity. For more details refer to the main text. Created with BioRender.com.

4.1.4 The role of macrophages in fibrosis

Macrophages play a central role in tissue response to injury or unresolved inflammation through their profibrotic and antifibrotic roles, depending on different activation states. They induce fibrinogenesis by switching to a wound-healing phenotype that promotes myofibroblast proliferation and activation, thereby stimulating ECM production. On the other hand, macrophages can also facilitate fibrosis resolution and ECM clearance by taking up collagen and degrading it through the secretion of MMPs and other proteolytic enzymes (Adhyatmika et al., 2015). Macrophages control ECM remodelling in the lungs, heart, liver, kidney, and intestine, and their depletion early during fibrosis onset results in reduced ECM deposition (Lis-

Lopez et al., 2021). While macrophages have also been suggested to play a role in WAT fibrosis (Marcelin et al., 2022), the evidence remains scarce, with elastin and TLR4 signalling being proposed to play a role in macrophage-induced WAT fibrosis during obesity (Martinez-Santibanez et al., 2015, Vila et al., 2014). ATMs have also been proposed to prevent pathological changes of ECM and limit the development of gWAT fibrosis (Chen et al., 2021) Nevertheless, it remains unclear which signals induce the macrophage pro- or anti-fibrotic phenotypic switch that could serve as important balance checkpoints and therapy targets in fibrotic diseases.

4.1.5 Chapter aims

In the first chapter, we observed the strong fibrotic phenotype in gWAT of *Atg7*^{Ad} mice. Given that WAT fibrosis is tightly associated with inflammation, we sought to understand how adipocyte autophagy changes the WAT immune landscape. Based on previous reports (Sakane et al., 2021, Cai et al., 2018), we hypothesized that *Atg7*^{Ad} gWAT adapts a pro-inflammatory state with immune cells shifting from anti- to pro-inflammatory phenotype. To this end, we (1) broadly characterized the SVF fraction of both gWAT and iWAT, (2) performed an in-depth analysis of immune cells, and (3) studied their impact on gWAT fibrosis.

4.2 Results

4.2.1 Adipocyte autophagy shapes WAT cellular composition

The profound shift in tissue and organ architecture is often a consequence of an altered cellular landscape (Gliniak et al., 2023). Multiple single-cell studies have demonstrated significant changes in cellular composition between distinct fat depots, including variations in adipocyte subsets and size, preadipocyte identity and adipogenic potential, immune cell infiltration, vascularisation, etc (Maniyadath et al., 2023, van Beek et al., 2015). To understand whether adipocyte autophagy can selectively affect tissue architecture between WAT depots through

modulation of cellular populations, we assessed their abundance in gWAT and iWAT. Nuclear density was notably increased in obese *Atg7*^{Ad} gWAT compared to WT, which was not true for iWAT (Fig 16A-B).

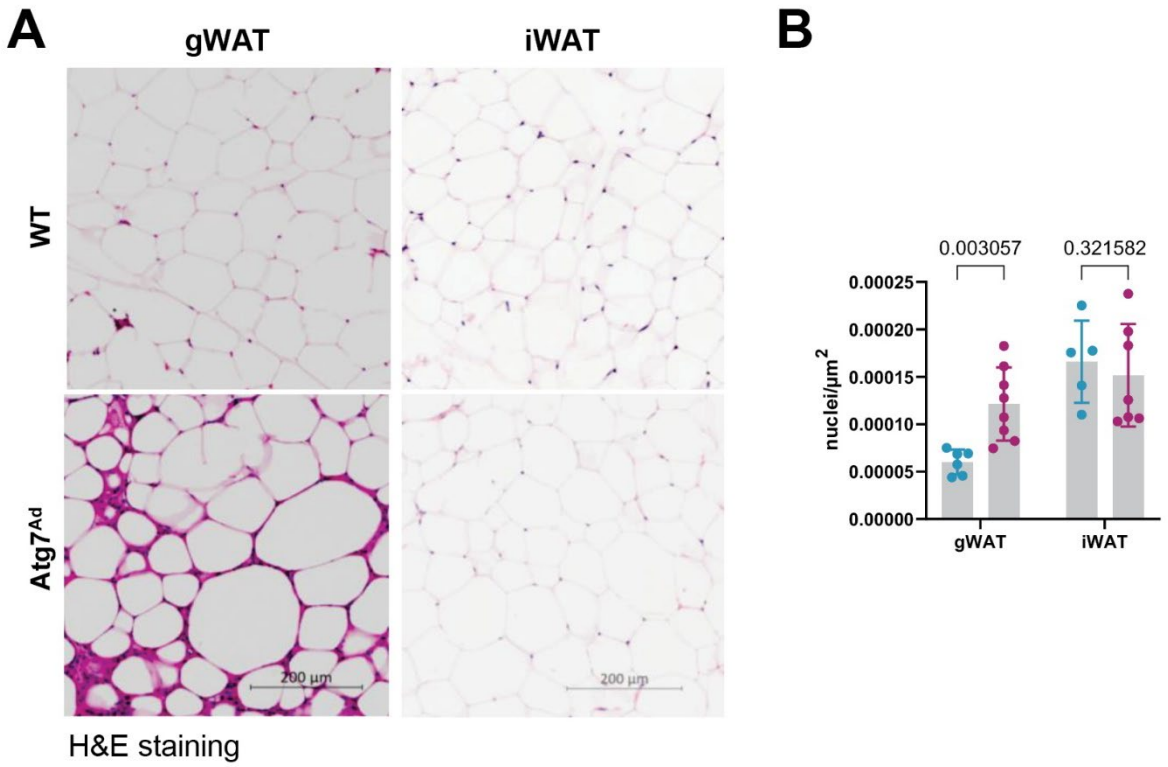

Figure 16: Autophagy limits cellular accumulation in gWAT. WT and *Atg7*^{Ad} mice were fed HFD for 16 weeks before tissue composition was assessed. (A) H&E staining of WT and *Atg7*^{Ad} gWAT and iWAT. Scale bar, 200 µm. (B) Quantification of nuclear staining presented as the number of nuclei per µm^2 of total tissue area from (A). Data are presented as mean ± SD. Statistical analysis by multiple unpaired t-test. Each data point represents one biological replicate. Representative of 3 independent experiments.

As noted in Fig 9B, adipocyte number in gWAT was not impacted by the loss of autophagy, indicating that adipocyte hyperplasia could therefore not explain a nearly 3-fold increase in cell number. Besides unilocular adipocytes, WAT contains a heterogeneous SVF, which includes endothelial, immune, and stromal cells (Emont et al., 2022). To assess the composition of WAT SVF in the absence of adipocyte autophagy, we performed flow cytometry analysis of lineage-specific markers for immune cell (CD45$^+$), endothelial cell (CD31$^+$) and fibroblast (PDGFRα$^+$) populations (Fig 17A). Notably, we observed a significant expansion of the immune cell

population in obese gWAT upon loss of adipocyte autophagy (Fig 17B, D). In contrast, the composition of iWAT SVF showed no considerable differences (Fig 17C). While immune cells accumulated, the abundance of endothelial cells and fibroblasts remained comparable or decreased in *Atg7*^{Ad} gWAT, respectively (Fig 17B, E-F). In line with the lower abundance of fibroblasts, the expression *Acta2*, a myofibroblast gene, was also found not to increase in obese *Atg7*^{Ad} gWAT (Fig 10D). Again, no differences in CD31^{+} and PDGFRα^{+} populations were observed in iWAT (Fig 17E-F).

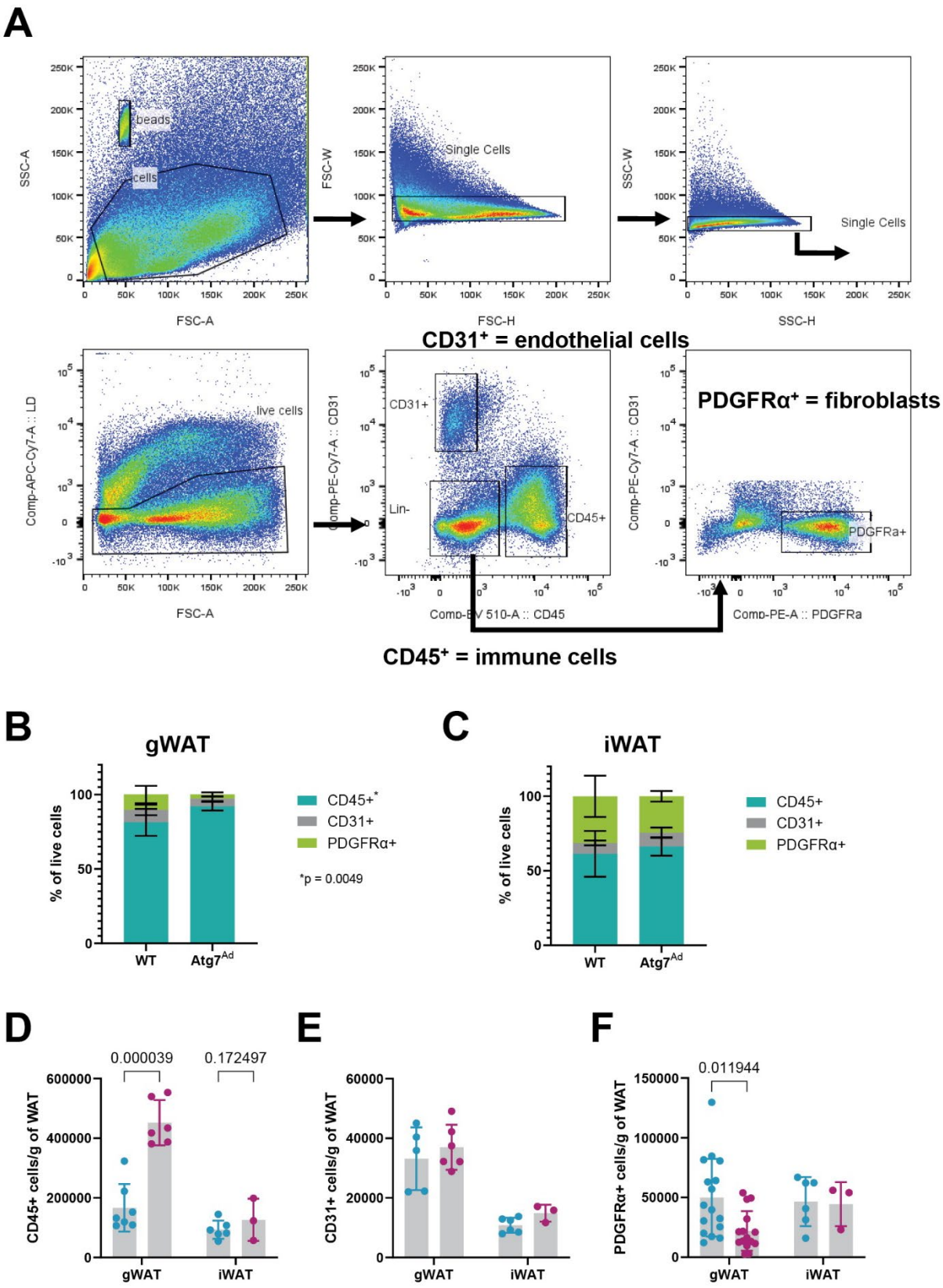

Figure 17: Adipocyte autophagy orchestrates gWAT cellular composition. (A) Gating strategy to determine WAT cellular composition by assessing CD45⁺, CD31⁺, and PDGFRα⁺ live cell subsets. (B-C) Flow cytometry analysis of CD45⁺, CD31⁺, and PDGFRα⁺ populations

in gWAT (B) and iWAT (C). n = 3-7 mice. (D-F) The absolute number of $CD45^+$ (D), $CD31^+$ (E), and $PDGFR\alpha^+$ (F) cells normalised to grams of WAT as in (B-C). Data are presented as mean ± SD. Each data point represents one biological replicate. Statistical analysis by two-way ANOVA with Šídák multi comparisons test (B) and multiple unpaired t-test (D, F). Representative of 3 independent experiments.

The $PDGFR\alpha^+$ population not only gives rise to fibroblasts but also supports WAT homeostasis by providing a pool of adipocyte precursors. To understand whether loss of autophagy in mature adipocytes and subsequent histological changes could shape the pool of adipose stem and progenitor cells (ASPCs) in gWAT, we performed flow cytometry characterisation (Fig 18A). Adipose stem and progenitor cells are defined as $CD45^-$ $CD31^-$ $TER119^-$ (lineage negative) fraction and are commonly identified by mesenchymal cell markers Sca-1 and CD29 (Ferrero et al., 2020) (Fig 18A). They do not express adiponectin, which is a distinctive marker of mature adipocytes (Korner et al., 2005). Our preliminary data show that the pool of ASPCs in gWAT of *Atg7*^{Ad} mice is approximately 50 % of that of WT (Fig 18B), indicating that mature adipocytes without autophagy control precursor abundance through a negative feedback loop, however not affecting adipose tissue formation. The ASPC population is heterogeneous with subsets differing in their stemness and adipogenic commitment. $CD55^+$ $CD26^-$ cells commonly display high proliferation and lower adipogenic differentiation potential, while $CD55^+$ $CD26^+$/$DPP4^+$ cells can give rise to preadipocyte and adipogenesis regulator pools (Ferrero et al., 2020). Interestingly, we found that not only was the abundance of ASPCs less in the gWAT of autophagy-deficient mice but also that their composition greatly differed between the two genotypes (Fig 18B-C). Preliminary data show that in *Atg7*^{Ad} mice there is a higher proportion of early precursors with lower adipogenic differentiation capacity ($CD55^+$ $CD26^-$) compared to WT mice (Fig 18C). In comparison, *Atg7*^{Ad} gWAT displays a reduced proportion of ASPCs that are found later in adipogenesis trajectory ($CD55^+$ $CD26^+$) compared to the WT gWAT. These preliminary data indicate that mature adipocyte autophagy shapes gWAT microenvironment to support not only the general ASPCs pool but also their adipogenic commitment, as evidenced by a dysregulated shift in early-to-late precursors in *Atg7*^{Ad} gWAT. Given that excessive WAT

fibrosis negatively affects adipogenesis and hyperplastic growth (Gliniak et al., 2023, Ghaben and Scherer, 2019), and considering no differences in mature adipocyte numbers between *Atg7*^{Ad} and WT gWAT (Fig 9B), it is plausible that the reduction in ASPCs is a consequence, rather than a cause, of the impaired tissue expansion. However, further experiments are necessary to determine the potential role of these cells in contributing to the *Atg7*^{Ad} phenotype.

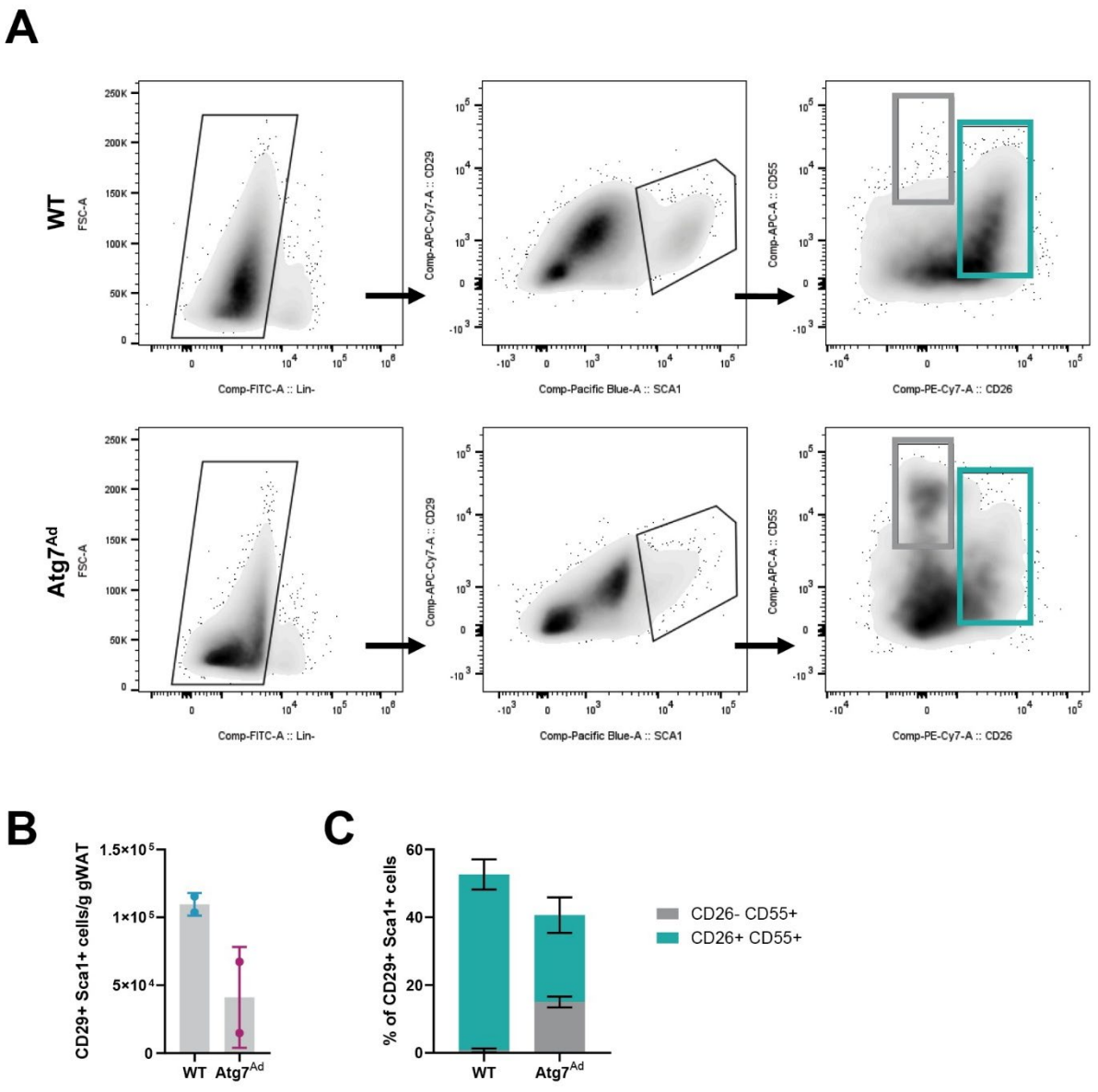

Figure 18: Mature adipocyte autophagy controls gWAT adipose stem and progenitor cells in DIO. (A) Gating strategy to study adipose stem and progenitor cell (ASPC) composition in gWAT. Lineage negative fraction includes CD45^{+}, CD31^{+} and TER119^{+} cells. Adipose stem and progenitor cell population (CD29^{+} Sca-1^{+}) can be divided into early progenitors (CD26^{-}

CD55$^+$) and adipose stem cells (ASCs; CD26$^+$ CD55$^+$), which give rise to preadipocytes. (B) Flow cytometry analysis of absolute CD29$^+$ Sca-1$^+$ number in obese gWAT of WT and *Atg7^{Ad}* mice. (C) The proportion of early progenitors and ASCs within the ASPC population in gWAT of WT and *Atg7^{Ad}* mice after 16 weeks of HFD. n = 2-3 mice. Each data point represents one biological replicate. Preliminary data from a single experiment.

To understand which immune cells contribute to the almost 3-fold expansion of the CD45$^+$ lineage in obese *Atg7^{Ad}* gWAT, we assessed the most common pro- and anti-inflammatory immune subsets by flow cytometry (Fig 19A-B).

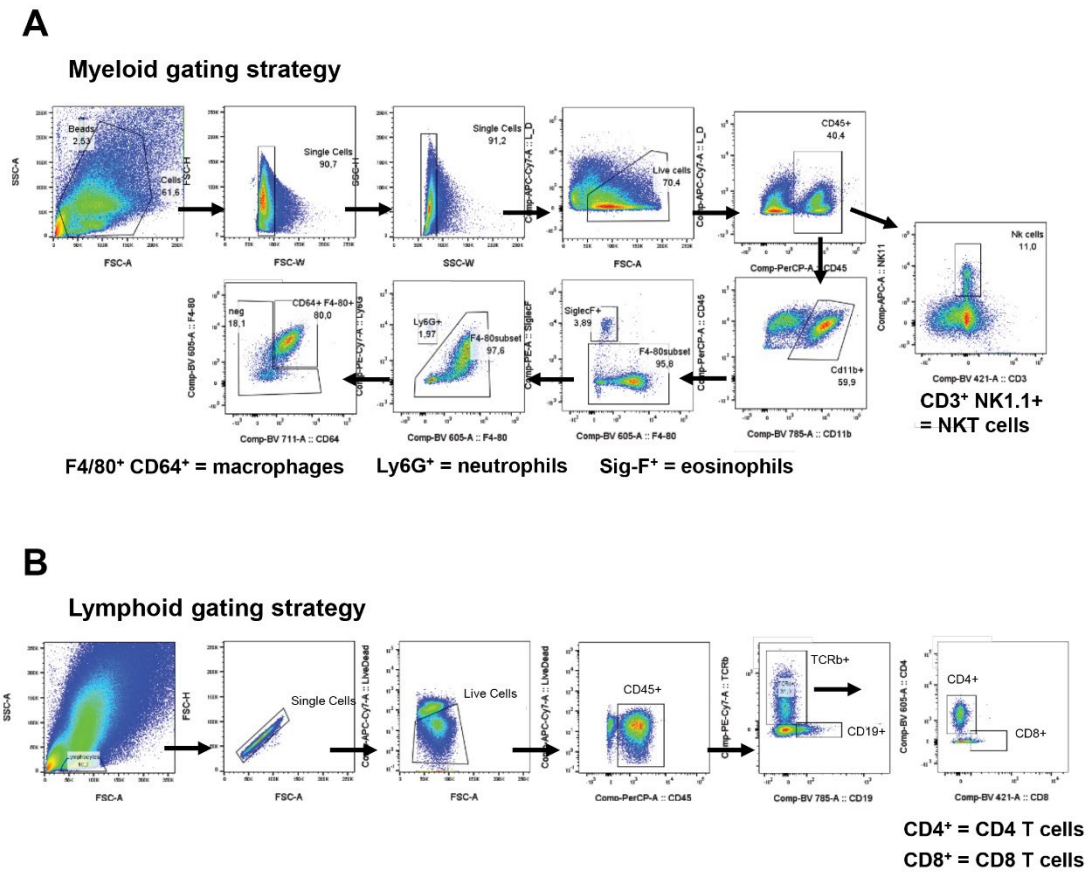

Figure 19: Gating strategy to study immune cell composition of WAT. (A) Myeloid cell gating strategy for neutrophils (Ly6G$^+$), eosinophils (Siglec-F$^+$), macrophages (F4/80$^+$ CD64$^+$), and natural killer T (NKT) cells (CD3$^+$ NK1.1$^+$) within CD45$^+$ live cells. (B) Lymphoid cell gating strategy for TCRβ$^+$ CD8$^+$ and CD4$^+$ T cells within CD45$^+$ live cells.

First, we compared immune cell frequencies between lean and obese gWAT to understand how our DIO mouse model recapitulates previous observations. We found no notable differences in the immune cell composition of gWAT and iWAT between NCD and HFD-fed WT

mice (Fig 20A-D). This contrasted with well-accepted obesity-induced macrophage accumulation (Biswas and Mantovani, 2012, Jaitin et al., 2019, Mathis, 2013, McNelis and Olefsky, 2014). We did, however, find macrophages being the most abundant immune cell type in obese WT gWAT (Fig 20B), in line with previous observations that macrophages contribute more than 50 % of the total immune cell population in WAT (Liu and Nikolajczyk, 2019). In addition, we observed an increased formation of CLS upon DIO in WT mice, as previously reported (Fig 20E-F) (Cinti et al., 2005).

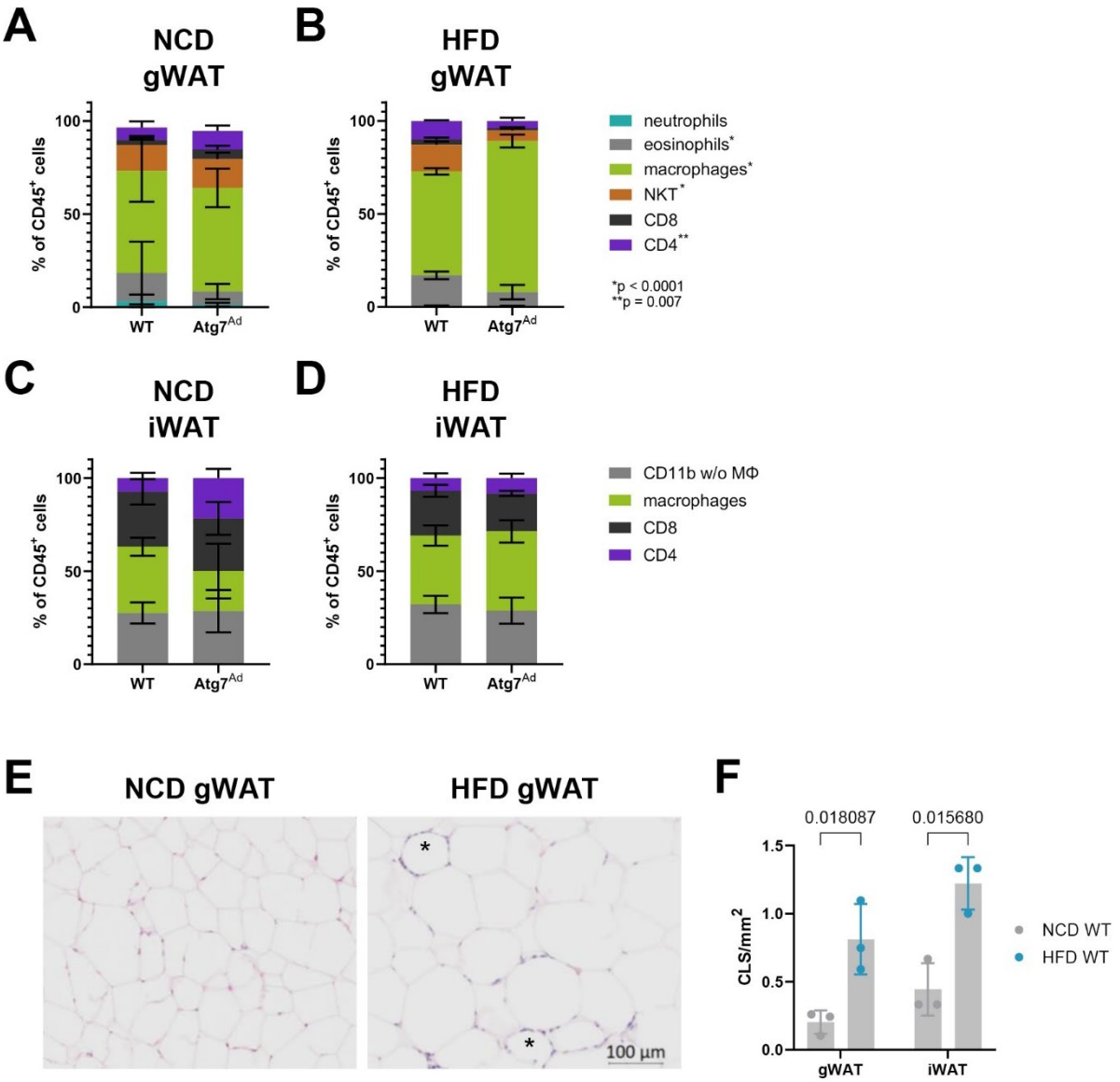

Figure 20: Autophagy directs immune cell composition in gWAT but not iWAT. (A-D) Immune cell ($CD45^+$) composition was assessed by flow cytometry in lean (A, C) and obese

(B, D) gWAT (A-B) and iWAT (C-D) after 16 weeks of altered diet feeding. NKT = natural killer T cell. n = 3-7 (E) Representative H&E image of crown-like structures (CLS) in WT lean and obese gWAT. CLS marked with asterisk. (F) Quantification of CLS as in (E). Each dot corresponds to a total number of CLS counted on three different tissue areas from a single animal. Data are presented as mean ± SD. Statistical analysis by two-way ANOVA with Šídák multi comparisons test (A-D) and multiple unpaired t-test (F). Representative of 3 independent experiments.

To understand how the loss of adipocyte autophagy influences these populations in obesity, we compared their frequencies between WT and *Atg7*^{Ad} in WAT (Fig 20A-D). Strikingly, we observed the macrophage population increase in frequency upon loss of adipocyte autophagy in DIO mice (Fig 20B). Macrophage frequency in iWAT of DIO mice, however, was not impacted by the lack of adipocyte autophagy (Fig 20D). Remarkably, the prevalence of macrophages increased more than 2-fold in obese *Atg7*^{Ad} gWAT, with around three million macrophages accumulated per gram of gWAT (Fig 20B and Fig 21A). This was also apparent with immunofluorescence staining, where macrophage-specific markers were abundant in *Atg7*^{Ad} gWAT (Fig 21B). On the other hand, we noted a reduction in the absolute number of CD4^{+} T cells (Fig 20B and Fig 21G), while the abundance of CD8^{+} T cells, neutrophils, eosinophils, and NKT cells remained unchanged (Fig 21C-F). These findings demonstrate that adipocyte autophagy has a profound impact on the immune cell composition of gWAT.

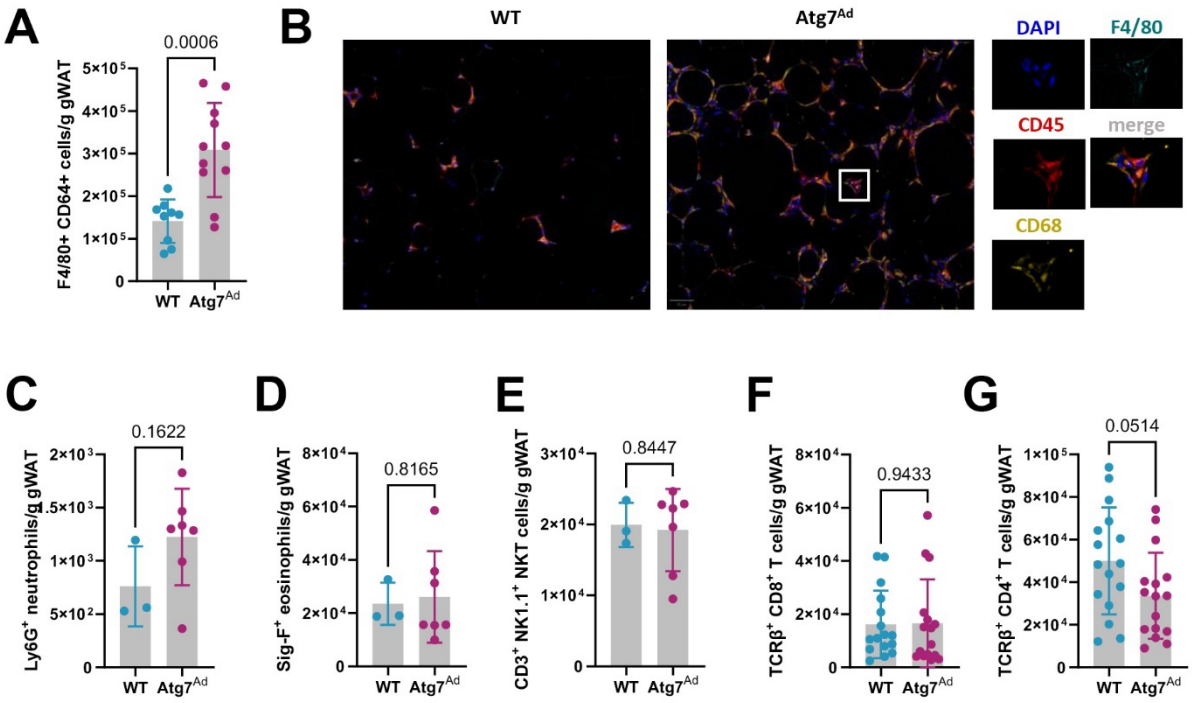

Figure 21: Autophagy limits macrophage expansion in gWAT. (A) Flow cytometry analysis of absolute F4/80$^+$ CD64$^+$ macrophage number in obese gWAT of WT and *Atg7^{Ad}* mice. (B) Representative immunofluorescence staining of WT and *Atg7^{Ad}* gWAT sections for F4/80 (turquoise), CD45 (red) and CD68 (gold). (C-G) Flow cytometry analysis of absolute numbers of immune cell subsets in WT and *Atg7^{Ad}* obese gWAT, including neutrophils (Ly6G$^+$) (C), eosinophils (Siglec-F$^+$) (D), NKT cells (CD3$^+$ NK1.1$^+$) (E), TCRβ$^+$ CD8$^+$ (F) and CD4$^+$ T cells (G). Data are presented as mean ± SD. Each data point represents one biological replicate. Statistical analysis by multiple unpaired t-test (A, C-G). Data merged from 3 independent experiments (A, F-G) or representative of 3 independent experiments (B-E).

In summary, our results demonstrate that adipocyte autophagy controls cell composition and abundance in a tissue-specific manner. Furthermore, it appears that immune cells, especially macrophages and CD4$^+$ T cells, dynamically respond to changes in adipocyte autophagy.

4.2.2 Macrophage fate is controlled by adipocyte autophagy

Given that the loss of adipocyte autophagy most profoundly impacts macrophages, we set out to investigate this immune cell subset more in detail. Considering that obesity is associated with an increase in pro-inflammatory macrophages (Trim and Lynch, 2022), we hypothesised that the observed accumulation of macrophages is a consequence of inflammation-promoted

macrophage recruitment and proliferation. Our hypothesis was supported by previous findings in adipocyte autophagy-deficient obese mice, where an increase in pro-inflammatory macrophage abundance was reported (Cai et al., 2018, Sakane et al., 2021).

To understand the identity of macrophages and how they change in relation to adipocyte autophagy, we separated macrophages using fluorescence-activated cell sorting (FACS) and performed transcriptomics (Fig 22A). While only DIO mice were analysed to reduce the experimental cost, both male and female mice were included to control for sex-dependent effects. Transcriptomics analysis was performed by Dr Amir H. Kayvanjoo from the Simon Lab in the Max-Delbrück Center for Molecular Medicine in the Helmholtz Association in Germany and Dr Lada Koneva at the Kennedy Institute of Rheumatology. The genotype explained 40 % of the observed variance (PC1) in the RNA-seq dataset (Fig 22B). As we observed a significant data separation based on the genotype, we analysed the dataset using the DEseq2 R package (Love et al., 2014) to assess differential gene expression resulting from the loss of adipocyte autophagy in DIO mice. Transcriptomics analysis revealed 1083 significantly differentially expressed genes (DEGs) between WT and *Atg7*^{Ad} ATMs (Fig 22C).

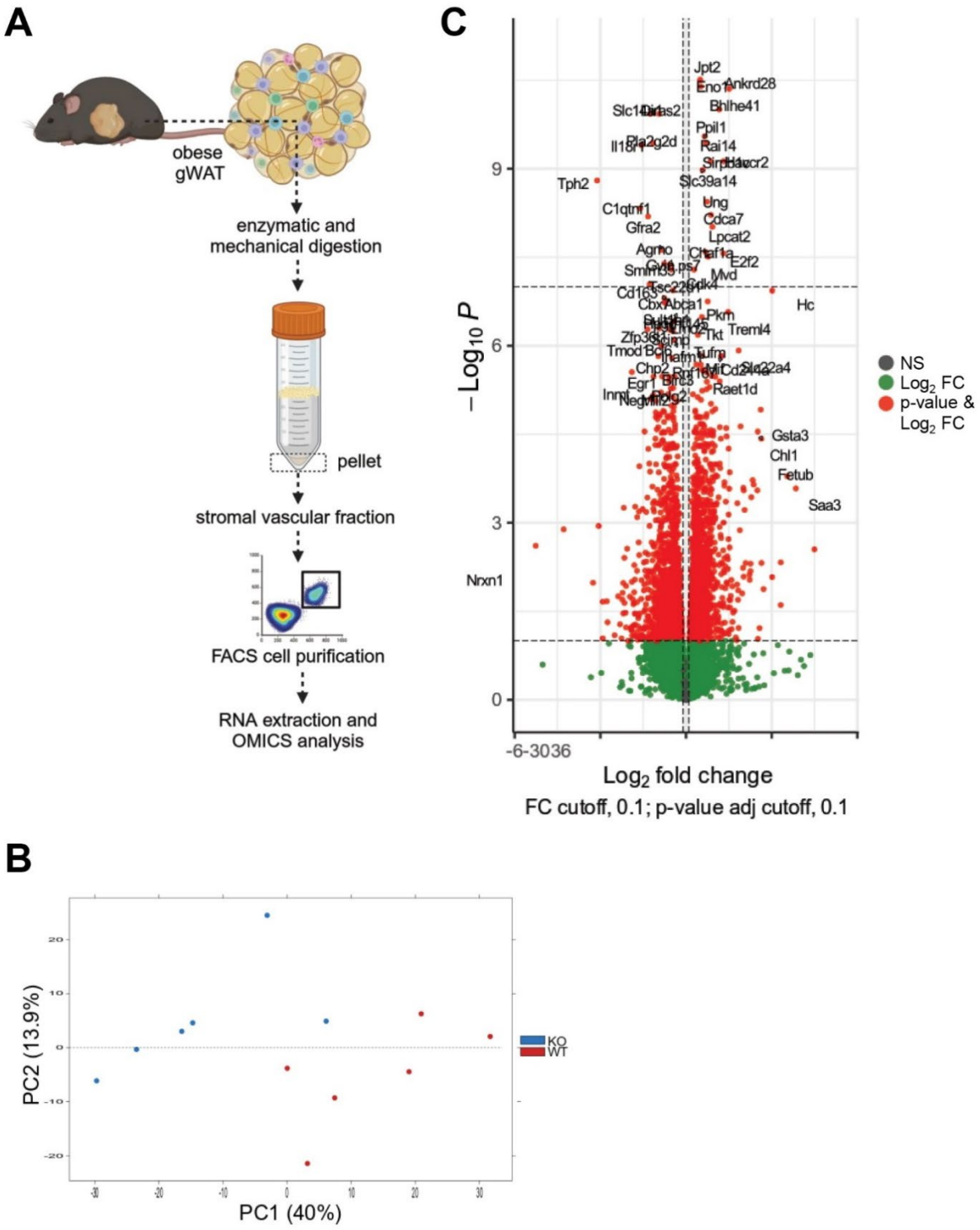

Figure 22: Loss of adipocyte autophagy dysregulates the macrophage transcriptome. (A) Schematic overview of experimental set-up for macrophage transcriptomics. Macrophages were isolated by FACS, and total RNA was extracted and sequenced. Created with BioRender.com. (B) PCA plot of individual samples. Each dot is a single biological replicate. (C) Volcano plot showing differentially expressed genes between macrophages isolated from WT and *Atg7*^{Ad} gWAT after 16 weeks of HFD feeding.

To reduce the complexity of transcriptomics datasets which revealed 515 downregulated and 568 upregulated DEGs, we performed gene ontology analysis using the clusterProfiler R package (Yu et al., 2012) (Fig 23A). Analysis of ATMs revealed that enriched gene sets downregulated upon the lack of adipocyte autophagy were involved in the activation of immune response and cytokine production (Fig 23B). On the other hand, enriched gene sets that were upregulated in ATMs of *Atg7*^{Ad} mice included proliferation, metabolic pathways, and interestingly, tissue remodelling processes (Fig 23C). Metabolic gene signatures between WT and *Atg7*^{Ad} ATMs highly suggested that in *Atg7*^{Ad} WAT, ATMs upregulated oxidative phosphorylation (OXPHOS) and pentose phosphate pathway (PPP), a metabolic shift that is commonly associated with tissue reparative macrophages (Russell et al., 2019, Galvan-Pena and O'Neill, 2014). In addition, while pro-inflammatory macrophages are mostly recruited to the tissue, ATMs that proliferate often display tissue-protective functions (Trim and Lynch, 2022, Matz et al., 2023). Furthermore, in *Atg7*^{Ad} ATMs we observed a drop in pathways associated with inflammatory cytokine secretion, including downregulation of a signature pro-inflammatory cytokine IL-1 (Fig 23B). A similar switch was previously reported for alveolar macrophages, where the upregulation of pro-inflammatory genes has been associated with a metabolic switch from OXPHOS to glycolysis and downregulation of proliferative capacity (Zhu et al., 2021). Altogether, these results suggested that loss of adipocyte autophagy in obese WAT leads to a shift to tissue-reparative ATM phenotype.

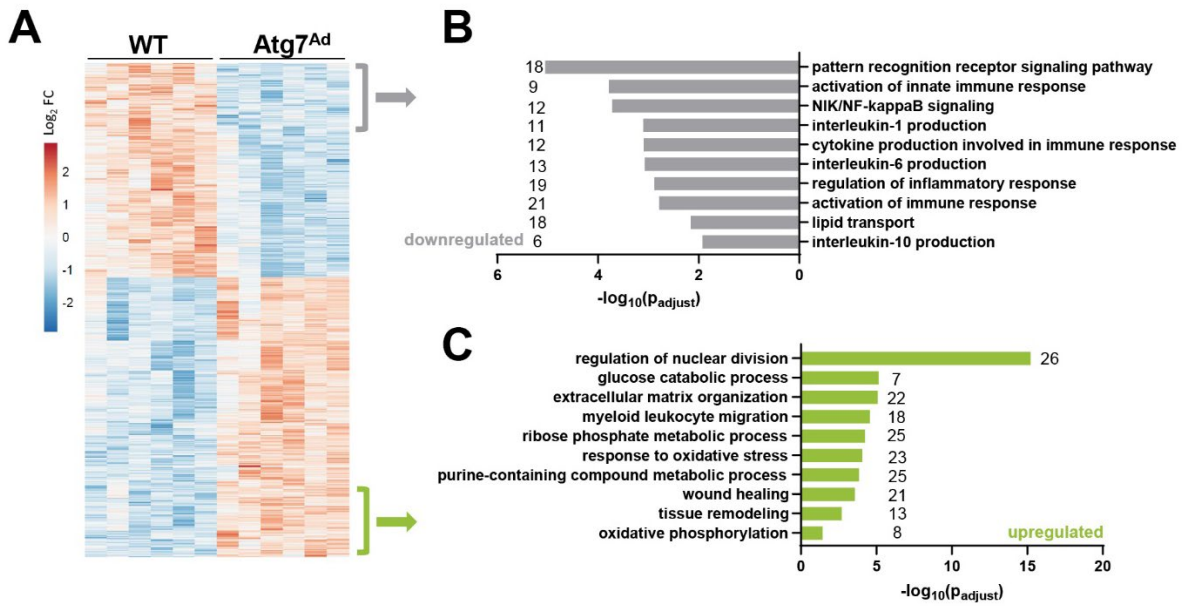

Figure 23: Macrophage transcriptome suggests a shift towards anti-inflammatory, tissue-reparative macrophages. (A) Hierarchical clustering of transcriptional profiles of the top 1000 differentially expressed genes in F4/80^{+} CD64^{+} macrophages extracted from WT and *Atg7*^{Ad} gWAT after 16 weeks of HFD. Colour denotes the $\log_2$ fold difference between WT and *Atg7*^{Ad} mice. (B-C) Enrichment gene ontology (GO) analysis of downregulated (B) or upregulated (C) biological processes in macrophages isolated from *Atg7*^{Ad} compared to WT gWAT. The number of genes identified for each term is labelled next to the bar. n = 6 mice.

To functionally validate transcriptomics findings which suggest a shift from pro- to anti-inflammatory, tissue-reparative phenotype, we assessed the *ex vivo* secretion of several cytokines associated with either state. We observed that *Atg7*^{Ad} compared to WT ATMs secreted considerably less pro-inflammatory (IL-1β and TNFα), pleiotropic (IL-6), as well as anti-inflammatory (IL-10) cytokines (Fig 24A-D). In addition, ATMs from *Atg7*^{Ad} mice upregulated transcription of key ECM remodelling genes, including *Col3a1* and *Mmp14* (Fig 24E). These macrophages, however, unexpectedly failed to upregulate TGFβ expression and secretion, at this timepoint at least (Fig 24E-F). This is in contrast to some reports suggesting that tissue repair macrophages decrease the secretion of pro- and anti-inflammatory cytokines at the expense of the pro-fibrotic TGFβ (Wynn and Vannella, 2016). To understand their proliferative behaviour and whether the increased abundance of ATMs was a consequence of proliferating tissue-resident macrophages or infiltrating monocytes, we transplanted congenic

CD45.1 bone marrow into WT or *Atg7*^{Ad} hosts. Reconstitution of bone marrow in *Atg7*^{Ad} mice revealed that the increased ATM abundance was due to monocyte-derived macrophages, which potentially gained proliferative capacity, and not self-renewing tissue-resident macrophages (Fig 24G).

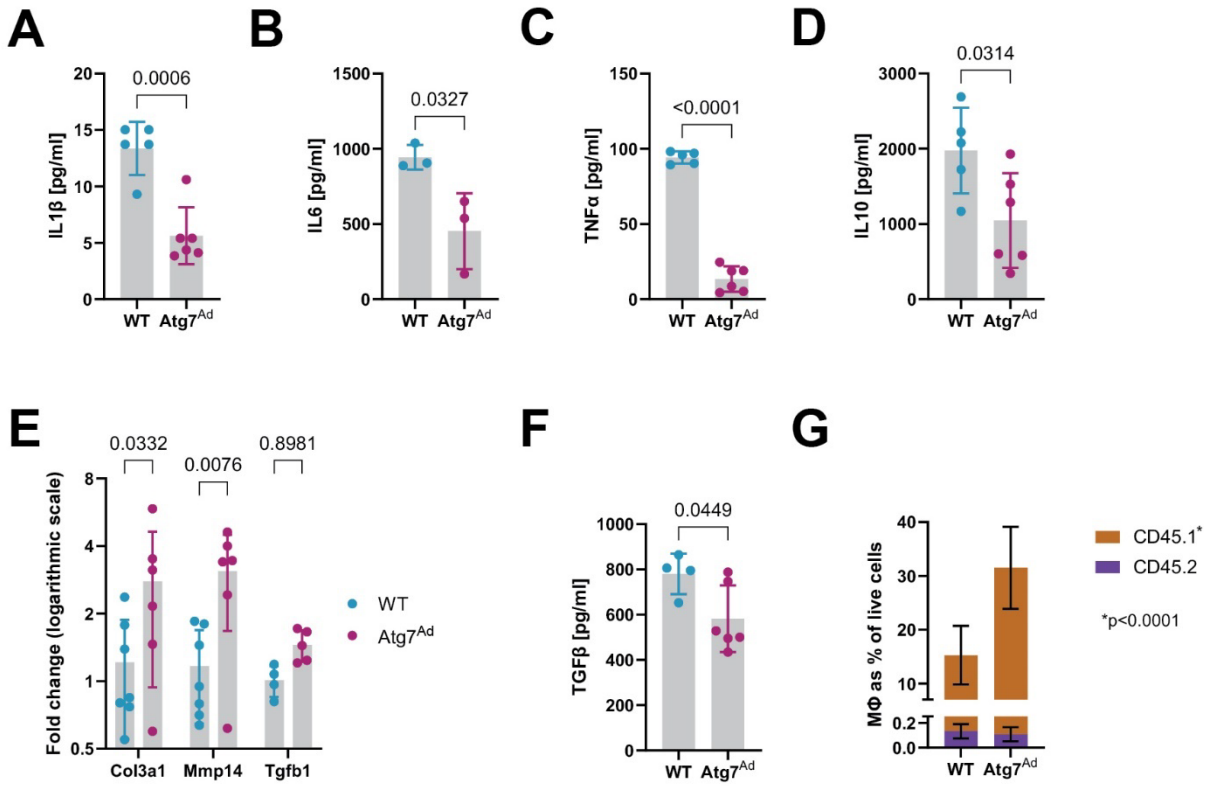

Figure 24: Macrophages in *Atg7*^{Ad} gWAT downregulate cytokine production, upregulate pro-fibrotic genes, and are monocyte-derived. (A-D) CD11b^{+} cells were isolated from gWAT of WT and *Atg7*^{Ad} mice after 16 weeks of HFD to measure the secretion of IL-1β (A), IL-6 (B), TNFα (C), and IL-10 (D). (E) Relative expression of ECM-related genes in sorted F4/80^{+} CD64^{+} macrophages from WT and *Atg7*^{Ad} gWAT. Expression was measured by qRT-PCR and is presented as a $\log_2$ fold difference. (F) Macrophages were isolated as in (A-D) to measure the secretion of TGFβ. (G) Frequency of CD45.1 (donor) or CD45.2 (host) congenic markers-labelled F4/80^{+} CD64^{+} macrophages in gWAT after adoptive transfer. CD45.1 bone marrow was transferred in CD45.2 WT and *Atg7*^{Ad} hosts. Adipocyte autophagy was deleted 25 days after the transfer, followed by HFD feeding for an additional 12 weeks. n = 6 mice. Representative of 2 independent experiments. Data are presented as mean ± SD. Each data point represents one biological replicate. Statistical analysis by unpaired t-test (A-D, F) or two-way ANOVA with Šídák multi comparisons test (E, G). Representative of 3 independent experiments unless otherwise stated.

Macrophage plasticity and heterogeneity are relatively young fields with new subsets being continuously identified, making a clear distinction highly complex. To make the differentiation between different ATM subtypes unbiased, we took advantage of two different approaches. First, we designed an extensive panel of macrophage-specific extracellular markers based on the existing literature and performed multidimensional flow cytometry analysis with Cytek Aurora. Unsupervised UMAP clustering overlaid with FlowSOM clusters (Kimball et al., 2018) identified 19 individual clusters inside the $CD11b^+$ population in gWAT (Fig 25A) . Differential analysis of cellular abundance within individual clusters revealed cluster 1 was significantly upregulated in *Atg7*^{Ad} gWAT, while clusters 4 and 10 were significantly downregulated in *Atg7*^{Ad} compared to WT gWAT (Fig 25B, D). This was further supported by cellular frequencies within individual clusters among the $CD11b^+$ population, indicating that indeed cluster 1 is highly abundant in *Atg7*^{Ad} gWAT (Fig 25C-D). As we have observed an increase in macrophage accumulation in *Atg7*^{Ad} gWAT (Fig 21A), we wondered about cluster 1 identity. Interestingly, by analysing the surface markers that define individual clusters, we found that cluster 1, in contrast to clusters 4 and 10, is characterised by a relatively low expression of antigen-presenting MHCII and a high expression of anti-inflammatory CD206 (Fig 25E). Furthermore, cluster 1 macrophages displayed a relatively high expression of macrophage-specific markers F4/80 and CD64, as well as low expression of CD9 and pro-inflammatory CD11c compared to the other two clusters that were reduced in *Atg7*^{Ad} gWAT (Fig 25E).

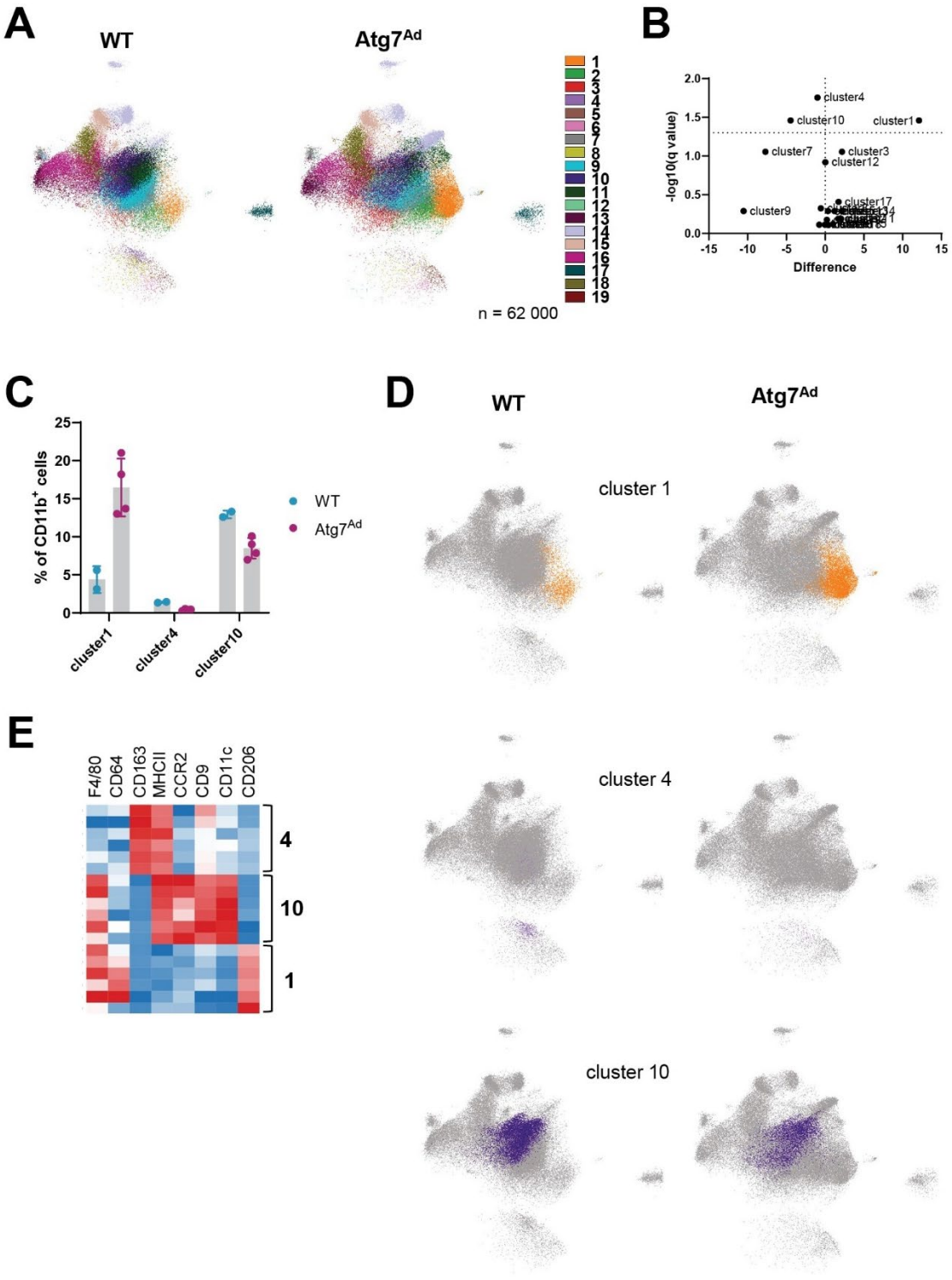

Figure 25: Macrophage phenotypic characterisation by Aurora reveals an accumulation of MHCII^{lo} cluster upon loss of adipocyte autophagy. (A) Representative UMAP of CD11b^{+} population in WT and Atg7^{Ad} gWAT after 16 weeks of HFD. n = 4. (B) Vulcano plot showing differences in cellular abundance within each cluster in *Atg7^{Ad}* compared to WT. (C) Frequencies of CD11b^{+} clusters 1, 4, and 10, which have been identified as significant in (B). Data are presented as mean ± SD. Each data point represents one biological replicate. (D)

Representative UMAPs displaying cellular abundance of clusters 1, 4, and 10 between WT and *Atg7*^{Ad}. (E) Heatmap of surface marker expression for differentially abundant clusters identified in (B). Each row corresponds to a single mouse. Legend: red = upregulated, blue = downregulated. Representative of 2 independent experiments.

Second, we took advantage of the published single-cell transcriptomics datasets from DIO mice to extract gene signatures of individual subsets (Sarvari et al., 2021, Chakarov et al., 2019, Jaitin et al., 2019). By applying the subtype-specific signature genes on our aggregated transcriptomics dataset, we identified that ATMs isolated from *Atg7*^{Ad} gWAT most closely aligned with LAM, P-LAM or CEM transcriptional signature (Fig 26A). To confirm these findings, we assessed the abundance of these ATM populations by flow cytometry. As currently no signature surface markers have been reported for P-LAM and CEM subtypes, we broadly screened published datasets for currently available macrophage markers (Sarvari et al., 2021). Genetic signatures of P-LAM and CEM suggested that P-LAM could be identified with the same markers as LAM, and CEM with the same markers as the PVM/VAM subset (Sarvari et al., 2021, Chakarov et al., 2019, Jaitin et al., 2019, Silva et al., 2019). The results showed that LAM and P-LAM (marked as CD9^{+} CD63^{+}) were, if anything, less frequent in *Atg7*^{Ad} gWAT compared to WT, and could therefore not explain the increase in macrophage numbers (Fig 26B-C). In contrast, we found that Lyve1^{hi} MHCII^{lo} ATMs, identifying pro-fibrotic CEM, accumulated more than 5-fold in *Atg7*^{Ad} gWAT (Fig 26D-E).

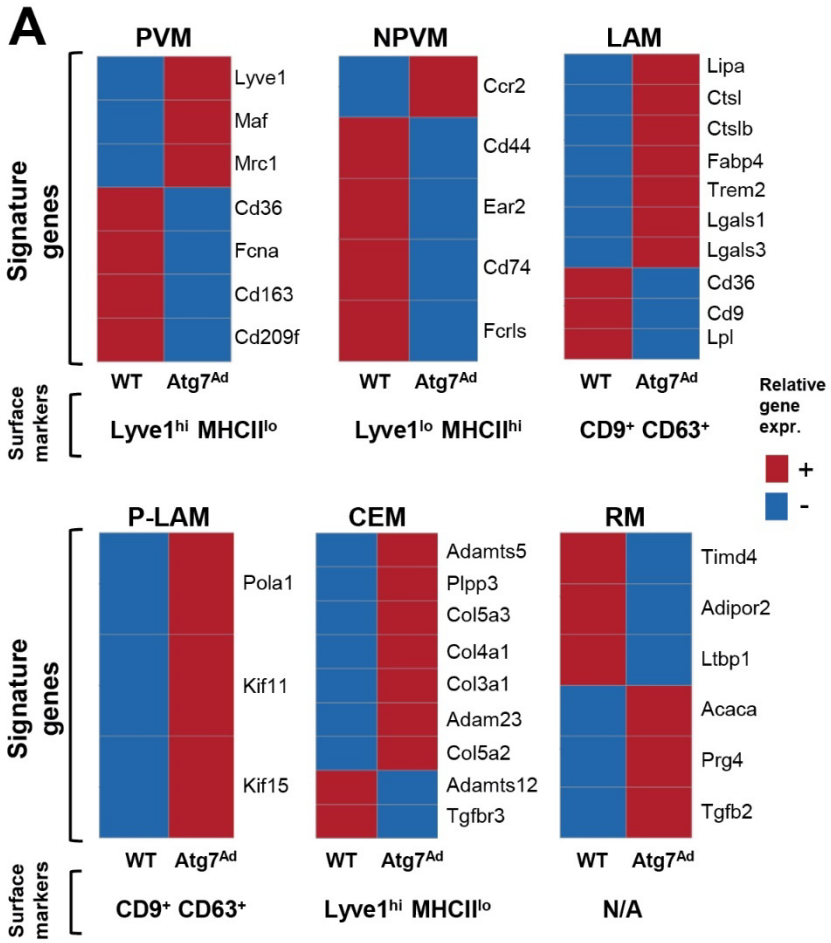
A
PVM
NPVM
LAM
Signature genes
Lyve1
Maf
Mrc1
Cd36
Fcna
Cd163
Cd209f
Ccr2
Cd44
Ear2
Cd74
Fcrls
Lipa
Ctsl
Ctslb
Fabp4
Trem2
Lgals1
Lgals3
Cd36
Cd9
Lpl
WT Atg7Ad
Surface markers
Lyve1hi MHCIIlo
Lyve1lo MHCIIhi
CD9+ CD63+
Relative gene expr.
+
-
P-LAM
CEM
RM
Pola1
Kif11
Kif15
Adamts5
Plpp3
Col5a3
Col4a1
Col3a1
Adam23
Col5a2
Adamts12
Tgfbr3
Timd4
Adipor2
Ltbp1
Acaca
Prg4
Tgfb2
CD9+ CD63+
Lyve1hi MHCIIlo
N/A

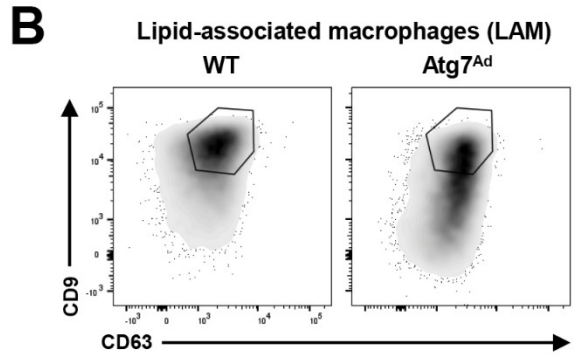
B
Lipid-associated macrophages (LAM)
WT
Atg7Ad
CD9
CD63

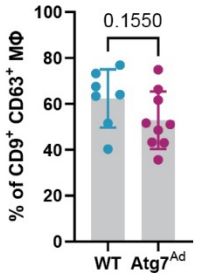
C
0.1550
% of CD9+ CD63+ MΦ
100
80
60
40
20
0
WT
Atg7Ad

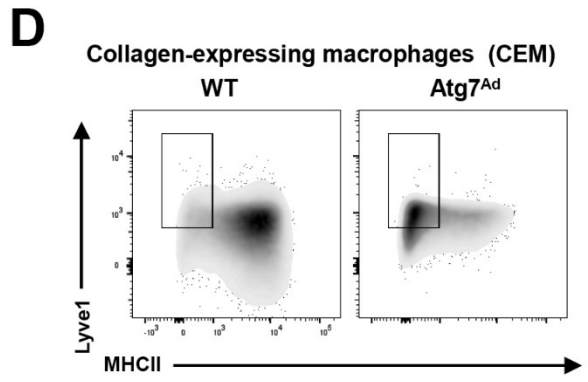
D
Collagen-expressing macrophages (CEM)
WT
Atg7Ad
Lyve1
MHCII

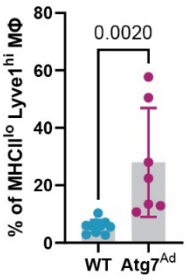
E
0.0020
% of MHCIIlo Lyve1hi MΦ
80
60
40
20
0
WT
Atg7Ad

Figure 26: Assessment of macrophage heterogeneity with single-cell transcriptomics data mining identifies a tissue-reparative phenotype in *Atg7^{Ad}* gWAT. (A) Heatmaps display macrophage gene expression profiles of signature genes associated with reported macrophage subsets and are based on macrophage transcriptomics data. Data were aggregated by the sample's mean expression for each genotype. PVM = perivascular-like macrophages; NPVM = non-perivascular-like macrophages; LAM = lipid-associated macrophages; P-LAM = proliferating LAM; CEM = collagen-expressing macrophages; RM = regulatory macrophages. (B-E) Representative flow cytometry plots and frequency quantification of CD63^{+} CD9^{+} (B-C) and MHCII^{lo} Lyve1^{hi} (D-E) macrophages. Data are presented as mean ± SD. Each data point represents one biological replicate. Statistical analysis by unpaired t-test (C, E). Representative of 3 independent experiments.

Considering that fibrosis developed between week 6 and week 9 of HFD feeding, we next asked whether the accumulation of tissue-reparative macrophages coincided with the onset of fibrosis. Furthermore, we wanted to understand whether the observed increase in macrophage abundance is primarily due to pro-inflammatory macrophages accumulating in obese gWAT or whether accumulated macrophages are directly polarised towards the pro-fibrotic phenotype in *Atg7^{Ad}*. This differentiation is important considering the complex sequence and kinetics of inflammation and fibrosis. While some studies claim that fibrosis is solely a consequence of excessive inflammation, other studies suggest that fibrosis can develop early during obesity onset and independent of inflammation (Reggio et al., 2013, Halberg et al., 2009, Wynn, 2007). By assessing the number of ATMs in obese gWAT after 6 and 9 weeks of HFD, we found that macrophages significantly accumulate by 9 weeks compared to 6 weeks of HFD in WT mice (Fig 27A). Strikingly, ATM accumulation in *Atg7^{Ad}* gWAT was even more pronounced during the three weeks and almost 3-fold higher compared to the WT gWAT (Fig 27A). In addition, while tissue-reparative MHCII^{lo} ATMs only contribute 20 % to the total macrophage pool at 6 weeks of HFD feeding, they attribute 30 % of total ATMs by 9 weeks of HFD in *Atg7^{Ad}* gWAT (Fig 27B). While MHCII^{lo} macrophages notably increase in *Atg7^{Ad}* gWAT, they seem to rather decline in WT gWAT by 9 weeks of HFD feeding. These data indicate that the ATM accumulation in *Atg7^{Ad}* obese gWAT is concomitant with the fibrosis onset and suggest that rather than switching from a pro-inflammatory phenotype, ATMs in *Atg7^{Ad}* mice are directly polarised to tissue-reparative phenotype.

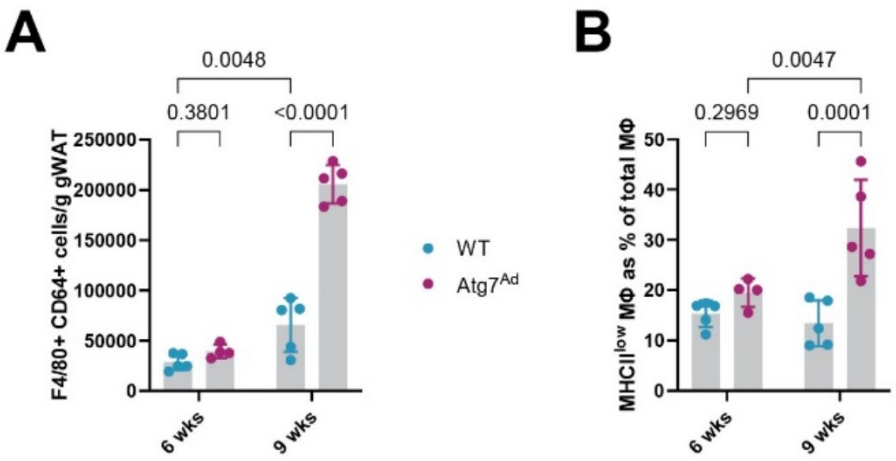

Figure 27: Autophagy limits macrophage expansion and controls tissue-reparative phenotype during early weight gain. (A-B) Flow cytometry analysis of absolute F4/80^{+} CD64^{+} macrophage number (A) and MHCII^{lo} macrophages frequency (B) in gWAT of WT and *Atg7^{Ad}* mice after 6 and 9 weeks of HFD feeding. Data are presented as mean ± SD. Each data point represents one biological replicate. Statistical analysis by two-way ANOVA with Fisher test (A, B). Representative of 2 independent experiments.

Taken together, we found that adipocyte autophagy in gWAT not only profoundly impacts ATM abundance but also their fate and function. When absent, ATMs polarise to a tissue-reparative phenotype, characterized by the signature surface markers, metabolic adaptation, expression of ECM genes and a drop in cytokine production.

4.2.3 Fibrosis of gWAT could be mediated by ATMs

Fibrosis onset and progression in multiple tissues and organs have traditionally been viewed as a consequence of inflammation (Henderson et al., 2020). However, it is now believed that immune cells execute ECM-modulating functions independent of inflammation (Marcelin et al., 2022). We therefore asked if tissue repair macrophages that we have phenotypically characterised, also have a functional role in exacerbated gWAT fibrosis in *Atg7^{Ad}* mice.

To address this question, we took advantage of multiple macrophage depletion models, which can reduce macrophage abundance in response to chemical compounds or antibodies.

Removal of resident macrophages enables a better understanding of their function. The first model we tested was clodronate-mediated macrophage depletion. This model takes advantage of liposomes, i.e., concentric phospholipid bilayer vesicles, which serve as a delivery vehicle for clodronate. Intracellular accumulation of clodronate through phagocytic activity of macrophages leads to apoptosis, resulting in a temporary controlled systemic or local macrophage depletion (Van Rooijen and Sanders, 1994). To deplete macrophages in gWAT of *Atg7*^{Ad} obese mice, we administered clodronate intraperitoneally once a week, which allowed us for a gradual depletion that could be maintained over a longer period. Treatment was commenced after 8 weeks of HFD feeding, an experimentally determined time window just before the onset of fibrosis (Fig 11) and a shift in macrophage abundance and cellular phenotype (Fig 27). Depletion of macrophages early in the fibrosis progression greatly diminishes its severity in other models (Duffield et al., 2005). Unexpectedly, clodronate administration resulted in severe outcomes, with several mice experiencing sudden death following the second administration of clodronate (Fig 28A). This occurred predominantly in male mice and was more predominant in the *Atg7*^{Ad} genotype but independent of the drug batch (Fig 28A). Females generally tended to experience less severe symptoms compared to males (data not shown). Studying the male mice that survived the 4-week treatment, we observed no difference in weight loss (Fig 28B). The macrophage abundance upon clodronate treatment was about 2-fold lower compared to PBS-treated controls (Fig 28C). By depleting macrophages, we observed no impact on gWAT fibrosis in female *Atg7*^{Ad} obese mice (data not shown). In contrast, however, clodronate-treated male *Atg7*^{Ad} obese mice showed a profound change in gWAT morphology and reduction in fibrosis (Fig 28D-E). Furthermore, the tissue morphology more closely resembled WT gWAT, showing fewer infiltrated cells and a more homogenous adipocyte structure (Fig 28D-E).

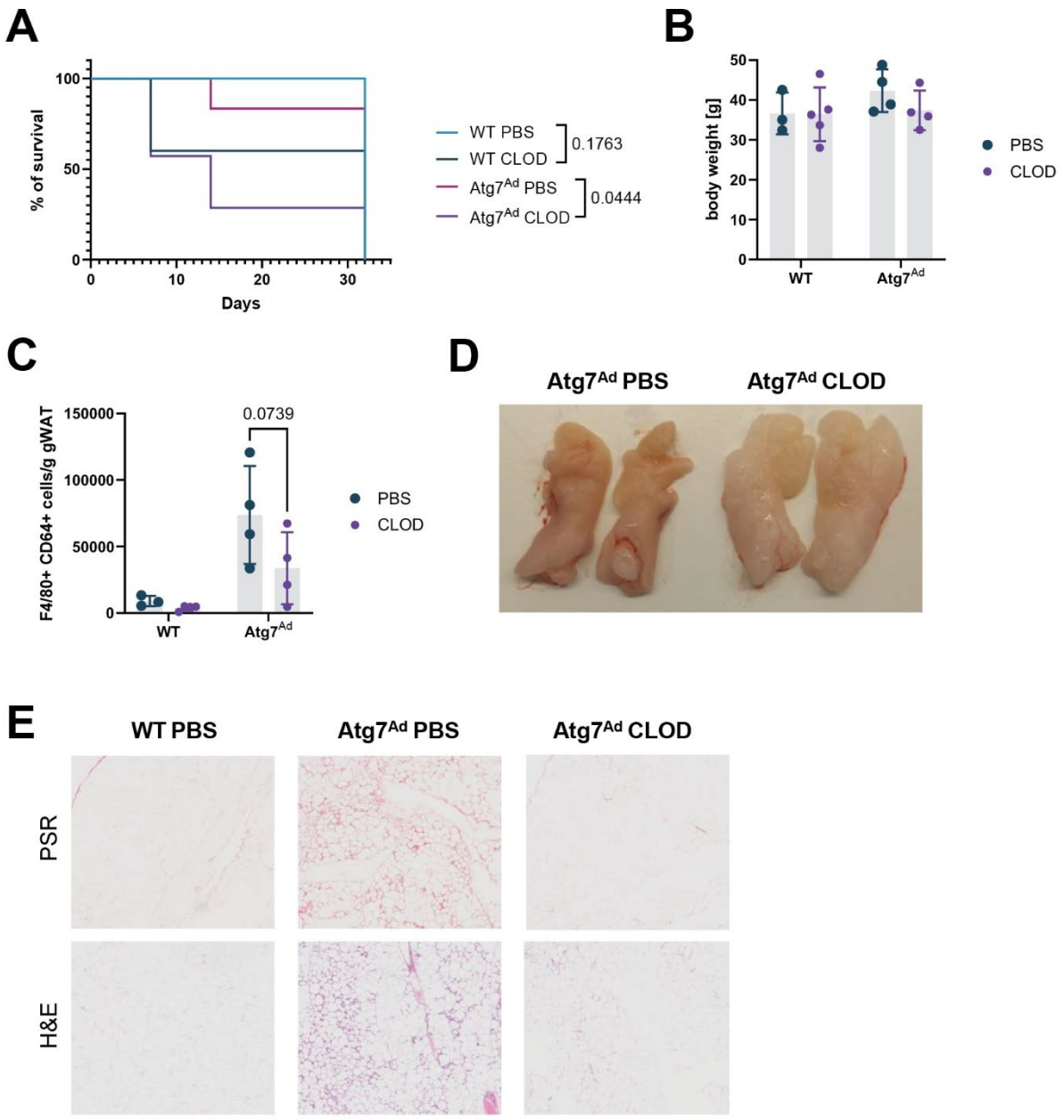

Figure 28: Clodronate-induced macrophage depletion is highly toxic but appears to limit fibrosis development in DIO male mice. (A) The proportion of survival of male WT and *Atg7*^{Ad} mice treated with clodronate over 4 weeks after 8 weeks on HFD. (B) Body weight after 4 weeks of clodronate treatment. (C) Flow cytometry analysis of F4/80^{+} CD64^{+} macrophage number in gWAT after clodronate treatment. (D) Photograph of gWAT fat pads of *Atg7*^{Ad} mice treated with PBS control or clodronate from a single experiment. (E) Representative PSR and H&E staining of gWAT harvested from WT and *Atg7*^{Ad} mice on PBS or clodronate treatment from a single experiment. Data are presented as mean ± SD. Each data point represents one biological replicate. Statistical analysis by log-rank (Mantel-Cox) test (A) or two-way ANOVA with Šídák multi comparisons test (C). Representative of 2 independent experiments unless otherwise stated.

Observing a noteworthy impact of macrophage depletion on gWAT fibrosis in obese *Atg7*^{Ad} males, we aimed to further validate these outcomes. Due to welfare considerations, this experiment could not be repeated. Therefore, we next decided to take advantage of monoclonal antibody-based macrophage depletion models. For this, we selected antibodies raised against macrophage colony-stimulating factor 1 receptor (α-CSF1R) and monocyte chemoattractant protein 1 (MCP1), also known as CCL2 (α-CCL2). Both antibodies have been reported to deplete tissue macrophages through distinct mechanisms and block respective proteins *in vivo* (Gordon et al., 2017, Singh et al., 2014). While CSF1R regulates monocyte and macrophage proliferation and differentiation, CCL2 acts as a chemokine, regulating the migration and infiltration of monocytes (Wculek et al., 2022). As we observed an increased accumulation of ATMs that were monocyte-derived, we hypothesised that these blocking antibodies would allow us to target two different mechanisms of ATM accumulation and ultimately their tissue-specific function. The antibody administration protocol was similar to clodronate liposomes' treatment and based on previous reports (Chen et al., 2021) and oral communication with experts in the field (Dr Tal Arnon, Dr Sarah Spear, Dr Elvira Mass). To test the protocol in our facility, we dosed two lean mice with 35 μg (α-CSF1R) or 5 μg (α-CCL2) of antibody per gram of body weight twice over a 4-week treatment window and observed a substantial depletion of ATMs (data not shown). Surprisingly, however, following the same protocol with the respective antibodies in HFD-fed obese mice resulted in negligible ATM depletion in gWAT (Fig 29A-B). Similar observations were made in iWAT and spleen (data not shown), indicating that the intraperitoneal administration of blocking antibodies failed to induce systemic macrophage depletion. Due to welfare constraints, we decided to not repeat the antibody-mediated macrophage depletion model.

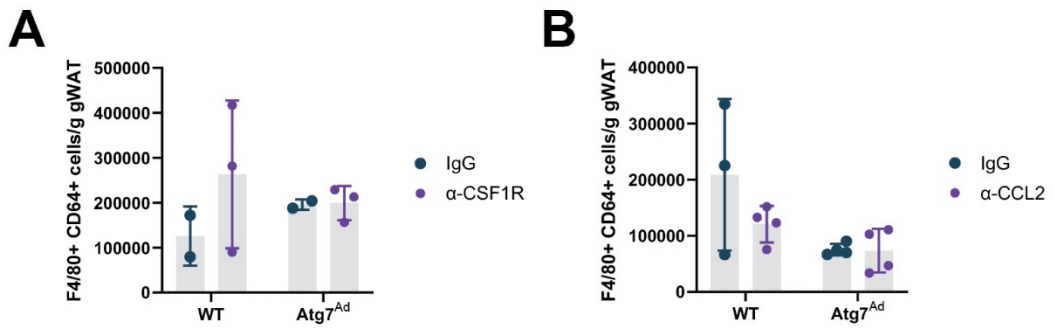

Figure 29: Monoclonal antibody-based macrophage depletion models do not sufficiently deplete ATMs in obese gWAT. (A-B) Flow cytometry analysis of F4/80$^+$ CD64$^+$ macrophage number in WT and *Atg7^{Ad}* gWAT after α-CSF1R (A) or α-CCL2 (B) treatment and 12 weeks of HFD feeding. WT and *Atg7^{Ad}* mice were treated with α-CSF1R (A) or α-CCL2 (B) antibodies which were administered intraperitoneally following 8 weeks on HFD twice, one week apart. Tissues were collected and analysed after 12 weeks of HFD. Each antibody administration was 35 µg (α-CSF1R) or 5 µg (α-CCL2) per gram of body weight. Data are presented as mean ± SD. Each data point represents one biological replicate. Representative of 3 (A) or one (B) independent experiment.

While clodronate-mediated macrophage depletion showed promising outcomes and indicated that ATMs may play a role in *Atg7^{Ad}* gWAT fibrosis, the high toxicity of clodronate, combined with the low efficiency of macrophage reduction in monoclonal antibody models, limited our ability to fully define the specific role of tissue-reparative macrophages in gWAT fibrosis in *Atg7^{Ad}* obese mice. Consequently, the precise contribution of these macrophages in our model remains unclear.

4.2.4 T cell fate is controlled by adipocyte autophagy

In addition to changes in macrophage abundance and function, we observed that adipocyte autophagy also impacts CD4$^+$ T cell abundance (Fig 21G). Changes in macrophage fate and function commonly shape T cell populations through cytokine secretion and antigen presentation (Jacks and Lumeng, 2024). We hypothesised that the decrease in CD4$^+$ T cells is a consequence of a profound shift in macrophage phenotype. Furthermore, as CD4$^+$ T cells are well-known to impact CD8$^+$ T cell priming and activation (Castellino and Germain, 2006),

we wondered whether their decrease also impacts $CD8^+$ T cells, despite no change in their abundance.

To understand how adipocyte autophagy modulates T cell populations, we sorted $CD4^+$ and $CD8^+$ T cells with FACS and performed RNA-seq as described above. In the $CD4^+$ T cell RNA-seq dataset PCA1 explained 18.3 % of sample variability, while it explained 20.5 % of the variance in the $CD8^+$ T cell subset (Fig 30A-B). Differential gene expression analysis between WT and *Atg7*^{Ad} DIO mice revealed 201 DEGs within the CD4+ T cell subset and 464 DEGs within the CD8+ T cell subset (Fig 30C-D). As we observed a batch effect whereby the separation by genotype failed to explain the sample variance (Fig 30A-B), gene ontology analysis revealed no meaningful enriched gene sets. To try and understand how both subsets change in response to loss of adipocyte autophagy, we overlapped DEGs between the two T cell subsets (Fig 30E). We found 18 genes upregulated in $CD4^+$ and $CD8^+$ subsets in *Atg7*^{Ad} gWAT, predominantly relating to oxidative stress and damage (*Mgst1, Morc1, Fth1, Mgme, Prdx1*) and T cell activation (*Cd276, Vtcn1*) (Fig 30E-F).

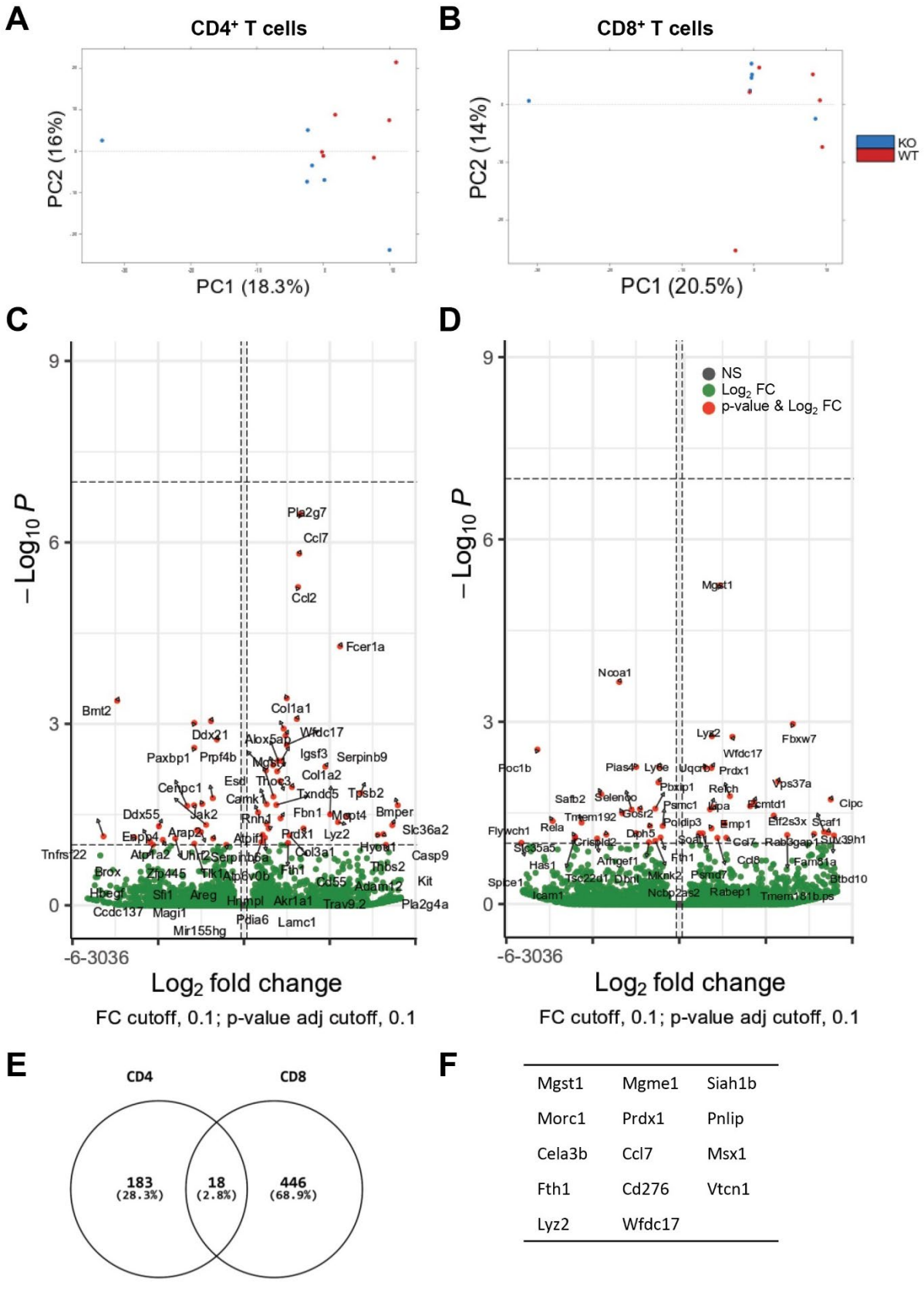

Figure 30: Loss of adipocyte autophagy dysregulates CD4⁺ and CD8⁺ T cell transcriptome. (A-B) PCA plot of individual samples for CD4⁺ (A) and CD8⁺ (B) T cell subsets.

Each dot represents a single biological replicate. (C-D) Volcano plots showing differentially expressed genes among $CD4^+$ (C) and $CD8^+$ (D) T cell subsets isolated from WT and *Atg7*^{Ad} gWAT after 16 weeks of HFD feeding. (E) Overlap of DEGs identified in $CD4^+$ and $CD8^+$ cells. (F) A list of overlapping DEGs. Note that 4 DEGs are excluded from the visualisation as they encode immunoglobulin (B cell contamination). n = 6 mice.

T cell function is often related to their activation in response to antigen stimulation (Castellino and Germain, 2006). Activation of naïve cells towards the effector and later memory stage can be characterized by the expression of CD44 and CD62L activation markers. Naïve T cells are identified as $CD44^{lo}$ $CD62L^{hi}$, effector as $CD44^{hi}$ $CD62L^{lo}$, and memory T cells as $CD44^{hi}$ $CD62L^{hi}$ populations (Shirakawa et al., 2016). To further understand how T cells change their phenotype and whether it relates to the observed transcriptome change, we designed a broad panel of T cell-specific extracellular and intracellular markers based on the published literature. Multidimensional flow cytometry data collected by Aurora was clustered into 21 individual $TCR\beta^+$ clusters by UMAP and FlowSOM (Kimball et al., 2018) (Fig 31A). Differential analysis of cluster cellular abundance identified cluster 18 as significantly upregulated in *Atg7*^{Ad} compared to WT gWAT, and clusters 5 and 19 as significantly downregulated ones (Fig 31B). This finding was further supported by cluster cellular frequencies within the $TCR\beta^+$ population (Fig 31C-D). Analysis of signature T cell markers revealed that cluster 5 corresponded to $CD4^+$ T cells, while clusters 18 and 19 were $CD8^+$ T cells (Fig 31E). We found that the two clusters downregulated in *Atg7*^{Ad}, namely clusters 5 and 19, shared a similar marker profile characterised by $CD44^{med}$ $CD62L^{hi}$ $TCF1^{hi}$ $Ly108^{hi}$ (Fig 31E). In contrast, the cluster 18, upregulated in *Atg7*^{Ad} mice, displayed $CD44^{hi}$ $CD62L^{lo}$ $PD1^{hi}$ $CD69^{lo/med}$ $CD39^{hi}$ $EOMES^{hi}$ signature (Fig 31E). Notably, the combination of these signature factors is commonly used to describe T cell exhaustion (Zhang et al., 2021a). Exhausted T cells (Tex) are formed through distinct consecutive phases. A high expression of TCF and Ly108 denotes the early development phase, while a high expression of PD1 and CD39 denotes terminal exhaustion (Beltra et al., 2020, Chen et al., 2019). Downregulated clusters 5 and 19 can thus be likely identified as proliferative circulating/precursor Tex, with a signature of $Ly108^+$ $CD69^-$ $TCF1^{hi}$.

On the other hand, upregulated cluster 18 is likely a terminally exhausted Tex cell cluster, characterised by PD1^{hi} CD39^{hi} Ly108^{-} CD69$^{med/hi}$ EOMES^{hi}. These results altogether suggested that adipocyte autophagy prevents the conversion of Tex to a terminally exhausted phenotype.

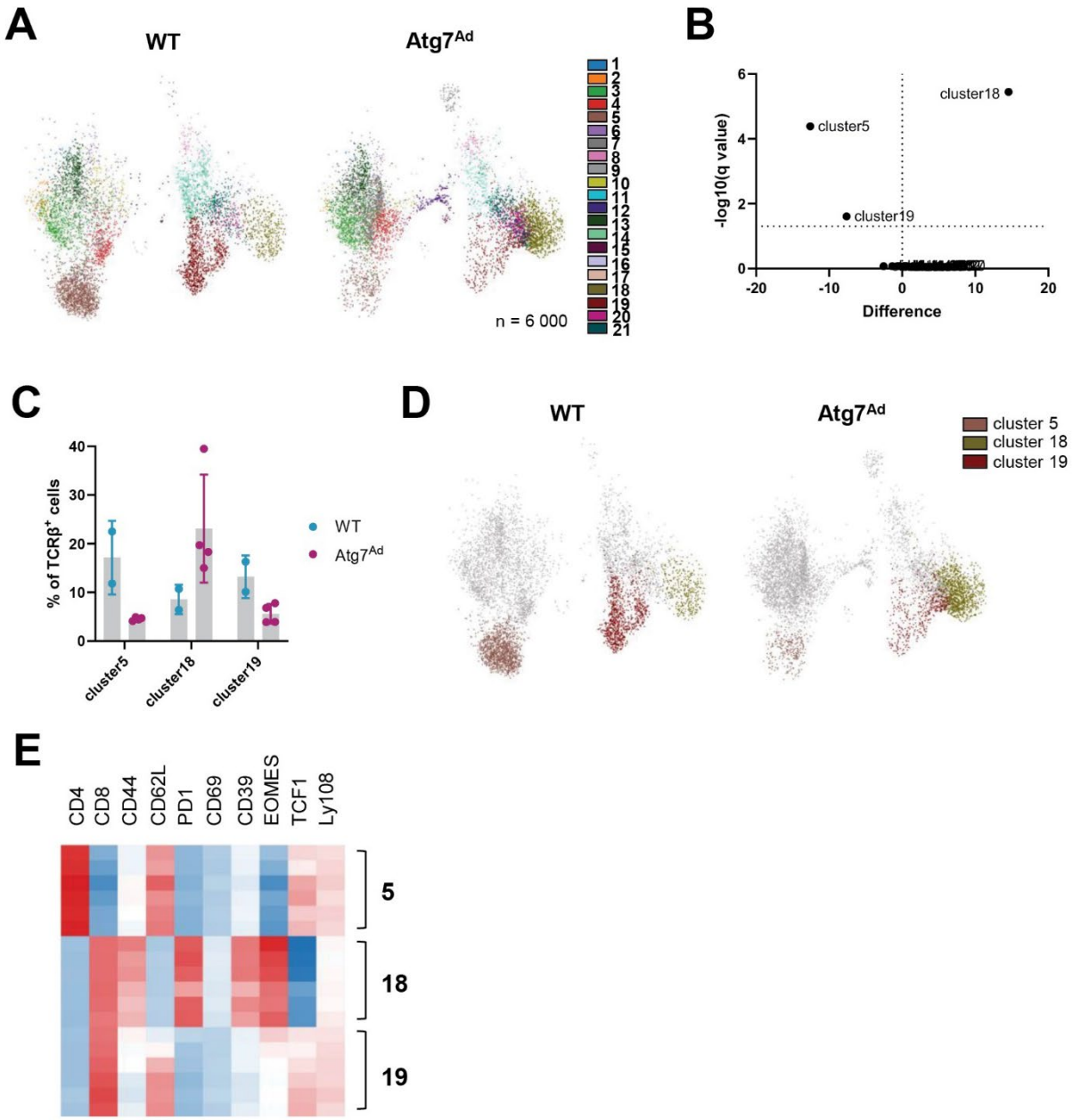

Figure 31: T cell phenotypic characterisation by Aurora reveals an accumulation of exhausted CD8^{+} T cell cluster upon loss of adipocyte autophagy. (A) Representative UMAP of TCRβ^{+} population in WT and Atg7^{Ad} gWAT after 16 weeks of HFD. n = 4 mice. (B) Vulcano plot showing differences in cellular abundance within each cluster in *Atg7^{Ad}* compared to WT. (C) Frequencies of TCRβ^{+} clusters 5, 18, and 19, which have been identified as significant in (B). Data are presented as mean ± SD. Each data point represents one biological

replicate. (D) Representative UMAP displaying cellular abundance of clusters 5, 18, and 19 between WT and *Atg7*^{Ad}. (E) Heatmap of surface marker expression for differentially abundant clusters identified in (B). Each row corresponds to a single mouse. Legend: red = upregulated, blue = downregulated. Representative of 3 independent experiments.

To further validate these observations, we manually gated conventional flow cytometry datasets. We observed a shift towards a CD44^{lo} population in both CD4^{+} and CD8^{+} T cells in *Atg7*^{Ad} obese gWAT (Fig 32A-D). As the expression of CD62L remained comparable, CD4^{+} and CD8^{+} T cells likely acquire either more naïve-like or memory-like properties in the absence of adipocyte autophagy. Since transcriptomics and Aurora analyses of T cells revealed dysregulation of several activation and exhaustion markers, it is likely that these cells display stem-like properties but are exhausted (Fig 30 and 31). To understand whether CD44^{lo} cells indeed become exhausted, we assessed the expression of a major regulator of T cell exhaustion, PD-1, by flow cytometry. Although we saw no differences in PD-1 expression among the general CD4^{+} and CD8^{+} populations (data not shown), PD-1 was highly upregulated within the CD44^{lo} population of both subsets when adipocyte autophagy was depleted (Fig 32E-H). While PD-1 upregulation indicates that these cells are exhausted, a simultaneous CD44 downregulation suggests a non-classic and unbalanced activation state of T cells in gWAT. Similar to observations made in macrophages, T cell exhaustion was documented to occur concomitantly with the onset of fibrosis, i.e., between week 6 and week 9 of HFD feeding (data not shown).

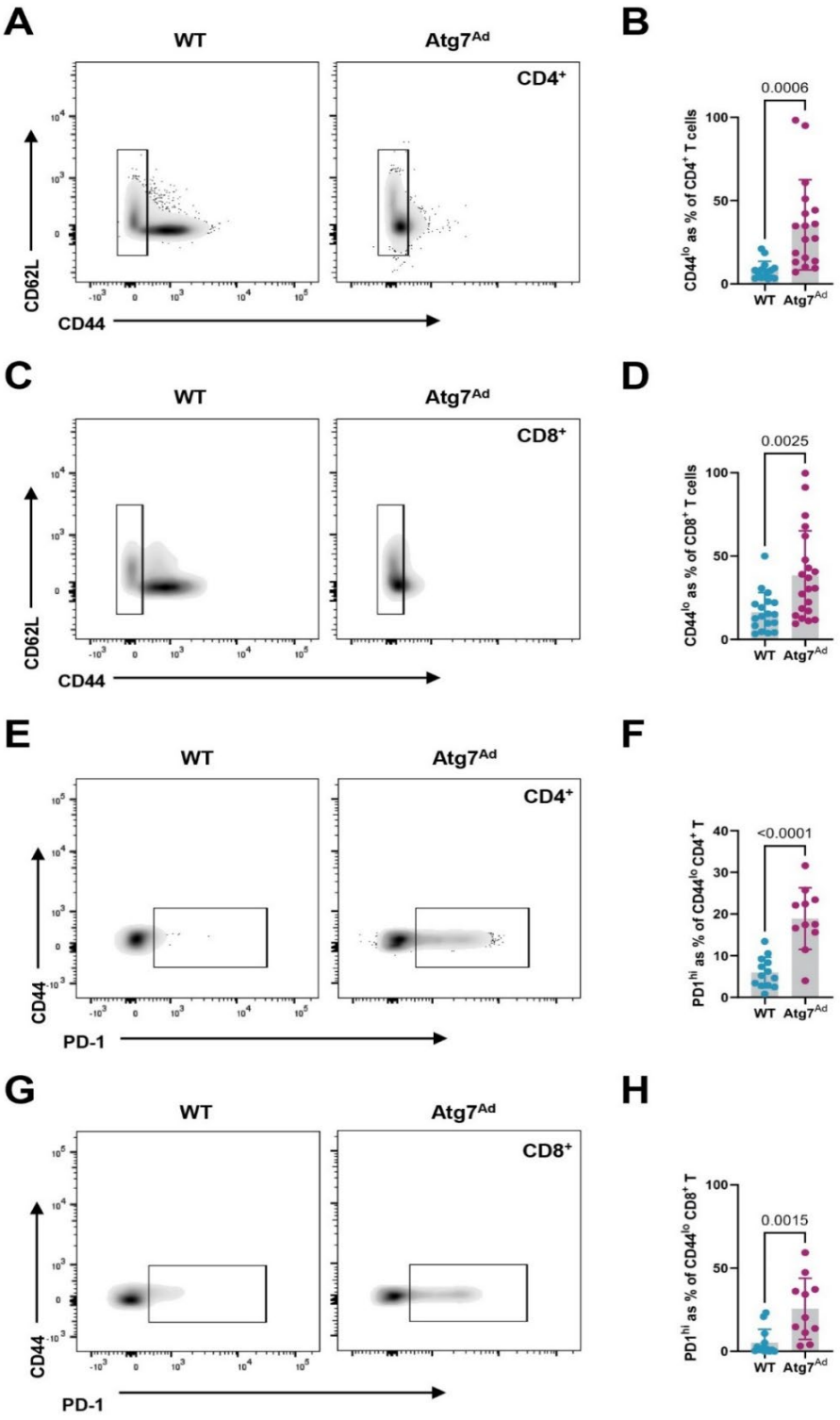

Figure 32: Adipocyte autophagy limits T cell exhaustion. (A-D) Representative flow cytometry plots of CD44 and CD62L expression between WT and *Atg7^{Ad}* gWAT within CD4^{+} (A) and CD8^{+} (C) T cell subset. Flow cytometry analysis of CD44^{lo} cell frequency within CD4^{+} (B) and CD8^{+} (D) T cells isolated from mice fed HFD for 16 weeks. (E-H) Representative flow cytometry plots of CD44 and PD1 expression between WT and *Atg7^{Ad}* gWAT within CD44^{lo} CD4^{+} (E) and CD8^{+} (G) T cell subset. Flow cytometry analysis of PD1^{hi} CD44^{lo} cell frequency

within $CD44^{lo}$ $CD4^{+}$ (F) and $CD8^{+}$ (H) T cells isolated from mice fed HFD for 16 weeks. Data are presented as mean ± SD. Each data point represents one biological replicate. Statistical analysis by unpaired t-test (B, D, F, H). Data are merged from 3 independent experiments.

To summarize, we have found that adipocyte autophagy not only impacts T cell homing to the gWAT but also supports their viability and activation state, ultimately preventing their exhaustion.

4.3 Discussion

4.3.1 Autophagy shapes immune cell accumulation in a tissue-specific manner

Excessive pericellular fibrosis positively correlated with a notable increase in nuclear density, which was specific for gWAT. We found that immune cell accumulation is the major contributing factor, with macrophage numbers doubling between obese WT and *Atg7*^{Ad} mice. Adipocyte autophagy has been previously reported to limit CLS formation and macrophage infiltration under both control and HFD diets (Sakane et al., 2021, Cai et al., 2018). Our results, however, failed to recapitulate a well-accepted increase in macrophage infiltration in obese versus lean mice (Biswas and Mantovani, 2012, Jaitin et al., 2019, Mathis, 2013, McNelis and Olefsky, 2014), and we found fewer macrophages present per gram of obese compared to lean WT gWAT. These disparities represent a noteworthy limitation of our study. The failure to recapitulate the phenotype between lean and obese WT WAT could potentially be explained by differences in digestion protocols, surface markers used for macrophage assessment, normalisation to tissue weight, as well as by general model variations, including diet duration and housing conditions. Experimental reproducibility in inflammation research is often impacted by variations in specific pathogen-free housing, microbiota composition, and diet, which are different between individual facilities (Moore and Stanley, 2016). While the composition of the reported chow diets used to feed lean mice is often not well defined in publications, we tried to minimise the confounding effects by using standard commercially available diets to feed the mice, with NCD sucrose matched to the HFD. Regardless, neither

chow (data not shown) nor standardized NCD could reproduce differences in macrophage accumulation observed between lean and obese WT mice. In addition, groups reporting an increase in macrophage infiltration would often only rely on a single macrophage marker, such as F4/80, which has been reported to also express on other immune cells, including eosinophils and dendritic cells (Dos Anjos Cassado, 2017). Due to this, we always used it in conjunction with another macrophage-specific marker, CD64, while simultaneously excluding other subsets in our gating strategy. Disparities in the macrophage number per gram of WAT could therefore to some extent also result from the reported overestimation. As we have continuously observed a reproducible increase in ATM abundance between obese WT and *Atg7*^{Ad} mice, as well as increased CLS formation between lean and obese WT gWAT across several C57BL/6J strains in our facility, we decided to accept this limitation and proceed with our study.

While we observed profound changes in gWAT, iWAT morphology appeared insensitive to adipocyte autophagy deletion. We noted that adipocyte autophagy loss primarily impacted the immune cell population. The absence of any cellular changes in iWAT could be explained by the fact that gWAT is more prone to immune cell infiltration and therefore has a much higher leukocyte and macrophage content (Marcelin et al., 2022). In line with this, a higher immune cell abundance in WT gWAT compared to iWAT was observed. It has been suggested that gWAT immune cell abundance is an evolutionary adaptation, having a protective role against intraperitoneal pathogens and abdominal injuries (Sakers et al., 2022). Interestingly, studying nuclear density increase in a tissue-specific manner also suggested that iWAT has a generally higher nuclear density compared to gWAT. While this could generally be explained by iWAT having more active adipogenesis and angiogenesis (Marcelin et al., 2022), the numbers of endothelial cells and adipocyte precursors suggest this is unlikely. High cellular abundance in iWAT could potentially be attributed to ASPCs, highly plastic cells characterised by CD29 and Sca-1 expression. These have been reported to be 8-fold more abundant in iWAT compared

to gWAT and hold great potential in regenerative research (Joe et al., 2009, Ferrero et al., 2020). Further research would be necessary to confirm these assumptions.

4.3.2 Macrophages obtain a tissue-reparative phenotype in *Atg7^{Ad}* gWAT

We found that adipocyte autophagy maintains a pro-inflammatory macrophage identity in the WAT of DIO mice. The role of autophagy in immunity and inflammation has been extensively studied, demonstrating that autophagy importantly contributes to balanced responses by maintaining immune cell homeostasis (Clarke and Simon, 2018, Levine et al., 2011). The loss of adipocyte autophagy resulted in a macrophage tissue-reparative fate. This was in contrast with previous reports, which concluded that loss of adipocyte autophagy results in a pro-inflammatory macrophage switch (Cai et al., 2018, Sakane et al., 2021). Despite making this conclusion, the two published studies failed to demonstrate the accumulation of pro-inflammatory macrophages. Their claims were based on the increased CLS formation, F4/80 immunobiological staining, and upregulation of *Serpin3j*, *Mcp1*, and *Cd68* transcripts, which are not specific for the pro-inflammatory subset and rather only describe macrophage attraction to the tissue. Simultaneously, these studies reported no change in pro- or anti-inflammatory cytokine secretion, with cytokines rather being transcriptionally downregulated, including *Il6*, *Il10* and *Il1b*. As these observations do not demonstrate a pro-inflammatory phenotype, they could also support our findings of a tissue-reparative macrophage switch in adipocyte autophagy-deficient WAT. In addition, we found that the increased abundance and tissue reparative macrophage phenotype appeared between weeks 6 and 9 of HFD feeding of *Atg7^{Ad}* mice, suggesting that these macrophages were unlikely to be pro-inflammatory at any point of HFD but were rather attracted to the tissue to directly polarise into the tissue-repair phenotype, which was corroborated by the bone marrow chimaera experiment.

While our understanding of adipose tissue reparative macrophages remains scarce, similar subsets have been described in the lung, bladder, liver, and tumour microenvironment

(Chakarov et al., 2019, Ma et al., 2022, Lacerda Mariano et al., 2020, Fabre et al., 2023, Sarvari et al., 2021). Three main lines of evidence support the emergence of tissue reparative macrophages in our model. First, ATMs emerging in *Atg7*^{Ad} gWAT downregulate the expression of immune response activation and antigen presentation genes and surface markers, including MHCII, pro- and anti-inflammatory cytokines (Chakarov et al., 2019, Lacerda Mariano et al., 2020). In addition, they upregulate genes and surface molecules associated with tissue integrity, including Lyve1, ECM remodelling and collagen genes (Sarvari et al., 2021, Chakarov et al., 2019, Silva et al., 2019). Second, their metabolic preferences closely resemble the tissue repair macrophage subset, with an upregulation of OXPHOS and rewired glycolysis through PPP, in contrast to pro-inflammatory macrophages that predominantly rely on glycolysis (Wculek et al., 2022, Viola et al., 2019). Macrophage reprogramming and reliance on aerobic pathways have been recently described as a distinguishing feature among ATMs (Wculek et al., 2023). Third, it has been reported that ECM can educate macrophages to acquire a tissue-remodelling and immunoregulatory phenotype, potentially through receptor-ECM interaction (Puttock et al., 2023). Accordingly, we observed an accumulation of macrophages in the fibrotic lesions in the gWAT. Nevertheless, to fully validate the changes in macrophage heterogeneity upon adipocyte autophagy depletion, we would have to perform single-cell RNA sequencing of the SVF. In addition, as subtype signatures are primarily transcriptionally defined, we could mine the published single-nucleus transcriptomics data (Sarvari et al., 2021) to identify unique surface markers of the CEM subset and validate these with flow cytometry.

While factors shaping macrophage fate have been proposed, it remains unknown which specific signals can shift macrophages towards a tissue-reparative phenotype (Bleriot et al., 2020). Proposals include secreted molecules, such as cytokines and metabolites, tissue stiffness, as well as ECM ligands, however, none of these hypotheses have been experimentally proven. Furthermore, the role of autophagy in this process remains completely unexamined.

4.3.3 Limitations of macrophage depletion models to understand their role in gWAT fibrosis

We tried to utilize various models of macrophage depletion to understand whether the increased infiltration and function of tissue-reparative macrophages are causative for gWAT fibrosis in *Atg7*^{Ad} mice. Despite testing three different models of macrophage depletion, we failed to conclusively demonstrate that ATMs drive gWAT fibrosis. Preliminary results obtained from clodronate-induced ATM depletion suggested that macrophages could indeed be responsible for exacerbated fibrosis in *Atg7*^{Ad} gWAT. Notably, macrophages have been described before as critical activators of the pro-fibrotic signalling cascade in many different organs and tumours (Lis-Lopez et al., 2021, Buechler et al., 2021). If these results were confirmed, they would suggest that fibrosis is not primarily fibroblast-driven. In line with this, the expression of expression of *Acta2*, a gene largely restricted to myofibroblasts, was not increased in the gWAT of obese *Atg7*^{Ad} mice. However, we do not have sufficient experimental evidence to definitively rule out a contribution from myofibroblasts, as this was not the focus of this study. Finally, our results remain inconclusive due to a lack of reproducibility.

A commonly described clodronate liposome limitation is its unspecific mode of action, targeting neutrophils, monocytes and dendritic cells, thus making it difficult to understand the contribution of individual cell subtypes to the phenotype (Culemann et al., 2023). However, the main challenge we faced trying to address this experimental question was a significant clodronate toxicity that resulted in severe outcomes in 40-70 % of male mice. While most of the published research and manufacturers do not report such severe side effects, clodronate liposomes have been reported as toxic before (Li et al., 2016). Despite a much lower mortality rate at around 30 % in recipient mice, they however reported complications like ours, including infarction and haemorrhage. As these led to sudden deaths, we were advised to stop the study by the Home Office.

While clodronate administration somewhat reduced ATM content, the antibody treatments were not successful in significantly reducing ATM population. These outcomes underlie the need for further technical optimisation of our protocols, which we chose not to pursue due to concerns for animal welfare. To minimize the number of mice used in these experiments, we developed protocols based on previously published studies targeting macrophage recruitment and accumulation in WAT and beyond (MacDonald et al., 2010, Mantovani et al., 2022, Baer et al., 2023, Chen et al., 2021). However, these studies differ slightly in terms of treatment dose and frequency. Future optimisations could involve fine-tuning these parameters, modulating the dose, frequency, route of administration, and treatment length, as well as potentially combining approaches to achieve sufficient depletion. In addition, as we observed a slightly delayed development of gWAT fibrosis in females compared to males, we could optimise the protocols for individual sex, initiating macrophage depletion in females at a later stage. Another option would be to reduce ATM abundance through genetic manipulation. Diphtheria-based macrophage depletion models, such as $CD169^{DTR}$ or LyzM-Cre^{DTR}, have been previously demonstrated to specifically deplete tissue resident $F4/80^{+}$ macrophages upon administration of diphtheria toxin (Chen et al., 2021, Berg et al., 2021, Shi et al., 2018, Nicolás-Ávila et al., 2020). Since ATMs in our model were predominantly monocyte-derived, these strains could be used to generate a bone marrow chimaera in WT or $Atg7^{Ad}$ hosts, potentially leading to higher efficiency of macrophage depletion.

Although further technical improvements and depletion models could enhance ATM depletion, we decided to conclude the study at this point. While we could not definitively prove that macrophages are the primary drivers of gWAT fibrosis in our model, it is highly plausible that they contribute due to their well-established pro-fibrotic role in multiple tissues (Lis-Lopez et al., 2021, Buechler et al., 2021) and their fibrotic gene signature. Thus, despite the technical limitations, it remains likely that macrophages play a role in fibrosis development.

4.3.4 Adipocyte autophagy limits T cell exhaustion

Loss of adipocyte autophagy resulted in exhausted $CD4^+$ and $CD8^+$ T cell population. T cell exhaustion is a consequence of continuous antigenic stimulation and is commonly reported to occur during chronic infections and cancer (Zhao et al., 2020). Obesity also leads to the exhaustion of WAT T cells, resulting in impaired secretion of inflammatory cytokines such as interferon gamma (IFN-γ) (Porsche et al., 2021). Interestingly, obesity-associated T cell exhaustion has been proposed to be independent of PD1 signalling (Porsche et al., 2021). As we only characterised T cell exhaustion phenotypically, it would be interesting to understand how it impacts T cell function by measuring cytokine production, proliferation as well as cytotoxic capability and antigen recognition. To this end, *in vitro* assays could be used to stimulate cytokine production as well as *in vivo* immunological challenge models, such as infection or tumour.

In addition, it would be beneficial to understand the signalling pathways through which adipocyte autophagy limits T cell exhaustion. Chronic antigen stimulation has been linked to MHCII expression, and macrophage-specific MHCII expression has been suggested to drive T cell impairment (Porsche et al., 2021). On the other hand, macrophage MHCII has also been reported to be critical for the proliferation and activation of $CD4^+$ T cells and WAT inflammation (Cho et al., 2014a, Morris et al., 2013), suggesting its multifaceted role in T cell activation and exhaustion. Furthermore, it has been proposed that $CD4^+$ T cell-mediated WAT inflammation could be improved by targeting the interaction with MHCII. As we have observed a significant decrease in MHCII expression in macrophages, it would be interesting to explore how this drop functionally modulates T cell populations in $Atg7^{Ad}$ gWAT. Oxidative stress has also been correlated to T cell exhaustion (Wu et al., 2023, Zhao et al., 2020). We found that oxidative stress response genes were dysregulated in both $CD4^+$ and $CD8^+$ T cell subsets in $Atg7^{Ad}$, similar to our findings in macrophages. These data could therefore suggest a common stress

signalling pathway that is a result of adipocyte autophagy loss, and it would be intriguing to test this hypothesis further.

We also found that adipocyte autophagy depletion resulted in an accumulation of $CD44^{lo}$ $CD4^{+}$ and $CD8^{+}$ T cell population, however, the kinetics of the expression as well as functional implications remain unclear. Interestingly, CD44 regulates $CD8^{+}$ T cell activation and migration through binding with its ligand OPN (Klement et al., 2018). While this interaction was reported in a paracrine manner, OPN has also been reported to be produced by senescent $PD1^{+}$ $CD4^{+}$ T cells, allowing for autocrine regulation of CD44 signalling (Shirakawa et al., 2016). Besides OPN, CD44 is known to bind and interact with many ECM ligands, including hyaluronic acid, collagens, and matrix metalloproteinases (Senbanjo and Chellaiah, 2017). This raises a question of whether the loss of CD44 on the T cell surface is related to dysregulated ECM deposition we observed in $Atg7^{Ad}$ mice, including increased OPN and collagen production, and further experiments would be necessary to validate the correlation or causation. Finally, a better understanding of adipocyte autophagy-mediated T cell CD44 expression could potentially also have a therapeutic value, since CD44 expression in WAT and resident immune cells highly correlates with the pathogenesis of obesity and type 2 diabetes in humans (Kodama et al., 2012).

4.4 Conclusion

In this chapter, we aimed to understand how adipocyte autophagy impacts WAT remodelling and inflammation during obesity. We uncovered that adipocyte autophagy supports low-grade gWAT inflammation through the maintenance of a pro-inflammatory macrophage population. Loss of autophagy leads to a phenotypic and functional shift of macrophages towards a tissue reparative fate, impacting T cell function and ECM deposition in the tissue. In the next chapter, we will address the molecular mechanisms underlying the autophagy-mediated crosstalk between adipocytes and immune cells.

5 Autophagy supports WAT integrity during obesity through adipocyte metabolic adaptation

5.1 Introduction

5.1.1 Adipocyte metabolism

White adipocytes are highly specialised in energy storage and mobilisation and previous research has predominantly focused on the core metabolic pathways supporting these critical functions. Fatty acid (FA) storage in a lipid droplet is initiated by the uptake of FAs either through passive diffusion or specific transporters. Once FAs get converted to acyl-CoA derivatives they are stored as TAG and can be mobilised via lipolysis (Morigny et al., 2021). TAG hydrolysis onto glycerol and FAs is facilitated by adipose triglyceride lipase (ATGL) and hormone-sensitive lipase (HSL), and FAs are either transported outside of the cell or oxidised in mitochondria via fatty acid oxidation (FAO) to generate ATP (Grabner et al., 2021). On the other hand, FAs can also originate from endogenous *de novo* lipogenesis (DNL), whereby glucose is metabolised via glycolysis and tricarboxylic acid (TCA) cycle to produce citrate and acetyl coenzyme A (acetyl-CoA) (Chouchani and Kajimura, 2019). DNL-generated FAs are primarily used as membrane building blocks and signalling molecules involved in inflammation and insulin sensitivity (Hsiao and Guertin, 2019). While lipolysis and lipogenesis are typically viewed as opposite independent pathways they are intimately interlinked with the intracellular fate of glucose and AAs. An important metabolic node is acetyl-CoA, which is a critical substrate in DNL, cholesterol synthesis and TCA cycle to generate ATP. It is produced through the metabolism of pyruvate, glutamine, FAO and branched-chain amino acid (BCAA) catabolism (Felix et al., 2021). BCAAs derived from protein catabolism contribute up to 30 % of the lipogenic acetyl-CoA pool, notably supporting mitochondrial metabolism and DNL, and ultimately adipogenesis (Green et al., 2016). Notably, glucose metabolism beyond lactate production, glycerol-3-phosphate synthesis for TAG backbone and DNL has not been

thoroughly studied, and it remains unclear how early steps in glycolysis impact adipocyte homeostasis (Morigny et al., 2021).

Most of these metabolic processes are tightly linked to functional mitochondria, therefore it is not surprising that mitochondrial dysfunction greatly impacts adipocyte function and is an important driver of obesity-associated metabolic pathologies (Chouchani and Kajimura, 2019). Obesity reduces mitochondrial function through the downregulation of mitochondrial biogenesis, OXPHOS, TCA cycle, and FAO pathway genes as well as reactive oxygen species (ROS) generation, leading to a drop in ATP levels and impaired adipogenesis, inflammation, and insulin resistance (Heinonen et al., 2020).

Adipocyte metabolism beyond lipid and glucose pathways and related mitochondrial oxidative metabolism remains poorly understood. Some advances in other metabolic pathways have been recently reported, whereby pentose phosphate pathway (PPP) and iron metabolism have been identified to regulate adipocyte function and systemic metabolism (Zhang et al., 2021b, Park et al., 2006). Furthermore, adipocyte metabolites have been described as messengers in intercellular and interorgan communication (Cai et al., 2018, Wen et al., 2017, Sakane et al., 2021). Since cellular metabolism is a dynamic interplay of multiple regulators, catabolic and anabolic pathways, its high complexity cannot only be explained by a handful of lipid metabolic pathways, and therefore a broader understanding of the metabolic landscape is needed. In addition, since most of the metabolic pathways described above significantly change during obesity, a better understanding of the obesity-related metabolic rewiring of cellular metabolism could lead to potential therapeutic applications.

5.1.2 Autophagy in the regulation of cellular metabolism

Autophagy plays a key role in promoting metabolic and nutrient homeostasis at both cellular and whole-organism levels. Through the control of energy and nutrient metabolism in normal

and diseased cells, it promotes survival during starvation. Importantly, autophagy can access internal nutrient stores, including glycogen and lipid droplets, as well as undedicated nutrient stores such as ribosomes, mobilising energy and nutrients when required (Deretic and Kroemer, 2022). By degrading proteins, lipids, carbohydrates and nucleic acids, autophagy generates amino and fatty acids, sugars, and nucleosides, respectively. These are released in the cytoplasm and reutilised in various metabolic processes, including glycolysis, PPP, TCA cycle, protein synthesis, ATP production, central carbon metabolism, and lipid synthesis (Rabinowitz and White, 2010).

Amino acids resulting from protein catabolism sustain cellular AA pools and can be catabolised to yield ATP through the TCA cycle or used as substrates for glucose production by gluconeogenesis. Free fatty acids are mobilised from complex lipids through lipophagy and converted into acetyl-CoA, which is utilised in the TCA cycle and FAO for energy production. Nucleosides are degraded to ribose-phosphate, which is used for ATP production or can be converted to glucose through nonoxidative PPP. Glycogen is degraded through glycophagy to salvage free glucose, which can be fuelled into glycolysis for ATP production. In addition, it can be used for the production of substrates for lipid, nucleotide, and FA synthesis, as well as to generate antioxidant responses. Autophagy also supports iron homeostasis and bioavailability through ferritinophagy of the iron-binding protein ferritin (Kaur and Debnath, 2015). As such, autophagy enables cells to salvage key metabolites by mobilising diverse cellular energy and nutrient stores. It is not surprising that cancer cells often exploit autophagy to support their growth and survival in nutrient-poor environments (Rabinowitz and White, 2010).

Autophagy also fuels biosynthetic capacity by providing anabolic substrates such as AA for protein synthesis, thereby facilitating and sustaining core cellular functions (Kaur and Debnath, 2015). Nucleosides can also be used as building blocks for adaptive anabolic reactions. The metabolic activity of autophagy is controlled by a central regulator of cellular metabolism mammalian target of rapamycin (mTOR), which promotes cellular growth and anabolism when

nutrients are abundant while suppressing autophagy. In contrast, when the AMP: ATP ratio rises, AMPK activates autophagy, favouring catabolic and degradative pathways (Zhang et al., 2018b). As such, autophagy not only controls cellular metabolism in health and disease but is also itself highly regulated by metabolic cues through these signalling pathways. Interestingly, autophagy-controlled metabolites, such as AAs and lipids, have also been described to be exchanged between adjacent cells, suggesting that autophagy additionally has a paracrine metabolic function (Sousa et al., 2016, Richter et al., 2023).

5.1.3 Metabolic control of macrophage fate

Cellular metabolism importantly shapes immune cell differentiation and function. As described in the previous chapter, macrophage pro- versus anti-inflammatory fate is closely associated with glycolysis and mitochondrial metabolism, respectively. Over the years, however, it became more apparent that not only is immune cell fate closely aligned with intracellular metabolic needs but is also dynamically modulated in response to local metabolic exchange and nutrient provision (Richter et al., 2018). Immune responses are shaped by a combination of cell-extrinsic metabolic signals that integrate information on nutrient availability, thereby guiding cell survival, activation, and function. These stimuli can either activate metabolic checkpoints that sense nutrients or directly signal to the cells as ligands, co-factors, and secondary messengers, linking cells to their microenvironment (Bacigalupa et al., 2024).

The local microenvironment also impacts macrophage fate. Traditionally, cytokines and adipokines were studied as tissue-specific factors impacting macrophage polarisation, including granulocyte-macrophage colony-stimulating factor (GM-CSF), interleukins 33 and 34, and TGFβ (Bleriot et al., 2020). The first studies suggesting that metabolites can act as signalling molecules in macrophage polarisation were published in 2014. The identity of peritoneal macrophages was described to rely on the extracellular concentration of retinoic acid, a metabolite of vitamin A, inducing expression of subset-specific *Gata6* transcription

factor (Okabe and Medzhitov, 2014). In obese WAT, macrophages were reported to acquire a metabolically activated phenotype when treated with a mixture of glucose, insulin, and palmitate, which signalled both through receptor binding and internalisation (Kratz et al., 2014). More recently, tryptophan-derived metabolites originating from microbiota have been reported to control macrophage function through binding to aryl hydrocarbon receptor in pancreatic tumours, suppressing anti-tumour immunity (Hezaveh et al., 2022). In WAT, adipocyte-derived lactate has been described to support pro-inflammatory ATM polarisation through binding and inhibition of the PHD2 enzyme (Feng et al., 2022).

Although accumulating evidence highlights the role of metabolic extracellular signals in the regulation of macrophage fate and function, the identity of these local metabolic cues is still largely unknown. In addition, it remains unclear how these signals change in response to disease, rendering functionally different macrophage responses.

5.1.4 Chapter aims

Autophagy is an important modulator of cellular and organ homeostasis. In the last chapter, we observed that loss of adipocyte autophagy impacted WAT immune cells, however, the molecular underpinnings of these changes remained unclear. To gain a deeper mechanistic understanding of potential adipocyte-macrophage crosstalk that could explain the phenotype, we sought to (1) understand how depletion of autophagy impacts adipocyte protein and metabolic homeostasis, (2) investigate whether these changes are communicated into the adipocyte microenvironment, and (3) assess adipocyte-macrophage interaction.

5.2 Results

5.2.1 Autophagy regulates adipocyte stress response and metabolism

Obesity-associated adipose tissue dysfunction is caused by a combination of impaired adipogenesis, exacerbated low-grade inflammation, and fibrosis (Sakers et al., 2022). While adipocyte autophagy is known to have a critical role in adipogenesis (Singh et al., 2009b, Zhang et al., 2009), it remains to be understood how it shapes WAT inflammation and fibrosis. Lack of adipocyte autophagy significantly altered gWAT architecture and cellular composition. To understand why adipocytes upregulate autophagy during DIO and control these profound tissue-wide changes, we performed transcriptomics, proteomics and metabolomics analyses of WT and *Atg7*^{Ad} adipocytes isolated from obese gWAT. For all methods, adipocytes were enriched as a floating fraction, the most commonly used method for mature adipocyte isolation (Wang et al., 2022) (Fig 33A). These were sent to collaborating laboratories at the Max-Delbrück Center for Molecular Medicine in the Helmholtz Association, Germany and UCLA Metabolomics Center, USA for analysis. For transcriptomics and metabolomics, both obese male and female mice were used for analysis. In contrast, proteomics analysis was performed with obese male mice only to reduce the complexity and cost of the experiment.

Transcriptomics analysis was performed in collaboration with Dr Amir H. Kayvanjoo based at the Max-Delbrück Center for Molecular Medicine in the Helmholtz Association, Germany. The genotype explained 74.9 % of the observed variance (PC1) in the RNA-seq dataset (Fig 33B). Similar to previously mentioned transcriptomics datasets, data were analysed using the DEseq2 R package (Love et al., 2014). As several hematopoietic lineage-specific genes were identified as significantly dysregulated genes (data not shown), the dataset was reduced to adipocyte-specific genes by using a published adipocyte-specific transcriptome, generated by *in vivo* labelling of adipocyte-specific ribosomes and chromatin immunoprecipitation sequencing (ChIP-seq) of Adipoq-Cre::NuTRAP mice (Roh et al., 2017). By improving the

quality of the dataset, loss of autophagy in DIO mice resulted in a total of 1249 significantly DEGs between WT and *Atg7*^{Ad} adipocytes (Fig 33C and Fig 34A).

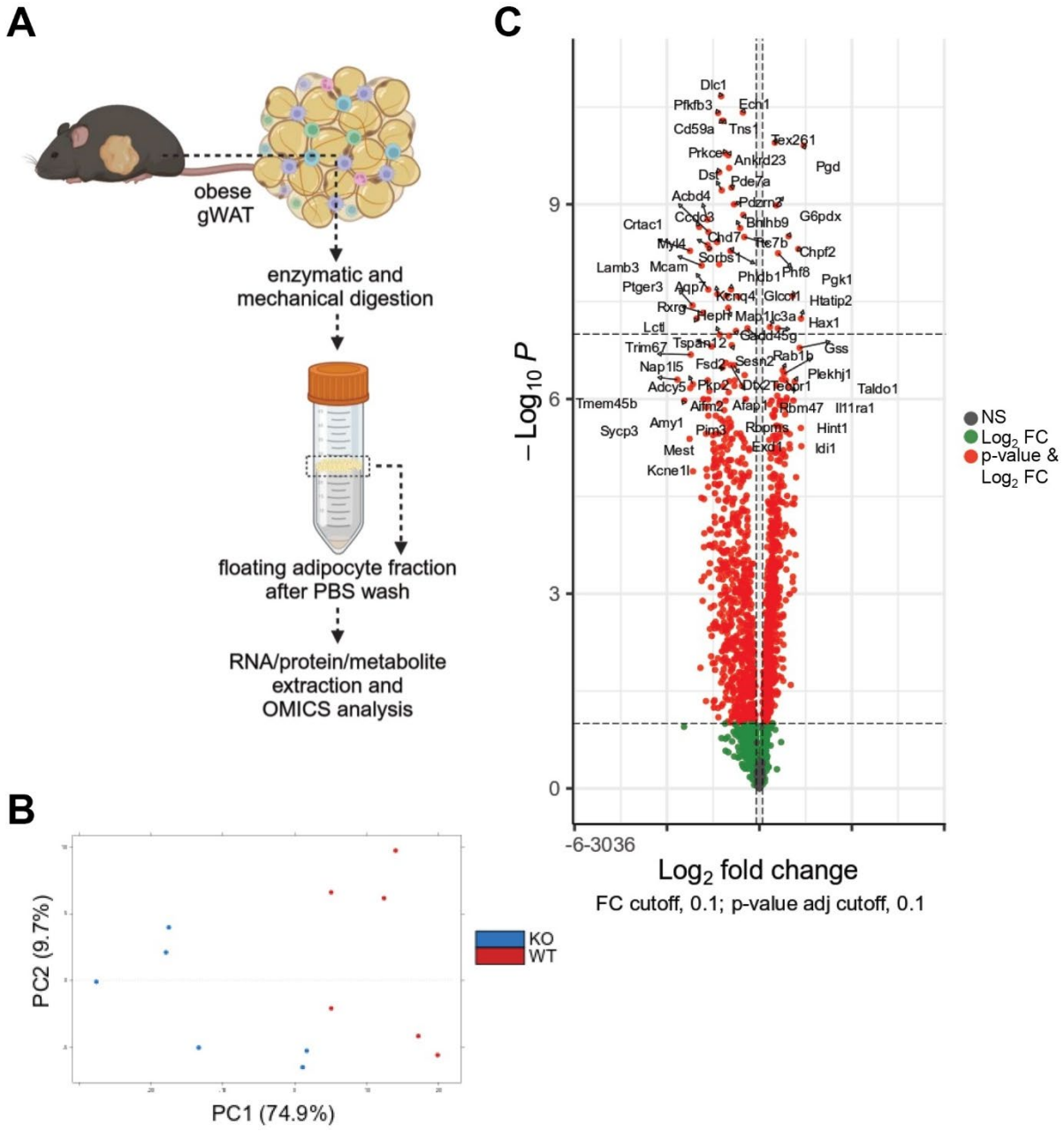

Figure 33: Loss of autophagy dysregulates adipocyte transcriptome. (A) Schematic overview of experimental set-up for adipocyte isolation used for all OMICS techniques described in this chapter. Adipocytes were isolated as a floating fraction and sent for analysis. Created with BioRender.com. (B) PCA plot of individual adipocyte samples. Each dot is a single biological replicate. (C) Volcano plot showing differentially expressed genes between WT and *Atg7*^{Ad} adipocytes isolated from gWAT after 16 weeks of HFD feeding. n = 6 mice in each group (WT and *Atg7*^{Ad}).

Gene ontology analysis revealed that loss of autophagy upregulates oxidative phosphorylation as well as nucleotide and nucleoside metabolic processes (Fig 34B). In contrast, loss of autophagy downregulated fatty acid metabolism, adipogenesis, and, as expected, autophagy in obese adipocytes (Fig 34C).

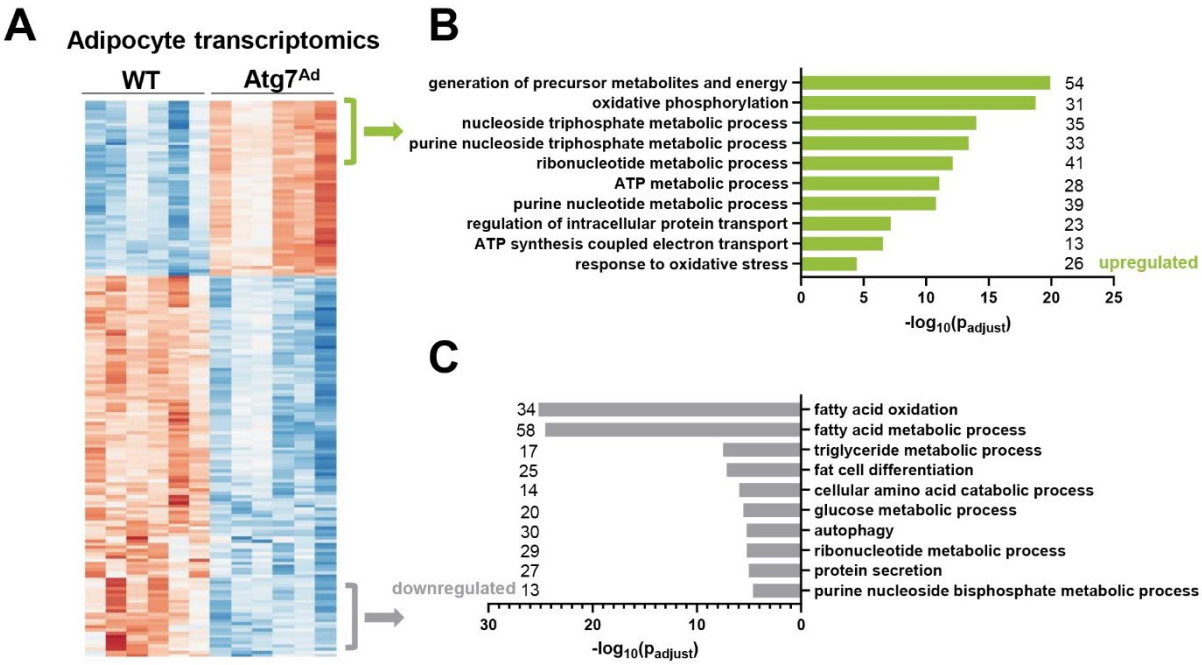

Figure 34: Autophagy transcriptionally regulates adipocyte metabolism. (A) Hierarchical clustering of transcriptional profiles of the top 1000 differentially expressed genes in WT and *Atg7*^{Ad} adipocytes isolated from gWAT after 16 weeks of DIO. Colour denotes the $\log_2$ fold difference between WT and *Atg7*^{Ad} mice. (B-C) Gene ontology (GO) analysis of upregulated (B) or downregulated (C) biological processes in autophagy-deficient adipocytes compared to WT. The number of genes identified for each term is labelled next to the bar. n = 6 mice in each group (WT and *Atg7*^{Ad}).

Proteomics analysis was performed in collaboration with Dr Oliver Popp based at the Max-Delbrück Center for Molecular Medicine in the Helmholtz Association, Germany. A comparison of WT and *Atg7*^{Ad} adipocyte proteome revealed a profound impact of autophagy on cellular proteostasis, as expected (Fig 35A). We found 3438 proteins differentially dysregulated, with 1402 significantly upregulated and 2036 significantly downregulated in *Atg7*^{Ad} compared to WT adipocytes. One of the key autophagy receptors and targets SQSTM1 was found elevated in *Atg7*^{Ad} adipocytes (Fig 35A), in line with being a degradation target of active autophagy

(Watson and Soilleux, 2015). Unexpectedly, we found ATG7 accumulated in *Atg7*^{Ad} compared to WT adipocytes (Fig 35A). This was in contrast with the western blot analysis of ATG7, which demonstrated that this autophagic protein is downregulated in *Atg7*^{Ad} adipocytes (Fig 35B). As the genetic deletion of Atg7 is a missense mutation rather than an excision at the start of the active catalytic Cys-Loop domain (Taherbhoy et al., 2011) (Fig 35C), it is plausible that the proteomics outcome is a consequence of the elevated accumulation of protein fragments rather than functional protein, detected by a western blot antibody. Visualising the ATG7 sequence with AlphaFold (Jumper et al., 2021), we found that one of the peptides identified by data-independent acquisition (DIA) proteomics positioned just before the Cys-Loop is notably reduced in *Atg7*^{Ad} compared to WT adipocytes (Fig 35D-E).

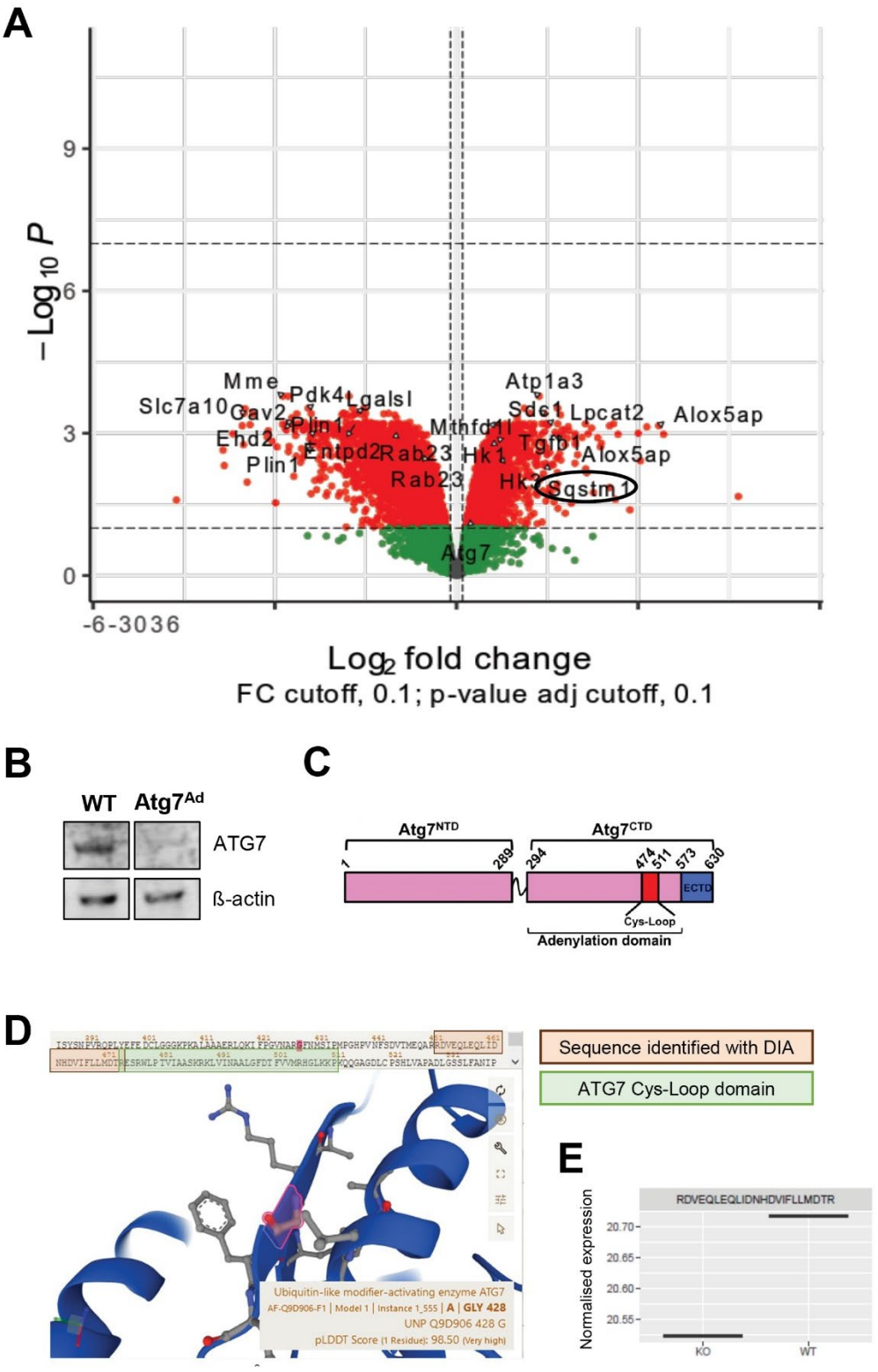

Figure 35: Loss of autophagy through ATG7 deletion significantly disrupts adipocyte proteostasis. (A) Vulcano plot of significantly dysregulated proteins in *Atg7*^{Ad} compared to WT adipocytes from gWAT after 16 weeks of HFD feeding. n = 4 male mice in each group (WT and *Atg7*^{Ad}). (B) Western blot analysis of ATG7 expression. Representative of 2 independent experiments. (C) Schematic of ATG7 protein sequence with N-terminal (NTD), C-terminal

(CTD) and adenylation domain marked. Cys-Loop is the catalytic site of the protein. Adapted from (Taherbhoy et al., 2011). (D-E) AlphaFold snapshot of ATG7 protein sequence with labelled Cys-Loop active domain (green) and protein sequence identified by DIA proteomics (orange) (D) and the normalised expression level of the identified "RDVEQLEQLIDNHDVIFLLMDTR" peptide (E).

To understand how proteome changes refer to biological processes, protein IDs were collapsed to gene names and analysed by GO analysis as described above. We found that loss of autophagy profoundly impacts adipocyte metabolism (Fig 36). The highest dysregulation was observed in nucleoside and lipid metabolism, as well as in oxidative stress (Fig 36B-C). These outcomes may be a consequence of highly dysregulated mitochondrial homeostasis, as most of the protein subunits encoding for complexes I-V of the electron transport chain were found significantly reduced in *Atg7*^{Ad} adipocytes (Fig 37A). Unexpectedly, we found several processes relating to nucleoside metabolism both up- and downregulated. While proteins supporting the early stage of nucleotide phosphate conversion were reduced, including ENPP and ENTPD, proteins involved in the late stage of nucleoside catabolism, such as NT5 were found to increase in *Atg7*^{Ad} adipocytes (Fig 37B). Finally, we found that loss of autophagy markedly impacted adipocyte function, as the global production of adipokines, including leptin, adiponectin, and DPP4 was found diminished in obese *Atg7*^{Ad} adipocytes (Fig 37C).

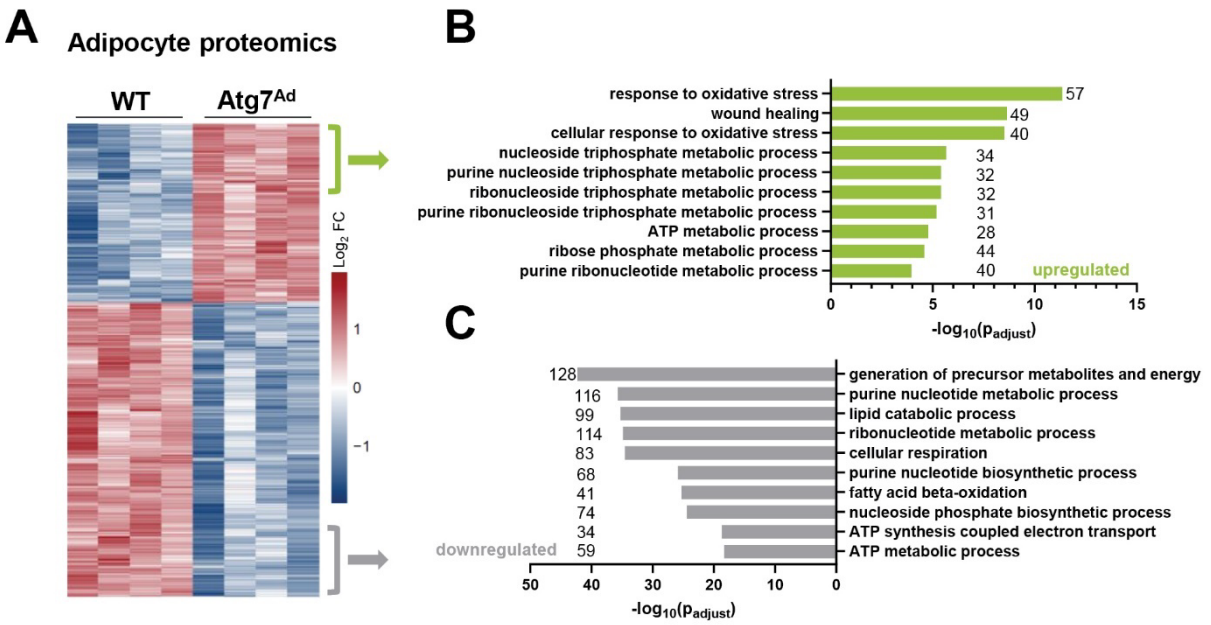

Figure 36: Loss of autophagy perturbs nucleoside and lipid metabolic pathways in obese adipocytes. (A) Hierarchical clustering of proteomics. The top 1886 proteins are shown (proteins identified with adjusted p-value ≤ 0.01) which were isolated from gWAT WT and *Atg7*^{Ad} adipocytes. Colour coding represents the $\log_2$ fold difference between the genotypes. n = 4 male mice in each group (WT and *Atg7*^{Ad}). (B-C) Enrichment GO analysis of significantly upregulated (B) or downregulated (C) pathways in *Atg7*^{Ad} adipocytes compared to WT. The number of genes identified for each term is labelled.

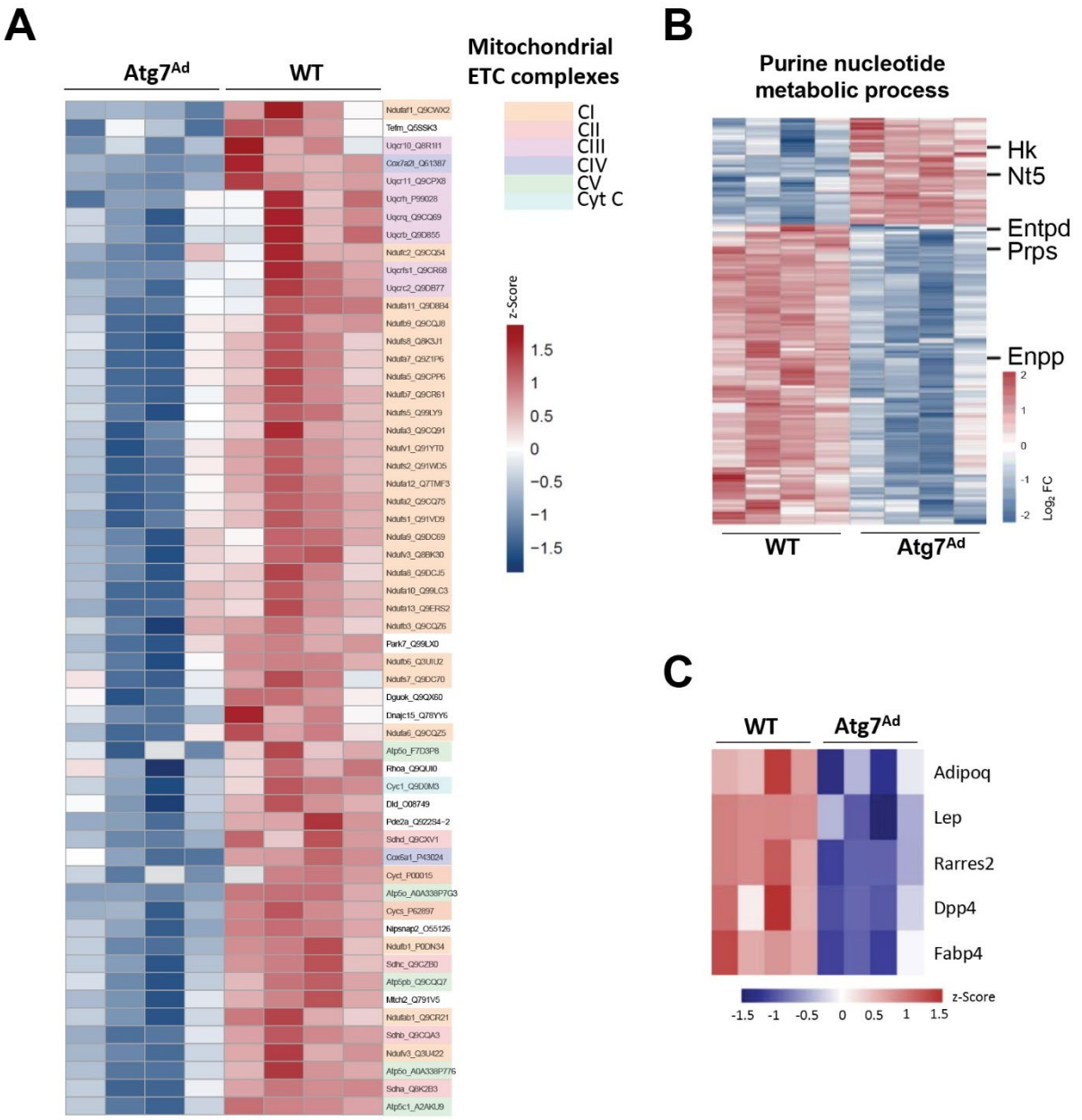

Figure 37: Autophagy depletion impairs mitochondrial and purine metabolism and impacts adipokine synthesis. (A) Heatmap of OXPHOS biological process (GO:0006119). Proteins building different mitochondrial complexes are colour-coded. Values are scaled by row (protein) using z-score. (B) Heatmap of purine nucleoside metabolic process (GO:0006163) with labelled proteins involved in enzymatic conversion. Colour coding represents the $\log_2$ fold difference between WT and *Atg7*^{Ad} mice. (C) Heatmap of adipokine expression. Lep = leptin, Adipoq = adiponectin. Values are scaled by row (protein) using z-score. n = 4 mice.

Autophagy loss has been previously reported to induce an oxidative response in *Atg3*^{Ad} and *Atg16*^{Ad} adipocytes under a control diet (Cai et al., 2018). Similarly, *Atg7*^{Ad} adipocytes

displayed a strong antioxidant response, with NQO1, HMOX1, GSR, and PRDX1 being highly accumulated (Fig 38A). This was further supported by a prominent increase of intracellular H_2O_2 in *Atg7*^{Ad} adipocytes (Fig 38B) as well as a drop in reduced/oxidised glutathione (GSH/GSSG) ratio (Fig 38C). The GSH/GSSG ratio commonly serves as an indicator of cellular health, whereby a low GSH/GSSG ratio, i.e. less GSH, indicates oxidative stress (Owen and Butterfield, 2010). In addition to increased oxidative stress in *Atg7*^{Ad} gWAT adipocytes, we found that the loss of autophagy moderately affected adipocyte viability, as indicated by adipocyte marker Perilipin-1 staining (Fig 38D-E). The impact of autophagy loss on adipocyte viability, however, was considerably lower compared to the impact of HFD feeding and obesity.

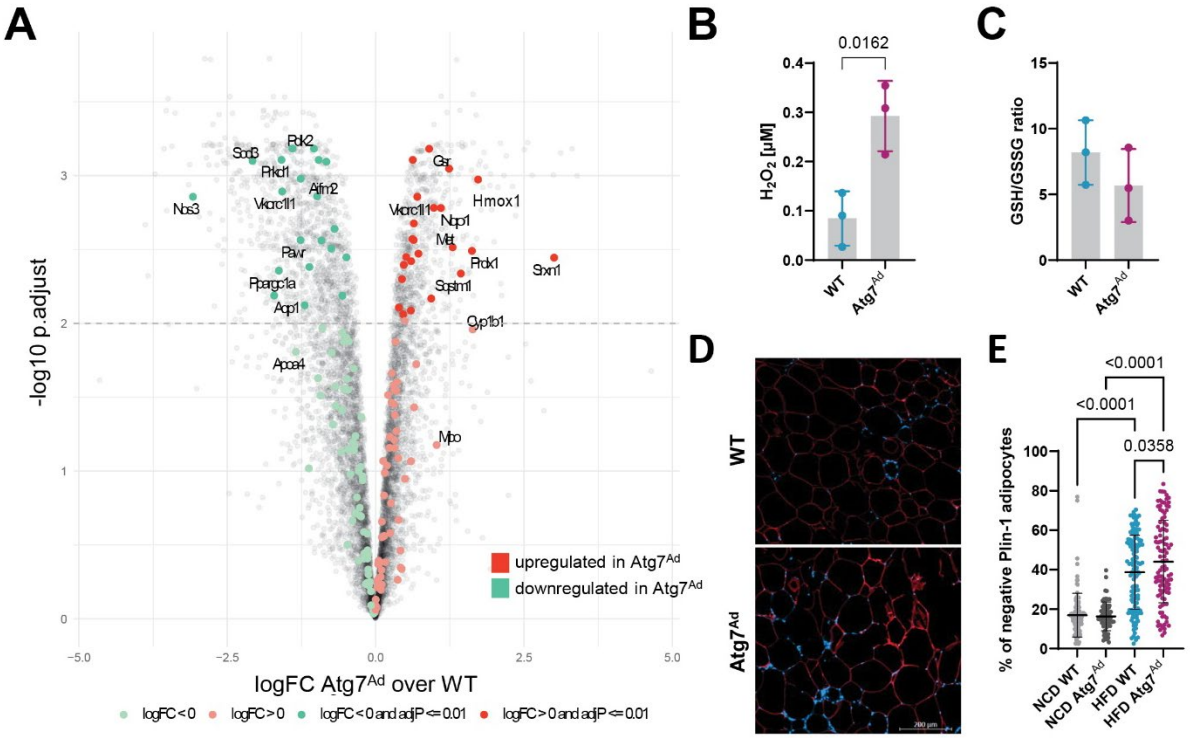

Figure 38: Autophagy limits oxidative stress and cell death in obese adipocytes. (A) Vulcano plot highlighting cellular response to oxidative stress pathway (GO:0034599) based on the proteomics dataset. (B) The concentration of intracellular H_2O_2 in WT and *Atg7*^{Ad} adipocytes isolated from gWAT of DIO mice. (C) The ratio of GSH/GSSG (reduced/oxidised form) in WT and *Atg7*^{Ad} adipocytes. D-E) Representative immunofluorescence staining of Perilipin-1 on gWAT sections from WT and *Atg7*^{Ad} mice following HFD feeding for 16 weeks

(D). Legend: blue = dapi, red = Perilipin-1. Quantification of Perilipin-1 staining as a percentage of Perilipin-1 negative adipocytes compared to total adipocytes (E). n = 7-8 mice. Data are presented as mean ± SD. Each data point represents one biological replicate. Statistical analysis by unpaired t-test (B) or two-way ANOVA with Tukey's multi comparisons test (E). Representative of 3 independent experiments (B, C) or merged from 3 independent experiments (E).

A comparison of adipocyte transcriptomics and proteomics data (Fig 39) revealed a high level of correlation (0.88) between the dysregulated genes and proteins. Similar to our previous remarks, this comparative analysis further supported that obese adipocytes upregulate oxidative stress pathways and nucleoside metabolic processes in response to a lack of autophagy (Fig 39). Furthermore, we again found that autophagy supports adiponectin expression and fat cell homeostasis (Fig 39).

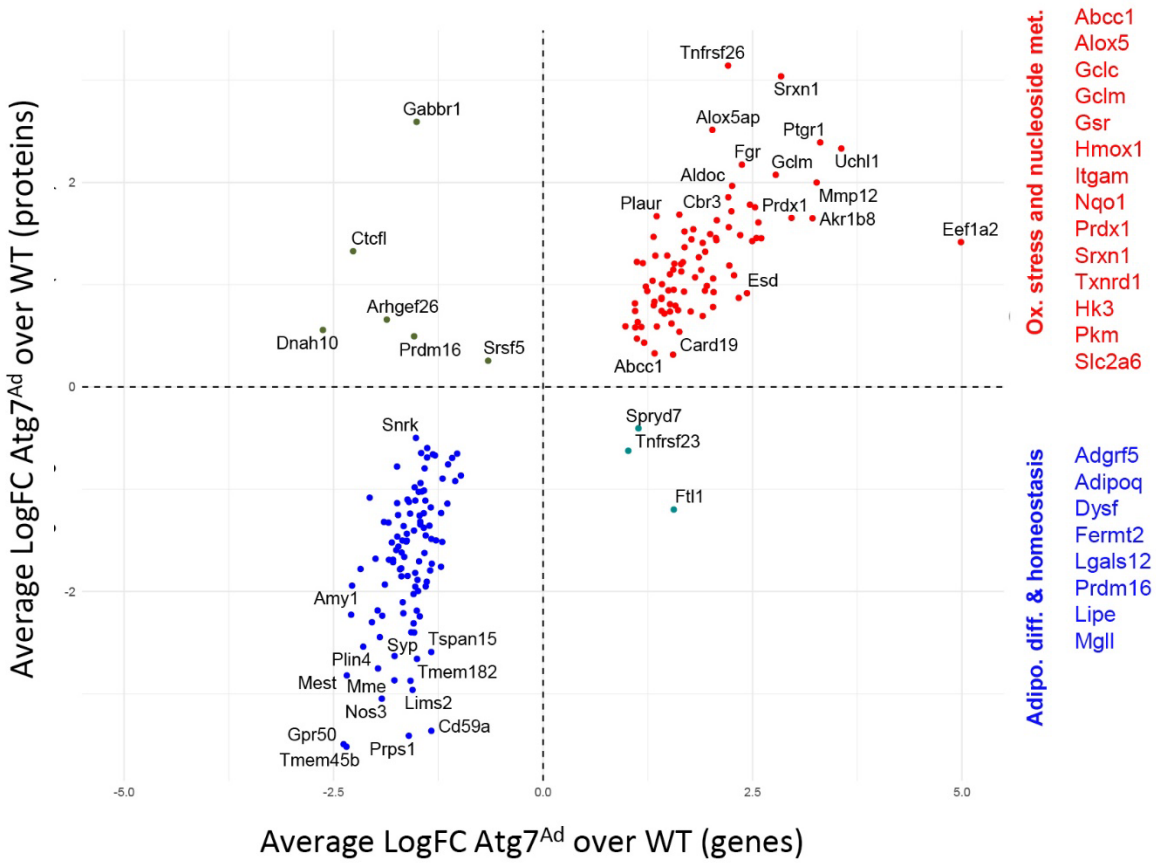

Figure 39: Integration of transcriptomics and proteomics datasets. Comparative analysis was performed with proteins and genes identified as significant in individual datasets. The average $\log_2$ fold changes for these proteins and genes are shown. Each protein and gene

datasets were filtered for significant results based on the adjusted p-value (adj.P.val) of less than 0.05. The intersection of a subset of mutual significant genes and proteins detected in both datasets is visualized in a dot plot, highlighting the correlation between the changes in gene and protein expression levels. Genes corresponding to pathways mentioned in the text are highlighted on the right side.

Metabolomics analysis was performed in collaboration with Dr Johanna ten Hoeve-Scott based at the UCLA Metabolomics Center, USA. Like proteomics data, metabolomics analysis confirmed substantial changes in adipocyte metabolism following autophagy loss (Fig 40A). A significant genotype-based data separation was observed, explaining 78.7 % of the observed variance (PC1) (Fig 40B). Data showed a significant accumulation of nucleosides in *Atg7*^{Ad} adipocytes, including cytidine, uridine, guanosine, and xanthine, a purine base derived from adenosine and guanine degradation (Fig 40A). In contrast, we observed a significant drop in nucleotide phosphates, including UMP and AMP; as well as in adenosine and ribose, essential for RNA synthesis (Fig 40A). These metabolic changes coupled with proteomic data suggest a significant dysregulation in nucleoside biosynthesis and degradation upon loss of autophagy.

Purine and pyrimidine metabolism is closely linked with PPP (Ferrier, 2014). *Atg7*^{Ad} adipocytes displayed a significant increase in N-acetylglucosamine (GlcNAc), an important post-translational modifier of glucose-6-phosphate dehydrogenase (G6PD), a rate-limiting enzyme of PPP (Rao et al., 2015). Glycolysis runs parallel to PPP and feeds substrates in the TCA cycle, which supports AA synthesis. Autophagy has been previously reported to maintain AA pools during starvation (Onodera and Ohsumi, 2005). Correspondingly, we observed a global reduction in essential and non-essential AAs in *Atg7*^{Ad} adipocytes, including glutamate, aspartate, methionine, tryptophan, threonine, lysine, alanine, serine, and asparagine (Fig 40C). This striking decrease could either be related to the dysregulation of the mitochondrial proteome (Fig 37A), where they are biosynthesised, or directly to impaired autophagy-mediated protein catabolism.

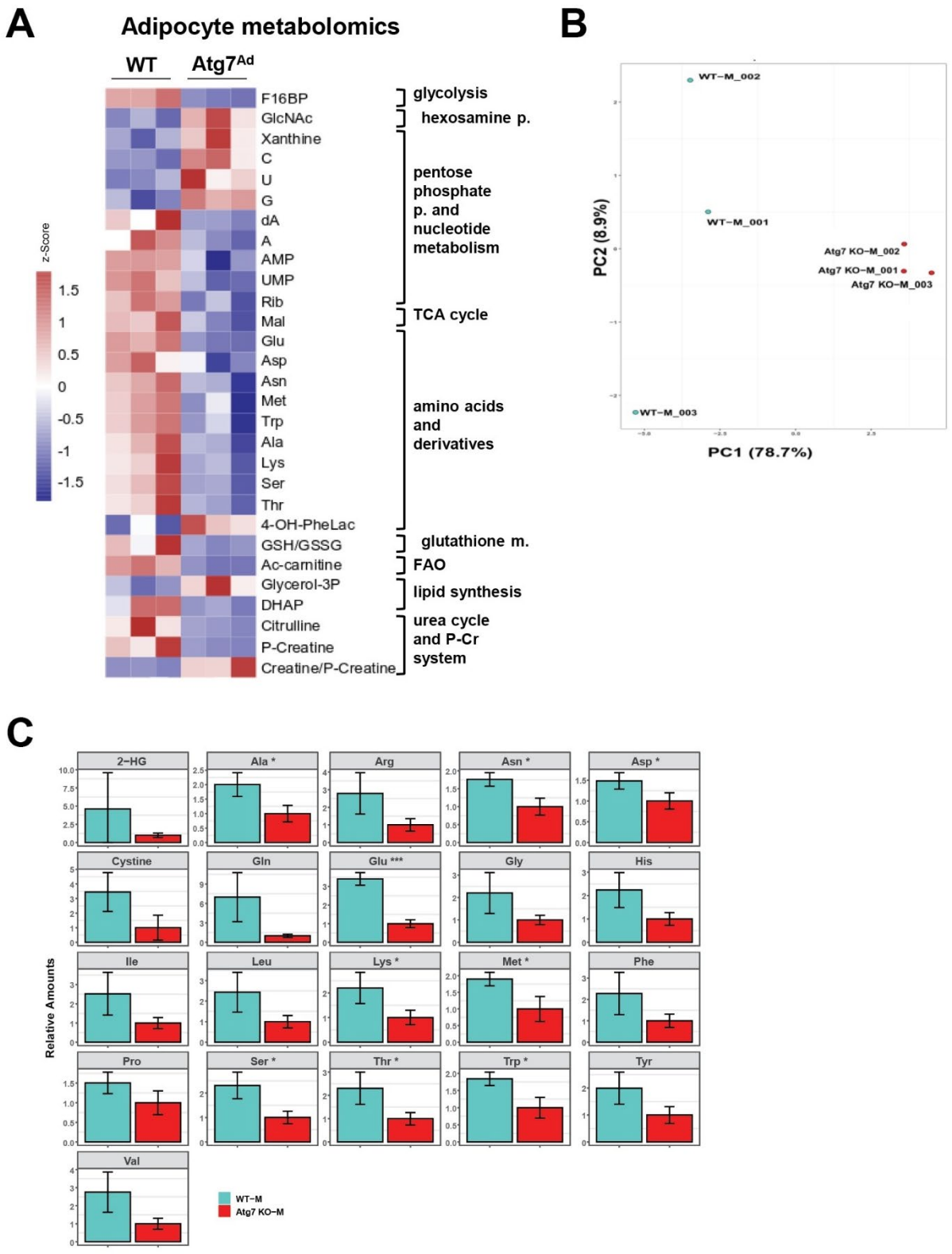

Figure 40: Autophagy controls adipocyte metabolism. (A) Heatmap of significantly ($p < 0.05$) abundant metabolites in WT and *Atg7*^{Ad} adipocytes isolated from gWAT of DIO mice. n = 3 male mice. All heatmap values were scaled by row (metabolite) using a z-score. (B) PCA plot for metabolomics analysis. (C) Relative abundance of amino acids in WT and *Atg7*^{Ad}

adipocytes measured by metabolomics analysis. The asterisk denotes significantly dysregulated AAs ($p < 0.05$).

Proteomics and metabolomics data showed a good overlap of pathways regulated by autophagy. Metabolite accumulation and depletion in *Atg7*^{Ad} adipocytes resembled changes in protein levels of critical enzymes supporting the respective pathways, including glycolysis, PPP, TCA cycle, and purine metabolism (Fig 41A-B). Loss of autophagy resulted in a general downregulation of enzymes involved in the TCA cycle and FAO. In contrast, *Atg7*^{Ad} adipocytes accumulated enzymes involved in oxidative PPP and purine metabolism, as well as specific glycolysis enzymes that support these metabolic axes, such as hexokinase (HK) (Fig 41A-B). The upregulation of oxidative PPP could be to provide reducing equivalents for antioxidant defence (Fig 38C). In addition, we observed an increase in non-oxidative PPP enzymes, including transketolase (TKT) and transaldolase (TAL, *Taldo*) (Fig 41A-B), which can support carbon metabolism by providing glycolytic intermediates (Ferrier, 2014).

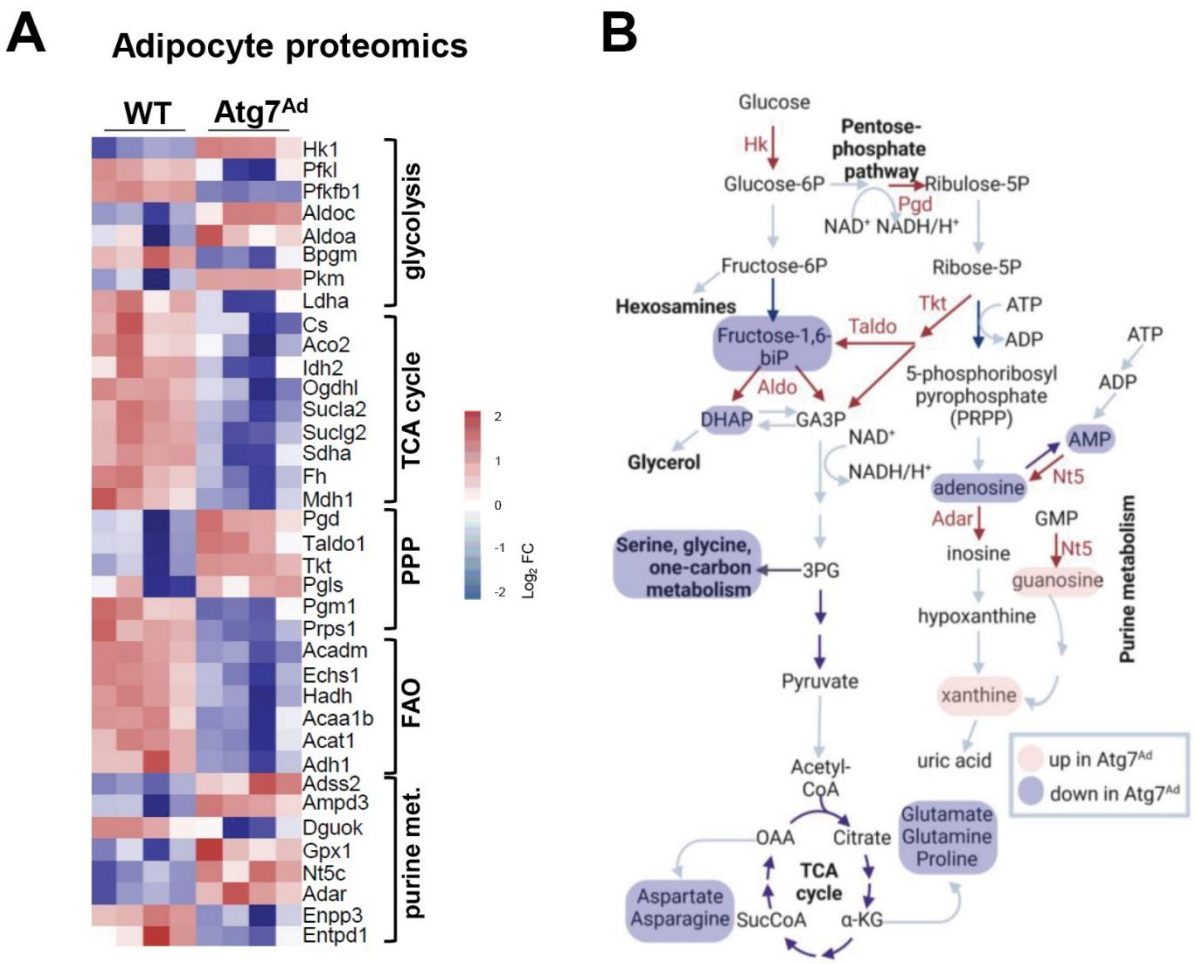

Figure 41: Adipocyte proteome and metabolome changes suggest a role of autophagy in the regulation of PPP and purine metabolism. (A) Heatmap of $\log_2$ fold changes for significantly differentially abundant proteins between WT and *Atg7*^{Ad} adipocytes. The heatmap highlights the enzymes according to the metabolic process they regulate. (B) Simplified schematic summary of autophagy-mediated adipocyte proteome and metabolome highlighting glycolysis, TCA cycle, PPP, and nucleoside degradation pathways. Enzymes and metabolic products are colour-coded based on the fold change (red ~ upregulated, blue ~ downregulated). Created with BioRender.com.

To validate omics data, we performed biochemical assays to assess total levels of ATP and downstream catabolites hypoxanthine and xanthine. Following OMICS observations, we found ATP levels downregulated, while hypoxanthine and xanthine accumulated in *Atg7*^{Ad} adipocytes (Fig 42A-B). Similar outcomes were seen in autophagy-deficient Ras-driven lung cancer cells upon starvation (Guo et al., 2016). Xanthine oxidase (XO) converts hypoxanthine to xanthine and finally to uric acid (Ferrier, 2014). We observed no change in uric acid accumulation and

the activity of XO between WT and *Atg7*^{Ad} (Fig 42C-D). These results indicate that the upregulation of purine catabolism is a consequence of a broader metabolic rewiring rather than the end-point production of uric acid.

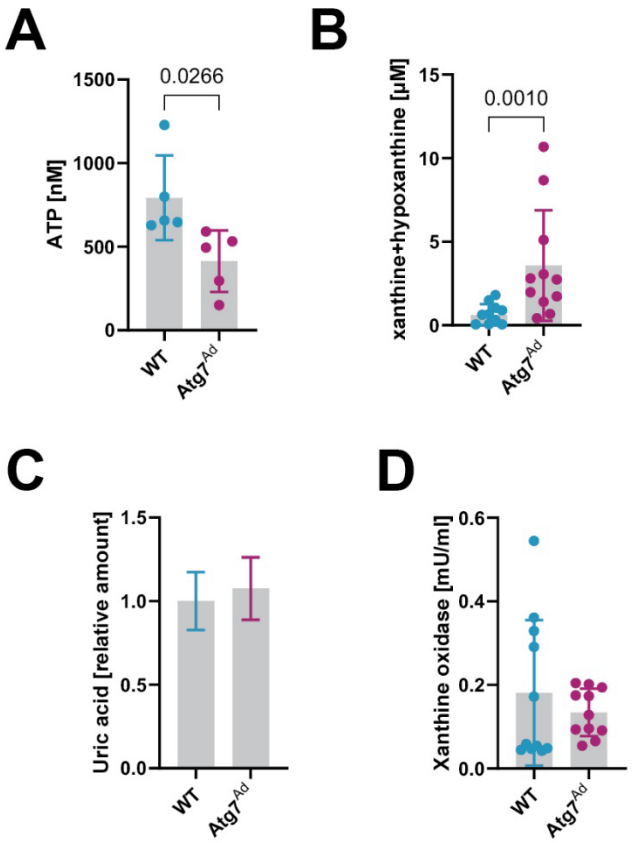

Figure 42: *In vitro* biochemical assays confirm autophagy controls adipocyte metabolism. (A-B) The concentration of ATP (A) or xanthine and hypoxanthine (B) was measured in gWAT adipocytes isolated from WT and *Atg7*^{Ad} mice fed with HFD for 16 weeks. (C) The relative amount of uric acid in WT and *Atg7*^{Ad} adipocytes was determined by metabolomics analysis. (D) Activity of xanthine oxidase (XO) after 2-hour incubation with WT and *Atg7*^{Ad} adipocyte lysates. Data are presented as mean ± SD. Each data point represents one biological replicate. Statistical analysis by unpaired t-test (A) or Mann-Whitney test (B). Representative of 3 independent experiments.

In summary, we found that autophagy controls adipocyte metabolism through substrate and energy provision, as well as by maintaining functional nucleotide and AA metabolic pools. When depleted, obese adipocytes upregulate nucleoside catabolism, leading to the accumulation of nucleosides and purine bases.

5.2.2 Loss of autophagy leads to changes in adipocyte secretome

The cellular microenvironment can reflect the profound intracellular protein and metabolite changes and autophagy-dependent intracellular rewiring has been previously reported to impact both tissue and body-wide outcomes. Notably, loss of host autophagy led to the secretion of arginine-degrading enzyme arginase I, impacting the levels of circulating arginine and tumour growth (Poillet-Perez et al., 2018). Similarly, loss of adipocyte autophagy resulted in dysregulation of extracellular oxylipin imbalance, exacerbating intestinal inflammation (Richter et al., 2023). Following these findings, we asked whether profound changes in the intracellular proteome and metabolome in *Atg7*^{Ad} adipocytes could impact their microenvironment and the respective morphological changes observed in gWAT.

Our hypothesis was based on an early observation, whereby *Atg7*^{Ad} gWAT explant culture or adipocyte *ex vivo* incubation for as little as 6 hours and up to 24 hours led to a noticeable change in cell culture medium colour (Fig 43A) (data for gWAT explants not shown). This was reminiscent of the yellowish tone of gWAT depots isolated from the mouse (Fig 10A). The shift in colour from pink to yellow is most commonly a sign of medium acidification, with phenol red in the medium serving as a colour indicator for the pH (Michl et al., 2019). Change in the medium pH is usually a result of an incubation time over several days as the cells use the medium for growing, or over 24 hours in case of bacterial infection. Despite observing a significantly lower pH in a conditioned medium (CM) of cultured Atg7^{Ad} adipocytes and gWAT explants (Fig 43B), neither long incubation nor bacterial infection were found to explain these differences (data not shown). Production of lactate and its secretion of the medium also leads to a yellow cell culture medium due to acidification (Michl et al., 2019). Biochemical assessment of lactate concentration, however, showed no significant difference in lactate secretion between WT and *Atg7*^{Ad} adipocytes (Fig 43C).

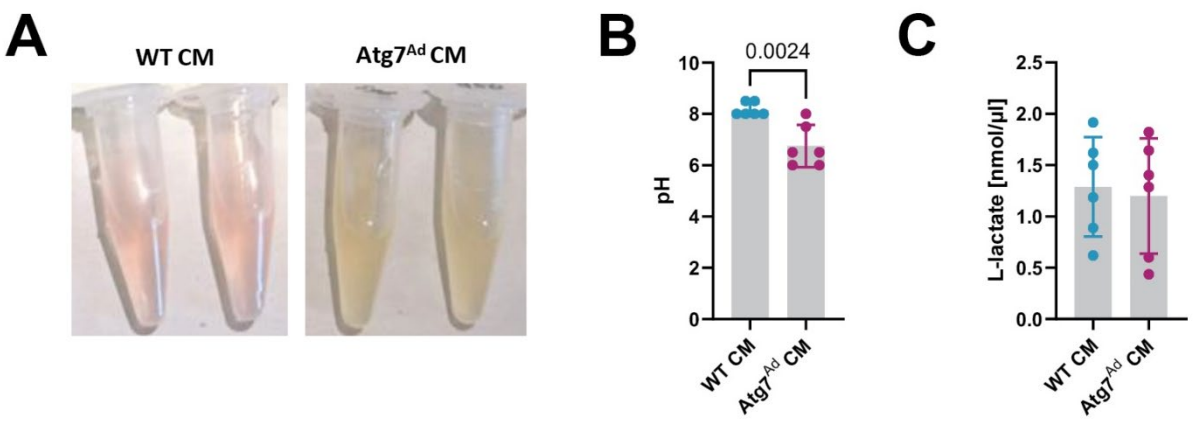

Figure 43: *Atg7*^{Ad} adipocytes acidify the cell culture medium. (A) Photograph of medium colour change after 24-hour *ex vivo* incubation of adipocytes isolated from obese WT and *Atg7*^{Ad} gWAT. CM = conditioned medium (B) pH change relating to medium colour change in (A). (C) The concentration of secreted L-lactate after 24-hour *ex vivo* cultivation of obese gWAT adipocytes. Data are presented as mean ± SD. Each data point represents one biological replicate. Statistical analysis by unpaired t-test (B). Representative of 3 independent experiments.

To understand which molecular entities contribute to the observed colour and pH shift and could potentially play a role in gWAT phenotype, we performed proteomics and targeted metabolomics analysis of adipocyte secretome following 24 hours of *ex vivo* cultivation. Proteomics analysis of serum-free medium unexpectedly uncovered numerous proteins that were significantly differentially secreted between WT and *Atg7*^{Ad} adipocytes (Fig 44A). Extracellular proteomics data confirmed the profound drop in adipokine secretion (Fig 44B). While some of the top hits included secretory proteins, such as CXCL1, B2M, and MCAM, we also found some proteins that we would not expect to be secreted or expressed by adipocytes, including ITGAM (Fig 44A). The latter is commonly associated with macrophages (Mantovani et al., 2022), suggesting that adipocyte purification as a floating fraction carried over a macrophage contamination. As this is a common technical limitation of working with adipocytes (Hagberg et al., 2018), we decided to continue the analysis of the dataset despite these constraints. To narrow down the candidate pool, we decided to perform a correlative analysis between the intracellular and extracellular proteome, thereby identifying co-regulated proteins.

The correlation of 3556 significantly differently secreted proteins with intracellular proteome was relatively high, with Pearson correlation at 0.669 (Fig 44C). 356 proteins were identified as upregulated in both *Atg7*^{Ad} medium and adipocytes compared to WT, while 557 proteins were identified as downregulated in both, representing 23% and 35.6% respectively. The co-upregulated proteins in *Atg7*^{Ad} cells and secretome were found involved in oxidative stress response, including SRXN1, ALOX5AP, HMOX1, GCLM, GCLC, and TFRC (Fig 44C). On the other hand, the co-downregulated proteins were mostly involved in lipid metabolic pathway, including PLIN4, ADIPOQ, and LEP (Fig 44C). We also found some proteins differentially abundant between adipocytes and medium (Fig 44C). The 18 proteins accumulated in *Atg7*^{Ad} cells but not medium were related to glycosylation and protein turnover (data not shown). In contrast, the 22 proteins accumulated in *Atg7*^{Ad} medium but not cells were surprisingly identified as ribosomal proteins (data not shown).

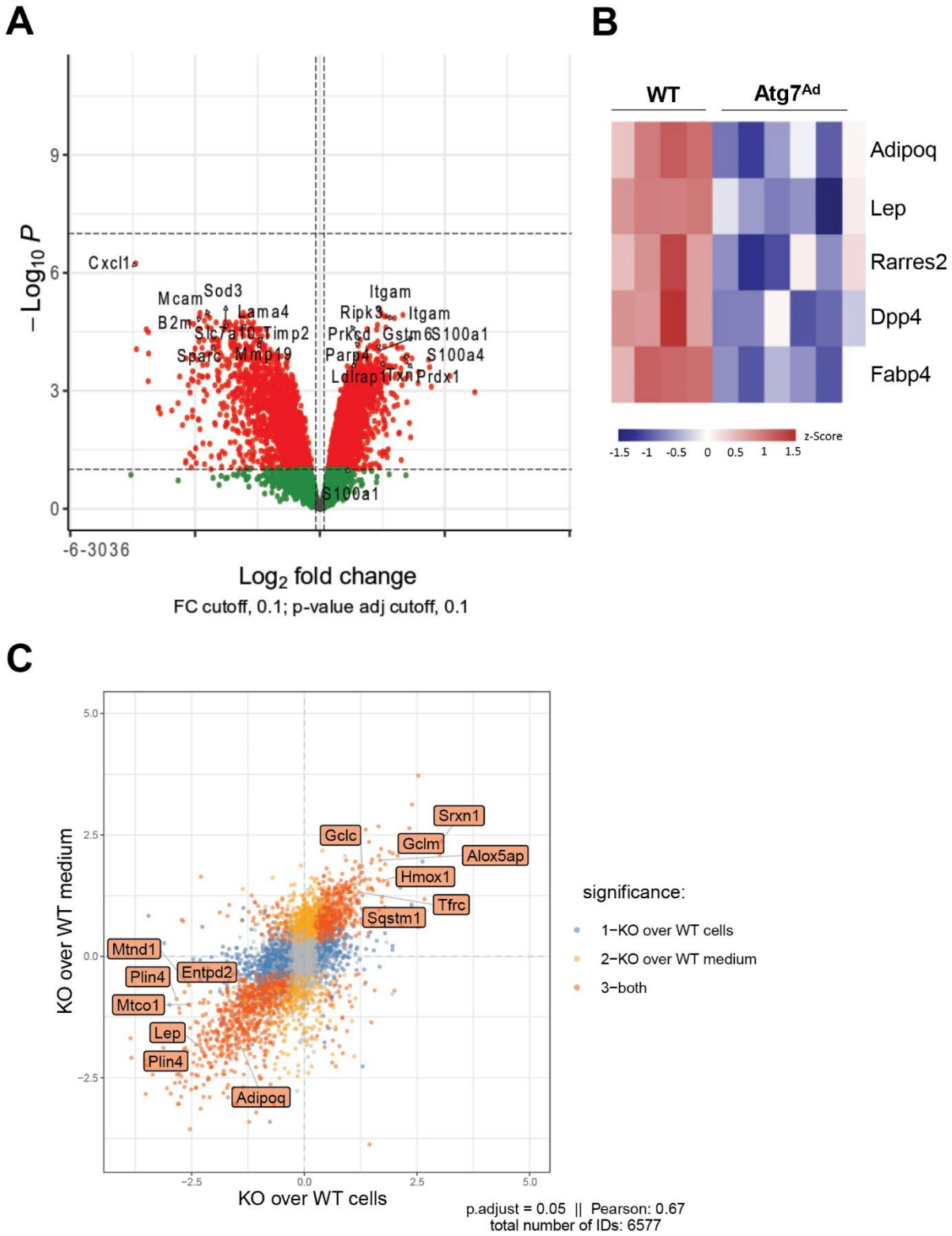

Figure 44: Autophagy controls the proteinaceous content of adipocyte secretome, which highly reflects intracellular proteostasis. (A) Vulcano plot of significantly dysregulated proteins secreted by WT or *Atg7*^{Ad} adipocytes over 24 h cultivation *ex vivo* in serum-free cell culture medium. Adipocytes were isolated from the gWAT of mice fed HFD for 16 weeks. n = 4-6 mice. (B) Heatmap of secreted adipokines Lep = leptin, Adipoq =

adiponectin. Values are scaled by row (protein) using z-score. (C) Scatter plot of log_2 fold changes compares differential expression in cellular and secreted proteins. Top co- and anti-regulated proteins are labelled.

Given strong metabolic rewiring in adipocytes upon autophagy depletion observed both with the intracellular metabolomics and proteomics as well as extracellular proteomics, we performed metabolomics of *Atg7*^{Ad} and WT adipocyte secretome. Analysis of significantly differentially abundant metabolites in adipocyte secretome revealed a much narrower repertoire compared to the intracellular metabolomics, with only 6 significantly upregulated metabolites in *Atg7*^{Ad} medium compared to WT (Fig 45A). Notably, half of those were related to nucleotide metabolism (AMP, dA, and dU). We found that intracellular accumulation of uridine and creatine reflected their extracellular accumulation (Fig 40A and 45A). In contrast, levels of AMP, adenosine, and glutamate were reduced in *Atg7*^{Ad} adipocytes but accumulated in their secretome (Fig 40A and 45A). We validated that the concentration of extracellular adenosine secreted from *Atg7*^{Ad} adipocytes increased 1.5-fold with a biochemical assay (Fig 45B). While not observing a high overlap between significant hits in the intracellular and extracellular metabolomics (Fig 40A and 45A), we found a considerable accumulation of nucleosides and purine bases, including cytidine, uridine, guanosine, and xanthine in the secretome derived from *Atg7*^{Ad} adipocytes compared to WT (Fig 45C). We could validate that the concentration of extracellular xanthine and hypoxanthine from *Atg7*^{Ad} adipocytes increased more than three-fold compared to the WT (Fig 45D).

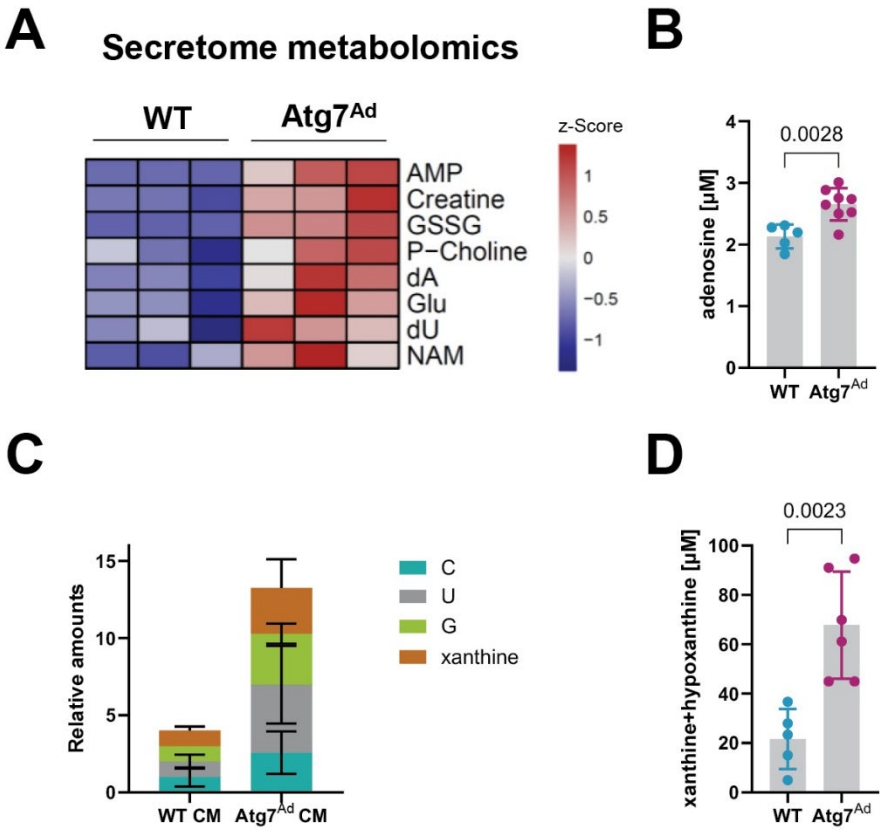

Figure 45: Autophagy in obese adipocytes controls the extracellular purine metabolite pool. (A) Heatmap of significantly ($p < 0.05$) abundant metabolites in the secretome of WT and *Atg7*^{Ad} adipocytes following 24-hour *ex vivo* incubation. Adipocytes were isolated from gWAT after 16 weeks of HFD feeding. n = 3 male mice. dA = deoxyadenosine, Glu = glutamate, dU = deoxyuridine, NAM = nicotinamide. (B) The concentration of adipocyte-secreted adenosine after 24-hour cultivation *ex vivo*. (C) The relative amount of nucleosides secreted by gWAT adipocytes isolated from obese WT and *Atg7*^{Ad} mice was measured by targeted metabolomics. n = 2-3 male mice. (D) The concentration of adipocyte-secreted xanthine and hypoxanthine after 24-hour cultivation *ex vivo*. Data are presented as mean ± SD. Each data point represents one biological replicate. Statistical analysis by unpaired t-test (B, D). Representative of 3 independent experiments (B, D).

To sum up, we demonstrated that upon loss of autophagy, the intracellular changes are communicated to the microenvironment as proteins and metabolites, including nucleoside messengers.

5.2.3 Autophagy-mediated nucleoside signalling directs macrophage tissue-reparative fate

To address whether obese adipocytes can communicate with ATMs via autophagy, we initially assessed macrophage phenotype and adipocyte homeostasis upon depletion of a core autophagy gene *Atg7*. Observing the profound impact autophagy loss had on these cells, we next sought to validate this interaction. First, we set to understand whether adipocyte secretome can signal to macrophages and drive their pro-fibrotic switch *in vivo*. To address this question, we set up a simplistic *in vitro* cellular assay by isolating $CD11b^{+}$ macrophages from lean visceral adipose tissues and cultivating them over 72 hours in the presence of obese WT or $Atg7^{Ad}$ adipocyte secretome (Fig 46A). This interaction resulted in a significant increase in the $Lyve^{hi}$ $MHCII^{low}$ macrophage population when subjected to $Atg7^{Ad}$ secretome (Fig 46B-D), resembling the CEM subset of macrophages observed *in vivo* (Fig 26D-E). Furthermore, these macrophages upregulated genes implicated in ECM remodelling, including *Col3a1*, *Mmp14*, and *Timp1* (Fig 46E). The *in vitro* macrophage phenotype thus closely resembled *in vivo* outcomes, suggesting that soluble adipocyte-derived messengers impact macrophage polarisation.

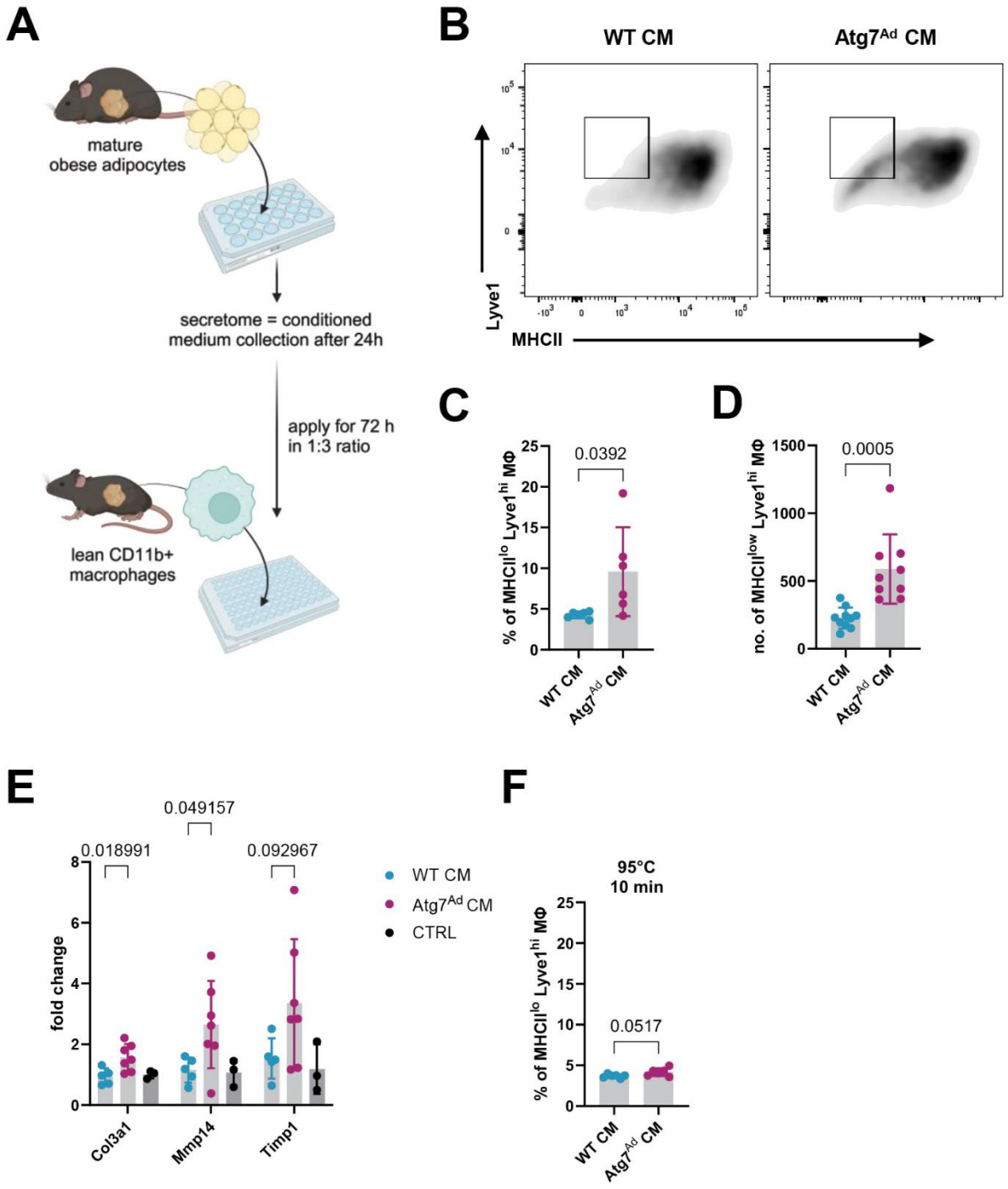

Figure 46: Autophagy controls adipocyte secretome signals that inhibit tissue-reparative macrophage switch. (A) Schematic summary of the *in vitro* experimental set-up. Adipocytes were isolated from WT and *Atg7*^{Ad} obese gWAT by flotation method and cultivated in a cell culture medium for 24 hours. Adipocyte conditioned medium (CM) was harvested and applied onto CD11b^{+} macrophages isolated from lean gWAT in a ratio of 1:3 with a cell culture medium. Macrophages were cultivated with adipocyte secretome for 72 hours before further analysis. Created with BioRender.com. (B-D) Flow cytometry analysis of MHCII and Lyve1 expression in lean ATMs cultured *in vitro* in the presence of WT and *Atg7*^{Ad} adipocyte secretome. Representative flow cytometry plots (B), frequency (C) and absolute number (D)

of MHCII^{lo} Lyve1^{hi} macrophages after treatment with WT and *Atg7*^{Ad} adipocyte CM. (E) Relative mRNA expression of ECM-related genes in macrophages after 72 hours of CM treatment from WT or *Atg7*^{Ad} adipocytes or baseline cell culture medium (CTRL). Levels measured by qRT-PCR. (F) Frequency of MHCII^{lo} Lyve1^{hi} macrophages after treatment with heat-inactivated WT and *Atg7*^{Ad} adipocyte CM for 10 min at 95°C. Data are presented as mean ± SD. Each data point represents one biological replicate. Statistical analysis by unpaired t-test (C, D, F) or multiple unpaired t-tests (E). Representative of 3 independent experiments.

Considering the severely impacted adipocyte metabolomics and proteomics landscape both intracellularly and in the WAT microenvironment, we next sought to understand which of the identified mediators could be responsible for a change in macrophage phenotype. To this end, we first heated the secretome to 95°C for 10 min, denaturing active proteins and heat-sensitive metabolites. Interestingly, exposing lean ATMs to the heated medium markedly reduced but did not completely abrogate the phenotype (Fig 46F), suggesting that the pro-fibrotic macrophage phenotype was actively potentiated by a soluble heat-sensitive messenger.

Since the extracellular adipocyte proteome was highly dysregulated, we found it difficult to narrow down our validation experiments to a single target. The macrophage phenotype could also be attributed to more than one factor. In addition, while the CEM-like phenotype was much less pronounced upon heating of CM, the difference between WT and *Atg7*^{Ad} was just above the significance threshold (Fig 46F). Furthermore, changes in adipocyte intra- and extracellular proteome to a large extent related to dysregulated metabolic pathways, of which nucleoside metabolism was the most commonly identified target. Due to this, we decided to examine whether nucleoside signals could drive macrophage polarisation towards a tissue-reparative phenotype. When exposing lean ATMs to baseline conditions of 50 ng/ml growth factor M-CSF and a cocktail of different nucleosides and purine bases (adenosine, uridine, xanthine and hypoxanthine each at 10 µM) over 72 hours we observed changes in expression of ECM-related genes, with *Col3a1* and *Timp1* significantly upregulated, denoting tissue-reparative polarisation (Fig 47A). In addition, we found a significant increase in the purine nucleoside transporter SLC28A2 protein levels in *Atg7*^{Ad} adipocytes (Fig 47B). Somewhat contradictory, we found adenosine A2B receptor (ADORA2B) notably downregulated on the surface of ATMs

isolated from obese *Atg7*^{Ad} gWAT (Fig 47C). This disparity could be explained by the role of purine base xanthine, which acts as an antagonist of adenosine receptors (Muller and Jacobson, 2011), and we indeed observed more than doubled secretion of this metabolite from *Atg7*^{Ad} adipocytes (Fig 45D). The downregulation of the ADORA2B receptor could also suggest that despite a higher concentration of secreted adenosine in the microenvironment (Fig 45B), this messenger cannot signal to macrophages found in *Atg7*^{Ad} gWAT due to receptor downregulation.

Based on these results, we wondered whether hypoxanthine and xanthine can serve as specific pro-fibrotic metabolic messengers in obese gWAT. Indeed, these metabolites were reported to act as signalling molecules in the nervous system (Huang et al., 2021). We treated the lean ATMs *in vitro* with 100 μM of individual purine nucleoside bases adenosine, guanosine, hypoxanthine and xanthine. Xanthine, and to a lesser extent hypoxanthine, led to a significant upregulation of ECM-related genes, whereas adenosine and guanosine did not (Fig 47D). To further validate that hypoxanthine and xanthine could indeed trigger a tissue-reparative switch, we decided to mimic the obese microenvironment by treating lean ATMs *in vitro* with the secretome of obese WT adipocytes, supplemented with a mixture of 100 μM of each xanthine and hypoxanthine. Strikingly, after 72 hours of treatment, we observed a significant upregulation of pro-fibrotic signature genes *Mmp14*, *Col3a1*, and *Timp1* (Fig 47E). These results altogether suggested that the upregulation of ECM-related genes is xanthine and hypoxanthine stimulation-specific and does not require a second factor.

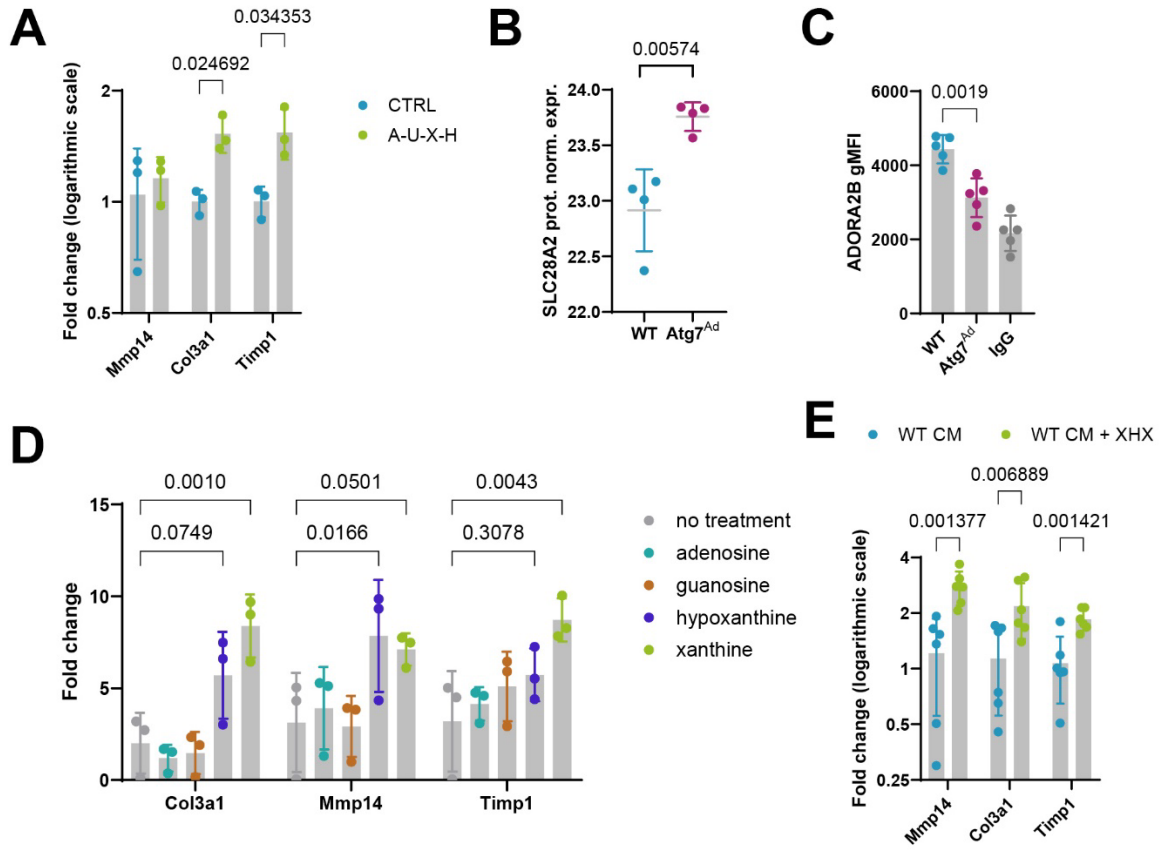

Figure 47: Adipocyte autophagy inhibits pro-fibrotic macrophage shift via nucleoside signalling in DIO. (A) Relative expression of ECM-related genes in lean ATM treated *in vitro* with 50 ng/ml growth factor M-CSF and 10 µM of each adenosine, uridine, xanthine, and hypoxanthine for 72 hours. mRNA expression was measured by qRT-PCR. (B) Normalised expression of SLC28A2 in WT and *Atg7*^{Ad} obese gWAT adipocytes measured by proteomics. (C) Flow cytometry analysis of ADORA2B receptor on F4/80^{+} CD64^{+} macrophages from WT and *Atg7*^{Ad} obese gWAT. Expression was quantified as geometric mean fluorescence intensity (gMFI). IgG was used as an isotype control. (D) Macrophages were isolated from lean WT gWAT and cultivated *in vitro* for 72 hours in baseline full medium supplemented with 50 ng/ml of M-CSF and 100 µM of either adenosine, guanosine, hypoxanthine or xanthine. Relative mRNA levels of ECM-related genes were measured by qRT-PCR. (E) Relative expression of ECM-related genes in lean ATMs following 72-hour treatment with secretome from obese WT adipocytes supplemented with or without 100 µM of both xanthine and hypoxanthine (XHX). Expression was measured by qRT-PCR and is presented as $\log_2$ fold difference. Data are presented as mean ± SD. Each data point represents one biological replicate. Statistical analysis by multiple unpaired t-tests (A, E), unpaired t-test (B, C), or two-way ANOVA with Dunnett's multi comparisons test (D). Representative of 3 independent experiments.

Lastly, considering the macrophage polarisation towards tissue reparative phenotype, we wondered about the plasticity of their phenotype and whether they would dynamically adapt

their phenotype further based on additional extracellular signals. To address this question, we treated ATMs isolated from WT and *Atg7*^{Ad} obese gWAT with ATP, a commonly described pro-inflammatory driver of macrophage phenotype in tissues (Mullen and Singh, 2023, Cauwels et al., 2014). This was based on our observations that loss of autophagy led to reduced intra- as well as extracellular ATP levels (Fig 42A and 48A). As expected, treatment of ATMs isolated from gWAT of obese WT mice led to a strong upregulation of *Il1b* expression (Fig 48B), in line with a generally pro-inflammatory macrophage phenotype found in the obese WAT (Russo and Lumeng, 2018). Interestingly, however, ATMs isolated from *Atg7*^{Ad} obese gWAT did not respond to the same ATP stimulation (Fig 48B). This response reproduced our earlier observation of reduced IL-1β secretion from *Atg7*^{Ad}-derived ATMs *in vivo* (Fig 24A). These findings suggest that not only is ATP absent from the *Atg7*^{Ad} secretome, but also tissue repair macrophages turn unresponsive towards the classical messenger of tissue damage.

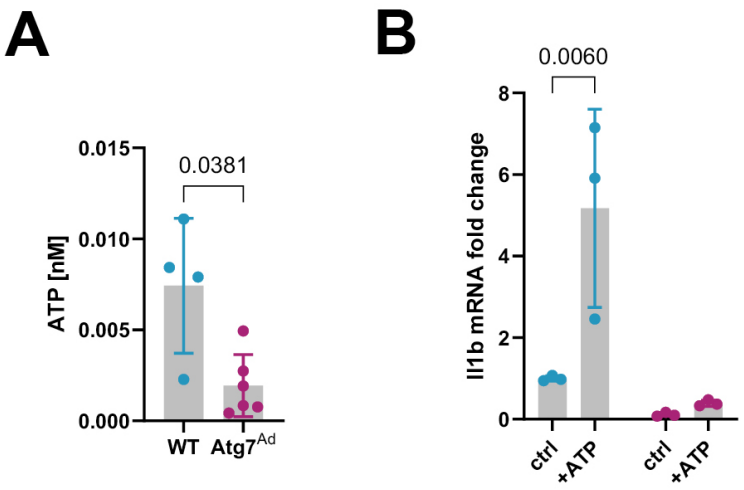

Figure 48: Tissue repair macrophages are not responsive towards classical messengers of tissue damage. (A) The concentration of secreted ATP from WT and *Atg7*^{Ad} obese gWAT adipocytes cultured for 24 hours *ex vivo*. (B) Relative *Il1b* mRNA expression was measured by qRT-PCR in macrophages isolated from gWAT of obese WT and *Atg7*^{Ad} mice and treated with 5 mM ATP *ex vivo* for 72 hours. Data are presented as mean ± SD. Each data point represents one biological replicate. Statistical analysis by Mann-Whitney test (A) or two-way ANOVA with Šídák multi comparisons test (B). Representative of 3 independent experiments.

All in all, we demonstrated that the adipocyte autophagy-mediated WAT microenvironment drives the macrophage pro-fibrotic switch in *Atg7*^{Ad} gWAT. The release of xanthine and hypoxanthine from autophagy-deficient obese adipocytes signals macrophages to obtain a tissue-reparative phenotype. This positions adipocyte autophagy as a critical regulator of tissue inflammation versus repair in obesity through the control of nucleotide intra- and extracellular pools.

5.3 Discussion

5.3.1 Multi-OMICS analysis reveals a key role of autophagy in metabolic support of obese adipocytes

To understand why adipocytes counter-intuitively upregulate autophagy during obesity, we performed transcriptomics, proteomics and metabolomics analyses. Understanding the role of autophagy in obese adipocytes remained elusive, despite several reports (Clemente-Postigo et al., 2020, Jansen et al., 2012, Kosacka et al., 2015, Mizunoe et al., 2017, Nuñez et al., 2013, Öst et al., 2010, Soussi et al., 2016, Soussi et al., 2015). In addition, contradictory conclusions were drawn on the molecular functions of autophagy upregulation (Cai et al., 2018, Sakane et al., 2021).

Performing multi-OMICS analysis, we found that the primary function of elevated autophagy is to meet the high metabolic demands of adipocytes during obesity-related WAT expansion. Transcriptomics, proteomics and metabolomics data pointed us towards changes in metabolic rewiring, indicated by the upregulation of nucleoside metabolic pathways and oxidative response and downregulation of AA and lipid metabolism in *Atg7*^{Ad} adipocytes. Understanding the adipocyte metabolism beyond glucose and lipid metabolism remains limited and only a handful of papers have described the role of other core metabolic pathways in adipocytes (Nagao et al., 2017, Kather, 1990, Park et al., 2017). Interestingly, the role of autophagy in the

maintenance of AA and nucleotide pools has been previously reported in hematopoietic stem cells and starved lung cancer cells (Borsa et al., 2024, Guo et al., 2016, Zhang et al., 2018a). Mature adipocytes are required to dynamically remodel their metabolism in response to fat mass expansion, and can be stimulated by adipokines to enter a pseudo-starvation state during obesity (James et al., 2021), reminiscent of the starved lung cancer cells.

Based on our experimental data, we propose that in a normal obese state, elevated autophagy is indispensable to maintain sufficient AA pools, active lipid metabolic turnover, and provide energy in mature adipocytes. Data suggest that autophagy critically supports mitochondrial metabolism, as evident by dysregulated mitochondrial protein synthesis, TCA cycle and FAO metabolism, as well as ATP availability. Acetyl-CoA is an important metabolic link between AA and lipid metabolism (Felix et al., 2021). It has been previously reported that nutrient starvation rapidly decreases acetyl-CoA cytosolic accumulation (Marino et al., 2014) and we hypothesise that autophagy actively depletes intermediate acetyl-CoA pool in adipocytes to fuel biosynthetic and energy-generating pathways. Interestingly, the deletion of autophagy led to the upregulation of enzymes and metabolites upstream and downstream of PPP. The pentose phosphate pathway is critical for the production of NADPH, a detoxifying agent, and five-carbon sugars, used in nucleotide synthesis (Ferrier, 2014). Through its oxidative and non-oxidative branches, it helps the cells mitigate oxidative stress and meet their anabolic demands, respectively (Patra and Hay, 2014). Glucose-6-phosphate (G6PD), a rate-limiting enzyme in PPP has been reported to increase with obesity, negatively impacting lipid and NADPH homeostasis (Park et al., 2006, Park et al., 2005). NADPH can contribute to NADPH oxidase (NOX)-mediated ROS generation or can be used for the reduction of oxidised glutathione (Park et al., 2017). Dysregulated glutathione metabolism in adipocytes has been described to contribute to insulin resistance through obesity-induced accumulation of reduced GSH (Kobayashi et al., 2009). We postulate that increased accumulation of H_2O_2 in *Atg7*^{Ad} adipocytes requires high concentration of reduced glutathione (GSH form) to mitigate oxidative

stress. As this step requires NADPH generation, *Atg7*^{Ad} adipocytes rewire their glucose metabolism through PPP to maximise NADPH synthesis. Nevertheless, due to G6PD's pleiotropic role in redox regulation across different cell types (Park et al., 2017), it remains to be determined whether the oxidative branch of PPP positively or negatively contributes to oxidative stress in *Atg7*^{Ad} adipocytes. Non-oxidative axis of PPP results in five-carbon sugar production and nucleoside metabolism (Ferrier, 2014). Salvage of five-carbon ribose has been recently shown to critically support glycolysis when nutrients are limited (Skinner et al., 2023). Furthermore, it has been previously demonstrated that TKT, a regulator of the non-oxidative branch of PPP regulates the balance between glycolysis and lipolysis in obese WAT by limiting mitochondrial function (Tian et al., 2020). Interestingly, dynamic regulation of intracellular purine metabolites has been described in both white and brown adipocytes, whereby adrenergic stimulation resulted in increased production and release of purine catabolites (Fromme et al., 2018, Kather, 1990).

Autophagy has been previously suggested to play a critical role in cellular metabolic rewiring. In starved Ras-driven lung cancer cells, autophagy supports energy charge and nucleotide pools, as well as reduces oxidative stress, thereby supporting cancer survival (Guo et al., 2016). The authors suggested that downregulating nucleotide pools while simultaneously upregulating nucleoside degradation helps *Atg7*-deficient cells maintain their energy charge. By removing AMP through degradation, cells can preserve their AMP/ADP to ATP ratio and maintain their metabolic homeostasis (Walther et al., 2010). Notably, it appears that the role of autophagy in the control of nucleoside catabolism is evolutionarily conserved. In yeast, nutrient starvation has been reported to upregulate autophagy and trigger nucleoside degradation for salvage of ribose and mediation of oxidative stress (Xu et al., 2013b). The incorporation of glucose in PPP to support NADPH and nucleotide pathways has been previously described in brown adipocytes, and it has been proposed that posttranscriptional mechanisms control glucose utilisation (Jung et al., 2021). It is plausible that autophagy, a posttranscriptional

mechanism, represents a common mechanism of glucose metabolic utilisation in both types of adipocytes. In addition, ATG7 isoform, ATG7(2), has been recently reported to directly interact with metabolic proteins, most notably mitochondrial membrane proteins and two key enzymes in glycolysis hexokinase II (HK2) and phosphofructokinase (PFKP) (Ostacolo et al., 2024). This close spatial interaction further supports the critical role of autophagy in the regulation of central energy metabolism.

A drop in both adipokine production and secretion revealed the profound functional impact that metabolic rewiring has on adipocytes. It has been previously reported that excessive mitochondrial perturbation leading to integrated stress response simultaneously reduces adiponectin and leptin secretion (Mann et al., 2023). We did not observe an activation of the integrated stress response when measuring the *Atf4* upregulation (data not shown). Therefore, it is plausible that loss of paracrine function is a consequence of a highly dysregulated AA pool. As the synthesis of adipokines is an amino acid-intensive process, it is likely that their production is blocked in *Atg7*^{Ad} adipocytes to conserve their AA pool. While the loss of adipokine production was apparent in gWAT adipocytes, we did not observe any profound systemic metabolic defects, suggesting that iWAT adipokine production buffers the dysfunction of gWAT paracrine function.

Notably, our data revealed some important study limitations. First, we found ATG7 protein to be upregulated in the *Atg7*^{Ad} compared to WT adipocytes. This was surprising, given the almost complete block of autophagy flux in these cells, suggesting that the autophagy process was indeed disrupted by *Atg7* deletion. Atg7 conditional knockout mice were generated by disruption of exon 14, which encodes an active site cysteine residue that is essential for ATG7 activation (Komatsu et al., 2005). While both peptide fragments identified in this region were downregulated in *Atg7*^{Ad} adipocytes, peptide fragments spanning other regions were upregulated, suggesting a compensatory mechanism and an accumulation of a likely dysfunctional protein in the *Atg7*^{Ad} cells. Nevertheless, the gold-standard assessments of

autophagic activity, i.e. LC3-II accumulation by western blot and double-membrane autophagosome accumulation observed on electron microscopy (data not shown) (Klionsky et al., 2021a), showed a notable reduction in mature autophagosome formation, therefore we were confident that *Atg7* deletion took place. In addition, *Atg7* expression was found reduced by qRT-PCR in both gWAT and iWAT. Furthermore, *Atg7* and autophagy flux were found reduced in the same model by a previous lab member (Richter et al., 2023). Lastly, we observed quite a strong phenotype in mice (fibrosis). Second, the identification of macrophage-specific markers, such as ITGAM revealed cross-contamination of adipocyte samples. Limitations related to the purity of adipocytes have been raised before with several studies describing cross-contamination with lipid-loaden ATMs identified through detection of macrophage-signature gene and cytokine profile (Ebke et al., 2014, Cho et al., 2014b). Another challenge in the process of adipocyte isolation besides their buoyancy is their large cell size and fragile nature (Hagberg et al., 2018). Therefore, no methods are currently available that would enable highly specific whole-adipocyte isolation (Villanueva-Carmona et al., 2023) and this limitation is generally accepted in the field of adipose tissue biology. Third, we observed sex-specific differences in adipocyte metabolome. In contrast to male, female metabolomics data demonstrated only a mild impact of autophagy loss (data not shown). Due to this significant sex-related difference and a noticeable overlap of metabolomics and proteomics data, we decided to proceed with the analysis of male-only samples. These disparities could be related to the observations we made throughout the project, whereby females developed the pro-fibrotic gWAT phenotype slower than males. This indicates that adipocytes from female gWAT are more resistant in responding to the loss of autophagy. Furthermore, it has been previously reported that metabolism and metabolic hormones are significantly different between females and males (Gavin and Bessesen, 2020, Varlamov et al., 2014). Nevertheless, all the experiments performed during this project were sex-balanced, meaning that the observed phenotypic differences could be attributed to both sexes in all cases except

metabolomics analysis. As sex-specific differences were not the subject of this project, we did not investigate this matter further.

To address some of the technical limitations related to adipocyte isolation, we could take advantage of adipocyte-labelled mouse models, such as AdipoChaser mice (Wang et al., 2013), allowing us to visualise and isolate mature adipocytes selectively. In addition, the Adipoq-Cre::NuTRAP mice (Roh et al., 2017) have been previously used to determine adipocyte-specific transcriptional profiles. While we exploited the published dataset to enhance our transcriptomics data, this approach could be further improved by feeding Adipoq-Cre::NuTRAP mice HFD so that the transcriptomics profile would better reflect the obesity state of adipocytes. In addition, different cellular models to study adipocyte biology *in vitro* could be implemented, including cultured adipocyte-like cell lines and differentiated pre-adipocytes. These models, however, could only be used to understand lean WAT as mimicking obese WAT microenvironment *in vitro* is difficult (Ruiz-Ojeda et al., 2016). Future experiments should explore adipocyte metabolic rewiring in-depth with advanced metabolic profiling. To this end, metabolic flux could be measured *in vivo*, whereby [U-^{13}C]-glucose isotope tracing could be used to follow glucose carbon incorporation into glycolysis, TCA cycle, PPP, nucleotide and lipid synthesis pathways (Nagao et al., 2017, Jung et al., 2021). In addition, biochemical assays measuring metabolic activity in the adipocytes could be performed, including the Seahorse XF Cell Mito Stress Test to measure mitochondrial function in cells (Bohm et al., 2020), and other assays measuring enzymatic conversion of specific metabolites. In addition, the existing metabolic measurements could be evaluated with respect to various inhibitors of pathways of interest, including 6-aminonicotinamide, which inhibits G6PD in the PPP pathway, forodesine, which inhibits purine nucleoside phosphorylase in the purine salvage pathway, as well as N-acetyl-L-cysteine, which is used to alleviate oxidative stress (Korycka et al., 2007, Halasi et al., 2013, Kaushik et al., 2021). Likewise, we could try to rescue *Atg7^{Ad}* adipocyte metabolism through the supplementation of metabolic intermediates that would enhance AA and nucleotide

pools (Guo et al., 2016). This would allow us to better understand the determinants of metabolic rewiring.

5.3.2 Loss of autophagy and disturbance of adipocyte homeostasis are communicated to the microenvironment

We found that profound transcriptomics, proteomics and metabolomics changes in *Atg7*^{Ad} adipocytes were reflected in their microenvironment. There was a strong overlap between intracellular and extracellular proteomics, with around 30 % of proteins co-regulated between cells and medium. Secreted proteins generally account for around 15 % of the total intracellular proteome (Miles et al., 2023). A 2-fold higher overlap between the two might be explained by the increased cell death observed in *Atg7*^{Ad} adipocytes compared to WT. In line with a modest cell death potentially contributing to the pool of extracellularly identified proteins, we found cytoskeletal actin and tubulin peptide fragments as well as ribosomal proteins significantly accumulated *Atg7*^{Ad} secretome. To better understand how the unspecific release of proteins could contribute to the identified pool, we could perform an additional experiment, where cell membranes would be gently disrupted to non-specifically release cell contents. Comparative proteomics analysis of these conditions with our existing data would reveal candidates of active secretion as well as identify contaminant proteins arising from cell lysis or death.

In contrast, metabolomics overlap was less significant, with only six metabolites identified to be significantly dysregulated between WT and *Atg7*^{Ad} adipocyte secretome. While uridine and creatine were both identified as upregulated inside and outside the adipocytes, AMP, adenosine and glutamine were significantly reduced in adipocytes but upregulated in their secretome. We found a strong intracellular nucleoside signature by transcriptomics, proteomics and metabolomics, as well as an extracellular nucleoside signature by proteomics. Extracellular metabolomics revealed there was a significant accumulation of nucleoside and nucleoside derivatives in the *Atg7*^{Ad} secretome compared to WT, however, it should be noted

that these metabolites were individually not significant. There could be two explanations for our observations. First, nucleoside species could be formed by nucleoside catabolism intracellularly and then secreted into the microenvironment. Several reports suggest nucleosides, including uridine, inosine, and xanthine, are produced in adipocytes and secreted in the WAT microenvironment (Deng et al., 2018, Pfeifer et al., 2024, Fromme et al., 2018). Second, adipocytes could secrete nucleotides, which would be converted extracellularly into nucleosides and purine bases. Such a cascade is known as purinergic signalling, whereby purine nucleotides are secreted as autocrine and paracrine signalling messengers (Huang et al., 2021). While the secretion of purines as signalling molecules has been broadly reported across different organs and diseases, the secretion of adenosine from adipocytes was previously reported as unspecific and a consequence of broken or damaged cells in a study from over 30 years ago (Kather, 1990). Combining proteomics, metabolomics, and biochemical assay data, our results mostly support the first hypothesis. However, it would be imperative to demonstrate which of the two hypotheses is true in an experimental setup. To this end, enzymes involved in the extracellular conversion of nucleotides to nucleosides, including ENPP, ENTPD, and 5-NT could be genetically or pharmacologically inhibited to see whether their block impairs extracellular nucleoside concentration. In addition, purine exporters could be genetically or pharmacologically blocked on adipocytes to see whether a block in AMP or adenosine export would alter extracellular nucleoside accumulation measured in *Atg7*^{Ad} secretome.

The role of secretory autophagy has become more appreciated over recent years, with nutrients, proteins, mitochondria, and extracellular vesicles being secreted as cargo (Piletic et al., 2023). While most reports to date describe an active role of autophagy in messenger secretion, several studies highlight how autophagy inhibition dysregulates the secretome and impacts cell-to-cell communication. Enzymes and lipid species, such as FFAs, oxylipins, and lipid peroxides have been reported in this context (Cai et al., 2018, Poillet-Perez et al., 2018,

Sakane et al., 2021, Richter et al., 2023). In line with these studies, we see profound differences in adipocyte secretome when autophagy is absent. While the accumulation of specific proteins in *Atg7*^{Ad} cells but not secretome could suggest either a failure of their degradation or an active role of autophagy in their secretion, these targets do not particularly match our other data and are mostly implicated in the glycosylation machinery and protein turnover.

Another important consideration regarding the formation of adipocyte secretome upon loss of autophagy is whether metabolites, especially nucleosides, are actively or passively secreted in the WAT microenvironment. As mentioned above, adenosine has been reported to be passively secreted from leaky adipocytes (Kather, 1990). In contrast, there are series of studies reporting the active secretion of adenosine derivatives. Inosine, hypoxanthine, and xanthine have been reported to be actively secreted as a consequence of intracellular metabolic changes in white adipocytes (Kather, 1990, Kather, 1988). Notably, similar dynamic regulation of intracellular purine metabolites has been described in brown adipocytes, whereby adrenergic stimulation resulted in increased production and release of purine derivatives, including hypoxanthine, xanthine, inosine, and guanosine (Fromme et al., 2018). Xanthine has also been reported to be actively secreted by T cells and involved in intercellular communication with the nervous system (Fan et al., 2019). Furthermore, inosine has been reported to be released from brown adipocytes upon stress, impacting whole-body metabolism and obesity-related outcomes (Pfeifer et al., 2024). In addition, adipocyte-derived uridine importantly contributes to plasma uridine availability (Deng et al., 2018). Importantly, the secretion of nucleosides and nucleoside derivatives, including hypoxanthine, inosine, and uridine has been identified as a consequence of cellular stress in multiple studies (Fan et al., 2019, Deng et al., 2018, Pfeifer et al., 2024). In line with this, autophagy depletion in adipocytes resulted in the upregulation of stress response pathways and led to the upregulation of purine nucleoside transporter SLC28A2. Altogether, these studies suggest that nucleoside

accumulation observed in *Atg7*^{Ad} secretome can indeed be a consequence of stress-induced secretion which is limited by active autophagy during obesity.

5.3.3 Nucleoside derivatives signal to macrophages for a pro-fibrotic phenotypic switch in the obese *Atg7*^{Ad} gWAT

We found that exposing lean ATMs to *Atg7*^{Ad} adipocyte secretome polarises them towards the tissue-reparative fate, mimicking the *in vivo* results. It is likely that the messengers that determine ATM fate are nucleosides and/or nucleoside derivatives, as the treatment with xanthine and hypoxanthine alone, as well as the supplementation of WT adipocyte secretome with these purine bases at physiological concentrations resulted in upregulation of pro-fibrotic genes in lean ATMs. Hereby, we for the first time identify the role of nucleoside catabolites in pro-fibrotic macrophage fate determination. To date, the mechanisms instructing macrophage tissue-reparative phenotype included lipid and cytokine signalling, including fatty acids, lipoxins, IL-4, IL-13, IL-33, IL-25, and IL-21 (Wynn and Vannella, 2016, Mitchell et al., 2002). While the role of local metabolic signalling in determining the immune cell fate is gaining increasing interest, the metabolic signals involved in macrophage fate remain rather unclear. We propose that xanthine and hypoxanthine serve as messengers of adipocyte oxidative stress. In turn, macrophages are attracted to the tissue and polarised to support ECM remodelling and prevent excessive adipocyte cell death and tissue necrosis. Furthermore, we hypothesise that the observed upregulation of macrophage nuclear division and consequently accumulation in *Atg7*^{Ad} gWAT is also a consequence of nucleoside-mediated signalling. Indeed, studies suggest that nucleosides, such as uridine and inosine, can be taken up from systemic circulation and microenvironment to support cellular anabolic needs and energetic intermediates, independent of glucose supply (Deng et al., 2018, Giannecchini et al., 2005). As extensive tissue damage and repair are energetically demanding, and fibrotic lesions limit the supply of metabolites (Gliniak et al., 2023), it is plausible that macrophages salvage *Atg7*^{Ad} adipocyte-derived nucleosides as their energy source.

Our *in vitro* experiments uncovered some further interesting insights. First, xanthine, and to a lesser part hypoxanthine, were sufficient to drive the polarization of lean ATMs towards the pro-fibrotic gene profile. This suggests that the treatment of lean ATMs with nucleosides alone is sufficient to signal for tissue repair. Considering that heating of the *Atg7*^{Ad} secretome profoundly reduced the extent of the phenotypic switch, it is plausible that these purine nucleosides are heat-sensitive, although heat stability of these metabolite species has not been reported. This observation is novel and challenges previous conclusions of cytokine-mediated pro-fibrotic phenotype (Wynn and Vannella, 2016). Second, pro-fibrotic macrophages failed to respond to the pro-inflammatory ATP stimulation (Cauwels et al., 2014). This suggests that the pro-fibrotic macrophages are locked in their fate due to prolonged stimulation. Time spent in tissue and tissue-specific signals have been described before as a major determinant of their identity and function (Bleriot et al., 2020).

Autophagy-controlled adipocyte-macrophage crosstalk requires further investigation. It would be critical to more definitively show the nucleoside exchange by using genetic and pharmacological models to inhibit release, secretome accumulation, as well as uptake by macrophages. In addition, since most of the nucleoside receptors are G protein-coupled receptors (Huang et al., 2021), it would be interesting to assess how the inhibition of downstream signalling pathways affects macrophage identity. Ultimately, it would be beneficial to demonstrate that nucleoside-mediated crosstalk has a functional consequence on macrophage fate and fibrosis development *in vivo*. To address this experimentally, we could take advantage of the most efficient pharmacological inhibitors validated *in vitro*. This, however, would have specific limitations, including non-specific systemic inhibition. Furthermore, it would be interesting to study whether the interaction between adipocytes is reciprocal, since macrophages have been previously reported to regulate adipocyte mitochondrial function and metabolic homeostasis (Keuper, 2019).

5.4 Conclusion

In this chapter, we wanted identified the mechanism by which autophagy impacts adipocyte homeostasis and adipocyte-to-macrophage crosstalk. By combining transcriptomic, proteomic, metabolomic, and functional analyses, we discovered a key role of autophagy in the support of adipocyte metabolic rewiring during obesity. When autophagy is blocked, adipocytes try to rescue their metabolism through PPP and nucleoside catabolism. In turn, the purine catabolites are secreted into the microenvironment, conveying adipocyte metabolic status and driving macrophage tissue repair phenotype.

6 General Discussion and Conclusion

6.1 Adipocyte autophagy in obesity: a pathway to metabolic regulation

The work presented in this thesis highlights the key role of autophagy in adipocyte metabolic remodelling, which is critically reflected at a tissue level and necessary for maintaining healthy WAT dynamics. While these findings underline the importance of increased adipocyte autophagy in obesity, its role remained unclear and controversial for more than a decade (Jansen et al., 2012, Kosacka et al., 2015, Kovsan et al., 2011, Mizunoe et al., 2017, Nuñez et al., 2013, Öst et al., 2010, Soussi et al., 2016, Soussi et al., 2015, Cai et al., 2018, Sakane et al., 2021). Autophagy is involved in the regulation of metabolic processes through distinct, however, interlinked extra- and intracellular processes; i) autophagy responds to nutrient and energy status, ii) autophagy controls the turnover of metabolic organelles and, iii) autophagy provides nutrients for cellular bioenergetic and biosynthetic processes (Kaur and Debnath, 2015, Deretic and Kroemer, 2022).

Positioned downstream of the master sensors of the nutrient and energy status, mTOR and AMPK, activation of autophagy tightly links to extra- as well as intracellular nutrient availability (Rabinowitz and White, 2010). When viewing the organism as a whole, the upregulation of adipocyte autophagy during times of systemic nutritional excess such as obesity goes against its traditional view as a starvation-driven cellular response. Furthermore, as the extent of calorie-rich food abundance and accessibility is greater than ever before, obesity-associated induction of autophagy cannot be rationalized as an evolutionary adaptation to systemic nutrient availability. Due to the general scarcity of nutrients available for consumption, organisms have evolved to preserve any excess energy in designated storage depots; these initially developed as simple lipid droplets in yeast and nematodes and slowly became more

complex, forming a fat body in *Drosophila*, and white adipose tissue in mammals (Parra-Peralbo et al., 2021).

In obese WAT, adipocyte autophagy may respond to nutrients at a level of tissue or individual cells. This rationale is further supported by the findings that obesity-related autophagy induction is specific for obese adipose tissue and has not been observed in other metabolic tissues, such as muscle and liver (Zhang et al., 2018b). By demonstrating the role of autophagy in the maintenance of nucleotide and AA pools, this thesis uncovers that obese white adipocytes need to critically regulate metabolic pathways beyond the classical lipid and glucose metabolism. Chronic obesity leads to adipose tissue dysfunction, characterised by an inflammatory and fibrotic microenvironment, hypoxic regions and reduced angiogenesis (Sakers et al., 2022). Such a restrictive adipocyte milieu represents a critical determinant of local nutrient availability and access. These conditions require substantial metabolic rewiring in order to optimally meet energy demands and preserve the lipid-storing function of obese white adipocytes. Parallels can be drawn with the tumour microenvironment, whereby both cancer as well as stromal cells adopt various metabolic strategies to survive and maintain function in the milieu of altered nutrient composition. In the cancer microenvironment, autophagy actively participates in regulating this metabolic rewiring, often promoting cancer progression (Pandey et al., 2021). Thus, the upregulation of adipocyte autophagy with increased adiposity could serve as an evolutionary adaptation to provide alternative nutrient sources and preserve the dynamics of adipocyte metabolism. While these alternative nutrient sources are likely to support well-described adipocyte metabolic processes such as lipid and glucose metabolism, understanding the supporting pathways might be critical to uncover metabolic dependencies with a therapeutic potential.

A question that remains to be addressed is how obesity-induced adipocyte autophagy actively supports these metabolic pathways at a molecular level. The function of autophagy in the control of metabolic processes can be split into quality control and metabolic autophagy

(Deretic and Kroemer, 2022). While these two aspects of autophagy have fundamentally different roles, current autophagy-based interventions and tools cannot differentiate between them. Adipocyte autophagy has been previously demonstrated to play a role in mitochondrial and lipid homeostasis through mitochondrial turnover via mitophagy and lipid droplet degradation via lipophagy (Zhang et al., 2022, Amorim et al., 2022, Cai et al., 2018). While the role of nucleotide and nucleoside metabolism in adipocyte homeostasis is not well understood, the role of autophagy in their regulation is even less so. Based on the results of this thesis, it is unlikely that autophagy supports this metabolic axis through non-specific bulk degradation. Instead, it is more plausible that autophagy regulates specific metabolic pathways and mobilises nutrients through directed degradation. Ribophagy has been proposed as a nucleotide-specific form of autophagy (Strefeler et al., 2024). In addition, since the role of autophagy in the control of the levels of metabolic enzymes is evolutionarily conserved (Lahiri et al., 2019), adipocyte autophagy could be responsible for specifically controlling the pathway by degrading nucleotide and nucleoside metabolism-regulating enzymes.

Altogether, this thesis highlights that obesity-induced autophagy is indispensable for adipocyte metabolic rewiring, essential for preserving adipocyte function. While some molecular mechanisms remain to be understood, this work calls for a more holistic view of adipocyte metabolism, which is necessary to fully understand metabolic determinants underpinning adipocyte and adipose tissue remodelling.

6.2 Adipose tissue fibrosis: balancing act between protection and pathology

Regeneration of a tissue or an organ after injury involves brief inflammation followed by a complete restoration of mass, structure and function. In contrast, tissue repair does not enable the tissue or organ to recover the original structure (Adler et al., 2020). Formation of fibrotic scars results in altered tissue or organ functionality. While tissue repair is often addressed as

a protective response to an injury, prolonged injury and inflammatory signals lead to excessive pathological scarring, referred to as fibrosis (Adler et al., 2020). Besides inflammatory cues, the transition from regeneration to fibrosis is tightly associated with the regenerative capacity of the tissue or organ. In contrast to muscle, lung epithelium, and liver, adipose tissue does not possess the regenerative capacity to restore morphological and functional structure in adults (Bohaud et al., 2021). Therefore, insults to WAT inevitably lead to tissue remodelling and fibrosis, disrupting tissue architecture and functionality. To understand the protective and pathological implications of adipose tissue remodelling and define targets for therapeutic reduction of fibrosis, it is important to assess ECM remodelling at histological, cellular and molecular levels.

While this thesis demonstrates that insulting WAT through loss of autophagy results in exacerbated pericellular fibrosis of gWAT this work also highlights that adipose tissue fibrosis cannot be simply labelled good or bad. *Atg7*^{Ad} mice display altered body fat distribution, improved metabolic health markers, and stiffening of gWAT, characterised by dysregulated cellular composition and altered metabolic and cytokine signalling. At the histological level, loss of autophagy results in pathological changes to gWAT architecture as well as in reduced adipokine-secreting function. It appears that the main pathological consequence of gWAT fibrosis is the loss of tissue's ability for dynamic expansion and shrinkage. Parallels can be drawn with severe skin damage, where scaring significantly impacts its dynamic remodelling and leads to skin contraction, which can in extreme cases induce function limitations to the movement of joints and limbs (Masanovic and Teot, 2020). In contrast, however, it can be argued that fibrosis specific to gWAT found in *Atg7*^{Ad} mice also has protective features. First, it limits fat deposition in the more pathophysiological WAT depot, resulting in more favourable body fat distribution and improved metabolic health. Second, even when fibrotic, gWAT can still execute some of its primary roles, including mechanic cushioning of internal organs and lipid storage. Although some studies have proposed that fibrotic WAT has decreased lipolytic

function which limits fat mass loss, this has not been experimentally proven (DeBari and Abbott, 2020). While we have no data on the lipolytic ability of *Atg7*^{Ad} fibrotic gWAT, it is likely that the pericellular fibrosis as a stiff matrix prevents dynamic release of lipids from WAT upon energy demand. Accordingly, gWAT appears to be functionally still preserving its lipid stores as evident by no increase in serum lipid content and less fatty liver in *Atg7*^{Ad} mice which would normally help to store excess fat.

At a molecular and cellular level, discerning the balance between fibrosis-mediated protection and pathology is more challenging. Macrophages are of paramount importance for tissue repair, responding to injury through recruitment and functional specialisation (Wynn and Vannella, 2016). Understanding the spatiotemporal cues for the functional specialisation of macrophages during remodelling, favouring inflammation versus fibrosis, is still limited. The work presented in this thesis outlines some critical determinants of the fibrotic tissue repair macrophage specialisation (Li et al., 2021, Bohaud et al., 2021). We show that the macrophages respond to metabolic cues in the gWAT microenvironment, in line with previous observations that fibrotic cues are matrix- and microenvironment-derived rather than intrinsic to cells (DeBari and Abbott, 2020). While our work describes a cell-to-cell interaction within stiffened ECM, a recent report suggests that extracellular ECM remodelling cues are evolutionarily conserved mechanisms that can directly impact mitochondrial homeostasis and promote the defence response (Zhang et al., 2024).

The observation that loss of autophagy severely exacerbates adipose tissue fibrosis has sparked a new project to develop nanoparticle-based targeted drug therapy that would selectively stimulate adipose tissue autophagy. A collaborative project was set up with Prof Dr Weiping Wang from The University of Hong Kong, China based on their previous work in nanoparticle and liposome-mediated selective drug delivery to WAT using adipose tissue homing peptide (CKGGRAKDC) (Chen et al., 2022, Jing et al., 2021). Considering that autophagy both positively and negatively mediates fibrosis across multiple organs through

various mechanisms (Li et al., 2020), it is paramount to develop targeted therapies that can be delivered to a specific organ, tissue or cell type. Selecting adipocyte autophagy as a target may represent a promising new venue for addressing the unmet need to alleviate visWAT fibrosis development.

6.3 Intercellular stress communication: the role of nucleoside signalling

Metabolites primarily serve as building blocks and energy sources inside the cells. Several classical metabolites, however, also serve as extracellular autocrine or paracrine signalling molecules to convey metabolic stress similar to neurotransmitters and hormones (Baker and Rutter, 2023). Extracellular metabolites, including TCA cycle intermediates succinate and acetate, as well as nucleotides ATP and adenosine, are sensed by dedicated G-protein-coupled receptors on the surface of metabolic, endocrine, and immune cells (Husted et al., 2017). In recipient cells, these molecules act to promote their activation, as well as metabolic and pro-inflammatory pathways. Furthermore, ROS, lactate and lipid species, including fatty acids and oxylipins, can also convey metabolic information between cells (Richter et al., 2023, Feng et al., 2022, Richter et al., 2018). While our understanding of metabolic signalling has significantly increased over the recent years, there is still much unknown, including how extracellular metabolic signals are integrated with classical signalling molecules to direct physiological functions and how they impact intracellular metabolic pathways and enzymes.

In this thesis, we found that purine nucleoside bases xanthine and hypoxanthine serve as metabolic messengers in the adipocyte-to-macrophage crosstalk, stimulating macrophages to acquire a tissue-reparative, pro-fibrotic phenotype. Increased secretion of xanthine and hypoxanthine has been previously associated with obesity, and these molecules have been described to signal intercellular stress in white and brown adipocytes and T cells (Fan et al., 2019, Deng et al., 2018, Pfeifer et al., 2024, Kather, 1988, Kather, 1990). While purine

nucleoside metabolites are gaining increasing attention in their role as metabolic signalling molecules across multiple cellular and disease states, the signalling mechanism and the function they promote in recipient cells remain unclear. Despite our narrow understanding of hypoxanthine and xanthine cell-extrinsic biological function, xanthine derivatives are a prominent class of mild stimulants and bronchodilators, used to treat asthma or influenza symptoms (2012). These drugs are known to non-specifically inhibit phosphodiesterase enzymes and/or non-selectively antagonise adenosine receptors (Singh et al., 2018, Muller and Jacobson, 2011). This results in the intracellular cAMP increase, activation of protein kinase A, and inhibition of TNFα and TGFβ release (Perez-Aso et al., 2015, Matsuhira et al., 2020, Spina and Page, 2017). Xanthine derivatives thus have a critical anti-inflammatory function in various inflammatory responses (2012). Drawing parallels with xanthine derivatives, it appears that hypoxanthine and xanthine might convey metabolic stress in the microenvironment by promoting anti-inflammatory responses. This is in line with our observations, whereby these molecules induced anti-inflammatory, tissue-reparative phenotype in macrophages, reducing their TNFα and TGFβ secretion. It remains to be determined; however, which xanthine and hypoxanthine-induced signalling events mediate this change.

While xanthine derivatives and thus likely xanthine have an anti-inflammatory function on recipient cells, it remains challenging to explain why autophagy-deficient adipocytes utilize these specific molecules as metabolic stress signals instead of some other metabolites. First, metabolic signalling molecules can stimulate both anti- and pro-inflammatory responses. In contrast to xanthine, acetate, and oxylipins, which are anti-inflammatory metabolites, ATP, adenosine, succinate and lactate activate a pro-inflammatory cascade (Husted et al., 2017, Winther et al., 2021). Based on our observations, conveying metabolic stress while simultaneously promoting anti-inflammatory responses might signal tissue repair. Second, the specificity of secreted metabolic signalling molecules might be a consequence of the

intracellular energy state. Cellular stress links to ATP depletion, resulting in impaired ATP: ADP ratios that need to be balanced via degradation (Baker and Rutter, 2023). In addition, the balance of purine salvage and *de novo* biosynthesis pathways is essential during high oxidative stress (Tian et al., 2022). To maintain energy balance cells therefore upregulate the purine catabolism pathway, making downstream metabolites such as xanthine and hypoxanthine a more direct indicator of energy stress in cells compared to other metabolites. Third, purine nucleosides act as chemical messengers on both ionotropic and metabotropic receptors, conveying messages in a very high sensitivity and fast manner (Huang et al., 2021). Purine receptors are conserved from bacteria to eukaryotes, including protozoa, algae, fungi, and mammals (Monteagudo-Cascales et al., 2024). Purine nucleosides convey information throughout tissues and species and their concentration can be fine-tuned in a spatiotemporal manner through a degradational activity of transmembrane and secreted proteins (Huang et al., 2021). Nevertheless, while xanthine and hypoxanthine represent highly potent signalling molecules, their action is still understudied due to extremely complex receptor and signalling networks, which often display high similarity with opposing function and are able to simultaneously impact multiple secondary messengers.

Overproduction of hypoxanthine and xanthine commonly results in the accumulation of uric acid, the end product of purine nucleoside metabolism (Chen et al., 2016). Data presented in this thesis, however, clearly demonstrate that overproduction and secretion of hypoxanthine and xanthine are independent of uric acid accumulation and the activity of the producing enzyme, XO. This could be due to adipocytes aiming to reduce additional oxidative stress, as the activity of XO produces ROS upon the synthesis of uric acid (Furuhashi, 2020). Furthermore, xanthine and hypoxanthine are more soluble than uric acid, excessive accumulation of which can lead to gout and hyperuricemia (Chen et al., 2016). Lastly, extracellular hypoxanthine and xanthine can be taken up by recipient cells, which can utilize them in the purine salvage pathway to regenerate energy-rich molecules such as ATP (Mullen

and Singh, 2023). While these hypotheses fit with the data presented in this thesis, they remain to be experimentally proven.

Altogether, this work underscores the importance of extracellular metabolic stress signalling in obesity and opens new research venues for the role of purine nucleoside metabolites in WAT signalling and modulation of ATM phenotypic switch. Xanthine and hypoxanthine-mediated signalling may also play a role in the fibrosis of other tissues, thus these findings may hold universal relevance for targeting the pro-fibrotic cascade.

6.4 From autophagy decline to ageing: consequences for metabolic health

Ageing is associated with numerous hallmarks, including loss of proteostasis, impaired nutrient sensing, mitochondrial dysfunction, cellular senescence, stem cell exhaustion and altered intercellular communication (Lopez-Otin et al., 2013). Ageing also impacts body fat distribution, with increased visWAT deposition and muscle wasting, accelerating metabolic disease (Kuk et al., 2009). Through profound adipose tissue dysfunction, ageing promotes low-grade inflammation and ectopic fat deposition. Furthermore, by impacting WAT energy storage and endocrine function, ageing dysregulates cellular and organismal metabolic and energy homeostasis, which are associated with the development of insulin resistance and type 2 diabetes mellitus (Ou et al., 2022). On the other hand, obesity is also a recognised major risk factor for age-related diseases, including cancer and cardiovascular disease (Aman et al., 2021). Autophagy activity declines with age across diverse species, contributing to a progressive accumulation of damaged organelles, misfolded proteins and lipid droplets (Zhang et al., 2022, Amorim et al., 2022, Kitada and Koya, 2021). As failure to eliminate cellular damage adversely impacts lifespan, autophagy is often portrayed as one of the key biological pathways promoting longevity (Kitada and Koya, 2021). Unpublished data from our research group indicates the same trend can be found in adipocytes and adipose tissues in both humans

and mice. Similar observations were previously made in adipose tissue SVF (Ghosh et al., 2016).

Loss of autophagy in obese *Atg7*^{Ad} mice could theoretically serve as an experimental model to study age-related autophagy decline and metabolic derangements. We found that in *Atg7*^{Ad}, similar to aged mice, WAT fibrosis is exacerbated and associated with increased ECM macromolecule secretion and pro-fibrotic macrophage phenotype. It has been recently reported that IgG is an ageing factor that induces WAT fibrosis through macrophage activation (Yu et al., 2024). The authors found that this effect is alleviated by caloric restriction, supporting our hypothesis that increased autophagy might be necessary to maintain healthy WAT remodelling dynamics. Furthermore, both loss of adipocyte autophagy and age resulted in reduced proliferation and differentiation capacity of adipocyte progenitors (Schipper et al., 2008). However, there are multiple disparities both at cellular and organismal levels that make it difficult to draw direct parallels between our experimental model and aged mice. First, despite both adipocyte autophagy-deficient and aged WAT displaying dysregulated secretomes, the signature of aged WAT is pro-inflammatory, with increased secretion of IL-1, IL-6, and TNFα (Ou et al., 2022). While pro-inflammatory cytokine secretion has been well studied, very few studies investigated the changes in WAT immune cells with age, and these results remain controversial. Second, aged mice preferentially deposit their fat in the visceral area, opposite to our findings in obese *Atg7*^{Ad} mice. This rather results in MUO, with increased lipotoxicity on other tissues and ectopic fat deposition in the liver (Kitada and Koya, 2021).

Therapies aimed at improving metabolic health, such as caloric restriction, exercise and antidiabetic drugs, often induce autophagy and are also implicated in increasing health and lifespan (Aman et al., 2021). Therefore, drawing parallels between metabolic health and longevity and understanding their divergence points is critical to better understanding which processes are directly mediated by autophagy and which are its consequences. This would

allow us to design more targeted therapies aimed at improving both metabolic health and longevity via a common mechanism of stimulating autophagy.

6.5 Thesis summary and outlook

White adipose tissue dysfunction is characterised by inflammation and fibrosis and critically contributes to obesity and metabolic syndrome pathophysiology. White adipocytes form complex cell-to-cell interactions with SVF, integrating a myriad of metabolic, stress, immunological, and endocrine signals. Control of these processes is imperative to maintain healthy and dynamic WAT that can support systemic nutrient and energy demands. At a cellular level, nutrient and energy sensing culminates in autophagy, and adipocyte autophagy has been previously positively associated with increased adiposity and WAT development. Its role in obesity-induced dysfunction, however, remained unclear.

In this thesis, we demonstrate that adipocyte autophagy plays a key role in the support of healthy WAT remodelling by limiting pericellular fibrosis (Fig 49). As these effects are specific to a more detrimental visceral fat depot, we find that adipocyte autophagy dictates local fat distribution, which is mirrored in the metabolic health of obese mice. Autophagy regulates gWAT remodelling and architecture through intercellular crosstalk between adipocytes and macrophages. Our data demonstrate that loss of autophagy induces a phenotypic and functional shift in ATMs to acquire a tissue-reparative, pro-fibrotic identity. Combining transcriptomics, proteomics, and metabolomics data with functional analyses, the work presented in this thesis highlights the key role of autophagy in the control of adipocyte metabolism in DIO. Unmet metabolic requirements of adipocytes upon loss of autophagy result in metabolic rewiring with the accumulation of purine nucleoside catabolic products that are secreted in the gWAT microenvironment. By depleting autophagy, we uncover a purine nucleoside-mediated pro-fibrotic signalling pathway that drives macrophage tissue repair

phenotype. Further research is necessary to elucidate whether these signalling molecules control fibrosis of other tissues and organs, potentially deeming them druggable targets.

Taken together, this study reveals a novel mechanism by which cells use autophagy to communicate their intracellular metabolic demands. Furthermore, we uncover autophagy as a determinant of WAT fibrosis and distribution, uncovering a potential new target for therapeutic intervention in obesity-induced WAT pathological remodelling.

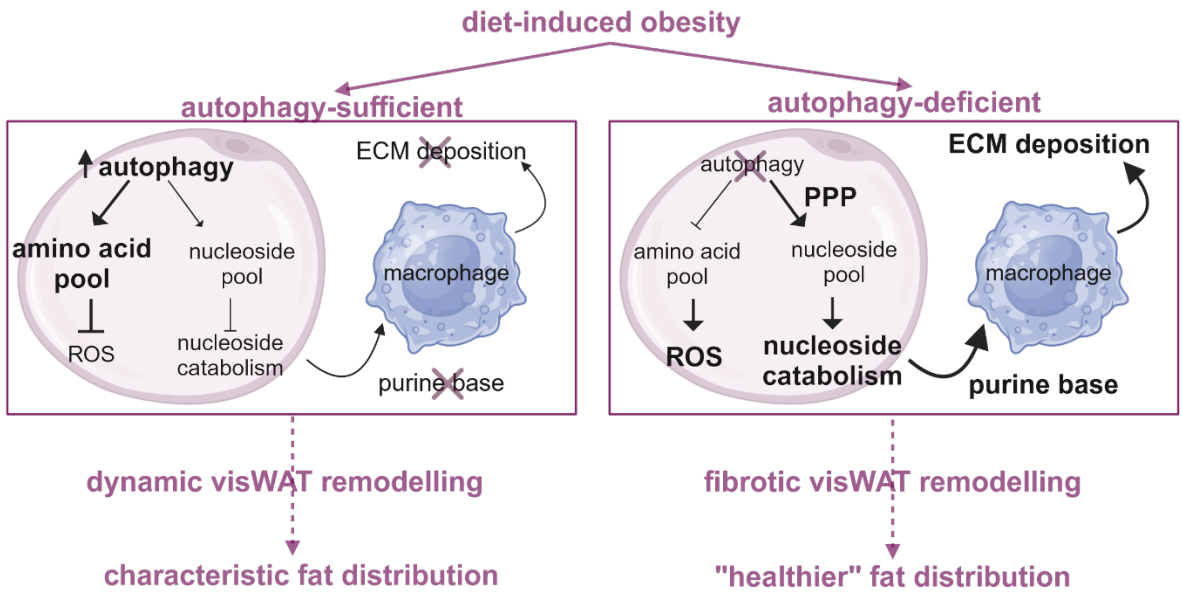

Figure 49: Graphical summary of the role of adipocyte autophagy in the control of obese WAT dysfunction. During DIO, autophagy serves as an indispensable metabolic pathway in hypertrophic visceral adipocytes, supporting amino acid and antioxidant metabolism. By supporting obese adipocyte metabolic demands, autophagy supports dynamic remodelling of visceral WAT (visWAT) and whole-body fat distribution. When autophagy is dysfunctional, however, obese adipocytes fail to meet their metabolic needs. This results in a profound metabolic rewiring through PPP to recover carbon and antioxidant substrates. As a result, purine catabolites are generated and released in the microenvironment, signalling for tissue repair through adipocyte-macrophage metabolic intercellular crosstalk. Created with BioRender.com.

References

2012. Xanthine Derivatives. *LiverTox: Clinical and Research Information on Drug-Induced Liver Injury.* Bethesda (MD).

ABDENNOUR, M., REGGIO, S., LE NAOUR, G., LIU, Y., POITOU, C., ARON-WISNEWSKY, J., CHARLOTTE, F., BOUILLOT, J. L., TORCIVIA, A., SASSO, M., MIETTE, V., ZUCKER, J. D., BEDOSSA, P., TORDJMAN, J. & CLEMENT, K. 2014. Association of adipose tissue and liver fibrosis with tissue stiffness in morbid obesity: links with diabetes and BMI loss after gastric bypass. *J Clin Endocrinol Metab,* 99**,** 898-907.

ADHYATMIKA, A., PUTRI, K. S., BELJAARS, L. & MELGERT, B. N. 2015. The Elusive Antifibrotic Macrophage. *Front Med (Lausanne),* 2**,** 81.

ADLER, M., MAYO, A., ZHOU, X., FRANKLIN, R. A., MEIZLISH, M. L., MEDZHITOV, R., KALLENBERGER, S. M. & ALON, U. 2020. Principles of Cell Circuits for Tissue Repair and Fibrosis. *iScience,* 23**,** 100841.

AMAN, Y., SCHMAUCK-MEDINA, T., HANSEN, M., MORIMOTO, R. I., SIMON, A. K., BJEDOV, I., PALIKARAS, K., SIMONSEN, A., JOHANSEN, T., TAVERNARAKIS, N., RUBINSZTEIN, D. C., PARTRIDGE, L., KROEMER, G., LABBADIA, J. & FANG, E. F. 2021. Autophagy in healthy aging and disease. *Nature Aging 2021 1:8,* 1**,** 634-650.

AMANO, S. U., COHEN, J. L., VANGALA, P., TENCEROVA, M., NICOLORO, S. M., YAWE, J. C., SHEN, Y., CZECH, M. P. & AOUADI, M. 2014. Local proliferation of macrophages contributes to obesity-associated adipose tissue inflammation. *Cell Metab,* 19**,** 162-171.

AMORIM, J. A., COPPOTELLI, G., ROLO, A. P., PALMEIRA, C. M., ROSS, J. M. & SINCLAIR, D. A. 2022. Mitochondrial and metabolic dysfunction in ageing and age-related diseases. *Nat Rev Endocrinol,* 18**,** 243-258.

AN, Y. A. & SCHERER, P. E. 2020. Mouse Adipose Tissue Protein Extraction. *Bio Protoc,* 10**,** e3631.

ANDERSEN, A., LUND, A., KNOP, F. K. & VILSBOLL, T. 2018. Glucagon-like peptide 1 in health and disease. *Nat Rev Endocrinol,* 14**,** 390-403.

ARCHER, A., STOLARCZYK, E., DORIA, M. L., HELGUERO, L., DOMINGUES, R., HOWARD, J. K., MODE, A., KORACH-ANDRE, M. & GUSTAFSSON, J. A. 2013. LXR activation by GW3965 alters fat tissue distribution and adipose tissue inflammation in ob/ob female mice. *J Lipid Res,* 54**,** 1300-11.

BACIGALUPA, Z. A., LANDIS, M. D. & RATHMELL, J. C. 2024. Nutrient inputs and social metabolic control of T cell fate. *Cell Metab,* 36**,** 10-20.

BAER, J. M., ZUO, C., KANG, L. I., DE LA LASTRA, A. A., BORCHERDING, N. C., KNOLHOFF, B. L., BOGNER, S. J., ZHU, Y., YANG, L., LAURENT, J., LEWIS, M. A., ZHANG, N., KIM, K. W., FIELDS, R. C., YOKOYAMA, W. M., MILLS, J. C., DING, L., RANDOLPH, G. J. & DENARDO, D. G. 2023. Fibrosis induced by resident macrophages has divergent roles in pancreas inflammatory injury and PDAC. *Nat Immunol,* 24**,** 1443-1457.

BAERGA, R., ZHANG, Y., CHEN, P. H., GOLDMAN, S. & JIN, S. 2009. Targeted deletion of autophagy-related 5 (atg5) impairs adipogenesis in a cellular model and in mice. *Autophagy,* 5**,** 1118-30.

BAGHERNIYA, M., BUTLER, A. E., BARRETO, G. E. & SAHEBKAR, A. 2018. The effect of fasting or calorie restriction on autophagy induction: A review of the literature. *Ageing Res Rev,* 47**,** 183-197.

BAKER, S. A. & RUTTER, J. 2023. Metabolites as signalling molecules. *Nat Rev Mol Cell Biol,* 24**,** 355-374.

BELTRA, J. C., MANNE, S., ABDEL-HAKEEM, M. S., KURACHI, M., GILES, J. R., CHEN, Z., CASELLA, V., NGIOW, S. F., KHAN, O., HUANG, Y. J., YAN, P., NZINGHA, K., XU, W., AMARAVADI, R. K., XU, X., KARAKOUSIS, G. C., MITCHELL, T. C., SCHUCHTER, L. M., HUANG, A. C. & WHERRY, E. J. 2020. Developmental Relationships of Four Exhausted CD8(+) T Cell Subsets Reveals Underlying Transcriptional and Epigenetic Landscape Control Mechanisms. *Immunity,* 52**,** 825-841 e8.

BERG, N. K., LI, J., KIM, B., MILLS, T., PEI, G., ZHAO, Z., LI, X., ZHANG, X., RUAN, W., ELTZSCHIG, H. K. & YUAN, X. 2021. Hypoxia-inducible factor-dependent induction of myeloid-derived netrin-1 attenuates natural killer cell infiltration during endotoxin-induced lung injury. *FASEB J,* 35**,** e21334.

BISWAS, S. K. & MANTOVANI, A. 2012. Orchestration of metabolism by macrophages. *Cell metabolism,* 15**,** 432-437.

BLERIOT, C., CHAKAROV, S. & GINHOUX, F. 2020. Determinants of Resident Tissue Macrophage Identity and Function. *Immunity,* 52**,** 957-970.

BLUHER, M. 2020. Metabolically Healthy Obesity. *Endocr Rev,* 41.

BOHAUD, C., JOHANSEN, M. D., JORGENSEN, C., KREMER, L., IPSEIZ, N. & DJOUAD, F. 2021. The Role of Macrophages During Mammalian Tissue Remodeling and Regeneration Under Infectious and Non-Infectious Conditions. *Front Immunol,* 12**,** 707856.

BOHM, A., KEUPER, M., MEILE, T., ZDICHAVSKY, M., FRITSCHE, A., HARING, H. U., DE ANGELIS, M. H., STAIGER, H. & FRANKO, A. 2020. Increased mitochondrial respiration of adipocytes from metabolically unhealthy obese compared to healthy obese individuals. *Sci Rep,* 10**,** 12407.

BOND, S. T., CALKIN, A. C. & DREW, B. G. 2022. Adipose-Derived Extracellular Vesicles: Systemic Messengers and Metabolic Regulators in Health and Disease. *Front Physiol,* 13**,** 837001.

BORSA, M., OBBA, S., RICHTER, F. C., ZHANG, H., RIFFELMACHER, T., CARRELHA, J., ALSALEH, G., JACOBSEN, S. E. W. & SIMON, A. K. 2024. Autophagy preserves hematopoietic stem cells by restraining MTORC1-mediated cellular anabolism. *Autophagy,* 20**,** 45-57.

BOWE, J. E., FRANKLIN, Z. J., HAUGE-EVANS, A. C., KING, A. J., PERSAUD, S. J. & JONES, P. M. 2014. Metabolic phenotyping guidelines: assessing glucose homeostasis in rodent models. *J Endocrinol,* 222**,** G13-25.

BUECHLER, M. B., FU, W. & TURLEY, S. J. 2021. Fibroblast-macrophage reciprocal interactions in health, fibrosis, and cancer. *Immunity,* 54**,** 903-915.

CAI, J., PIRES, K. M., FERHAT, M., CHAURASIA, B., BUFFOLO, M. A., SMALLING, R., SARGSYAN, A., ATKINSON, D. L., SUMMERS, S. A., GRAHAM, T. E. & BOUDINA, S. 2018. Autophagy Ablation in Adipocytes Induces Insulin Resistance and Reveals Roles for Lipid Peroxide and Nrf2 Signaling in Adipose-Liver Crosstalk. *Cell Reports,* 25**,** 1708-1717.e5.

CASTELLINO, F. & GERMAIN, R. N. 2006. Cooperation between CD4+ and CD8+ T cells: when, where, and how. *Annu Rev Immunol,* 24**,** 519-40.

CAUWELS, A., ROGGE, E., VANDENDRIESSCHE, B., SHIVA, S. & BROUCKAERT, P. 2014. Extracellular ATP drives systemic inflammation, tissue damage and mortality. *Cell Death Dis,* 5**,** e1102.

CHAKAROV, S., LIM, H. Y., TAN, L., LIM, S. Y., SEE, P., LUM, J., ZHANG, X. M., FOO, S., NAKAMIZO, S., DUAN, K., KONG, W. T., GENTEK, R., BALACHANDER, A., CARBAJO, D., BLERIOT, C., MALLERET, B., TAM, J. K. C., BAIG, S., SHABEER, M., TOH, S. A. E. S., SCHLITZER, A., LARBI, A., MARICHAL, T., MALISSEN, B., CHEN, J., POIDINGER, M., KABASHIMA, K., BAJENOFF, M., NG, L. G., ANGELI, V. & GINHOUX, F. 2019. Two distinct interstitial macrophage populations coexist across tissues in specific subtissular niches. *Science,* 363.

CHEN, C., LU, J. M. & YAO, Q. 2016. Hyperuricemia-Related Diseases and Xanthine Oxidoreductase (XOR) Inhibitors: An Overview. *Med Sci Monit,* 22**,** 2501-12.

CHEN, K., CHEONG, L. Y., GAO, Y., ZHANG, Y., FENG, T., WANG, Q., JIN, L., HONORE, E., LAM, K. S. L., WANG, W., HUI, X. & XU, A. 2022. Adipose-targeted triiodothyronine therapy counteracts obesity-related metabolic complications and atherosclerosis with negligible side effects. *Nat Commun,* 13**,** 7838.

CHEN, Q., LAI, S. M., XU, S., TAN, Y., LEONG, K., LIU, D., TAN, J. C., NAIK, R. R., BARRON, A. M., ADAV, S. S., CHEN, J., CHONG, S. Z., NG, L. G. & RUEDL, C. 2021. Resident macrophages restrain pathological adipose tissue remodeling and protect vascular integrity in obese mice. *EMBO Rep,* 22**,** e52835.

CHEN, Z., JI, Z., NGIOW, S. F., MANNE, S., CAI, Z., HUANG, A. C., JOHNSON, J., STAUPE, R. P., BENGSCH, B., XU, C., YU, S., KURACHI, M., HERATI, R. S., VELLA, L. A., BAXTER, A. E., WU, J. E., KHAN, O., BELTRA, J. C., GILES, J. R., STELEKATI, E., MCLANE, L. M., LAU, C. W., YANG, X., BERGER, S. L., VAHEDI, G., JI, H. & WHERRY, E. J. 2019. TCF-1-Centered Transcriptional Network Drives an Effector versus Exhausted CD8 T Cell-Fate Decision. *Immunity,* 51**,** 840-855 e5.

CHO, K. W., MORRIS, D. L., DELPROPOSTO, J. L., GELETKA, L., ZAMARRON, B., MARTINEZ-SANTIBANEZ, G., MEYER, K. A., SINGER, K., O'ROURKE, R. W. & LUMENG, C. N. 2014a. An MHC II-dependent activation loop between adipose tissue macrophages and CD4+ T cells controls obesity-induced inflammation. *Cell Rep,* 9**,** 605-17.

CHO, K. W., MORRIS, D. L. & LUMENG, C. N. 2014b. Flow cytometry analyses of adipose tissue macrophages. *Methods Enzymol,* 537**,** 297-314.

CHOUCHANI, E. T. & KAJIMURA, S. 2019. Metabolic adaptation and maladaptation in adipose tissue. *Nature Metabolism,* 1**,** 189-200.

CHUNG, K. W. & CHUNG, H. Y. 2019. The Effects of Calorie Restriction on Autophagy: Role on Aging Intervention. *Nutrients,* 11.

CINTI, S., MITCHELL, G., BARBATELLI, G., MURANO, I., CERESI, E., FALOIA, E., WANG, S., FORTIER, M., GREENBERG, A. S. & OBIN, M. S. 2005. Adipocyte death defines macrophage localization and function in adipose tissue of obese mice and humans. *J Lipid Res,* 46**,** 2347-55.

CLARKE, A. J. & SIMON, A. K. 2018. Autophagy in the renewal, differentiation and homeostasis of immune cells. *Nature Reviews Immunology 2018 19:3,* 19**,** 170-183.

CLEMENTE-POSTIGO, M., TINAHONES, A., BEKAY, R. E., MALAGÓN, M. M. & TINAHONES, F. J. 2020. The Role of Autophagy in White Adipose Tissue Function: Implications for Metabolic Health. *Metabolites,* 10.

COATS, B. R., SCHOENFELT, K. Q., BARBOSA-LORENZI, V. C., PERIS, E., CUI, C., HOFFMAN, A., ZHOU, G., FERNANDEZ, S., ZHAI, L., HALL, B. A., HAKA, A. S., SHAH, A. M., REARDON, C. A., BRADY, M. J., RHODES, C. J., MAXFIELD, F. R. & BECKER, L. 2017. Metabolically Activated Adipose Tissue Macrophages Perform Detrimental and Beneficial Functions during Diet-Induced Obesity. *Cell Reports,* 20**,** 3149-3161.

CORNIER, M. A., DABELEA, D., HERNANDEZ, T. L., LINDSTROM, R. C., STEIG, A. J., STOB, N. R., VAN PELT, R. E., WANG, H. & ECKEL, R. H. 2008. The metabolic syndrome. *Endocr Rev,* 29**,** 777-822.

CREWE, C., FUNCKE, J.-B., LI, S., KUSMINSKI, C. M., KLEIN, S. & SCHERER CORRESPONDENCE, P. E. 2021. Extracellular vesicle-based interorgan transport of mitochondria from energetically stressed adipocytes.

CULEMANN, S., KNAB, K., EULER, M., WEGNER, A., GARIBAGAOGLU, H., ACKERMANN, J., FISCHER, K., KIENHOFER, D., CRAINICIUC, G., HAHN, J., GRUNEBOOM, A., NIMMERJAHN, F., UDERHARDT, S., HIDALGO, A., SCHETT, G., HOFFMANN, M. H. & KRONKE, G. 2023. Stunning of neutrophils accounts for the anti-inflammatory effects of clodronate liposomes. *J Exp Med,* 220.

DATTA, R., PODOLSKY, M. J. & ATABAI, K. 2018. Fat fibrosis: friend or foe? *JCI insight,* 3.

DEBARI, M. K. & ABBOTT, R. D. 2020. Adipose Tissue Fibrosis: Mechanisms, Models, and Importance. *Int J Mol Sci,* 21.

DEMICHEV, V., MESSNER, C. B., VERNARDIS, S. I., LILLEY, K. S. & RALSER, M. 2020. DIA-NN: neural networks and interference correction enable deep proteome coverage in high throughput. *Nat Methods,* 17**,** 41-44.

DENG, Y., WANG, Z. V., GORDILLO, R., ZHU, Y., ALI, A., ZHANG, C., WANG, X., SHAO, M., ZHANG, Z., IYENGAR, P., GUPTA, R. K., HORTON, J. D., HILL, J. A. & SCHERER, P. E. 2018. Adipocyte Xbp1s overexpression drives uridine production and reduces obesity. *Mol Metab,* 11**,** 1-17.

DERETIC, V. & KROEMER, G. 2022. Autophagy in metabolism and quality control: opposing, complementary or interlinked functions? *Autophagy,* 18**,** 283-292.

DESPRÉS, J.-P. 2021. Taking a closer look at metabolically healthy obesity. *Nature Reviews Endocrinology 2021***,** 1-2.

DICK, S. A., WONG, A., HAMIDZADA, H., NEJAT, S., NECHANITZKY, R., VOHRA, S., MUELLER, B., ZAMAN, R., KANTORES, C., ARONOFF, L., MOMEN, A., NECHANITZKY, D., LI, W. Y., RAMACHANDRAN, P., CROME, S. Q., BECHER, B., CYBULSKY, M. I., BILLIA, F., KESHAVJEE, S., MITAL, S., ROBBINS, C. S., MAK, T. W. & EPELMAN, S. 2022. Three tissue resident macrophage subsets coexist across organs with conserved origins and life cycles. *Science Immunology,* 7**,** 7777-7777.

DIKIC, I. & ELAZAR, Z. 2018. Mechanism and medical implications of mammalian autophagy. *Nat Rev Mol Cell Biol,* 19**,** 349-364.

DOS ANJOS CASSADO, A. 2017. F4/80 as a Major Macrophage Marker: The Case of the Peritoneum and Spleen. *Results Probl Cell Differ,* 62**,** 161-179.

DUFFIELD, J. S., FORBES, S. J., CONSTANDINOU, C. M., CLAY, S., PARTOLINA, M., VUTHOORI, S., WU, S., LANG, R. & IREDALE, J. P. 2005. Selective depletion of macrophages reveals distinct, opposing roles during liver injury and repair. *J Clin Invest,* 115**,** 56-65.

DUNCAN, R. E., AHMADIAN, M., JAWORSKI, K., SARKADI-NAGY, E. & SUL, H. S. 2007. Regulation of lipolysis in adipocytes. *Annu Rev Nutr,* 27**,** 79-101.

EBKE, L. A., NESTOR-KALINOSKI, A. L., SLOTTERBECK, B. D., AL-DIERI, A. G., GHOSH-LESTER, S., RUSSO, L., NAJJAR, S. M., VON GRAFENSTEIN, H. & MCINERNEY, M. F. 2014. Tight association between macrophages and adipocytes in obesity: implications for adipocyte preparation. *Obesity (Silver Spring),* 22**,** 1246-55.

EMONT, M. P., JACOBS, C., ESSENE, A. L., PANT, D., TENEN, D., COLLELUORI, G., DI VINCENZO, A., JORGENSEN, A. M., DASHTI, H., STEFEK, A., MCGONAGLE, E., STROBEL, S., LABER, S., AGRAWAL, S., WESTCOTT, G. P., KAR, A., VEREGGE, M. L., GULKO, A., SRINIVASAN, H., KRAMER, Z., DE FILIPPIS, E., MERKEL, E., DUCIE, J., BOYD, C. G., GOURASH, W., COURCOULAS, A., LIN, S. J., LEE, B. T., MORRIS, D., TOBIAS, A., KHERA, A. V., CLAUSSNITZER, M., PERS, T. H., GIORDANO, A., ASHENBERG, O., REGEV, A., TSAI, L. T. & ROSEN, E. D. 2022. A single-cell atlas of human and mouse white adipose tissue. *Nature,* 603**,** 926-933.

EPELMAN, S., LAVINE, K. J. & RANDOLPH, G. J. 2014. Origin and functions of tissue macrophages. *Immunity,* 41**,** 21-35.

FABRE, T., BARRON, A. M. S., CHRISTENSEN, S. M., ASANO, S., BOUND, K., LECH, M. P., WADSWORTH, M. H., 2ND, CHEN, X., WANG, C., WANG, J., MCMAHON, J., SCHLERMAN, F., WHITE, A., KRAVARIK, K. M., FISHER, A. J., BORTHWICK, L. A., HART, K. M., HENDERSON, N. C., WYNN, T. A. & DOWER, K. 2023. Identification of a broadly fibrogenic macrophage subset induced by type 3 inflammation. *Sci Immunol,* 8**,** eadd8945.

FAN, K. Q., LI, Y. Y., WANG, H. L., MAO, X. T., GUO, J. X., WANG, F., HUANG, L. J., LI, Y. N., MA, X. Y., GAO, Z. J., CHEN, W., QIAN, D. D., XUE, W. J., CAO, Q., ZHANG, L., SHEN, L., ZHANG, L., TONG, C., ZHONG, J. Y., LU, W., LU, L., REN, K. M., ZHONG, G.,

WANG, Y., TANG, M., FENG, X. H., CHAI, R. J. & JIN, J. 2019. Stress-Induced Metabolic Disorder in Peripheral CD4(+) T Cells Leads to Anxiety-like Behavior. *Cell,* 179**,** 864-879 e19.

FÉLIX, I., JOKELA, H., KARHULA, J., KOTAJA, N., SAVONTAUS, E., SALMI, M. & RANTAKARI, P. 2021. Single-Cell Proteomics Reveals the Defined Heterogeneity of Resident Macrophages in White Adipose Tissue. *Frontiers in Immunology,* 12**,** 2995-2995.

FELIX, J. B., COX, A. R. & HARTIG, S. M. 2021. Acetyl-CoA and Metabolite Fluxes Regulate White Adipose Tissue Expansion. *Trends Endocrinol Metab,* 32**,** 320-332.

FENG, T., ZHAO, X., GU, P., YANG, W., WANG, C., GUO, Q., LONG, Q., LIU, Q., CHENG, Y., LI, J., CHEUNG, C. K. Y., WU, D., KONG, X., XU, Y., YE, D., HUA, S., LOOMES, K., XU, A. & HUI, X. 2022. Adipocyte-derived lactate is a signalling metabolite that potentiates adipose macrophage inflammation via targeting PHD2. *Nat Commun,* 13**,** 5208.

FENG, Y., HE, D., YAO, Z. & KLIONSKY, D. J. 2014. The machinery of macroautophagy. *Cell Research,* 24**,** 24-24.

FERRANTE, A. W. 2013. The immune cells in adipose tissue. *Diabetes, Obesity and Metabolism,* 15**,** 34-38.

FERRERO, R., RAINER, P. & DEPLANCKE, B. 2020. Toward a Consensus View of Mammalian Adipocyte Stem and Progenitor Cell Heterogeneity. *Trends Cell Biol,* 30**,** 937-950.

FERRIER, D. R. 2014. *Biochemistry*, Wolters Kluwer Health.

FROMME, T., KLEIGREWE, K., DUNKEL, A., RETZLER, A., LI, Y., MAURER, S., FISCHER, N., DIEZKO, R., KANZLEITER, T., HIRSCHBERG, V., HOFMANN, T. & KLINGENSPOR, M. 2018. Degradation of brown adipocyte purine nucleotides regulates uncoupling protein 1 activity. *Mol Metab,* 8**,** 77-85.

FRUHBECK, G., CATALAN, V., RODRIGUEZ, A. & GOMEZ-AMBROSI, J. 2018. Adiponectin-leptin ratio: A promising index to estimate adipose tissue dysfunction. Relation with obesity-associated cardiometabolic risk. *Adipocyte,* 7**,** 57-62.

FURUHASHI, M. 2020. New insights into purine metabolism in metabolic diseases: role of xanthine oxidoreductase activity. *Am J Physiol Endocrinol Metab,* 319**,** E827-E834.

GALVAN-PENA, S. & O'NEILL, L. A. 2014. Metabolic reprograming in macrophage polarization. *Front Immunol,* 5**,** 420.

GAVIN, K. M. & BESSESEN, D. H. 2020. Sex Differences in Adipose Tissue Function. *Endocrinol Metab Clin North Am,* 49**,** 215-228.

GHABEN, A. L. & SCHERER, P. E. 2019. Adipogenesis and metabolic health. *Nature Reviews Molecular Cell Biology,* 20**,** 242-258.

GHOSH, A. K., MAU, T., O'BRIEN, M., GARG, S. & YUNG, R. 2016. Impaired autophagy activity is linked to elevated ER-stress and inflammation in aging adipose tissue. *Aging (Albany NY),* 8**,** 2525-2537.

GIANNECCHINI, M., MATTEUCCI, M., PESI, R., SGARRELLA, F., TOZZI, M. G. & CAMICI, M. 2005. Uptake and utilization of nucleosides for energy repletion. *Int J Biochem Cell Biol,* 37**,** 797-808.

GLINIAK, C. M., PEDERSEN, L. & SCHERER, P. E. 2023. Adipose tissue fibrosis: the unwanted houseguest invited by obesity. *J Endocrinol,* 259.

GOMEZ PERDIGUERO, E., KLAPPROTH, K., SCHULZ, C., BUSCH, K., AZZONI, E., CROZET, L., GARNER, H., TROUILLET, C., DE BRUIJN, M. F., GEISSMANN, F. & RODEWALD, H. R. 2015. Tissue-resident macrophages originate from yolk-sac-derived erythro-myeloid progenitors. *Nature,* 518**,** 547-51.

GONZÁLEZ-MUNIESA, P., MÁRTINEZ-GONZÁLEZ, M. A., HU, F. B., DESPRÉS, J. P., MATSUZAWA, Y., LOOS, R. J. F., MORENO, L. A., BRAY, G. A. & MARTINEZ, J. A. 2017. Obesity. *Nature Reviews Disease Primers,* 3.

GORDON, S. R., MAUTE, R. L., DULKEN, B. W., HUTTER, G., GEORGE, B. M., MCCRACKEN, M. N., GUPTA, R., TSAI, J. M., SINHA, R., COREY, D., RING, A. M., CONNOLLY, A. J. & WEISSMAN, I. L. 2017. PD-1 expression by tumour-associated macrophages inhibits phagocytosis and tumour immunity. *Nature,* 545**,** 495-499.

GRABNER, G. F., XIE, H., SCHWEIGER, M. & ZECHNER, R. 2021. Lipolysis: cellular mechanisms for lipid mobilization from fat stores. *Nat Metab,* 3**,** 1445-1465.

GREEN, C. R., WALLACE, M., DIVAKARUNI, A. S., PHILLIPS, S. A., MURPHY, A. N., CIARALDI, T. P. & METALLO, C. M. 2016. Branched-chain amino acid catabolism fuels adipocyte differentiation and lipogenesis. *Nat Chem Biol,* 12**,** 15-21.

GUILLIAMS, M. & SCOTT, C. L. 2017. Does niche competition determine the origin of tissue-resident macrophages? *Nat Rev Immunol,* 17**,** 451-460.

GUO, J. Y., TENG, X., LADDHA, S. V., MA, S., VAN NOSTRAND, S. C., YANG, Y., KHOR, S., CHAN, C. S., RABINOWITZ, J. D. & WHITE, E. 2016. Autophagy provides metabolic substrates to maintain energy charge and nucleotide pools in Ras-driven lung cancer cells. *Genes Dev,* 30**,** 1704-17.

HAGBERG, C. E., LI, Q., KUTSCHKE, M., BHOWMICK, D., KISS, E., SHABALINA, I. G., HARMS, M. J., SHILKOVA, O., KOZINA, V., NEDERGAARD, J., BOUCHER, J., THORELL, A. & SPALDING, K. L. 2018. Flow Cytometry of Mouse and Human Adipocytes for the Analysis of Browning and Cellular Heterogeneity. *Cell Reports,* 24**,** 2746-2756.e5.

HALASI, M., WANG, M., CHAVAN, T. S., GAPONENKO, V., HAY, N. & GARTEL, A. L. 2013. ROS inhibitor N-acetyl-L-cysteine antagonizes the activity of proteasome inhibitors. *Biochem J,* 454**,** 201-8.

HALBERG, N., KHAN, T., TRUJILLO, M. E., WERNSTEDT-ASTERHOLM, I., ATTIE, A. D., SHERWANI, S., WANG, Z. V., LANDSKRONER-EIGER, S., DINEEN, S., MAGALANG, U. J., BREKKEN, R. A. & SCHERER, P. E. 2009. Hypoxia-inducible factor 1alpha induces fibrosis and insulin resistance in white adipose tissue. *Mol Cell Biol,* 29**,** 4467-83.

HAN, S. J., GLATMAN ZARETSKY, A., ANDRADE-OLIVEIRA, V., COLLINS, N., DZUTSEV, A., SHAIK, J., MORAIS DA FONSECA, D., HARRISON, O. J., TAMOUTOUNOUR, S.,

BYRD, A. L., SMELKINSON, M., BOULADOUX, N., BLISKA, J. B., BRENCHLEY, J. M., BRODSKY, I. E. & BELKAID, Y. 2017. White Adipose Tissue Is a Reservoir for Memory T Cells and Promotes Protective Memory Responses to Infection. *Immunity,* 47**,** 1154-1168 e6.

HEINONEN, S., JOKINEN, R., RISSANEN, A. & PIETILAINEN, K. H. 2020. White adipose tissue mitochondrial metabolism in health and in obesity. *Obes Rev,* 21**,** e12958.

HENDERSON, N. C., RIEDER, F. & WYNN, T. A. 2020. Fibrosis: from mechanisms to medicines. *Nature,* 587**,** 555-566.

HEZAVEH, K., SHINDE, R. S., KLOTGEN, A., HALABY, M. J., LAMORTE, S., CIUDAD, M. T., QUEVEDO, R., NEUFELD, L., LIU, Z. Q., JIN, R., GRUNWALD, B. T., FOERSTER, E. G., CHAHARLANGI, D., GUO, M., MAKHIJANI, P., ZHANG, X., PUGH, T. J., PINTO, D. M., CO, I. L., MCGUIGAN, A. P., JANG, G. H., KHOKHA, R., OHASHI, P. S., O'KANE, G. M., GALLINGER, S., NAVARRE, W. W., MAUGHAN, H., PHILPOTT, D. J., BROOKS, D. G. & MCGAHA, T. L. 2022. Tryptophan-derived microbial metabolites activate the aryl hydrocarbon receptor in tumor-associated macrophages to suppress anti-tumor immunity. *Immunity,* 55**,** 324-340 e8.

HILL, D. A., LIM, H.-W., KIM, Y. H., HO, W. Y., FOONG, Y. H., NELSON, V. L., NGUYEN, H. C. B., CHEGIREDDY, K., KIM, J., HABERTHEUER, A., VALLABHAJOSYULA, P., KAMBAYASHI, T., WON, K.-J. & LAZAR, M. A. 2018. Distinct macrophage populations direct inflammatory versus physiological changes in adipose tissue. *Proceedings of the National Academy of Sciences,* 115**,** E5096-E5105.

HOTAMISLIGIL, G. S., SHARGILL, N. S. & SPIEGELMAN, B. M. 1993. Adipose expression of tumor necrosis factor-alpha: direct role in obesity-linked insulin resistance. *Science,* 259**,** 87-91.

HSIAO, W. Y. & GUERTIN, D. A. 2019. De Novo Lipogenesis as a Source of Second Messengers in Adipocytes. *Curr Diab Rep,* 19**,** 138.

HUANG, Z., XIE, N., ILLES, P., DI VIRGILIO, F., ULRICH, H., SEMYANOV, A., VERKHRATSKY, A., SPERLAGH, B., YU, S. G., HUANG, C. & TANG, Y. 2021. From purines to purinergic signalling: molecular functions and human diseases. *Signal Transduct Target Ther,* 6**,** 162.

HUSTED, A. S., TRAUELSEN, M., RUDENKO, O., HJORTH, S. A. & SCHWARTZ, T. W. 2017. GPCR-Mediated Signaling of Metabolites. *Cell Metab,* 25**,** 777-796.

ICER, M. A. & GEZMEN-KARADAG, M. 2018. The multiple functions and mechanisms of osteopontin. *Clin Biochem,* 59**,** 17-24.

JACKS, R. D. & LUMENG, C. N. 2024. Macrophage and T cell networks in adipose tissue. *Nat Rev Endocrinol,* 20**,** 50-61.

JAHANGIRI, B., SAEI, A. K., OBI, P. O., ASGHARI, N., LORZADEH, S., HEKMATIRAD, S., RAHMATI, M., VELAYATIPOUR, F., ASGHARI, M. H., SALEEM, A. & MOOSAVI, M. A. 2022. Exosomes, autophagy and ER stress pathways in human diseases: Cross-regulation and therapeutic approaches. *Biochimica et Biophysica Acta - Molecular Basis of Disease,* 1868.

JAITIN, D. A., ADLUNG, L., THAISS, C. A., WEINER, A., LI, B., DESCAMPS, H., LUNDGREN, P., BLERIOT, C., LIU, Z., DECZKOWSKA, A., KEREN-SHAUL, H., DAVID, E., ZMORA, N., ELDAR, S. M., LUBEZKY, N., SHIBOLET, O., HILL, D. A., LAZAR, M. A., COLONNA, M., GINHOUX, F., SHAPIRO, H., ELINAV, E. & AMIT, I. 2019. Lipid-Associated Macrophages Control Metabolic Homeostasis in a Trem2-Dependent Manner. *Cell,* 178**,** 686-698.e14.

JAMES, D. E., STÖCKLI, J. & BIRNBAUM, M. J. 2021. The aetiology and molecular landscape of insulin resistance. *Nature Reviews Molecular Cell Biology 2021 22:11,* 22**,** 751-771.

JANSEN, H. J., VAN ESSEN, P., KOENEN, T., JOOSTEN, L. A. B., NETEA, M. G., TACK, C. J. & STIENSTRA, R. 2012. Autophagy Activity Is Up-Regulated in Adipose Tissue of Obese Individuals and Modulates Proinflammatory Cytokine Expression. *Endocrinology,* 153**,** 5866-5874.

JING, M., LI, Y., WANG, M., ZHANG, H., WEI, P., ZHOU, Y., ISHIMWE, N., HUANG, X., WANG, L., WEN, L., WANG, W. & ZHANG, Y. 2021. Photoresponsive PAMAM-Assembled Nanocarrier Loaded with Autophagy Inhibitor for Synergistic Cancer Therapy. *Small,* 17**,** e2102295.

JOE, A. W., YI, L., EVEN, Y., VOGL, A. W. & ROSSI, F. M. 2009. Depot-specific differences in adipogenic progenitor abundance and proliferative response to high-fat diet. *Stem Cells,* 27**,** 2563-70.

JU, L., HAN, J., ZHANG, X., DENG, Y., YAN, H., WANG, C., LI, X., CHEN, S., ALIMUJIANG, M., LI, X., FANG, Q., YANG, Y. & JIA, W. 2019. Obesity-associated inflammation triggers an autophagy–lysosomal response in adipocytes and causes degradation of perilipin 1. *Cell Death & Disease 2019 10:2,* 10**,** 1-16.

JUMPER, J., EVANS, R., PRITZEL, A., GREEN, T., FIGURNOV, M., RONNEBERGER, O., TUNYASUVUNAKOOL, K., BATES, R., ZIDEK, A., POTAPENKO, A., BRIDGLAND, A., MEYER, C., KOHL, S. A. A., BALLARD, A. J., COWIE, A., ROMERA-PAREDES, B., NIKOLOV, S., JAIN, R., ADLER, J., BACK, T., PETERSEN, S., REIMAN, D., CLANCY, E., ZIELINSKI, M., STEINEGGER, M., PACHOLSKA, M., BERGHAMMER, T., BODENSTEIN, S., SILVER, D., VINYALS, O., SENIOR, A. W., KAVUKCUOGLU, K., KOHLI, P. & HASSABIS, D. 2021. Highly accurate protein structure prediction with AlphaFold. *Nature,* 596**,** 583-589.

JUNG, S. M., DOXSEY, W. G., LE, J., HALEY, J. A., MAZUECOS, L., LUCIANO, A. K., LI, H., JANG, C. & GUERTIN, D. A. 2021. In vivo isotope tracing reveals the versatility of glucose as a brown adipose tissue substrate. *Cell Rep,* 36**,** 109459.

KANASAKI, K. & KOYA, D. 2011. Biology of obesity: lessons from animal models of obesity. *J Biomed Biotechnol,* 2011**,** 197636.

KATHEDER, N. S., KHEZRI, R., O'FARRELL, F., SCHULTZ, S. W., JAIN, A., SCHINK, M. K. O., THEODOSSIOU, T. A., JOHANSEN, T., JUHÁSZ, G., BILDER, D., BRECH, A., STENMARK, H. & RUSTEN, T. E. 2017. Microenvironmental autophagy promotes tumour growth. *Nature 2017 541:7637,* 541**,** 417-420.

KATHER, H. 1988. Purine accumulation in human fat cell suspensions. Evidence that human adipocytes release inosine and hypoxanthine rather than adenosine. *J Biol Chem,* 263**,** 8803-9.

KATHER, H. 1990. Pathways of purine metabolism in human adipocytes. Further evidence against a role of adenosine as an endogenous regulator of human fat cell function. *J Biol Chem,* 265**,** 96-102.

KAUR, J. & DEBNATH, J. 2015. Autophagy at the crossroads of catabolism and anabolism. *Nat Rev Mol Cell Biol,* 16**,** 461-72.

KAUSHIK, N., KAUSHIK, N. K., CHOI, E. H. & KIM, J. H. 2021. Blockade of Cellular Energy Metabolism through 6-Aminonicotinamide Reduces Proliferation of Non-Small Lung Cancer Cells by Inducing Endoplasmic Reticulum Stress. *Biology (Basel),* 10.

KEUPER, M. 2019. On the role of macrophages in the control of adipocyte energy metabolism. *Endocr Connect,* 8**,** R105-R121.

KIMBALL, A. K., OKO, L. M., BULLOCK, B. L., NEMENOFF, R. A., VAN DYK, L. F. & CLAMBEY, E. T. 2018. A Beginner's Guide to Analyzing and Visualizing Mass Cytometry Data. *J Immunol,* 200**,** 3-22.

KITADA, M. & KOYA, D. 2021. Autophagy in metabolic disease and ageing. *Nat Rev Endocrinol,* 17**,** 647-661.

KLEINERT, M., CLEMMENSEN, C., HOFMANN, S. M., MOORE, M. C., RENNER, S., WOODS, S. C., HUYPENS, P., BECKERS, J., DE ANGELIS, M. H., SCHURMANN, A., BAKHTI, M., KLINGENSPOR, M., HEIMAN, M., CHERRINGTON, A. D., RISTOW, M., LICKERT, H., WOLF, E., HAVEL, P. J., MULLER, T. D. & TSCHOP, M. H. 2018. Animal models of obesity and diabetes mellitus. *Nat Rev Endocrinol,* 14**,** 140-162.

KLEMENT, J. D., PASCHALL, A. V., REDD, P. S., IBRAHIM, M. L., LU, C., YANG, D., CELIS, E., ABRAMS, S. I., OZATO, K. & LIU, K. 2018. An osteopontin/CD44 immune checkpoint controls CD8+ T cell activation and tumor immune evasion. *J Clin Invest,* 128**,** 5549-5560.

KLIONSKY, D. J., ABDEL-AZIZ, A. K., ABDELFATAH, S., ABDELLATIF, M., ABDOLI, A., ABEL, S., ABELIOVICH, H., ABILDGAARD, M. H., ABUDU, Y. P., ACEVEDO-AROZENA, A., ADAMOPOULOS, I. E., ADELI, K., ADOLPH, T. E., ADORNETTO, A., AFLAKI, E., AGAM, G., AGARWAL, A., AGGARWAL, B. B., AGNELLO, M., AGOSTINIS, P., AGREWALA, J. N., AGROTIS, A., AGUILAR, P. V., AHMAD, S. T., AHMED, Z. M., AHUMADA-CASTRO, U., AITS, S., AIZAWA, S., AKKOC, Y., AKOUMIANAKI, T., AKPINAR, H. A., AL-ABD, A. M., AL-AKRA, L., AL-GHARAIBEH, A., ALAOUI-JAMALI, M. A., ALBERTI, S., ALCOCER-GOMEZ, E., ALESSANDRI, C., ALI, M., ALIM AL-BARI, M. A., ALIWAINI, S., ALIZADEH, J., ALMACELLAS, E., ALMASAN, A., ALONSO, A., ALONSO, G. D., ALTAN-BONNET, N., ALTIERI, D. C., ALVAREZ, E. M. C., ALVES, S., ALVES DA COSTA, C., ALZAHARNA, M. M., AMADIO, M., AMANTINI, C., AMARAL, C., AMBROSIO, S., AMER, A. O., AMMANATHAN, V., AN, Z., ANDERSEN, S. U., ANDRABI, S. A., ANDRADE-SILVA, M., ANDRES, A. M., ANGELINI, S., ANN, D., ANOZIE, U. C., ANSARI, M. Y., ANTAS, P., ANTEBI, A., ANTON, Z., ANWAR, T., APETOH, L., APOSTOLOVA, N., ARAKI, T., ARAKI, Y., ARASAKI, K., ARAUJO, W. L., ARAYA, J., ARDEN, C., AREVALO, M. A., ARGUELLES, S., ARIAS, E., ARIKKATH, J., ARIMOTO, H., ARIOSA, A. R., ARMSTRONG-JAMES, D., ARNAUNE-PELLOQUIN, L., AROCA, A., ARROYO, D. S., ARSOV, I., ARTERO, R., ASARO, D. M. L., ASCHNER, M., ASHRAFIZADEH, M., ASHUR-FABIAN, O., ATANASOV, A. G., AU, A. K., AUBERGER, P., AUNER, H. W., AURELIAN, L., et al. 2021a. Guidelines for the use and interpretation of assays for monitoring autophagy (4th edition)(1). *Autophagy,* 17**,** 1-382.

KLIONSKY, D. J., PETRONI, G., AMARAVADI, R. K., BAEHRECKE, E. H., BALLABIO, A., BOYA, P., BRAVO-SAN PEDRO, J. M., CADWELL, K., CECCONI, F., CHOI, A. M. K., CHOI, M. E., CHU, C. T., CODOGNO, P., COLOMBO, MARIA I., CUERVO, A. M., DERETIC, V., DIKIC, I., ELAZAR, Z., ESKELINEN, E. L., FIMIA, G. M., GEWIRTZ, D. A., GREEN, D. R., HANSEN, M., JÄÄTTELÄ, M., JOHANSEN, T., JUHÁSZ, G., KARANTZA, V., KRAFT, C., KROEMER, G., KTISTAKIS, N. T., KUMAR, S., LOPEZ-OTIN, C., MACLEOD, K. F., MADEO, F., MARTINEZ, J., MELÉNDEZ, A., MIZUSHIMA, N., MÜNZ, C., PENNINGER, J. M., PERERA, RUSHIKA M., PIACENTINI, M., REGGIORI, F., RUBINSZTEIN, D. C., RYAN, KEVIN M., SADOSHIMA, J., SANTAMBROGIO, L., SCORRANO, L., SIMON, H. U., SIMON, A. K., SIMONSEN, A., STOLZ, A., TAVERNARAKIS, N., TOOZE, S. A., YOSHIMORI, T., YUAN, J., YUE, Z., ZHONG, Q., GALLUZZI, L. & PIETROCOLA, F. 2021b. Autophagy in major human diseases. *The EMBO Journal,* 40.

KOBAYASHI, H., MATSUDA, M., FUKUHARA, A., KOMURO, R. & SHIMOMURA, I. 2009. Dysregulated glutathione metabolism links to impaired insulin action in adipocytes. *Am J Physiol Endocrinol Metab,* 296**,** E1326-34.

KODAMA, K., HORIKOSHI, M., TODA, K., YAMADA, S., HARA, K., IRIE, J., SIROTA, M., MORGAN, A. A., CHEN, R., OHTSU, H., MAEDA, S., KADOWAKI, T. & BUTTE, A. J. 2012. Expression-based genome-wide association study links the receptor CD44 in adipose tissue with type 2 diabetes. *Proceedings of the National Academy of Sciences of the United States of America,* 109**,** 7049-7054.

KOMATSU, M., WAGURI, S., UENO, T., IWATA, J., MURATA, S., TANIDA, I., EZAKI, J., MIZUSHIMA, N., OHSUMI, Y., UCHIYAMA, Y., KOMINAMI, E., TANAKA, K. & CHIBA, T. 2005. Impairment of starvation-induced and constitutive autophagy in Atg7-deficient mice. *J Cell Biol,* 169**,** 425-34.

KORNER, A., WABITSCH, M., SEIDEL, B., FISCHER-POSOVSZKY, P., BERTHOLD, A., STUMVOLL, M., BLUHER, M., KRATZSCH, J. & KIESS, W. 2005. Adiponectin expression in humans is dependent on differentiation of adipocytes and down-regulated by humoral serum components of high molecular weight. *Biochem Biophys Res Commun,* 337**,** 540-50.

KORYCKA, A., BLONSKI, J. Z. & ROBAK, T. 2007. Forodesine (BCX-1777, Immucillin H)--a new purine nucleoside analogue: mechanism of action and potential clinical application. *Mini Rev Med Chem,* 7**,** 976-83.

KOSACKA, J., KERN, M., KLÖTING, N., PAESCHKE, S., RUDICH, A., HAIM, Y., GERICKE, M., SERKE, H., STUMVOLL, M., BECHMANN, I., NOWICKI, M. & BLÜHER, M. 2015. Autophagy in adipose tissue of patients with obesity and type 2 diabetes. *Molecular and cellular endocrinology,* 409**,** 21-32.

KOVSAN, J., BLÜHER, M., TARNOVSCKI, T., KLÖTING, N., KIRSHTEIN, B., MADAR, L., SHAI, I., GOLAN, R., HARMAN-BOEHM, I., SCHÖN, M. R., GREENBERG, A. S., ELAZAR, Z., BASHAN, N. & RUDICH, A. 2011. Altered autophagy in human adipose tissues in obesity. *The Journal of clinical endocrinology and metabolism,* 96.

KRATZ, M., COATS, B. R., HISERT, K. B., HAGMAN, D., MUTSKOV, V., PERIS, E., SCHOENFELT, K. Q., KUZMA, J. N., LARSON, I., BILLING, P. S., LANDERHOLM, R. W., CROUTHAMEL, M., GOZAL, D., HWANG, S., SINGH, P. K. & BECKER, L. 2014. Metabolic dysfunction drives a mechanistically distinct proinflammatory phenotype in adipose tissue macrophages. *Cell Metab,* 20**,** 614-25.

KUK, J. L., SAUNDERS, T. J., DAVIDSON, L. E. & ROSS, R. 2009. Age-related changes in total and regional fat distribution. *Ageing Res Rev,* 8**,** 339-48.

KURAMOTO, K., KIM, Y. J., HONG, J. H. & HE, C. 2021. The autophagy protein Becn1 improves insulin sensitivity by promoting adiponectin secretion via exocyst binding. *Cell Reports,* 35.

LACERDA MARIANO, L., ROUSSEAU, M., VARET, H., LEGENDRE, R., GENTEK, R., SAENZ CORONILLA, J., BAJENOFF, M., GOMEZ PERDIGUERO, E. & INGERSOLL, M. A. 2020. Functionally distinct resident macrophage subsets differentially shape responses to infection in the bladder. *Sci Adv,* 6.

LAHIRI, V., HAWKINS, W. D. & KLIONSKY, D. J. 2019. Watch What You (Self-) Eat: Autophagic Mechanisms that Modulate Metabolism. *Cell Metab,* 29**,** 803-826.

LATTOUF, R., YOUNES, R., LUTOMSKI, D., NAAMAN, N., GODEAU, G., SENNI, K. & CHANGOTADE, S. 2014. Picrosirius red staining: a useful tool to appraise collagen networks in normal and pathological tissues. *J Histochem Cytochem,* 62**,** 751-8.

LAVIN, Y., WINTER, D., BLECHER-GONEN, R., DAVID, E., KEREN-SHAUL, H., MERAD, M., JUNG, S. & AMIT, I. 2014. Tissue-resident macrophage enhancer landscapes are shaped by the local microenvironment. *Cell,* 159**,** 1312-26.

LAWLER, H. M., UNDERKOFLER, C. M., KERN, P. A., ERICKSON, C., BREDBECK, B. & RASOULI, N. 2016. Adipose Tissue Hypoxia, Inflammation, and Fibrosis in Obese Insulin-Sensitive and Obese Insulin-Resistant Subjects. *J Clin Endocrinol Metab,* 101**,** 1422-8.

LEE, J. H., VERMA, N., THAKKAR, N., YEUNG, C. & SUNG, H. K. 2020. Intermittent Fasting: Physiological Implications on Outcomes in Mice and Men. *Physiology (Bethesda),* 35**,** 185-195.

LEIDAL, A. M., HUANG, H. H., MARSH, T., SOLVIK, T., ZHANG, D., YE, J., KAI, F. B., GOLDSMITH, J., LIU, J. Y., HUANG, Y. H., MONKKONEN, T., VLAHAKIS, A., HUANG, E. J., GOODARZI, H., YU, L., WIITA, A. P. & DEBNATH, J. 2020. The LC3-conjugation machinery specifies the loading of RNA-binding proteins into extracellular vesicles. *Nature Cell Biology,* 22**,** 187-199.

LEMPESIS, I. G., TSILINGIRIS, D., LIU, J. & DALAMAGA, M. 2022. Of mice and men: Considerations on adipose tissue physiology in animal models of obesity and human studies. *Metabol Open,* 15**,** 100208.

LEVINE, B. & KLIONSKY, D. J. 2004. Development by self-digestion: molecular mechanisms and biological functions of autophagy. *Dev Cell,* 6**,** 463-77.

LEVINE, B., MIZUSHIMA, N. & VIRGIN, H. W. 2011. Autophagy in immunity and inflammation. *Nature,* 469**,** 323-35.

LI, M., HOU, Q., ZHONG, L., ZHAO, Y. & FU, X. 2021. Macrophage Related Chronic Inflammation in Non-Healing Wounds. *Front Immunol,* 12**,** 681710.

LI, Y., LIU, R., WU, J. & LI, X. 2020. Self-eating: friend or foe? The emerging role of autophagy in fibrotic diseases. *Theranostics,* 10**,** 7993-8017.

LI, Z., XU, X., FENG, X. & MURPHY, P. M. 2016. The Macrophage-depleting Agent Clodronate Promotes Durable Hematopoietic Chimerism and Donor-specific Skin Allograft Tolerance in Mice. *Sci Rep,* 6**,** 22143.

LIN, X. & LI, H. 2021. Obesity: Epidemiology, Pathophysiology, and Therapeutics. *Front Endocrinol (Lausanne),* 12**,** 706978.

LIS-LOPEZ, L., BAUSET, C., SECO-CERVERA, M. & COSIN-ROGER, J. 2021. Is the Macrophage Phenotype Determinant for Fibrosis Development? *Biomedicines,* 9.

LIU, R. & NIKOLAJCZYK, B. S. 2019. Tissue Immune Cells Fuel Obesity-Associated Inflammation in Adipose Tissue and Beyond. *Front Immunol,* 10**,** 1587.

LOPEZ-OTIN, C., BLASCO, M. A., PARTRIDGE, L., SERRANO, M. & KROEMER, G. 2013. The hallmarks of aging. *Cell,* 153**,** 1194-217.

LOVE, M. I., HUBER, W. & ANDERS, S. 2014. Moderated estimation of fold change and dispersion for RNA-seq data with DESeq2. *Genome Biol,* 15**,** 550.

LUTZ, T. A. & WOODS, S. C. 2012. Overview of animal models of obesity. *Curr Protoc Pharmacol,* Chapter 5**,** Unit5 61.

MA, R. Y., BLACK, A. & QIAN, B. Z. 2022. Macrophage diversity in cancer revisited in the era of single-cell omics. *Trends Immunol,* 43**,** 546-563.

MACDONALD, K. P., PALMER, J. S., CRONAU, S., SEPPANEN, E., OLVER, S., RAFFELT, N. C., KUNS, R., PETTIT, A. R., CLOUSTON, A., WAINWRIGHT, B., BRANSTETTER, D., SMITH, J., PAXTON, R. J., CERRETTI, D. P., BONHAM, L., HILL, G. R. & HUME, D. A. 2010. An antibody against the colony-stimulating factor 1 receptor depletes the resident subset of monocytes and tissue- and tumor-associated macrophages but does not inhibit inflammation. *Blood,* 116**,** 3955-63.

MANIYADATH, B., ZHANG, Q., GUPTA, R. K. & MANDRUP, S. 2023. Adipose tissue at single-cell resolution. *Cell Metab,* 35**,** 386-413.

MANN, J. P., DUAN, X., PATEL, S., TABARA, L. C., SCURRIA, F., ALVAREZ-GUAITA, A., HAIDER, A., LUIJTEN, I., PAGE, M., PROTASONI, M., LIM, K., VIRTUE, S., O'RAHILLY, S., ARMSTRONG, M., PRUDENT, J., SEMPLE, R. K. & SAVAGE, D. B. 2023. A mouse model of human mitofusin-2-related lipodystrophy exhibits adipose-specific mitochondrial stress and reduced leptin secretion. *Elife,* 12.

MANTOVANI, A., ALLAVENA, P., MARCHESI, F. & GARLANDA, C. 2022. Macrophages as tools and targets in cancer therapy. *Nat Rev Drug Discov,* 21**,** 799-820.

MARCELIN, G., GAUTIER, E. L. & CLEMENT, K. 2022. Adipose Tissue Fibrosis in Obesity: Etiology and Challenges. *Annu Rev Physiol,* 84**,** 135-155.

MARINO, G., PIETROCOLA, F., EISENBERG, T., KONG, Y., MALIK, S. A., ANDRYUSHKOVA, A., SCHROEDER, S., PENDL, T., HARGER, A., NISO-SANTANO, M., ZAMZAMI, N., SCOAZEC, M., DURAND, S., ENOT, D. P., FERNANDEZ, A. F., MARTINS, I., KEPP, O., SENOVILLA, L., BAUVY, C., MORSELLI, E., VACCHELLI, E., BENNETZEN, M., MAGNES, C., SINNER, F., PIEBER, T., LOPEZ-OTIN, C., MAIURI, M. C., CODOGNO, P., ANDERSEN, J. S., HILL, J. A., MADEO, F. & KROEMER, G. 2014. Regulation of autophagy by cytosolic acetyl-coenzyme A. *Mol Cell,* 53**,** 710-25.

MARTINEZ-SANTIBANEZ, G., SINGER, K., CHO, K. W., DELPROPOSTO, J. L., MERGIAN, T. & LUMENG, C. N. 2015. Obesity-induced remodeling of the adipose tissue elastin network is independent of the metalloelastase MMP-12. *Adipocyte,* 4**,** 264-72.

MARTINS, I., WANG, Y., MICHAUD, M., MA, Y., SUKKURWALA, A. Q., SHEN, S., KEPP, O., METIVIER, D., GALLUZZI, L., PERFETTINI, J. L., ZITVOGEL, L. & KROEMER, G. 2014. Molecular mechanisms of ATP secretion during immunogenic cell death. *Cell Death Differ,* 21**,** 79-91.

MASANOVIC, M. G. & TEOT, L. 2020. Scar Contractures. *In:* TEOT, L., MUSTOE, T. A., MIDDELKOOP, E. & GAUGLITZ, G. G. (eds.) *Textbook on Scar Management: State of the Art Management and Emerging Technologies.* Cham (CH).

MATHIS, D. 2013. Immunological Goings-on in Visceral Adipose Tissue. *Cell Metabolism,* 17**,** 851-859.

MATSUHIRA, T., NISHIYAMA, O., TABATA, Y., KAJI, C., KUBOTA-ISHIDA, N., CHIBA, Y., SANO, H., IWANAGA, T. & TOHDA, Y. 2020. A novel phosphodiesterase 4 inhibitor, AA6216, reduces macrophage activity and fibrosis in the lung. *Eur J Pharmacol,* 885**,** 173508.

MATZ, A. J., QU, L., KARLINSEY, K., VELLA, A. T. & ZHOU, B. 2023. Capturing the multifaceted function of adipose tissue macrophages. *Front Immunol,* 14**,** 1148188.

MCNELIS, J. C. & OLEFSKY, J. M. 2014. Macrophages, Immunity, and Metabolic Disease. *Immunity,* 41**,** 36-48.

MEDZHITOV, R. 2021. The spectrum of inflammatory responses. *Science,* 374**,** 1070-1075.

MENG, X. M., NIKOLIC-PATERSON, D. J. & LAN, H. Y. 2016. TGF-beta: the master regulator of fibrosis. *Nat Rev Nephrol,* 12**,** 325-38.

MICHAUD, M., MARTINS, I., SUKKURWALA, A. Q., ADJEMIAN, S., MA, Y., PELLEGATTI, P., SHEN, S., KEPP, O., SCOAZEC, M., MIGNOT, G., RELLO-VARONA, S., TAILLER, M., MENGER, L., VACCHELLI, E., GALLUZZI, L., GHIRINGHELLI, F., DI VIRGILIO, F., ZITVOGEL, L. & KROEMER, G. 2011. Autophagy-dependent anticancer immune responses induced by chemotherapeutic agents in mice. *Science,* 334**,** 1573-7.

MICHL, J., PARK, K. C. & SWIETACH, P. 2019. Evidence-based guidelines for controlling pH in mammalian live-cell culture systems. *Commun Biol,* 2**,** 144.

MILES, H. N., TOMLIN, D., RICKE, W. A. & LI, L. 2023. Integrating intracellular and extracellular proteomic profiling for in-depth investigations of cellular communication in a model of prostate cancer. *Proteomics,* 23**,** e2200287.

MITCHELL, S., THOMAS, G., HARVEY, K., COTTELL, D., REVILLE, K., BERLASCONI, G., PETASIS, N. A., ERWIG, L., REES, A. J., SAVILL, J., BRADY, H. R. & GODSON, C. 2002. Lipoxins, aspirin-triggered epi-lipoxins, lipoxin stable analogues, and the resolution of inflammation: stimulation of macrophage phagocytosis of apoptotic neutrophils in vivo. *J Am Soc Nephrol,* 13**,** 2497-507.

MIZUNOE, Y., SUDO, Y., OKITA, N., HIRAOKA, H., MIKAMI, K., NARAHARA, T., NEGISHI, A., YOSHIDA, M., HIGASHIBATA, R., WATANABE, S., KANEKO, H., NATORI, D., FURUICHI, T., YASUKAWA, H., KOBAYASHI, M. & HIGAMI, Y. 2017. Involvement of

lysosomal dysfunction in autophagosome accumulation and early pathologies in adipose tissue of obese mice. *Autophagy,* 13**,** 642-642.

MONTEAGUDO-CASCALES, E., GUMEROV, V. M., FERNANDEZ, M., MATILLA, M. A., GAVIRA, J. A., ZHULIN, I. B. & KRELL, T. 2024. Ubiquitous purine sensor modulates diverse signal transduction pathways in bacteria. *Nat Commun,* 15**,** 5867.

MOORE, R. J. & STANLEY, D. 2016. Experimental design considerations in microbiota/inflammation studies. *Clin Transl Immunology,* 5**,** e92.

MORIGNY, P., BOUCHER, J., ARNER, P. & LANGIN, D. 2021. Lipid and glucose metabolism in white adipocytes: pathways, dysfunction and therapeutics. *Nat Rev Endocrinol,* 17**,** 276-295.

MORRIS, D. L., CHO, K. W., DELPROPOSTO, J. L., OATMEN, K. E., GELETKA, L. M., MARTINEZ-SANTIBANEZ, G., SINGER, K. & LUMENG, C. N. 2013. Adipose tissue macrophages function as antigen-presenting cells and regulate adipose tissue CD4+ T cells in mice. *Diabetes,* 62**,** 2762-72.

MRAZ, M. & HALUZIK, M. 2014. The role of adipose tissue immune cells in obesity and low-grade inflammation. *J Endocrinol,* 222**,** R113-27.

MULLEN, N. J. & SINGH, P. K. 2023. Nucleotide metabolism: a pan-cancer metabolic dependency. *Nat Rev Cancer,* 23**,** 275-294.

MULLER, C. E. & JACOBSON, K. A. 2011. Xanthines as adenosine receptor antagonists. *Handb Exp Pharmacol***,** 151-99.

NAGAO, H., NISHIZAWA, H., BAMBA, T., NAKAYAMA, Y., ISOZUMI, N., NAGAMORI, S., KANAI, Y., TANAKA, Y., KITA, S., FUKUDA, S., FUNAHASHI, T., MAEDA, N., FUKUSAKI, E. & SHIMOMURA, I. 2017. Increased Dynamics of Tricarboxylic Acid Cycle and Glutamate Synthesis in Obese Adipose Tissue: IN VIVO METABOLIC TURNOVER ANALYSIS. *J Biol Chem,* 292**,** 4469-4483.

NANCE, S. A., MUIR, L. & LUMENG, C. 2022. Adipose tissue macrophages: Regulators of adipose tissue immunometabolism during obesity. *Mol Metab,* 66**,** 101642.

NGUYEN, T. A. & DEBNATH, J. 2022. Control of unconventional secretion by the autophagy machinery. *Current Opinion in Physiology,* 29.

NHS. 2022. *Health Survey for England* [Online]. Available: https://digital.nhs.uk/data-and-information/publications/statistical/health-survey-for-england/2021# [Accessed May 1st 2024].

NICOLÁS-ÁVILA, J. A., LECHUGA-VIECO, A. V., ESTEBAN-MARTÍNEZ, L., SÁNCHEZ-DÍAZ, M., DÍAZ-GARCÍA, E., SANTIAGO, D. J., RUBIO-PONCE, A., LI, J. L. Y., BALACHANDER, A., QUINTANA, J. A., MARTÍNEZ-DE-MENA, R., CASTEJÓN-VEGA, B., PUN-GARCÍA, A., TRAVÉS, P. G., BONZÓN-KULICHENKO, E., GARCÍA-MARQUÉS, F., CUSSÓ, L., A-GONZÁLEZ, N., GONZÁLEZ-GUERRA, A., ROCHE-MOLINA, M., MARTIN-SALAMANCA, S., CRAINICIUC, G., GUZMÁN, G., LARRAZABAL, J., HERRERO-GALÁN, E., ALEGRE-CEBOLLADA, J., LEMKE, G., ROTHLIN, C. V., JIMENEZ-BORREGUERO, L. J., REYES, G., CASTRILLO, A., DESCO, M., MUÑOZ-CÁNOVES, P., IBÁÑEZ, B., TORRES, M., NG, L. G., PRIORI, S. G., BUENO, H., VÁZQUEZ, J., CORDERO, M. D., BERNAL, J. A., ENRÍQUEZ, J. A. &

HIDALGO, A. 2020. A Network of Macrophages Supports Mitochondrial Homeostasis in the Heart. *Cell,* 183**,** 94-109.e23.

NUÑEZ, C. E., RODRIGUES, V. S., GOMES, F. S., DE MOURA, R. F., VICTORIO, S. C., BOMBASSARO, B., CHAIM, E. A., PAREJA, J. C., GELONEZE, B., VELLOSO, L. A. & ARAUJO, E. P. 2013. Defective regulation of adipose tissue autophagy in obesity. *International Journal of Obesity,* 37**,** 1473-1480.

OH, J., PARK, C., KIM, S., KIM, M., KIM, C. S., JO, W., PARK, S., YI, G. S. & PARK, J. 2023. High levels of intracellular endotrophin in adipocytes mediate COPII vesicle supplies to autophagosome to impair autophagic flux and contribute to systemic insulin resistance in obesity. *Metabolism,* 145**,** 155629.

OKABE, Y. & MEDZHITOV, R. 2014. Tissue-specific signals control reversible program of localization and functional polarization of macrophages. *Cell,* 157**,** 832-44.

OKUNO, Y., FUKUHARA, A., HASHIMOTO, E., KOBAYASHI, H., KOBAYASHI, S., OTSUKI, M. & SHIMOMURA, I. 2018. Oxidative Stress Inhibits Healthy Adipose Expansion Through Suppression of SREBF1-Mediated Lipogenic Pathway. *Diabetes,* 67**,** 1113-1127.

ONODERA, J. & OHSUMI, Y. 2005. Autophagy is required for maintenance of amino acid levels and protein synthesis under nitrogen starvation. *J Biol Chem,* 280**,** 31582-6.

OSORIO-CONLES, O., VIDAL, J. & DE HOLLANDA, A. 2021. Impact of Bariatric Surgery on Adipose Tissue Biology. *J Clin Med,* 10.

ÖST, A., SVENSSON, K., RUISHALME, I., BRÄNNMARK, C., FRANCK, N., KROOK, H., SANDSTRÖM, P., KJOLHEDE, P. & STRÅLFORS, P. 2010. Attenuated mTOR signaling and enhanced autophagy in adipocytes from obese patients with type 2 diabetes. *Molecular medicine (Cambridge, Mass.),* 16**,** 235-246.

OSTACOLO, K., LOPEZ GARCIA DE LOMANA, A., LARAT, C., HJALTALIN, V., HOLM, K. Y., HLYNSDOTTIR, S. S., SOUCHERAY, M., SOOMAN, L., ROLFSSON, O., KROGAN, N. J., STEINGRIMSSON, E., SWANEY, D. L. & OGMUNDSDOTTIR, M. H. 2024. ATG7(2) Interacts With Metabolic Proteins and Regulates Central Energy Metabolism. *Traffic,* 25**,** e12933.

OU, M. Y., ZHANG, H., TAN, P. C., ZHOU, S. B. & LI, Q. F. 2022. Adipose tissue aging: mechanisms and therapeutic implications. *Cell Death Dis,* 13**,** 300.

OUCHI, N., PARKER, J. L., LUGUS, J. J. & WALSH, K. 2011. Adipokines in inflammation and metabolic disease. *Nat Rev Immunol,* 11**,** 85-97.

OWEN, J. B. & BUTTERFIELD, D. A. 2010. Measurement of oxidized/reduced glutathione ratio. *Methods Mol Biol,* 648**,** 269-77.

PANDEY, A., YADAV, P. & SHUKLA, S. 2021. Unfolding the role of autophagy in the cancer metabolism. *Biochem Biophys Rep,* 28**,** 101158.

PARK, J., CHOE, S. S., CHOI, A. H., KIM, K. H., YOON, M. J., SUGANAMI, T., OGAWA, Y. & KIM, J. B. 2006. Increase in glucose-6-phosphate dehydrogenase in adipocytes stimulates oxidative stress and inflammatory signals. *Diabetes,* 55**,** 2939-49.

PARK, J., RHO, H. K., KIM, K. H., CHOE, S. S., LEE, Y. S. & KIM, J. B. 2005. Overexpression of glucose-6-phosphate dehydrogenase is associated with lipid dysregulation and insulin resistance in obesity. *Mol Cell Biol,* 25**,** 5146-57.

PARK, Y. J., CHOE, S. S., SOHN, J. H. & KIM, J. B. 2017. The role of glucose-6-phosphate dehydrogenase in adipose tissue inflammation in obesity. *Adipocyte,* 6**,** 147-153.

PARRA-PERALBO, E., TALAMILLO, A. & BARRIO, R. 2021. Origin and Development of the Adipose Tissue, a Key Organ in Physiology and Disease. *Front Cell Dev Biol,* 9**,** 786129.

PARZYCH, K. R. & KLIONSKY, D. J. 2014. An Overview of Autophagy: Morphology, Mechanism, and Regulation. *Antioxidants & Redox Signaling,* 20**,** 460-460.

PATRA, K. C. & HAY, N. 2014. The pentose phosphate pathway and cancer. *Trends Biochem Sci,* 39**,** 347-54.

PATRO, R., DUGGAL, G., LOVE, M. I., IRIZARRY, R. A. & KINGSFORD, C. 2017. Salmon provides fast and bias-aware quantification of transcript expression. *Nat Methods,* 14**,** 417-419.

PEREZ-ASO, M., MONTESINOS, M. C., MEDIERO, A., WILDER, T., SCHAFER, P. H. & CRONSTEIN, B. 2015. Apremilast, a novel phosphodiesterase 4 (PDE4) inhibitor, regulates inflammation through multiple cAMP downstream effectors. *Arthritis Res Ther,* 17**,** 249.

PFEIFER, A., MIKHAEL, M. & NIEMANN, B. 2024. Inosine: novel activator of brown adipose tissue and energy homeostasis. *Trends Cell Biol,* 34**,** 72-82.

PILETIC, K., ALSALEH, G. & SIMON, A. K. 2023. Autophagy orchestrates the crosstalk between cells and organs. *EMBO Rep,* 24**,** e57289.

PIRZGALSKA, R. M., SEIXAS, E., SEIDMAN, J. S., LINK, V. M., SANCHEZ, N. M., MAHU, I., MENDES, R., GRES, V., KUBASOVA, N., MORRIS, I., ARUS, B. A., LARABEE, C. M., VASQUES, M., TORTOSA, F., SOUSA, A. L., ANANDAN, S., TRANFIELD, E., HAHN, M. K., IANNACONE, M., SPANN, N. J., GLASS, C. K. & DOMINGOS, A. I. 2017. Sympathetic neuron-associated macrophages contribute to obesity by importing and metabolizing norepinephrine. *Nat Med,* 23**,** 1309-1318.

POILLET-PEREZ, L., XIE, X., ZHAN, L., YANG, Y., SHARP, D. W., HU, Z. S., SU, X., MAGANTI, A., JIANG, C., LU, W., ZHENG, H., BOSENBERG, M. W., MEHNERT, J. M., GUO, J. Y., LATTIME, E., RABINOWITZ, J. D. & WHITE, E. 2018. Autophagy maintains tumour growth through circulating arginine. *Nature,* 563**,** 569-573.

PORSCHE, C. E., DELPROPOSTO, J. B., GELETKA, L., O'ROURKE, R. & LUMENG, C. N. 2021. Obesity results in adipose tissue T cell exhaustion. *JCI Insight,* 6.

PUTTOCK, E. H., TYLER, E. J., MANNI, M., MANIATI, E., BUTTERWORTH, C., BURGER RAMOS, M., PEERANI, E., HIRANI, P., GAUTHIER, V., LIU, Y., MANISCALCO, G., RAJEEVE, V., CUTILLAS, P., TREVISAN, C., POZZOBON, M., LOCKLEY, M., RASTRICK, J., LAUBLI, H., WHITE, A. & PEARCE, O. M. T. 2023. Extracellular matrix educates an immunoregulatory tumor macrophage phenotype found in ovarian cancer metastasis. *Nat Commun,* 14**,** 2514.

RABINOWITZ, J. D. & WHITE, E. 2010. Autophagy and metabolism. *Science,* 330**,** 1344-8.

RAO, X., DUAN, X., MAO, W., LI, X., LI, Z., LI, Q., ZHENG, Z., XU, H., CHEN, M., WANG, P. G., WANG, Y., SHEN, B. & YI, W. 2015. O-GlcNAcylation of G6PD promotes the pentose phosphate pathway and tumor growth. *Nat Commun,* 6**,** 8468.

REGGIO, S., PELLEGRINELLI, V., CLÉMENT, K. & TORDJMAN, J. 2013. Fibrosis as a Cause or a Consequence of White Adipose Tissue Inflammation in Obesity. *Current Obesity Reports,* 2**,** 1-9.

RICHTER, F. C., FRIEDRICH, M., KAMPSCHULTE, N., PILETIC, K., ALSALEH, G., ZUMMACH, R., HECKER, J., POHIN, M., ILOTT, N., GUSCHINA, I., WIDEMAN, S. K., JOHNSON, E., BORSA, M., HAHN, P., MORRISEAU, C., HAMMOCK, B. D., SCHIPPER, H. S., EDWARDS, C. M., ZECHNER, R., SIEGMUND, B., WEIDINGER, C., SCHEBB, N. H., POWRIE, F. & SIMON, A. K. 2023. Adipocyte autophagy limits gut inflammation by controlling oxylipin and IL-10. *EMBO J,* 42**,** e112202.

RICHTER, F. C., OBBA, S. & SIMON, A. K. 2018. Local exchange of metabolites shapes immunity. *Immunology,* 155**,** 309-319.

RITCHIE, M. E., PHIPSON, B., WU, D., HU, Y., LAW, C. W., SHI, W. & SMYTH, G. K. 2015. limma powers differential expression analyses for RNA-sequencing and microarray studies. *Nucleic Acids Res,* 43**,** e47.

ROH, H. C., TSAI, L. T., LYUBETSKAYA, A., TENEN, D., KUMARI, M. & ROSEN, E. D. 2017. Simultaneous Transcriptional and Epigenomic Profiling from Specific Cell Types within Heterogeneous Tissues In Vivo. *Cell Rep,* 18**,** 1048-1061.

RUIFROK, A. C. & JOHNSTON, D. A. 2001. Quantification of histochemical staining by color deconvolution. *Anal Quant Cytol Histol,* 23**,** 291-9.

RUIZ-OJEDA, F. J., RUPEREZ, A. I., GOMEZ-LLORENTE, C., GIL, A. & AGUILERA, C. M. 2016. Cell Models and Their Application for Studying Adipogenic Differentiation in Relation to Obesity: A Review. *Int J Mol Sci,* 17.

RUSSELL, D. G., HUANG, L. & VANDERVEN, B. C. 2019. Immunometabolism at the interface between macrophages and pathogens. *Nat Rev Immunol,* 19**,** 291-304.

RUSSO, L. & LUMENG, C. N. 2018. Properties and functions of adipose tissue macrophages in obesity. *Immunology,* 155**,** 407-417.

SAKANE, S., HIKITA, H., SHIRAI, K., MYOJIN, Y., SASAKI, Y., KUDO, S., FUKUMOTO, K., MIZUTANI, N., TAHATA, Y., MAKINO, Y., YAMADA, R., KODAMA, T., SAKAMORI, R., TATSUMI, T. & TAKEHARA, T. 2021. White Adipose Tissue Autophagy and Adipose-Liver Crosstalk Exacerbate Nonalcoholic Fatty Liver Disease in Mice. *Cellular and Molecular Gastroenterology and Hepatology,* 12**,** 1683-1699.

SAKERS, A., DE SIQUEIRA, M. K., SEALE, P. & VILLANUEVA, C. J. 2022. Adipose-tissue plasticity in health and disease. *Cell,* 185**,** 419-446.

SARVARI, A. K., VAN HAUWAERT, E. L., MARKUSSEN, L. K., GAMMELMARK, E., MARCHER, A. B., EBBESEN, M. F., NIELSEN, R., BREWER, J. R., MADSEN, J. G. S. & MANDRUP, S. 2021. Plasticity of Epididymal Adipose Tissue in Response to Diet-Induced Obesity at Single-Nucleus Resolution. *Cell Metab,* 33**,** 437-453 e5.

SASSMANN, A., OFFERMANNS, S. & WETTSCHURECK, N. 2010. Tamoxifen-inducible Cre-mediated recombination in adipocytes. *Genesis,* 48**,** 618-625.

SCHIPPER, B. M., MARRA, K. G., ZHANG, W., DONNENBERG, A. D. & RUBIN, J. P. 2008. Regional anatomic and age effects on cell function of human adipose-derived stem cells. *Ann Plast Surg,* 60**,** 538-44.

SENBANJO, L. T. & CHELLAIAH, M. A. 2017. CD44: A Multifunctional Cell Surface Adhesion Receptor Is a Regulator of Progression and Metastasis of Cancer Cells. *Front Cell Dev Biol,* 5**,** 18.

SHI, J., HUA, L., HARMER, D., LI, P. & REN, G. 2018. Cre Driver Mice Targeting Macrophages. *Methods Mol Biol,* 1784**,** 263-275.

SHIRAKAWA, K., YAN, X., SHINMURA, K., ENDO, J., KATAOKA, M., KATSUMATA, Y., YAMAMOTO, T., ANZAI, A., ISOBE, S., YOSHIDA, N., ITOH, H., MANABE, I., SEKAI, M., HAMAZAKI, Y., FUKUDA, K., MINATO, N. & SANO, M. 2016. Obesity accelerates T cell senescence in murine visceral adipose tissue. *Journal of Clinical Investigation,* 126**,** 4626-4639.

SILVA, H. M., BAFICA, A., RODRIGUES-LUIZ, G. F., CHI, J., SANTOS, P. D. A., REIS, B. S., HOYTEMA VAN KONIJNENBURG, D. P., CRANE, A., ARIFA, R. D. N., MARTIN, P., MENDES, D., MANSUR, D. S., TORRES, V. J., CADWELL, K., COHEN, P., MUCIDA, D. & LAFAILLE, J. J. 2019. Vasculature-associated fat macrophages readily adapt to inflammatory and metabolic challenges. *J Exp Med,* 216**,** 786-806.

SINGH, M., KHONG, H., DAI, Z., HUANG, X. F., WARGO, J. A., COOPER, Z. A., VASILAKOS, J. P., HWU, P. & OVERWIJK, W. W. 2014. Effective innate and adaptive antimelanoma immunity through localized TLR7/8 activation. *J Immunol,* 193**,** 4722-31.

SINGH, N., SHRESHTHA, A. K., THAKUR, M. S. & PATRA, S. 2018. Xanthine scaffold: scope and potential in drug development. *Heliyon,* 4**,** e00829.

SINGH, R., KAUSHIK, S., WANG, Y., XIANG, Y., NOVAK, I., KOMATSU, M., TANAKA, K., CUERVO, A. M. & CZAJA, M. J. 2009a. Autophagy regulates lipid metabolism. *Nature,* 458**,** 1131-5.

SINGH, R., XIANG, Y., WANG, Y., BAIKATI, K., CUERVO, A. M., LUU, Y. K., TANG, Y., PESSIN, J. E., SCHWARTZ, G. J. & CZAJA, M. J. 2009b. Autophagy regulates adipose mass and differentiation in mice. *Journal of Clinical Investigation,* 119**,** 3329-3339.

SKINNER, O. S., BLANCO-FERNANDEZ, J., GOODMAN, R. P., KAWAKAMI, A., SHEN, H., KEMENY, L. V., JOESCH-COHEN, L., REES, M. G., ROTH, J. A., FISHER, D. E., MOOTHA, V. K. & JOURDAIN, A. A. 2023. Salvage of ribose from uridine or RNA supports glycolysis in nutrient-limited conditions. *Nat Metab,* 5**,** 765-776.

SOUSA, C. M., BIANCUR, D. E., WANG, X., HALBROOK, C. J., SHERMAN, M. H., ZHANG, L., KREMER, D., HWANG, R. F., WITKIEWICZ, A. K., YING, H., ASARA, J. M., EVANS, R. M., CANTLEY, L. C., LYSSIOTIS, C. A. & KIMMELMAN, A. C. 2016. Pancreatic stellate cells support tumour metabolism through autophagic alanine secretion. *Nature 2016 536:7617,* 536**,** 479-483.

SOUSSI, H., CLÉMENT, K. & DUGAIL, I. 2016. Adipose tissue autophagy status in obesity: Expression and flux—two faces of the picture. *Autophagy,* 12**,** 588-589.

SOUSSI, H., REGGIO, S., ALILI, R., PRADO, C., MUTEL, S., PINI, M., ROUAULT, C., CLÉMENT, K. & DUGAIL, I. 2015. DAPK2 downregulation associates with attenuated adipocyte autophagic clearance in human obesity. *Diabetes,* 64**,** 3452-3463.

SPINA, D. & PAGE, C. P. 2017. Xanthines and Phosphodiesterase Inhibitors. *Handb Exp Pharmacol,* 237**,** 63-91.

STEFAN, N., BIRKENFELD, A. L., SCHULZE, M. B. & LUDWIG, D. S. 2020. Obesity and impaired metabolic health in patients with COVID-19. *Nat Rev Endocrinol,* 16**,** 341-342.

STREFELER, A., BLANCO-FERNANDEZ, J. & JOURDAIN, A. A. 2024. Nucleosides are overlooked fuels in central carbon metabolism. *Trends Endocrinol Metab,* 35**,** 290-299.

SUN, K., LI, X. & SCHERER, P. E. 2023. Extracellular Matrix (ECM) and Fibrosis in Adipose Tissue: Overview and Perspectives. *Compr Physiol,* 13**,** 4387-4407.

TAHERBHOY, A. M., TAIT, S. W., KAISER, S. E., WILLIAMS, A. H., DENG, A., NOURSE, A., HAMMEL, M., KURINOV, I., ROCK, C. O., GREEN, D. R. & SCHULMAN, B. A. 2011. Atg8 transfer from Atg7 to Atg3: a distinctive E1-E2 architecture and mechanism in the autophagy pathway. *Mol Cell,* 44**,** 451-61.

THOMOU, T., MORI, M. A., DREYFUSS, J. M., KONISHI, M., SAKAGUCHI, M., WOLFRUM, C., RAO, T. N., WINNAY, J. N., GARCIA-MARTIN, R., GRINSPOON, S. K., GORDEN, P. & KAHN, C. R. 2017. Adipose-derived circulating miRNAs regulate gene expression in other tissues. *Nature,* 542**,** 450-455.

TIAN, N., LIU, Q., LI, Y., TONG, L., LU, Y., ZHU, Y., ZHANG, P., CHEN, H., HU, L., MENG, J., FENG, M., LI, M., ZHENG, L., LI, B., XU, T., WU, L. & TONG, X. 2020. Transketolase Deficiency in Adipose Tissues Protects Mice From Diet-Induced Obesity by Promoting Lipolysis. *Diabetes,* 69**,** 1355-1367.

TIAN, R., YANG, C., CHAI, S. M., GUO, H., SEIM, I. & YANG, G. 2022. Evolutionary impacts of purine metabolism genes on mammalian oxidative stress adaptation. *Zool Res,* 43**,** 241-254.

TRIM, W. V. & LYNCH, L. 2022. Immune and non-immune functions of adipose tissue leukocytes. *Nat Rev Immunol,* 22**,** 371-386.

VAN BEEK, L., VAN KLINKEN, J. B., PRONK, A. C., VAN DAM, A. D., DIRVEN, E., RENSEN, P. C., KONING, F., WILLEMS VAN DIJK, K. & VAN HARMELEN, V. 2015. The limited storage capacity of gonadal adipose tissue directs the development of metabolic disorders in male C57Bl/6J mice. *Diabetologia,* 58**,** 1601-9.

VAN ROOIJEN, N. & SANDERS, A. 1994. Liposome mediated depletion of macrophages: mechanism of action, preparation of liposomes and applications. *J Immunol Methods,* 174**,** 83-93.

VARLAMOV, O., BETHEA, C. L. & ROBERTS, C. T., JR. 2014. Sex-specific differences in lipid and glucose metabolism. *Front Endocrinol (Lausanne),* 5**,** 241.

VILA, I. K., BADIN, P. M., MARQUES, M. A., MONBRUN, L., LEFORT, C., MIR, L., LOUCHE, K., BOURLIER, V., ROUSSEL, B., GUI, P., GROBER, J., STICH, V., ROSSMEISLOVA, L., ZAKAROFF-GIRARD, A., BOULOUMIE, A., VIGUERIE, N., MORO, C., TAVERNIER, G. & LANGIN, D. 2014. Immune cell Toll-like receptor 4 mediates the

development of obesity- and endotoxemia-associated adipose tissue fibrosis. *Cell Rep,* 7**,** 1116-29.

VILLANUEVA-CARMONA, T., CEDO, L., NUNEZ-ROA, C., MAYMO-MASIP, E., VENDRELL, J. & FERNANDEZ-VELEDO, S. 2023. Protocol for the in vitro isolation and culture of mature adipocytes and white adipose tissue explants from humans and mice. *STAR Protoc,* 4**,** 102693.

VILLARROYA, F., CEREIJO, R., GAVALDÀ-NAVARRO, A., VILLARROYA, J. & GIRALT, M. 2018. Inflammation of brown/beige adipose tissues in obesity and metabolic disease. *Journal of Internal Medicine,* 284**,** 492-504.

VILLARROYA, F., CEREIJO, R., VILLARROYA, J. & GIRALT, M. 2017. Brown adipose tissue as a secretory organ. *Nat Rev Endocrinol,* 13**,** 26-35.

VIOLA, A., MUNARI, F., SANCHEZ-RODRIGUEZ, R., SCOLARO, T. & CASTEGNA, A. 2019. The Metabolic Signature of Macrophage Responses. *Front Immunol,* 10**,** 1462.

VIRTUE, S. & VIDAL-PUIG, A. 2010. Adipose tissue expandability, lipotoxicity and the Metabolic Syndrome--an allostatic perspective. *Biochim Biophys Acta,* 1801**,** 338-49.

WALTHER, T., NOVO, M., ROSSGER, K., LETISSE, F., LORET, M. O., PORTAIS, J. C. & FRANCOIS, J. M. 2010. Control of ATP homeostasis during the respiro-fermentative transition in yeast. *Mol Syst Biol,* 6**,** 344.

WANG, Q. A., TAO, C., GUPTA, R. K. & SCHERER, P. E. 2013. Tracking adipogenesis during white adipose tissue development, expansion and regeneration. *Nat Med,* 19**,** 1338-44.

WANG, T., SHARMA, A. K. & WOLFRUM, C. 2022. Novel insights into adipose tissue heterogeneity. *Rev Endocr Metab Disord,* 23**,** 5-12.

WATSON, A. S. & SOILLEUX, E. J. 2015. Detection of p62 on Paraffin Sections by Immunohistochemistry. *Cold Spring Harb Protoc,* 2015**,** 756-60.

WCULEK, S. K., DUNPHY, G., HERAS-MURILLO, I., MASTRANGELO, A. & SANCHO, D. 2022. Metabolism of tissue macrophages in homeostasis and pathology. *Cell Mol Immunol,* 19**,** 384-408.

WCULEK, S. K., HERAS-MURILLO, I., MASTRANGELO, A., MANANES, D., GALAN, M., MIGUEL, V., CURTABBI, A., BARBAS, C., CHANDEL, N. S., ENRIQUEZ, J. A., LAMAS, S. & SANCHO, D. 2023. Oxidative phosphorylation selectively orchestrates tissue macrophage homeostasis. *Immunity,* 56**,** 516-530 e9.

WEISBERG, S. P., MCCANN, D., DESAI, M., ROSENBAUM, M., LEIBEL, R. L. & FERRANTE, A. W., JR. 2003. Obesity is associated with macrophage accumulation in adipose tissue. *J Clin Invest,* 112**,** 1796-808.

WEN, Y. A., XING, X., HARRIS, J. W., ZAYTSEVA, Y. Y., MITOV, M. I., NAPIER, D. L., WEISS, H. L., MARK EVERS, B. & GAO, T. 2017. Adipocytes activate mitochondrial fatty acid oxidation and autophagy to promote tumor growth in colon cancer. *Cell Death Dis,* 8**,** e2593.

WHO. 2024. *Obesity and overweight* [Online]. Available: https://www.who.int/news-room/fact-sheets/detail/obesity-and-overweight [Accessed May 1st 2024].

WINTHER, S., TRAUELSEN, M. & SCHWARTZ, T. W. 2021. Protective succinate-SUCNR1 metabolic stress signaling gone bad. *Cell Metab,* 33**,** 1276-1278.

WU, H., ZHAO, X., HOCHREIN, S. M., ECKSTEIN, M., GUBERT, G. F., KNOPPER, K., MANSILLA, A. M., ONER, A., DOUCET-LADEVEZE, R., SCHMITZ, W., GHESQUIERE, B., THEURICH, S., DUDEK, J., GASTEIGER, G., ZERNECKE, A., KOBOLD, S., KASTENMULLER, W. & VAETH, M. 2023. Mitochondrial dysfunction promotes the transition of precursor to terminally exhausted T cells through HIF-1alpha-mediated glycolytic reprogramming. *Nat Commun,* 14**,** 6858.

WYNN, T. A. 2007. Common and unique mechanisms regulate fibrosis in various fibroproliferative diseases. *J Clin Invest,* 117**,** 524-9.

WYNN, T. A. & VANNELLA, K. M. 2016. Macrophages in Tissue Repair, Regeneration, and Fibrosis. *Immunity,* 44**,** 450-462.

XU, X., GRIJALVA, A., SKOWRONSKI, A., VAN EIJK, M., SERLIE, M. J. & FERRANTE, A. W. 2013a. Obesity activates a program of lysosomal-dependent lipid metabolism in adipose tissue macrophages independently of classic activation. *Cell Metabolism,* 18**,** 816-830.

XU, Y. F., LETISSE, F., ABSALAN, F., LU, W., KUZNETSOVA, E., BROWN, G., CAUDY, A. A., YAKUNIN, A. F., BROACH, J. R. & RABINOWITZ, J. D. 2013b. Nucleotide degradation and ribose salvage in yeast. *Mol Syst Biol,* 9**,** 665.

YU, G., WANG, L. G., HAN, Y. & HE, Q. Y. 2012. clusterProfiler: an R package for comparing biological themes among gene clusters. *OMICS,* 16**,** 284-7.

YU, L., WAN, Q., LIU, Q., FAN, Y., ZHOU, Q., SKOWRONSKI, A. A., WANG, S., SHAO, Z., LIAO, C. Y., DING, L., KENNEDY, B. K., ZHA, S., QUE, J., LEDUC, C. A., SUN, L., WANG, L. & QIANG, L. 2024. IgG is an aging factor that drives adipose tissue fibrosis and metabolic decline. *Cell Metab,* 36**,** 793-807 e5.

ZHANG, H., ALSALEH, G., FELTHAM, J., SUN, Y., NAPOLITANO, G., RIFFELMACHER, T., CHARLES, P., FRAU, L., HUBLITZ, P., YU, Z., MOHAMMED, S., BALLABIO, A., BALABANOV, S., MELLOR, J. & SIMON, A. K. 2019. Polyamines Control eIF5A Hypusination, TFEB Translation, and Autophagy to Reverse B Cell Senescence. *Mol Cell,* 76**,** 110-125 e9.

ZHANG, H., TSUI, C. K., GARCIA, G., JOE, L. K., WU, H., MARUICHI, A., FAN, W., PANDOVSKI, S., YOON, P. H., WEBSTER, B. M., DURIEUX, J., FRANKINO, P. A., HIGUCHI-SANABRIA, R. & DILLIN, A. 2024. The extracellular matrix integrates mitochondrial homeostasis. *Cell,* 187**,** 4289-4304 e26.

ZHANG, J., LYU, T., CAO, Y. & FENG, H. 2021a. Role of TCF-1 in differentiation, exhaustion, and memory of CD8(+) T cells: A review. *FASEB J,* 35**,** e21549.

ZHANG, N., YANG, X., YUAN, F., ZHANG, L., WANG, Y., WANG, L., MAO, Z., LUO, J., ZHANG, H., ZHU, W. G. & ZHAO, Y. 2018a. Increased Amino Acid Uptake Supports Autophagy-Deficient Cell Survival upon Glutamine Deprivation. *Cell Rep,* 23**,** 3006-3020.

ZHANG, S., PENG, X., YANG, S., LI, X., HUANG, M., WEI, S., LIU, J., HE, G., ZHENG, H., YANG, L., LI, H. & FAN, Q. 2022. The regulation, function, and role of lipophagy, a form of selective autophagy, in metabolic disorders. *Cell Death Dis,* 13**,** 132.

ZHANG, Y., GOLDMAN, S., BAERGA, R., ZHAO, Y., KOMATSU, M. & JIN, S. 2009. Adipose-specific deletion of autophagy-related gene 7 (atg7) in mice reveals a role in adipogenesis. *Proceedings of the National Academy of Sciences of the United States of America,* 106**,** 19860-19865.

ZHANG, Y., SOWERS, J. R. & REN, J. 2018b. Targeting autophagy in obesity: From pathophysiology to management. *Nature Reviews Endocrinology,* 14**,** 356-376.

ZHANG, Z., FUNCKE, J. B., ZI, Z., ZHAO, S., STRAUB, L. G., ZHU, Y., ZHU, Q., CREWE, C., AN, Y. A., CHEN, S., LI, N., WANG, M. Y., GHABEN, A. L., LEE, C., GAUTRON, L., ENGELKING, L. J., RAJ, P., DENG, Y., GORDILLO, R., KUSMINSKI, C. M. & SCHERER, P. E. 2021b. Adipocyte iron levels impinge on a fat-gut crosstalk to regulate intestinal lipid absorption and mediate protection from obesity. *Cell Metabolism,* 33**,** 1624-1639.e9.

ZHAO, Y., SHAO, Q. & PENG, G. 2020. Exhaustion and senescence: two crucial dysfunctional states of T cells in the tumor microenvironment. *Cell Mol Immunol,* 17**,** 27-35.

ZHU, B., WU, Y., HUANG, S., ZHANG, R., SON, Y. M., LI, C., CHEON, I. S., GAO, X., WANG, M., CHEN, Y., ZHOU, X., NGUYEN, Q., PHAN, A. T., BEHL, S., TAKETO, M. M., MACK, M., SHAPIRO, V. S., ZENG, H., EBIHARA, H., MULLON, J. J., EDELL, E. S., REISENAUER, J. S., DEMIREL, N., KERN, R. M., CHAKRABORTY, R., CUI, W., KAPLAN, M. H., ZHOU, X., GOLDRATH, A. W. & SUN, J. 2021. Uncoupling of macrophage inflammation from self-renewal modulates host recovery from respiratory viral infection. *Immunity,* 54**,** 1200-1218 e9.